Polymer Materials for the Encapsulation and Degradation of Chemical Warfare Agents

Alexander Joseph Wright

A thesis submitted to the University of Kent in partial fulfilment of the requirements for the degree of Doctor of Philosophy.

University of Kent, Canterbury,
Kent,
CT2 7NH

September 2018

Declaration

I declare that this thesis is my own work, and has been written in my own words. Appropriate care has been taken to accurately reference the works of others where necessary.

Signed -

Alexander Joseph Wright

19th September 2018

Acknowledgements

Firstly, I would like to thank Dr Simon Holder for giving me the opportunity to carry out this project. I would like to thank him for the support, huge range of knowledge, and the time he put in to keep my work moving in the correct direction, not only throughout my PhD, but also in my undergraduate studies. Secondly, I would like to thank Dr Barry Blight who acted as my co-supervisor until he sadly moved back to Canada. His enthusiasm and commitment even after leaving the University helped to solidify the collaborative efforts of mine and Yarry's work.

Thanks goes to Dr Kate Belsey and Dr Olivia Monaghan who gave me so much help during the first two years of my PhD, and taught me many of the core techniques which I used throughout my work. Additionally, Dr Ewan Clarke for help with many aspects of synthesis, Dr Jennifer Hiscock for help with NMR, and all the other academics and technical staff who have proposed solutions to problems during my time at Kent.

I would also like to acknowledge firstly; Yarry who has travelled through this experience parallel with me since our first day in lab 310, and who acted as a great friend, housemate and also academic competition which helped to keep both of us on track. My thanks go to all my other friends in the School of Physical Sciences past and present: Francesco, Brad, Aaron, Nanami, Matt, Jed, Barbora, Saeed, Andryj, JJ and Ian.

Huge thanks goes to Hannah for always giving me something to look forward to and for being the person who motivates me to be the best I can be.

I would finally like to thank my whole family, especially Mum and Dad, who have always encouraged me to take the right path and have done all they can to support me unconditionally throughout all my choices.

Abstract

Superabsorbent polymer hydrogel networks are found in everyday life, such as in nappies and spill kits. This research would focus on the development of a highly absorbent, catalytically active polymer system, for the encapsulation and degradation of organic materials and chemical warfare agents (CWAs) such as VX and sulfur mustard (HD).

The superabsorbent nature of a series of styrene based polyelectrolyte networks, crosslinked with divinylbenzene, were examined. The electrolytic nature of the networks was established through the introduction of a quaternary ammonium ionic monomer at increasing mol% weighting. The resulting *net*-poly(styrene-*co*-4-vinylbenzyl trihexylammonium chloride-*co*-divinylbenzene) systems were studied for their ability to absorb common solvents. The swelling performance was then correlated with various physical properties including dielectric and solubility parameters. The predicted swelling degrees of additional solvents were calculated and showed good similarity to experimental results. The swelling behaviour of CWAs in this system was examined and a suitable simulant for HD and VX was determined from these results. In an attempt to increase the swelling of the CWAs, alternative low polarity monomers were screened using predictions from solubility parameter data. Alternative anions to the chloride were also screened in an attempt to increase the swelling performance in the electrolytic polymers. A poly(styrene-*co*-vinylbenzyl chloride-*co*-divinylbenzene) lightly cross-linked poly high internal phase emulsion (pHIPE) was also developed. The record breaking absorption capacities of a variety of CWAs, including sulfur mustard (HD) (Q = 40) and V-series (VM, VX, *i*-Bu-VX, *n*-Bu-VX) of nerve agents (Q $\geqslant$ 45) and a simulant, methyl benzoate (Q = 55) were observed in this polymer. The polymer showed fast swelling, (<5 min to total absorption) and the ability to swell both from a monolithic state and from a compressed state. The polymer was then produced on increased scale (10 kg).

The absorbent pHIPEs were further adapted to include a catalytically active MOF inside the pores at 25 wt%, in addition to internal buffer as part of the polymer matrix. This combination

of changes led to a polymer sorbent which was able to swell and degrade a VX simulant (methyl paraoxon) and VX in situ without the need for external buffering.

Modification of the styrene based pHIPE to include increasing amounts of myrcene was also investigated briefly as an approach to creating an elastomeric oil / CWA absorption capability, using a greener feedstock. To facilitate this, an alternative crosslinking monomer was synthesised and found to be an effective linker unit.

Publications and Presentations

Peer-Reviewed Journal Publication:

Poly High Internal Phase Emulsion for the Immobilization of Chemical Warfare Agents, A. J. Wright, M. J. Main, N. J. Cooper, B. A. Blight, S. J. Holder, *ACS Appl. Mater. Interfaces*, **2017**, *9* (37), pp 31335–31339.

Oral presentations:

'Encapsulation and decontamination of chemical warfare agents in a polyHIPE / MOF composite,' Macro Group Young Researchers Meeting, Dublin, 2018. Second prize award received.

'Superabsorbent Polymers for Encapsulation of Chemical Warfare Agents,' School of Physical Sciences Functional Materials Group Colloquium, University of Kent, 2016

Poster Presentations:

'PolyHIPE composition modification; Towards a versatile chemical warfare agent absorbent,' 256th ACS National Meeting and Exposition, Boston (USA), 2018, presented by Dr. Simon Holder.

'Poly High Internal Phase Emulsions for the Effective Encapsulation of Chemical Warfare Agents,' Polymers For Advanced Technologies conference, Manchester, 2017.

'Styrene Based Superabsorbents for the Encapsulation of Chemical Agents – Rationalisation of Swelling Performance Using Hansen Solubility Parameters,' Warwick International Polymer Conference, University of Warwick, 2016.

'Synthesis and Characterisation of Styrene Based Superabsorbents for the Immobilization and Degradation of Organophosphorus Compounds,' European Science Foundation's Precision Polymer Materials Conference, Lacanau (France), 2015

List of Abbreviations

2-CEES	2-Chloroethyl Ethyl Sulfide
AChE	Acetylcholine Esterase
ATRP	Atom-Transfer Radical Polymerisation
CWA	Chemical Warfare Agent
Đ	Dispersity Index
DCM	Dichloromethane
DCP	Diethyl chlorophosphate
DDMA	1,10-Decanedimethacrylate
DMF	Dimethylformamide
DMMP	Dimethyl methyl phosphonate
DMNP	Methyl Paraoxon
DMSO	Dimethyl sulfoxide
DSC	Differential Scanning Calorimetry
DVB	Divinylbenzene
EGDMA	Ethylene glycol dimethacrylate
FRP	Free Radical Polymerisation
GB (Sarin)	isopropyl methyl phosphonofluoridate
GPC	Gel Permeation Chromatography
HBA	Hydrogen Bond Acceptor
HD	Sulfur Mustard (bis (2-chloroethyl) sulfide)
HIPE	High Internal Phase Emulsion
HSP	Hansen Solubility Parameters
HSPiP	Hansen Solubility Parameters in Practice (software)
i-Bu-VX	diethylaminoethyl O-isobutyl methylphosphonthioate
IP_{xx}	Internal phase fraction
FT-IR	Fourier Transform Infra-Red Spectroscopy

K_{ass}	Ion Association Constant
M_n	Number Average Molecular Weight
MOF	Metal-Organic Framework
M_w	Weight Average Molecular Weight
n-Bu-VX	diethylaminoethyl O-nbutyl methylphosphonothioate
NMR	Nuclear Magnetic Resonance Spectroscopy
ODMA	Octadecylmethacrylate
pHIPE	Poly High Internal Phase Emulsion
PSS	Poly(styrenesulfonate)
PTFE	Poly(tetrafluoroethylene)
PXRD	Powder X-Ray Diffraction
Q	Mass swelling ratio
QAS-xx	Quaternary ammonium monomer (xx = associated anion)
Q_{mod}	Modified mass swelling ratio
Q_v	Volume swelling ratio
RAFT	Reversible Addition-Fragmentation Chain-Transfer Polymerisation
SDM	Self-Decontaminating Material
SEM	Scanning Electron Microscopy
St	Styrene
T_g	Glass Transition Temperature
THF	Tetrahydrofuran
THVBAC	N,N,N-trihexyl-N-(4-vinylbenzyl)ammonium chloride
VBC	Vinyl Benzyl Chloride (4-chloromethyl styrene)
VBPP	Vinyl Benzyl Piperidine (1-(4-vinylbenzyl)piperidine))
VM	diethylaminoethyl O-ethyl methylphosphonothioate
VX	diisopropylaminoethyl O-ethyl methylphosphonothioate

δd	Hansen Dispersion Component
δh	Hansen Hydrogen Bonding Component
δp	Hansen Polarity Component

Contents

Chapter 1 - Introduction

This thesis focusses on the development of absorbent polymer materials with the ultimate aim of creating a matrix for absorbing chemical warfare agents (CWAs) and degrading them in situ. This section of my thesis is aimed at introducing some of the central topics relating to the various investigations that were carried out throughout the project. More specific introductions and motivations are found at the start of each chapter.

1.1 Free radical polymerisation

For the purposes of this thesis, all of the polymers would be grown through free-radical polymerisation (FRP). Free radical polymerisation (FRP) is a very widely used and industrially important technique for the production of polymers, many of which are found throughout daily life.[1] FRP utilizes monomers which have unsaturated bonds, specifically unsaturated vinyl bonds such as acrylates, methacrylates and styrenes.[2] The first crucial step in a FRP is the initiation of the polymerisation. In general, initiators for FRP undergo a reaction based upon homolytic cleavage of a covalent bond in a molecular species to leave one or more reactive species known as radicals. Two examples of this which are extremely common are the thermolysis of azobisisobutyronitrile (AIBN) and potassium persulfate, which are oil and water soluble respectively (Figure 1.1). It is important to note here that thermolysis is only one method of radical formation. Other forms include photolysis, exposure to electric potential, or through a redox reaction.[3]

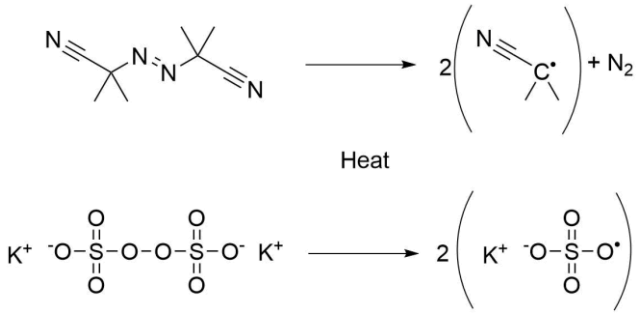

Figure 1.1 – The thermolysis causing homolytic cleavage of AIBN and potassium persulfate which forms two radicals.

The chain growth mechanism of FRP occurs through the propagation of a radical as the kinetic chain carrier. The initiators first cleave, forming the radical initator species. This radical then attacks the unsaturated bond of a monomer unit, which in turn moved the racial onto the monomer. More units are subsequently added as the chain grows, this stage is known as propagation. The propagation steps for the FRP of styrene, initiated with an AIBN radical is shown in Figure 1.2.

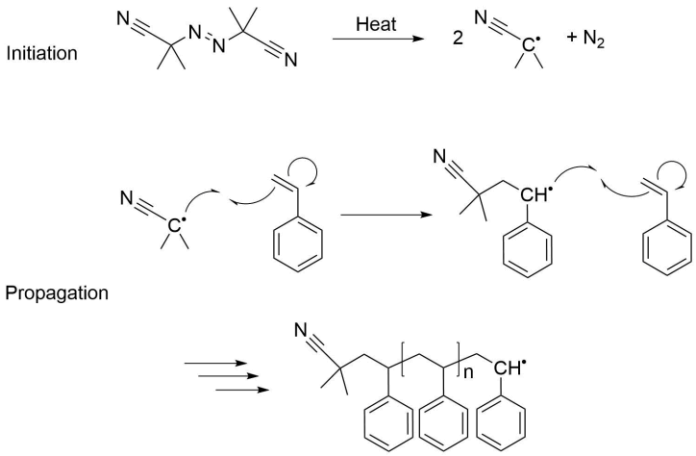

Figure 1.2 – The FRP mechanism for the initiation and propagation of polystyrene initiated with AIBN and heat.

Termination is the final important step with regards to FRP. Termination can occur through three main mechanisms (Figure 1.3). Disproportionation is a process in which hydrogen is abstracted from one growing polymer chain onto another which results in one saturated and one unsaturated polymer chain. Combination termination occurs when two radicals come together and cause extinction of the active site. This can occur between growing chains or between growing chains and initiating radicals. If the combination is between two chains, the resulting polymer length is increased. Disproportionation results in smaller variation in chain length than combination.[4] Chain transfer is the third type of termination and is the act of the propagating radical transferring from the active end of the polymer chain to another substance such as a chain transfer agent, impurity, solvent or even to another propagating chain. Oxygen is one such example of a chain transfer agent which can slow polymerisation rates significantly when oxygen is not excluded from a FRP reaction.[5] Chain transfer however does not necessarily cause extinction of the radical as with the other two routes.

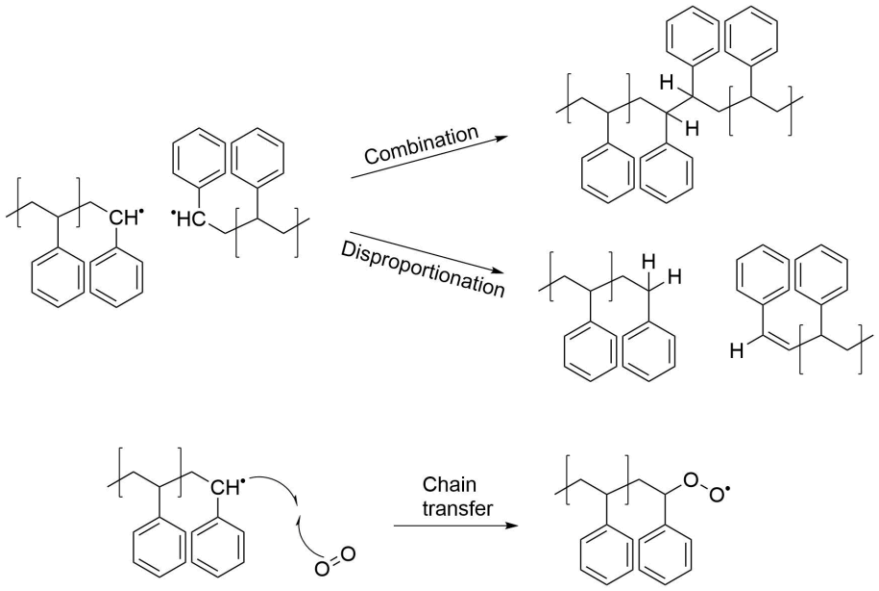

Figure 1.3 – The termination mechanism of polystyrene. Disproportionation and combination (top), and chain transfer to molecular oxygen (below).

The overall rate of polymerisation (R_p) is a function of all three steps and is given in a generalised equation (for thermally initiated FRP);

$$R_p = k_p \left(\frac{f k_d}{k_t}\right)^{0.5} [M][I]^{0.5}$$

(Equation 1.1)

Where the k_p is the propagation constant, f is the initator efficiency, k_t is the rate of termination, k_d is the rate of initiator dissociation, [M] is the concentration of the monomer, and the concentration of initiator is [I].[6] The equation assumes a steady-state throughout the polymerisation. This is that the rate of termination and rate of initiator formation is equal and therefore the quantity of active chains is constant. Most polymerisations are generally accepted to be in steady state; however one notable exception is when auto-acceleration occurs. This is sometimes known as the gel-effect, or Tromssdorff effect and is observed when the localised increase in viscosity of a polymerisation causes the R_p to increase significantly due to a decrease in k_t chain termination (disproportionation and combination).[7,8] The M_w of the polymer is also seen to increase under this effect as the propagating radical is active for longer due to less termination likelihood. This effect is commonly observed in FRPs where

multifunctional monomers, such as a crosslinker are utilized. Due to the formation of networks, the active chain ends are restricted which reduces the k_t similarly to a viscosity increase.[9]

1.1.1 Copolymers and Crosslinking

1.1.1.1 Copolymerisation

A copolymer is defined as a polymer which is comprised of more than one monomer in its chain. Copolymers are split into categories which are defined by the pattern in which the monomers are incorporated in the polymer chain.[10] Random copolymers are formed when the monomers randomly react together to form the chain irrespective of the adjacent molecules. Block copolymers are obtained from extended sequences of repeating units of the same monomer, commonly forming di-block and tri-block copolymers. Alternating copolymers are formed when the monomers are incorporated into the polymer one after the other in complete regularity. Finally, gradient copolymers form when each monomer has a slight tendency to react with itself more so than with the other, causing a high concentration of one monomer, followed by a more statistical distribution, and then a high concentration of the other polymer at the subsequent chain end. The rate of reaction of a monomer or growing chain to the other monomers in the reaction is not always identical. That is, the rate of heteropolymerisation and homopolymerisation for a monomer is unique to the copolymerisation. This is what leads to the variation in ratios of monomer through the polymer, and the subsequent patterns mentioned above.[6]

1.1.1.2 Crosslinking

Crosslinking in its most simple form is the act of joining multiple polymer chains together to form a network. The earliest forms of crosslinking were the vulcanisation of liquid rubbers with agents such as sulfur, to form hard rubbers suitable for applications such as car tyres. [11] Crosslinking can be carried out in nearly all polymer systems, for example by using a bi-functional monomer such as ethylene glycol dimethacrylate in the free radical copolymerisation of acrylic acid to form a hydrogel, or by post synthetically crosslinking

polymers, such as in vulcanisation of rubbers (Figure 1.4). All polymers which are considered 'thermosetting,' where they are unable to melt once cured, are crosslinked.[12] Some examples of which include polyurethanes (foams), epoxy resins (glues) and silicones (cooking equipment).

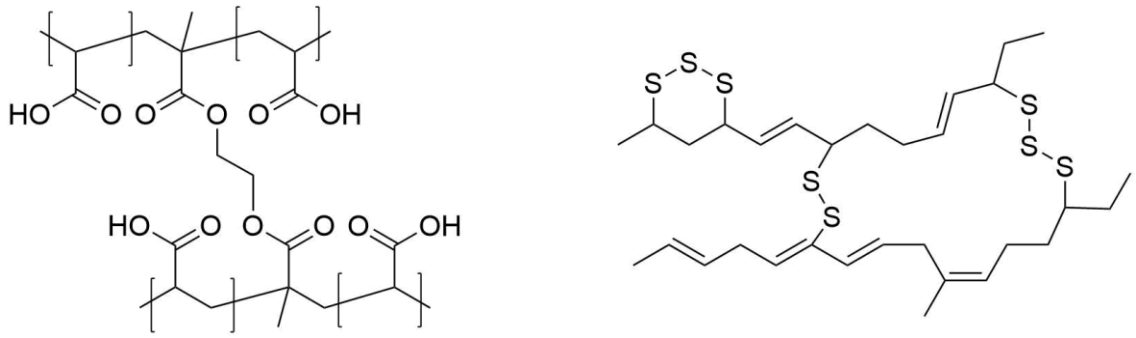

Figure 1.4 – A representation of crosslinking in polyacrylic acid with ethylene glycol dimethacrylate (left) and the vulcanization of natural rubber by the addition of sulfur bridges (right).

The joining of polymer chains into networks significantly changes the physical properties of the system. Some of the most obvious changes are that the polymer will no longer exhibit a true melting point and heating will only lead to pyrolysis/decomposition. The strength and brittleness of the polymer will also increase. Whilst the melting point is lost, the glass transition should still be observed, however it is generally largely increased by increasing levels of crosslinking.[13] T_g elevation in ethylene glycol dimethacrylate crosslinked isobutyl methacrylate systems can increase from 45 °C to 105 °C,[14] and natural rubbers can increase from -50 °C to over 150 °C with varying fractions of linking.[15] The most important characteristic of crosslinking in terms of the work in the following chapters, is that the solubility of polymers change when they are crosslinked. More specifically, the ability of the polymer chains to completely dissolve is lost.

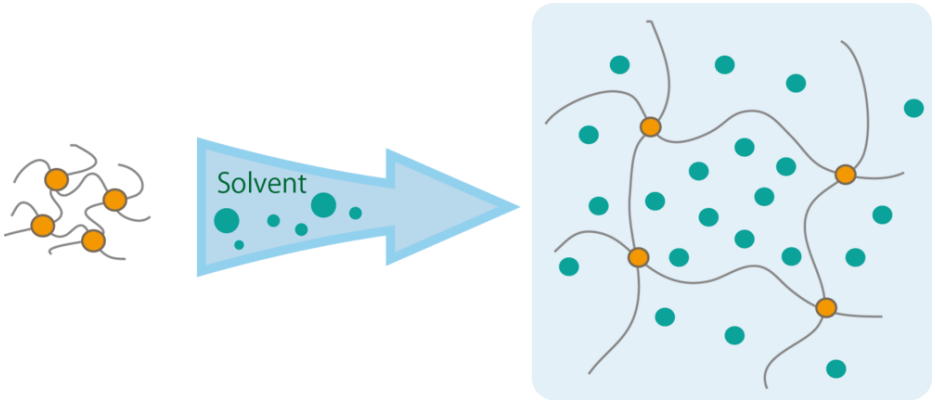

Figure 1.5 - A demonstration of how crosslinks in a polymer network prevent full dissolution, causing a swelling effect.

When a crosslinked polymer is exposed to a suitable solvent, the chains will begin to dissolve, but the links will prevent full dissolution, this causes a swelling effect where the solvent is trapped into the network (Figure 1.5). This swelling phenomenon is the principle for the areas of the work which will be presented in further chapters.

1.2 Emulsions and high internal phase emulsion polymers

1.2.1 Emulsions

An emulsion is defined by the IUPAC gold book as a colloidal system where liquid droplets or liquid crystals are dispersed in another liquid. Usually these droplets are immiscible and form opaque solutions when formed. An emulsion consists of an organic, nonpolar, hydrophobic solution known as the 'oil' and a hydrophilic aqueous mixture known as the 'water'. The phase in which either of these liquids are in denoted the type of emulsion. In an oil in water emulsion (o/w), the oil is in the internal phase (dispersed phase) and the water is the external (continuous phase). In water in oil emulsions (w/o), the opposite is true (Figure 1.6).[16]

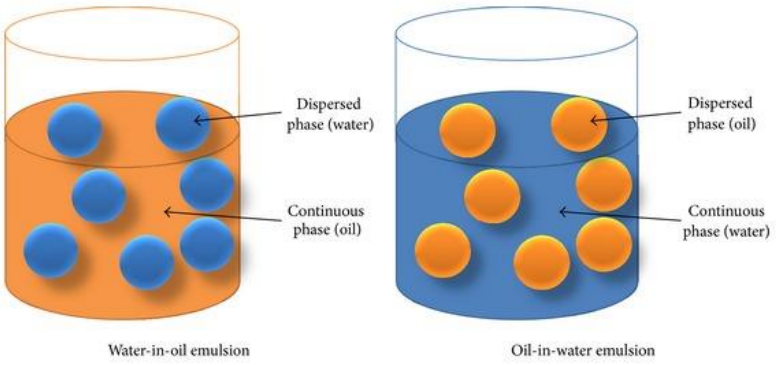

Figure 1.6 – A diagram from reference showing the difference between a w/o and a o/w emulsion.[17]

Energy is required to form an emulsion, and this is normally introduced through mixing of some kind. This is because there is an energy requirement when increasing the interfacial area of the system through the formation of the emulsion.[18] Interface molecules, which are referred to as surfactants are required for the long term stability of the emulsion. Without surfactants stabilizing the interface of the phases, the emulsion would instantly phase separate back to a lower energy level. Surfactants are normally amphiphilic; they possess both hydrophilic and hydrophobic segments. This feature is what allows them to assemble at the interface of the phases. The class of surfactant is denoted by the charge of the hydrophilic portion, such as cationic, anionic and non-ionic.

1.2.1.1 O/W vs W/O

One of the critical rules in emulsions is that of Bancroft. The work of Bancroft *et al*. showed that the phase into which the surfactant is most soluble will normally become the continuous phase of the emulsion.[19] Therefore a surfactant most soluble in the water will lead to an o/w emulsion. This leads on to a term which is used to predict which type of emulsion will form based upon the surfactant choice, known as the hydrophilic-lipophilic balance (HLB).[20] The HLB is derived from the weight fraction of the respective hydrophilic and hydrophobic portions of the surfactant and is calculated;

$$HLB = 20\ x\ \frac{M_h}{M}$$

(Equation 1.2)

Where M_h is the molecular mass of the hydrophilic portion and M is the total molecular mass. The resulting HLB number can then be used to predict the type of emulsion as shown in Figure 1.7. The higher the HLB number the higher the hydrophilicity.

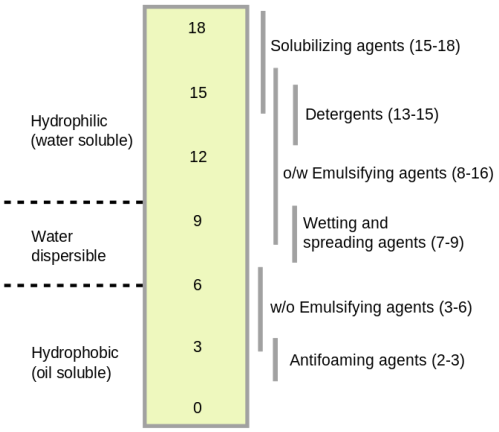

Figure 1.7 –A scale showing a range of HLB numbers and the subsequent type of surfactant represented by the number.[21]

HLB is an established theory, although it is important to note one reported exception. It was reported by Shinoda *et al*. that the HLB does not correlate in all cases, specifically at elevated temperatures. This group observed an effect known as 'phase inversion temperature' where an increased temperature caused dehydration of the hydrophilic end of a non-ionic poly(ethoxylated) surfactant.[22] This caused the formerly o/w emulsion to preferentially form a w/o emulsion. This concept is of slight concern with respect to curing of emulsion, or emulsion derived systems at high temperatures where the solubility of the respective ends of the surfactant can vary with temperature.[23]

1.2.1.2 Stability of emulsions

A brief distinction between macro and micro emulsions must be made. Macro emulsions (droplets > 0.1 μm) are not thermodynamically stable due to the increase in energy required to

increase the interfacial area of the system, but they are kinetically stable due to the surfactant assembling at the interface. Micro emulsions (droplets < 0.1 μm) conversely are thermodynamically stable, due to the normally large amounts of surfactant which reduces the interfacial tension. The scope of this thesis only covers the macro-emulsion stability.[24] The kinetic stability of macro emulsions means that they are liable to undergo destabilization related processes. These are flocculation, coalescence, creaming/sedimentation and Ostwald ripening.[18] Flocculation is small droplets coming together in a dilute emulsion to form larger droplets. Coalescence is the breaking of the interface between two nearby droplets which forms one larger droplet. Creaming or sedimentation is the aggregation of the emulsion due to density differences in the phases. The last and most significant in terms of the thesis is Ostwald ripening (Figure 1.8), which is where the dispersed phase is very slightly soluble in the continuous phase. This permits the diffusion of the dispersed phase across the continuous which leads to larger droplets growing in preference to smaller droplets. This leads to increases in average droplet size, which is satisfying thermodynamically due to decreasing the overall interfacial area.

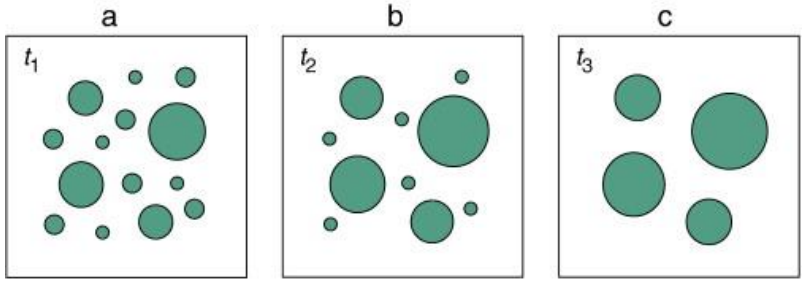

Figure 1.8 – A schematic of the Ostwald ripening process, where smaller droplets are lost in favour of larger droplets.[25]

Polymerisation of emulsions, such as through FRP, is a versatile and industrially proven synthetic route to polymer synthesis. Polymerisation of emulsions where the dispersed phase consists of monomers results in a latex which is a dispersion of polymer micro particles. The emulsion polymerisation process has some distinct advantages over bulk polymerisation. Some

of these advantages are that high M_w polymers can be achieved in faster reaction times than the bulk.[26] The viscosity of the system remains constant relative to a bulk which generally would increase in viscosity, and the continuous phase of an emulsion regulates the heat of the system exceeding well which is useful for preventing industrial accidents as may be seen by auto-acceleration due to the gel-effect in bulk.[27] Emulsion polymerisations are industrially critical and are used for the synthesis of paints, coatings and bulk polymers amongst many other applications.[28]

1.2.2 High internal phase emulsions

Based upon the internal phase volume ratio of the emulsion, the system can be classed as a low, medium or high internal phase emulsion. The classification requires the internal phase volume to be: less than 30 %, between 31 % and 74 %, and above 74 % of the total volume respectively. The internal phase can be calculated;[29]

$$Vol_{\%I} = \frac{V_i x\ 100}{(V_i + V_e)}$$

(Equation 1.3)

Where V_i is the volume of the internal phase and the V_e is the volume of the external phase. A high internal phase emulsion (HIPE) is classes as having an internal phase over 74 % of the total volume fraction of the mixture. The value of 74 % is important as it represents the most efficient packing possible for spheres in any unit cell.[30] As this value of 74 % is surpassed by introduction of increasing amounts of internal phase; the once discreet droplets of internal begin to come together and form polyhedra. High internal phase emulsions have been known for many years and are commonplace in food and cosmetic technology.[16]

1.2.3 Poly high internal phase emulsions

1.2.3.1 Introduction to pHIPEs

A poly high internal phase emulsion (pHIPE) is the name of a polymer morphology formed through the polymerisation of a high internal phase emulsion. Conventionally preparation

requires the dispersed phase to be added with mixing to a mixture of monomers and surfactant which form the continuous phase. Curing of the monomeric continuous phase of the HIPE emulsion leads to the formation of a porous, templated polymer monolith known as a pHIPE (polyHIPE) (Figure 1.9), as opposed to curing of a standard emulsion which forms a latex. The porosity is derived from 'windows' forming between the 'voids/pores' where the walls between the polyhedra are thinnest.[31] The formation of the windows is due to the shrinkage of the polymer continuous phase during curing (a common feature of polymerisation), which effectively rips holes in the thin walls between the droplets of internal phase. This mechanism has been shown by cryoSEM in styrene-DVB based systems and the formation of windows was shown to align with the gel point of the polymer network.[32]

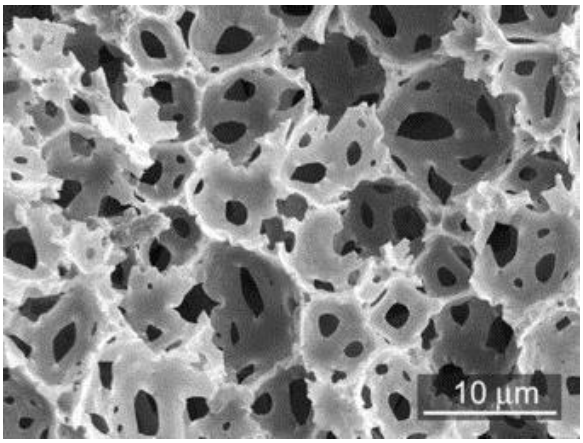

Figure 1.9 – An electron microscope image of a typical styrene-co-divinylbenzene pHIPE, clearly showing the large voids, connected by the smaller windows. Taken from reference.[33]

In some cases the surface area of these systems can be as high as 1200 m^2g^{-1}.[34] These structures have shown great promise in recent works, with some pHIPEs being able to; support active catalysts made of platinum nanoparticles in the pores, which could be cycled over 1500 times,[35] reversibly adsorb gasses such as CO_2,[36] and show exceedingly good swelling degrees, an example of which; a hydrogel which can absorb water to over Q = 300 (wt/wt).[37] Introducing a substance into the pores of these systems can be as easy as mixing the material into the internal phase before foam formation as shown in Figure 1.10).

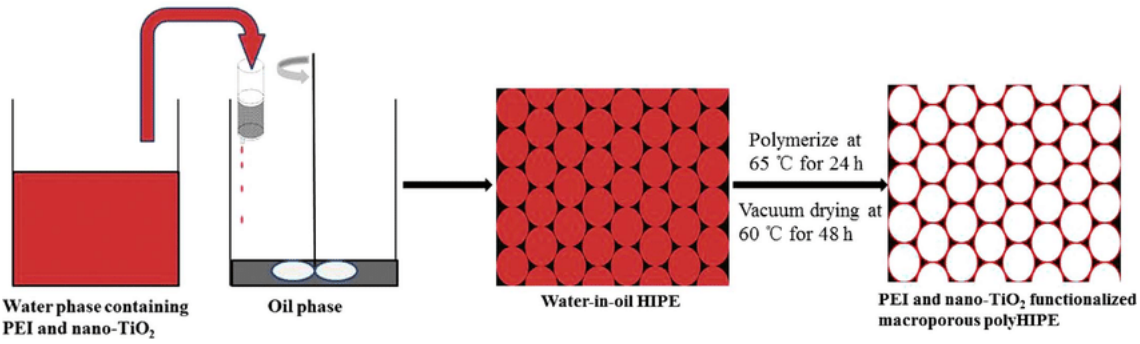

Figure 1.10 – A scheme taken from an article[38] which demonstrates the encapsulation of titania in the pores of a pHIPE by mixing the material into the foam's internal phase.

1.2.3.2 Surfactant and monomer choice

The large set of research presented in this area is to do with styrene based systems, most commonly, crosslinked with DVB. This is due to the fact that styrene is sufficiently hydrophobic for the w/o emulsion to be stable at high internal phase. The most common surfactants which are suitable for preparing the traditional w/o emulsions are non-ionic and have a HLB of between 3 and 6 which is suitable for the formation of water in oil emulsions.[39] An example of a common surfactant Span-80 is shown in Figure 1.11.

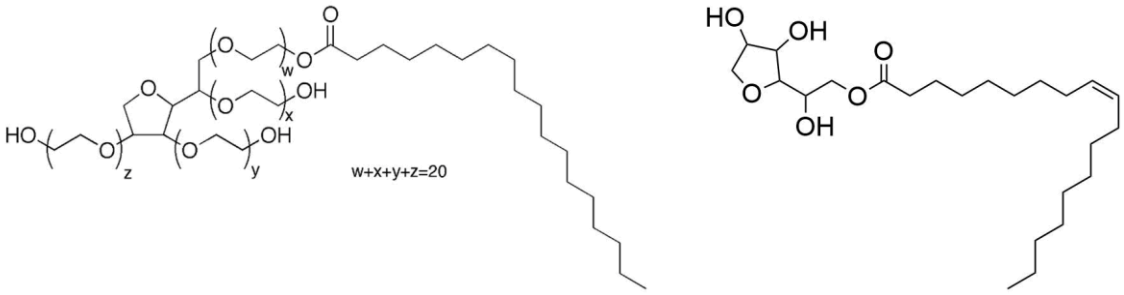

Figure 1.11 - Showing the structures of two common non-ionic surfactants for pHIPEs; Tween-40 (o/w, left) and Span-80 (w/o, right).

Whilst pHIPEs with other hydrophobic monomers have been produced (for example hexyl methacrylate amongst many others[40,41]), as soon as the monomer shows a certain level of hydrophilicity, the emulsion stability is reduced and destabilization can occur. For systems where the monomers are significantly hydrophilic, such as in poly(vinylalcohol) and poly(acrylamides), pHIPEs have be formed by using supercritical CO_2 as the internal phase, in

conjunction with the common surfactant 'tween 40'.[42,43] Normally the internal phase is aqueous; however non-aqueous systems have also been reported, but require strongly immiscible organic solvent pairs such as petroleum ether and DMSO, and a bespoke surfactant such as polyethylene oxide-block-polypropylene oxide.[44] The correct choice of monomer and surfactant in the preparation of a bespoke pHIPE is critical to prevent the splitting, or ripening of the emulsion either at the mixing stage, or later on in the curing stage at elevated temperatures.

1.2.3.3 Open or closed cell

The cellular nature of pHIPEs does not always have to be open-celled (with windows), it was shown early on that a styrene-DVB pHIPE consisting of only 5 % SPAN-80 surfactant and an internal phase fraction of 97 % lead to a closed cell pHIPE.[45] Originally it was believed that the windows are formed by the splitting of the thin walls during curing. This theory helped to develop the knowledge of how the interconnectivity can be modified. The knowledge was built upon to the point where it is now generally accepted that as the surfactant is increased, the walls between droplets become thinner, and therefore the propensity for the windows to form during shrinkage of the curing polymer is increased. The elasticity of the polymer is also important however and this is demonstrated in Figure 1.12 where an increasing amount of shrinkage during curing of methyl acrylate / styrene based pHIPEs showed pore variation from closed to open cell due to the increased shrinkage of the curing system with increase methyl acrylate content.[46] A paper in 2006 proposed that the theory of window formation through shrinkage was partially incorrect and invited discussion about how the window formation could actually be due to processed involved after the curing, such as through drying. The justification for this was that the previous works required sublimation of the internal phase out of the network before cryo-SEM study which meant the pore formation could have actually occurred prior to the SEM analysis.[47] To this date, the exact mechanism of the window formation is still not firmly agreed upon.

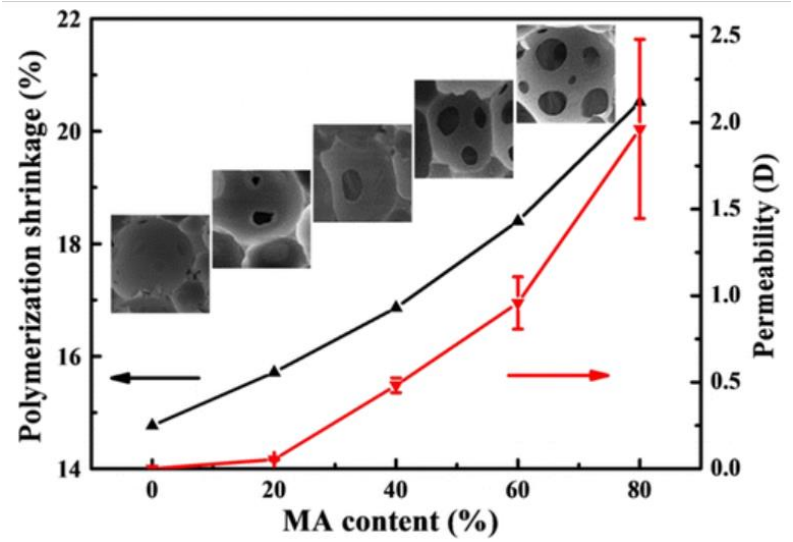

Figure 1.12 – A diagram showing how an increase in methyl acrylate monomer relative to styrene and DVB causes increasing shrinkage during curing of the resulting polymer and how this increased shrinkage changes the pores from closed to open-celled.[46]

1.2.3.4 Pore sizes in pHIPEs

A very large amount of the data for the pore size variation in styrene based pHIPEs was gathered by Williams et al.[48] They found that pore sizes can be controlled through nearly every variable in the polymerisation process. They found that varying the crosslinking content in a DVB : styrene pHIPE, the pore size was reduced from 15 µm with 100 % styrene, to 5 µm in the 100 % DVB polymer. This was due to the increased hydrophobicity of the DVB reducing the propensity for Ostwald ripening. The effect of electrolyte concentration on the pore size was also investigated in the same paper where the addition of K_2SO_4 to the aqueous phase up from 0 to 10 g/L was seen to result in the reduction of pore size from 50 µm to 5 µm. This was due to the increased emulsion stability, where the electrolyte prevented Ostwald ripening from occurring. Similar effects have also been shown to support this theory with aqueous solutions containing NaCl, $CaCl_2$ and Na_2SO_4.[49]

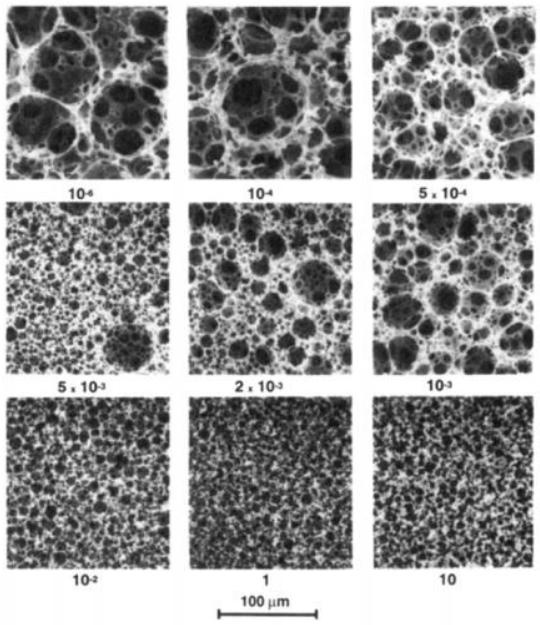

Figure 1.13 – The effect of pore size on a styrene/DVB pHIPE with increasing content of K_2SO_4 in the aqueous internal phase. The numbers represent the mass of salt per litre of water. Picture is taken from Williams *et al*.

The monomer choice and the relative hydrophobicity (just as with the stability of non-HIPE emulsions) play a large part in the pore sizes. This has been shown with vinylbenzyl chloride (VBC) as a co-monomer to styrene, crosslinked with DVB, where the pore sizes were shown to decrease dramatically with increasing VBC content up to 30 %. This was theorised to have occurred due to the VBC aggregating at the interface of the emulsion, acting as a co-surfactant and therefore increasing the emulsion stability and reducing the subsequent pore sizes.[50]

1.2.3.5 Porogens in pHIPEs

The final big influence on the porosity and structure of pHIPEs can be through the addition of a porogen to the continuous (external) phase. A porogen is an organic solvent which does not take a role in the polymerisation, but can affect the porosity of the pHIPE through the way it interacts with the polymer and the two phases. Three common porogens for styrene-DVB pHIPEs are chlorobenzene, toluene and chloromethyl benzene. These can increase the total surface area of the foam if they are able to swell the polymer matrix during curing. This has been shown to be correlated to the similarity of the solubility parameters of the porogen and

polymer where the better swelling solvents increase the surface area.[51] Porogens can also reduce the interfacial tension of the phases by acting as a co-surfactant, which reduces the cell size and increases the window size.[52] The influence of porogens on emulsions is a wide ranging topic[53], and as with all the other factors; specific to each system.

1.2.3.6 The form-factor of pHIPEs

Preparation of a pHIPE requires first the mixing of the HIPE foam, followed by curing, normally in an oven and finally removal of the internal phase. The circumstance that a pHIPE is a templated system means that the resulting polymer is always one single monolith which takes the form of the curing vessel. Recent advances however have seen these systems formed as membranes for cell culture[54] and electrochemical sensing,[55] as well as formed as discreet beads (Figure 1.14). One such example was the formation of poly(acrylamide) hydrogel beads, crosslinked with N,N-methylene bisacrylamide. These were formed through suspension polymerisation of a pre-mixed HIPE in an additional aqueous phase to form water in oil in water in oil system (o/w/o) where the HIPE droplets were subsequently cured.[56] The resulting beads could be dried very quickly and would have the porous nature of the pHIPE, as well as the much enlarged surface area from being formed as a bead when compared to a monolith. The beads produced by this method were then subsequently submerged in solutions of tetraethylorthosilicate and then the excess removed. The polymers were calcified which left an inorganic/organic composite bead.[57] Similar approaches for the preparation of pHIPE beads have also been carried out with thermally cured w/o/w emulsions such as the synthesis of VBC based networks, crosslinked with DVB.[58] The beads were modified by the addition of amines to the pendant chloride of the VBC after the formation of the beads.

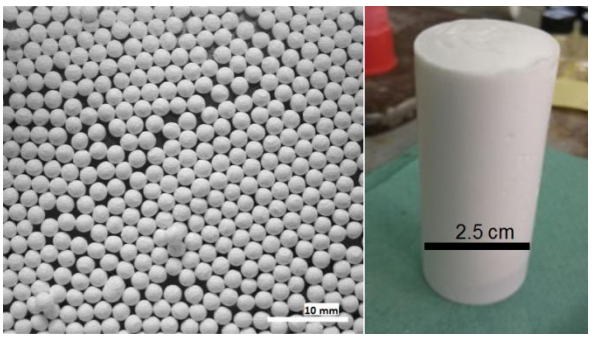

Figure 1.14 – A comparison of a standard pHIPE monolith, formed in a plastic cylinder (right), and pHIPE beads formed through a w/o/w suspension polymerisation (left).[59]

The same principles of pHIPE batch bead synthesis have been carried over to the field of microfluidics where monodisperse microbeads have been formed in fluidic cells.[60] Whilst these beads are mostly similar to those presented above, they can be formed in a continuous production and at much smaller diameters which represent progress toward industrialization of the technology. [61]

1.2.3.7 Post synthetic modification of pHIPEs

The potential for post synthetic modification of pHIPEs are wide-ranging. On a well-defined polymer with good mechanical strength, reactions can be carried out on the matrix after synthesis of the monolith in a very similar way to any other polymer. This capability provides new routes to porous functional materials. A map of a tiny portion of the huge array of modifications which have been carried out on styrene and methacrylate based polymers is shown in (Figure 1.15).

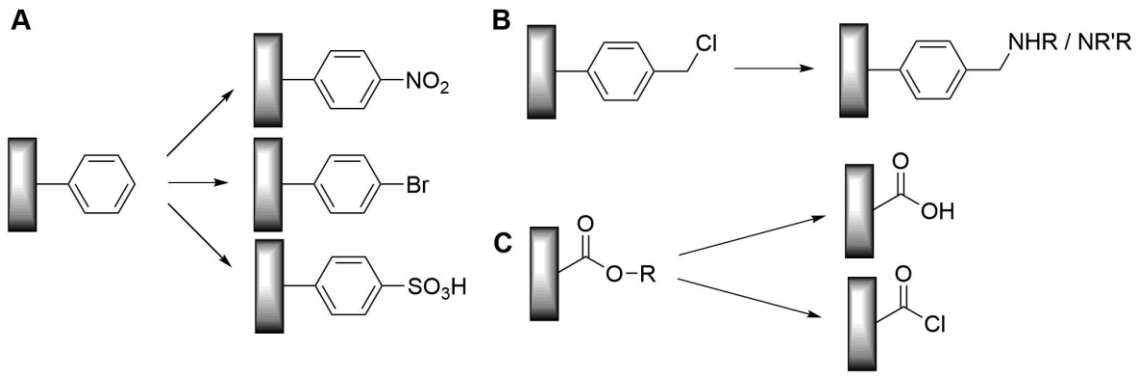

Figure 1.15 – Examples of possible modifications which have been carried out on pHIPEs. (A) Sulfonation, nitration and bromination of styrene,[62] (B) amination of a pendant VBC functionality[63] and (C) substitution of poly(methacrylates)[64] have all been shown to be successful on a pHIPE scaffold.

Increased rates of reaction should also be seen due to the increased porosity and reagent movement through the polymer compared to a traditional gel. In contrary to this, removal of the surfactant is usually necessary to stop side reactions occurring which increases the processing time requirement.[65] An alternative approach to the functionalisation was reported through the carbonization of a Styrene/DVB pHIPE. The pHIPE was formed, followed by hypercrosslinking through a friedel crafts mechanism. After pyrolysis of the hypercrosslinked pHIPE, an industrially competitive carbon foam remained which was easily formed with very high surface areas of 417 m^2g^{-1}.[66] As the research into suitable reactive monomers for preparation of pHIPEs expands, so does the options for polymer modification.

Aspects of all of the research mentioned in the above sections regarding pHIPEs are pertinent to this thesis. The versatility and ability the monoliths to be formed in various form factors, with controllable pore sizes and interconnectivity, the ability for alternative reactive monomers to be incorporated and utilized for post synthetic modification, as well as the ability for the structures to support materials in the pores are all aspects which would be ideal for the design of an absorbent decontamination system for chemical warfare agents. The final

important property of pHIPEs is that they are able to swell solvents into the matrix as well as encapsulate liquid in the pores which can lead to large swelling ability through void-expansion effects.[67] The literature on the use of pHIPEs as absorbents for bulk volumes of solvent is limited and so this feature is reviewed in more detail at the start of chapter 4.

1.3 Polymers as absorbent materials

1.3.1 History of absorbent polymers

Absorbent polymer systems, specifically covalent polymer networks with high swelling ability, are very common in everyday life, such as in nappies and supermarket spill kits. These products are based on the absorption of water, or mixtures of water with low levels of other components. Polymers which are crosslinked and are able to absorb water are formerly known as hydrogels. W. Kern was the first to report a water absorbing system comprised of crosslinked poly(acrylic acid) in 1938. The distinct advantage of this polymer system over the traditional cellulose sorbents was that the liquid could not be removed by squeezing, and the swelling magnitude was also much larger. Further work on the properties and swelling theory of such materials continued into the 50's by Kuhn and Katchalsky, amongst others, and showed that by generating the salt form of the acids, the swelling could be increased to over Q = 200, much larger than a non-ionic network (Figure 1.16).[68,69]

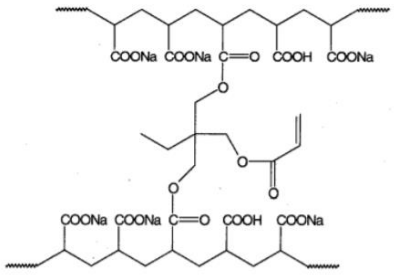

Figure 1.16 – An example of the structure of poly(acrylic acid) which has been crosslinked with a multi-functional acrylate based monomer and partially modified into the sodium salt to form a weak polyelectrolyte hydrogel.[70]

These ionic polymers were to be known as polyelectrolytes and one of the first patents describing the use of a polyelectrolyte hydrogel was ratified in 1966 for use in firefighting,[71] and thereafter the published works on hydrogels significantly increased in volume. The first medical use of hydrogels was then seen in the 1980s in Japan for the production of nappies and sanitary products.[72] There are significant amounts of work still occurring around hydrogels, especially for more specialized applications.[73] The swelling ability of water in hydrogels can easily exceed Q = 800 in weakly crosslinked electrolytic poly(acrylamide/acrylate) systems,[74] and products have been developed which are responsive to various stimuli for medical purposes, including magnetic field[75] and light irradiation.[76] Some recent reviews discuss the plethora of advances across many fields in hydrogel systems generally,[77] specifically for green chemistry,[78] and for biomedical and applied uses.[79]

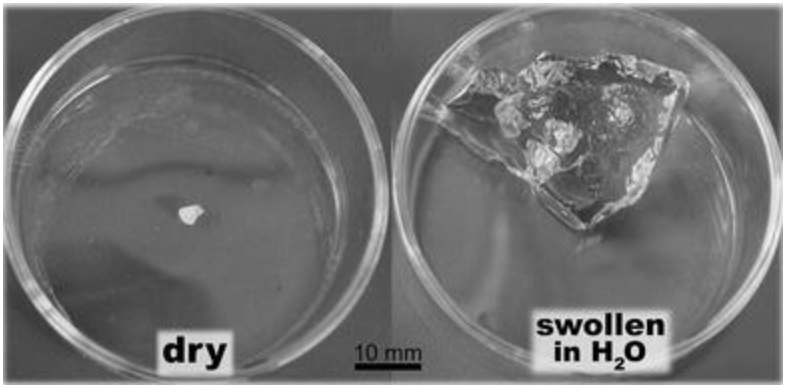

Figure 1.17 – A graphical representation of the volume increase of a polymeric hydrogel which has been swollen in 870 times its own mass of water.[80]

1.3.2 Absorbents for organic materials

Early superabsorbent polymers which were designed for water absorption could absorb water in massive excesses due to them exploiting increased osmotic pressure due to the higher free ion content in the polyelectrolyte hydrogel matrix. The theory behind the swelling related osmotic pressure gained from free ions is explained further in section 1.3.3. Since the early hydrogels, there has been lots of interest in the design of polymers with the ability to absorb organic solvents to the same, huge swelling degrees. However unlike water, organic solvents

cover a range of physical properties and compatibilities which make the design of sorbents more bespoke.

1.3.2.1 Low polarity organics

Low polarity organic solvents and oils have been a specific target for polymeric absorbent design; one specific reason for this is for the cleaning up of spills of crude oil. Initial work with the absorption of low polarity organics into polymer networks looked at simple crosslinked polymer systems. An example of this is work by Errede *et al*. which focused on styrene/DVB networks and examined the sorption of binary mixtures of toluene and other solvents by these polymer networks. They showed how the polarity of the co-solvent and crosslinking affected the swelling of the polymer. The swelling in these systems was low, and never exceeded Q = 5 The swelling was also reduced further when the co-solvent was slightly polar due to the incompatibility with the polymer matrix.[81] One approach to the encapsulation of low polarity solvents from Kiatkamjornwong *et al*. built upon the previous earlier work, and created styrene/DVB porous beads with a diameter of around 0.5 mm through seeded suspension polymerisation. The resulting beads were able to reach a maximum swelling of Q = 12.9 in 90 minutes exposure to toluene.[82] A paper presented by Morcellet *et al*. synthesised similar porous hydrophobic styrene/DVB/vinyl aniline networks with an affinity for the absorption of benzene and benzene derivatives however they only achieved swelling values only around Q = 5. Shan *et al*. also utilized a suspension polymerisation to form resin of styrene and butadiene with DVB crosslinking. The maximum swelling did not exceed Q = 17.5 in benzene.[83] A more recent and advanced approach by Zhao *et al*. was to graft *t*-butyl styrene and DVB onto an ethylene-propylene-diene elastomer (polymer with both viscoelasticity and a sub-room-temperature T_g) backbone, where the swelling of 10 % crude oil in toluene was seen to exceed Q = 80 in a very slow swelling polymer, and Q = 50 in the faster swelling version. This was a significant advancement through better polymer design.[84] Another more recent advancement was presented in a very thorough paper by Ceylan *et al*. who crosslinked butyl rubber to form an elastomeric absorbent. The polymer showed very good swelling capability in crude oil (Q =

20), diesel (Q = 20), gasoline and toluene (Q = 15).[85] A paper published in 2016 reported a novel 1-decene / DVB elastomer of varying form factors, which exhibited a crude oil absorption capacity of Q = 26, and toluene and diesel swelling of Q = 30.

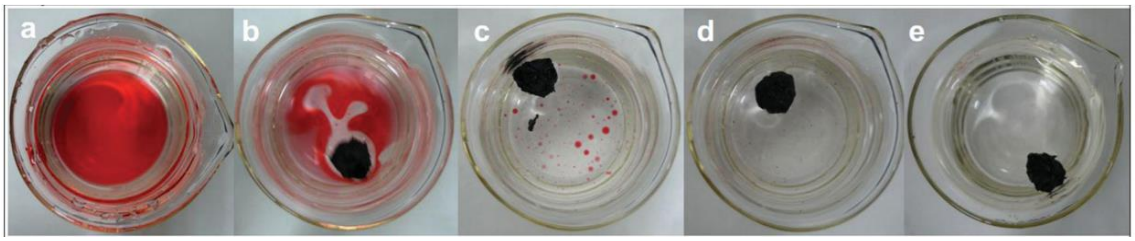

Figure 1.18 – A schematic from reference[86] showing the absorption of dyed dodecane from the surface of artificial seawater using a spongy graphene absorbent.

Figure 1.18 shows a diagram taken from a paper by Ruoff *et al.* which demonstrates success in one of the main targets from the previously mentioned works. Specifically the ability of the sorbent to take in oil selectively from the surface of water is clearly shown. The paper contrasts the work with polymer sorbents as they were able to absorb Q = 16 of dodecane using a spongy graphene material.[86] A range of techniques, including green approaches to the challenge of oil absorption were presented well in a recently published review.[87] One trend observed through all the research presented was that the authors were designing their systems to be as compatible with the oils as possible to increase the degrees of intermolecular attraction between the network and the solvent.

1.3.2.2 Polyelectrolytes for organic solvents

Whilst many groups looked at only the compatibility of the polymer for oil absorption, a big jump in knowledge for organic solvent absorption came from exploiting the same osmotic effects which were observed in hydrogel polyelectrolytes. This area of research was initiated with a paper published in 2007 by the group of Sada *et al*.[88] who acknowledged that polyelectrolytes were imperative for being able to observe high swelling especially in polar solvents. His work followed on from previous reports which had attempted to swell organic solvents in other polyelectrolytes and these would collapse in organic solvents and show no

swelling. Two of these previous works were on partially quaternised 4-vinylpyrdine[89] and poly(allylamine)[90] polyelectrolytes and both showed significantly decreasing swelling capacity as the amount of organic solvent such as acetonitrile or ethanol was mixed with the water which swelled well. The proposal by Sada was that through radical polymerisation of a stearyl methacrylate chain, crosslinked with 1 mol% ethylene glycol dimethacrylate, as well as an alkyl quaternary ammonium monomer and a weakly coordinating anion 'BARF' (Figure 1.19), they could form a lipophilic/hydrophobic polyelectrolyte network which would not collapse in organic solvents. They did observe hugely increased swelling in the polyelectrolyte gel across some solvents for example THF of Q = 23 to Q = 122 and chloroform from Q = 49 to Q = 99 in this system. Some non-polar solvents however decreased in swelling for example hexane Q = 25 to Q = 24.

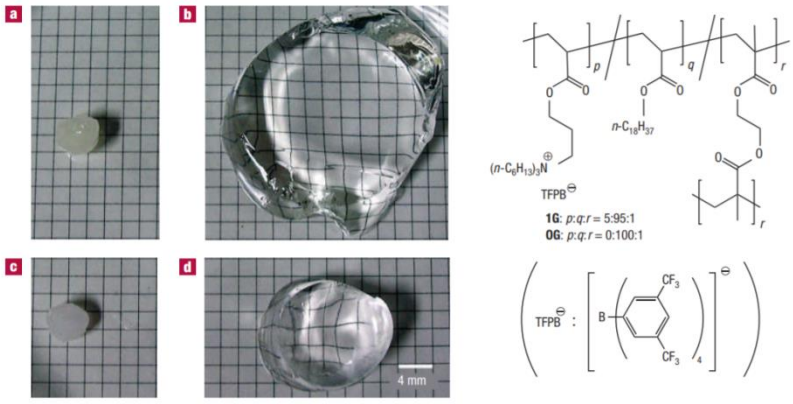

Figure 1.19 – Picture taken from reference[88] which shows the swelling of THF in (b) polyelectrolyte and (d) nonelectrolyte gel against the starting dry gels (a and c), as well as the polymers scheme and the BARF anion.

The group led by Sada continued to develop polyelectrolyte lipophilic gels for organic solvent encapsulation, specifically focused at absorbing non-polar media.[91] They modified the alkyl chain length of the acrylate monomer and the quantity of the ionic moiety to try to improve the non-polar solvent absorption.[92] They also looked at applying the same principles to a styrene based system with a bespoke styrene based quaternary ammonium monomer and noted how the swelling could be achieved even at low temperature.[93] Both of these reports

and the claims they made regarding the correlation of swelling to various physical properties are explained in more detail in the introductions for chapter 2 and 3. The group further investigated some binary mixtures of methanol with chloroform, toluene and THF in the same polyelectrolyte system as first mentioned, where they observed non-continuous swelling behaviour due to the solubility differences of the contrasting solvents.[94] More recent work by the group looked at incorporating mesogenic liquid crystalline co-monomers to the system to increase the swelling, again with the same quaternary ammonium BARF monomer which they claim was crucial to the increased swelling of solvents such as DMSO from Q = 5 to Q > 200.[95] A review was published by Sada in 2017 which covered the majority of the work carried out in his group utilizing the polyelectrolytes, and it is important to note that the true non-polar solvents (hexane, dodecane) struggled to swell any of the gels presented.[96] Since the work of Sada, other groups have taken inspiration for polyelectrolytes designed for the absorption of solvents of varying nature.

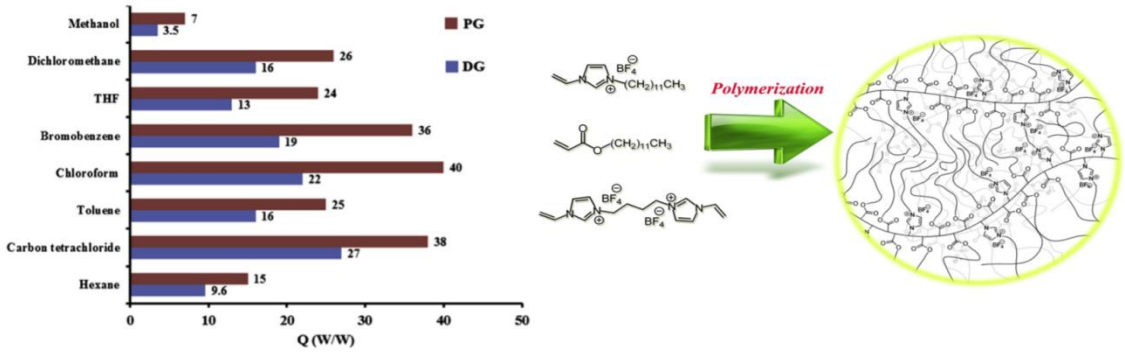

Figure 1.20 – Pictures taken from reference showing (left) the swelling of low polarity solvents in a non-ionic gel (DG) and polyelectrolyte (PG), and (right) the monomers used.[97]

Figure 1.20 shows how the swelling of low polarity solvents such as hexane in addition to the more polar solvents was increased by introducing an electrolyte group based upon alkyl imidazolium ionic liquid monomers at 1 % of the total monomers. The report however did not observe as large increases in swelling from introducing the polyelectrolyte as what was published by Sada.[97] This represents a part of a recent body of work which stemmed from

Sada's on poly electrolytes for organic solvent absorption. Some of the other works on absorbent polyelectrolytes include: the synthesis of absorbent gel beads from imidazolium ionic liquid monomers in suspension polymerisation for catalytic application[98] and absorbents which can switch between swelling organic solvents and water based upon a reversible amino-acid electrolytic group.[99] The importance of introducing ionic groups into polymer absorbents to increase the osmotic pressure inside the system, which causes increased swelling to be observed over non-ionic networks, especially in polar solvents and hydrogels is clear.[100]

1.3.3 Absorption theory

1.3.3.1 Osmotic pressure and elasticity

Models of absorption into a polymer matrix are based upon the features of solvation of the polymer chains. In a non-ionic polymer network in equilibrium it is understood that swelling is driven by the osmotic pressure of the system. The equilibrium swelling of a system is said to be achieved when there is no residual osmotic pressure (Π_s); or when the osmotic potentials inside and outside (μ_s^{in} and μ_s^{out}) of a system of given volume v_s are equal; [101]

$$\Pi_s = 0 = \frac{\mu_s{}^{in} - \mu_s{}^{out}}{v_s}$$

(Equation 1.4)

The Flory-Rehner description of swelling explains that the osmotic pressure in a non-ionic system arises from the increase in entropy gained through the mixing of the polymer and solvent, along with the reduction in total chain conformations which occurs through the expansion of the weakly cross-linked polymer.[102]

$$\Delta F = \Delta F_{mix} + \Delta F_{el}$$

(Equation 1.5)

Where ΔF_{mix} is the energy change due to solvent-polymer interactions, ΔF_{el} describes the free energy change due to elastic response of the polymer. As a network swells its osmotic pressure decreases due to the decrease in polymer concentration, whilst its elastic modulus increases

due to conformational changes in the polymer strands leading to increasing resistance to stress. Thus a polymer gel takes in solvent and swells until the elastic modulus of the gel matches the osmotic pressure of the polymer-solvent system

In a polyelectrolyte gel solvent system, the osmotic pressure arising from the increase in entropy due to the polymer-solvent interactions still contributes to the equilibrium swelling, but the osmotic pressure arising from the increase in entropies of the free ions is far more significant to the total osmotic pressure. Thus the change in free energy in the system can be summarised as a combination of 3 factors;

$$\Delta F = \Delta F_{mix} + \Delta F_{el} + \Delta F_{ion}$$

(Equation 1.6)

Where the new term ΔF_{ion} is the free energy change resulting from the dissociated ions in solution. When there are no added salts in the absorbed solvent, this latter contribution results from the ionic content of polymer network only. Thus in the absence of any dissociated ions the equation devolves to that describing a non-ionic polymer network. The osmotic pressure of a polyelectrolyte gel-solvent system, such as a sodium poly(acrylate) network for example, can be described as follows;

$$\pi = \pi_{mix} + \pi_{el} + \pi_{ion}$$

(Equation 1.7)

Where π_{el} is the elastic osmotic potential and π_{ion} is the osmotic potential from ion/solvent interaction, the equilibrium point would be satisfied when $\pi = 0$. The osmotic pressure resulting from dissociated counter-anions in polyelectrolyte networks is generally substantially larger than that of polymer-solvent mixing ($\pi_{mix} << \pi_{ion}$). Consequently, the swelling for electrolyte systems would be up to several degrees of magnitude larger than for the simple non-ionic/ ionomer systems do to the increased osmotic pressure. This basically shows that

osmotic pressure in polyelectrolytes from dissociation of the ion pairs is the largest driving factor for superabsorbent swelling.

1.3.3.2 Crosslinking and swelling

The crosslinking of a polymer network will directly affect its ability to swell a given solvent. It is generally accepted that the lower the crosslinking density the more mobile the polymer chains and therefore the higher the swelling ability.[103] As crosslinking increases the modulus of the network increases[104] and therefore the osmotic elastic potential (π_{el}) is decreased. This in turn decreases the total osmotic pressure π of the system, which reduces the swelling degree in both non-ionic networks ($\pi_{mix} + \pi_{el}$) and ionic ($\pi_{mix} + \pi_{el} + \pi_{ion}$) networks. This theory is supported by numerous works which have looked at the effect of swelling on crosslinking[105,106] and means that the design of effective absorbent polymer networks with high swelling capacity requires crosslinking to be low.

1.4 Compatibility of the solvent and polymer - solubility parameters

1.4.1 Hildebrand solubility parameters

One of the earliest lessons taught to prospective chemists and physical scientists when talking about solvation is that 'like dissolves like.' This principle was the basis for work which has been done on classifications which are known as solubility parameters; an area of physical chemistry which aims to de-trivialise understanding of molecular interaction. Solvent parameters expanded upon the theories of what makes certain molecules 'alike'.

One of the first mentions of a solubility parameter in the modern sense was in 1936 in the PhD. thesis of Hildebrand where he proposed the first definition of a 'solubility parameter'. The purpose of his work was to develop a system whereby the miscibility of solvents (other materials) could be explained mathematically. The Hildebrand solubility parameter (δ) is also

referred to in literature as a cohesive energy parameter, due to its derivation as the square root of the cohesive energy of a system; the heat of vaporisation divided by the molar volume of the solvent:[107]

$$\delta = \frac{\Delta \mathrm{H_v} - RT}{V_m}$$

(Equation 1.8)

The cohesive energy parameter is simply no more than the expression of the total van der waals force of a molecule. Whilst this solubility parameter can be utilized to a good degree in simple non-polar systems, the lack of a specific term for polarity, dielectric or hydrogen bonding of the molecule was the major limitation in this parameter. An example of this limitation is that poly(styrene) has a Hildebrand parameter of 9.13 $cal^{1/2}cm^{-3/2}$, and chloroform and ethyl acetate have values of 9.21 $cal^{1/2}cm^{-3/2}$ and 9.10 $cal^{1/2}cm^{-3/2}$ respectively.[108] These values would suggest that poly(styrene) is highly soluble in both these solvents due to the fact they are very closely matched, however in reality; chloroform is the only one of the two solvents to interact with polystyrene well.

1.4.2 Hansen solubility parameters

Hansen solubility parameters (HSPs) were established in 1967 by Hansen as his attempt to further predict the relative miscibility of two components of a mixture. The model was originally designed to forecast the solubility of a solid in a liquid, similarly to Hildebrand. However, the Hansen model improves over the Hildebrand as it takes into account the polarity and the hydrogen bonding potential of the molecules, making it a three-component parameter; allowing the HPSs to be very useful in more complex applications where polarity is significant.[109]

1.4.2.1 Development of HSPs

The first assumption was that the cohesive energy of the system is equal to the sum of the components which affect the thermodynamic properties; the dispersive forces, the polar forces and the hydrogen bonding forces;

$$E = E_d + E_p + E_h$$

(Equation 1.9)

This assumption is what gave rise to the now commonly known 'total Hansen parameter' value;

$$\delta\mathrm{tot} = \sqrt{\delta\mathrm{d}^2 + \delta\mathrm{p}^2 + \delta\mathrm{h}^2}$$

(Equation 1.10)

Hansen used various methods to calculate each of the terms in the equation for dispersion, dipole, and hydrogen bonding. The original works looked at the calculation of parameters through experimental data gathered for 90 liquids and 32 polymer systems,[110] with the non-polar contribution (δd) being gathered from procedures presented by Blanks and Prausnitz, which is still used currently, and is similar to the work of Hildebrand.[111] The polar contribution (δp) was developed firstly by Hansen and Skaarup with a calculation based upon the dielectric, dipole, refractive index and molar volume of the compound.[112] Finding all of these terms is usually difficult and so the most popular method for calculating δp is now carried out using the equation;[113]

$$\delta\mathrm{p} = \frac{37.4\,(DM)}{V^{0.5}}$$

(Equation 1.11)

Where DM is the dipole moment and V is the molar volume of the compound. For the purposes of deciphering the hydrogen bonding component (δh), this is done by subtracting the polar and dispersive components from the total energy which is gathered experimentally. It is

claimed that using group contribution data for the hydrogen bonding data is more than sufficient in most cases for when the polar, dispersive and total energies are not known.

1.4.2.2 Ra

A set of HSPs (non-polar (δd), polar (δp), and hydrogen bonding (δh)) from each of two materials, such as a polymer and solvent, can be compared mathematically to give a difference; known as the Ra. The Ra is a measure of how similar the solubility parameters of the two components are. When Ra = 0, the components would be the most ideally compatible (having exactly the same HSPs), with less compatibility as the value increases. Ra is useful for showing how alike two components are with a single number.

$$Ra = \sqrt{4\left(\delta\mathrm{d}_{\mathrm{poly}} - \delta\mathrm{d}_{\mathrm{solv}}\right)^2 + \left(\delta\mathrm{p}_{\mathrm{poly}} - \delta\mathrm{p}_{\mathrm{solv}}\right)^2 + \left(\delta\mathrm{h}_{\mathrm{poly}} - \delta\mathrm{h}_{\mathrm{solv}}\right)^2}$$

(Equation 1.12)

The HSP system is used widely as a powerful tool for determining the mixing potential of various systems, from the sorption of dyes onto biodegradable polymers,[114] to the selection of appropriate excipients for the improvement of drug delivery in poorly soluble medicines.[115] Hansen quotes in his handbook that there are still many limitations to his solubility parameter, regardless of the improvements made over previous parameters. He mentions that some properties might overwhelm the parameter, specifically volume and size effects; therefore methanol and other highly polar molecules may not fit certain systems.[116] For this project, HSPs would be used to help explain the various swelling behaviours of several solvents and chemical warfare agents in the polymer sorbents which were to be designed and synthesised.

1.5 Introduction to chemical warfare agents

1.5.1 General categories of CWAs

Chemical warfare agents (CWAs) are a group of chemicals which have the propensity to be used in warfare due to their extremely high toxicity and irritancy. There are many different categories of CWA, in which there are many individually identifiable chemicals. Some of the

most common agents fit into the categories of; nerve agents and blister agents/vesicants, amongst others. Each category of agent is defined around the biochemical action which the molecule takes upon a body. The nerve agent series of chemicals contains those which act upon the nervous system. Blister agents damage cells' DNA causing irreversible damage to tissue. Two large groups which fall into the nerve agent category are the 'V' and 'G' series of agents, some examples of which include sarin (GB) and VX, respectively. The large group of compounds into which blister agents fall, is that of the mustards; including sulfur mustard (HD), or mustard gas (Figure 1.21). There are many more categories of agent, and many more compounds for each class, however the V, G and mustards are some of the most commonly used, both historically and presently.[117]

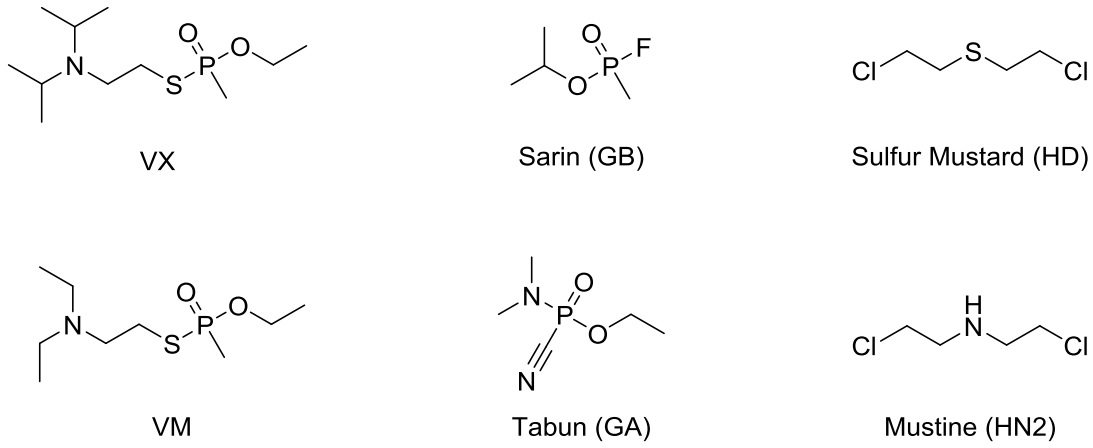

Figure 1.21 – The structures of many of the common known CWAs. VX and VM represent the V-series, GB and GA represents the G-series and HD and Mustine represent the mustards.

1.5.2 Nerve agent mechanism of action

Nerve agents are generally known as acetylcholinesterase (AChE) inhibitors, this means they inhibit the ability of the body to break down and remove acetylcholine. This is particularly important because acetylcholine is a neurotransmitter which is found throughout the body and is used primarily to signal muscles to contract. When the nerve agents inhibit AChE, the acetylcholine is not removed from the muscle's receptors, causing it to remain in a state of contraction, which eventually fatigues and paralyses it. The common symptoms of a nerve

agent poisoning are; fitting, respiratory depression, and in many cases death.[118] The lethal dose for an agent such as sarin (GB) varies; but has been reported to be as low as 0.3 g skin contact for an average male. VX on the other hand is even more toxic with a lethal dose by skin contact averaging around 0.01 g, which is less than a small drop.[119] The incredible action of these nerve agents is derived from their ability to covalently bond with a pendant hydroxyl of a serine molecule in the AChE, deactivating the enzyme (Figure 1.22).[120,121]

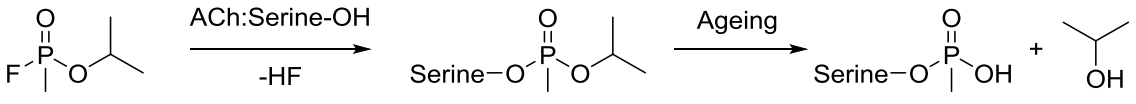

Figure 1.22 –The mechanism of action of nerve agents (sarin) on acetylcholine esterase. The second step where further hydrolysis occurs is sometimes referred to as ageing, where the receptor is irreversibly inhibited.

1.5.3 Mustard mechanism of action

Common blister agents, sulfur mustard (HD) and mustine (HN2), work by damaging DNA on a cellular level. The molecule infiltrates the cells of any contact surface, whether that is the lungs on inhalation, retinas, or skin contact and damages the cells by alkylating the guanine units of the DNA. The mustards eliminate a terminal chlorine to form a highly reactive sulfonium or nitrogen cation which goes on to react with the guanine (Figure 1.23).[122]

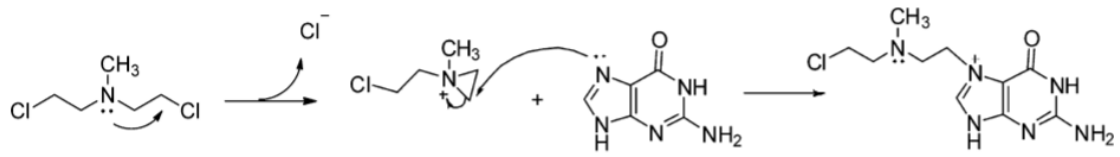

Figure 1.23 – A scheme depicting the mechanism for the alkylation of a guanine unit by a nitrogen mustard (mustine) molecule. This reaction mechanism is the stereotypical route of reaction for all mustards.

In the long term this leads to the inability of the cells to function, leading to death of many of these cells, which causes the characteristic blistering and irreparable damage to certain organs such as the eyes and respiratory system. In most cases, exposure to mustards is an acute problem, however in severe cases the exposure can also lead to death through infection, respiratory arrest, or other secondary illness.

1.5.4 Chemical warfare agent absorbents and decontaminants

1.5.4.1 Absorption/encapsulation of CWAs

Just as the reactivity of the three agent species varies because of the functional groups, so does the physical properties. For the absorption of bulk volumes of agent, by any method polymeric or otherwise, there is simply very little research. The operationally advised method to collect spills has been by use of natural materials such as vermiculite, pearlite, wood shavings or sand, which are subsequently destroyed by burning[123] and alternatives are not presented in any of the large reviews.[124,117] One report by Sullivan *et al*. presented inorganic/organic hybrid polyoxometalate systems which would act as a gelator when exposed to polar aprotic solvents. This group used a simulant in place of the true agent which would mimic the physical and chemical properties of the CWA whilst reducing user risk during the research. They were able to hydrolyse a common simulant dimethyl methyl phosphonate (DMMP) and absorb it through gelation. They achieved a Q = 9.6 in the simulant DMMP but were unable to report the effectiveness of their system on other agents or simulants.[125] Other work with gelators demonstrated how the introduction of DMMP to a urea based gel could strengthen the gels.[126] Additionally, an oximate containing organogel was used to gelate and then break down the simulant diethylchlorophosphate (DCP) with an observable color change.[127] In both these systems however, the simulant is only a small proportion (<20 %) of the liquid used in the gelation which means they are not designed for bulk scale encapsulation of agent. One area of work which is available in this area presented a viable sorbent through the formation of a hypercrosslinked network (HCN) by Wilson *et al*. [128] A relatively facile

synthesis, HCNs can be produced with a huge variety of substituents and crosslinking densities (Figure 1.24). This synthesis provided a polymeric system with an absorption capability in; VX of Q = 12, Sarin Q = 21 and HD Q = 19.

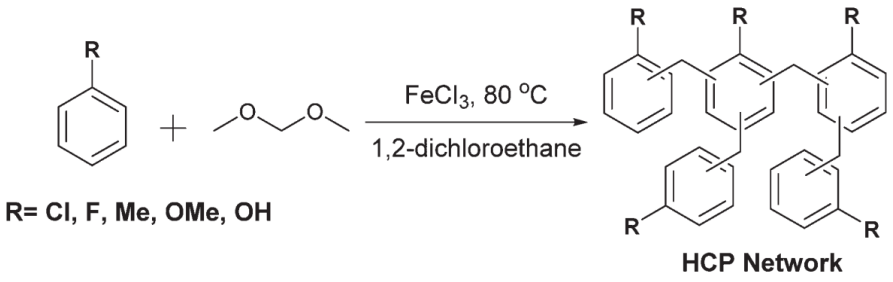

Figure 1.24 – The synthetic procedure for the creation of a hyper-cross-linked network, cross-linked with the Friedel-Crafts addition of the formaldehyde dimethyl acetal. Taken from reference.[128]

These capacities were significant and represented the first true 'all-agents-in-one' polymeric CWA sorbent. Many routes to decontamination of CWAs mentioned in the following section reply on the adsorption of the agents onto the material, such as in activated charcoal filters[129] and amorphous silica,[130] however this is not true absorption, and none of the articles are seen to quote a swelling value of any kind. In reports where sensing of CWAs is carried out, similar trends are observed. Specifically where the adsorption of agents was monitored, but absorption into a substance for encapsulation was not.[131,132] The lack of development into the bulk absorption of chemical warfare agents was one of the motivators for the work in this thesis.

1.5.4.2 Functional decontamination of CWAs

The approach to decontamination of nerve agents in most cases is the liberal application of strong bases. Hydrolysis of the P-O bonds in the G-agents, and P-S bonds in the V-agents by aqueous strong bases has been the longstanding recommended route for decontamination. Oxidation of the sulphur in HD by the application of strong bleach is the most common approach to decontamination of mustard agents.[133]

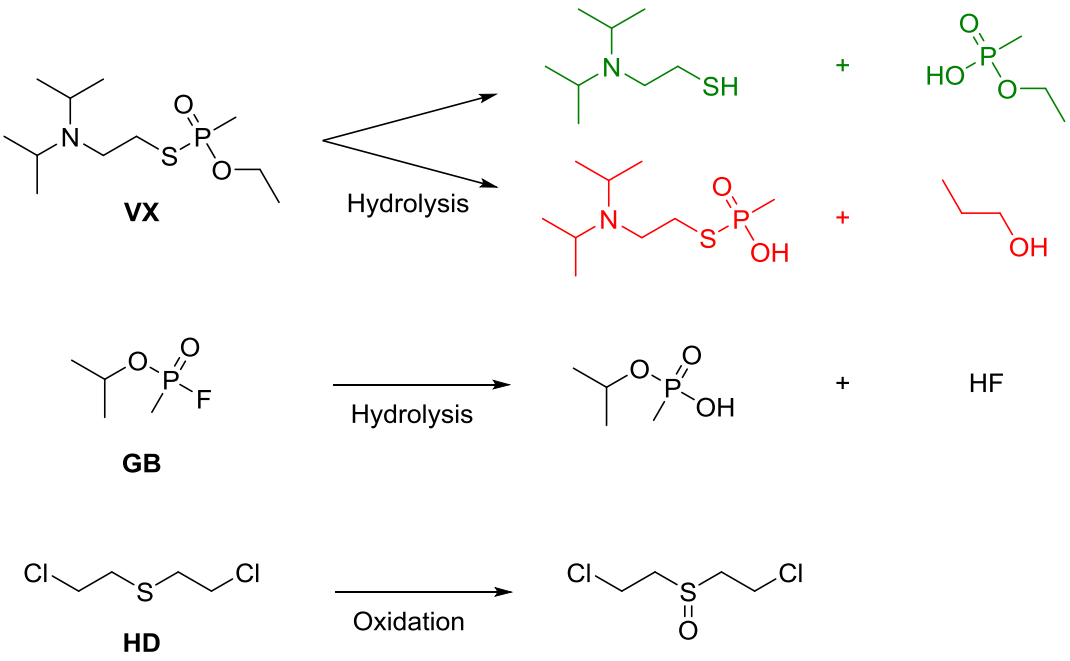

Figure 1.25 – The decontamination routes for VX, GB and HD. The hydrolysis routes for VX can occur mostly at the P-S bond, but also at the P-O bond in more basic environments. GB hydrolyses to form HF but can also hydrolyse over the P-O bond in very strong bases, leaving 2-propanol. Oxidation of HD leaves the sulfoxide which prevents the production of the reactive sulfonium ion.

The go-to chemical for most decontamination efforts was bleach, however due to its low shelf life, less than ideal conversion ratio and corrosive nature to many surfaces, this was superseded in 1960 by 'decontamination solution 2 (DS2)'. This solution was the mixture of around 70 % diethylenetriamine, 28 % ethylene glycol monomethyl ether and 2 % sodium hydroxide. This non-aqueous solution reacted instantly with VX, GB and HD and had long shelf life, making it the industry standard surface decontamination approach for military forces. In terms of personnel decontamination; a different personal decontamination kit (PDK) was developed which was not so harmful to the skin, based upon 72 % ethanol, 10 % phenol, 5 % sodium hydroxide, 12 % water and <1 % ammonia.[134] Whilst these official products are available, the application of various basic household chemicals has also been shown to be

effective at decontamination for emergency situations, with mixtures of household ammonia and 3 % hydrogen peroxide decontaminating both GD and VX in 1 and 6 minutes.[135]

1.5.4.3 Catalytic degradation of CWAs

Where traditional decontamination routes are both effective and cheap, they are only useful for decontamination of surfaces where the agents have been deposited. Logistically it is difficult to transport huge quantities of decontamination equipment if bulk stockpiles of agent were to be found. The breakdown of bulk agents, specifically the highly persistent VX and HD, is what has led to the research into catalytic degradation systems. One such system uses a polymer matrix, swollen with water to degrade VX catalytically. They used polymer supported ammonium fluoride salts to form an ion exchange resin, which degraded VX with a half-life of less than 2 hours. The swelling of water into the polymer facilitated the hydrolysis significantly, however when large excesses of agent were added (6 eq.) the hydrolysis rate dropped significantly to 6 days.[136] Zirconium based metal-organic frameworks (MOFs) have also been shown to be effective at the buffered catalytic hydrolysis of V-agents. MOF-808,[137] Nu-1000,[138] and UiO-67-NH_2,[139] have all shown promise in this area, however they all shared the same feature which is that they required a buffered environment, commonly with N–ethyl morpholine, to allow the reaction to take place. It would be ideal for a system to not require an external liquid buffer for the hydrolysis of V agents. With respect to sulphur mustard (HD), MOFs have also shown promise for catalytic degradation. The photocatalytic degradation of 2-CEES (HD simulant) in porphyrin based MOFs is based upon the production of singlet oxygen which oxidizes the sulphur to the sulfoxide. Two reports from the same group have noted this effective route to the degradation of 2-chloroethylethyl sulfide (2-CEES) with a PCN-222/MOF-545 (zirconium) based system,[140,141] and a further report with Nu-1000 has also been made.[142] The importance of these systems is that the only consumable is oxygen which can be scavenged from air. In addition to work with MOFs, metal-oxides have also been trialled in various agents as a simple approach to degradation. Active forms of cerium oxide with lots of –OH surface functionalities have been synthesised in an attempt to produce sorbents which can

break down VX.[143] Nano tubular titanium oxide has also been synthesised and shown to hydrolyse VX and GB.[144] One of the largest issues with these approaches is the large ratio of 'catalyst' to substrate required. pHIPEs have also been used very recently in CWA sequestration. A poly(dicyclopentadiene) based pHIPE foam was oxidized and was then used to oxidize the VX simulant demeton-S. This polymer approach however was not catalytic, as the oxygen stored in the polymer was used to oxidise the simulant.[145] A final approach to mention was a recent paper in which presented supramolecular 1-3,diindolylureas and thioureas which would act as receptors for DCP and DCNP (VX simulants) and increased the hydrolysis rates by up to 45 % compared to systems without the receptors.[146]

1.5.5 Modern day usage of CWAs

Many of the chemical agents were developed in and around the two world wars, with widespread use of choking and blister agents such as phosgene and sulfur mustard in WW1. Despite this, there are still regular, and in some opinions; growing risks from the use of chemical warfare agents in this modern age.[147] G and V nerve agents are still used sporadically in and outside conflicts around the world. An example of such is the recent Syrian civil war where sarin was confirmed to have been used.[148] Estimates quote over 1400 died and over 3000 were injured from one such release in the capital of Damascus.[149] An example of chemical weapon use outside of a country ravaged by war was in the recent poisoning of British citizen Sergei Skripal and his daughter; using a newly disclosed nerve agent belonging to the Russian 'novichok' series (Figure 1.26). The clean-up of all the affected areas caused some locations to be off limits for over 8 weeks. Two further members of the public were then exposed fatally nearly 4 months later by the same agent in a nearby town.[150]

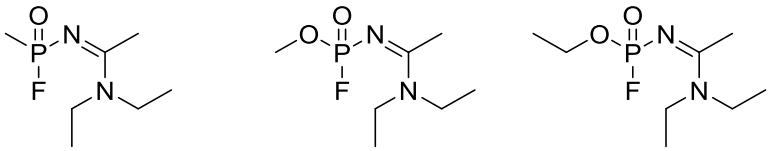

A-230 A-232 A-234

Figure 1.26 – Three agents of the 'novichok' series of nerve agents.

The relatively low reactivity, low vapour density and very high boiling points of V-agents and novichok agents mean that they are extremely persistent in the environment and the dangers they pose long after an initial attack is evidenced by these recent events. Stockpiles of agents and precursors are still found around the world and the biological damage they can do is huge. It is important to control the chemicals but in instances when they have already been used or are found ready for use, methods to neutralise them safely are of great importance.

1.6 Aims of the thesis

The primary aim of this thesis was to develop a polymeric system which has the ability to encapsulate a wide range of chemical warfare agents to very high swelling magnitudes (Q > 30, 3000wt %). The system developed would ideally comprise a variety of factors which would make its use truly practical in a real world scenario: low physical volume and high swelling capacity across a range of CWAs, economic viability, long shelf life, stability under harsh conditions, and the potential for inclusion of reactive/catalytic components into the matrix. With specific regard to inclusion of catalytic or reactive components; the polymer would ideally function not only as a sorbent, but also as a scaffold for the components required to permit the in-situ breakdown of the absorbed agents. By combining all these criteria in a single polymer, the final product would work as a viable self-contained immobilisation and decontamination system (a self-decontaminating material (SDM)). The capability of the system to be scaled up in its entirety is a condition which would then determine the viability of the polymer as a operationally capable product as opposed to a proof of concept, for this reason the polymer and catalyst production would be tested for its ease of synthesis and performance

on larger scales. The work would begin on determining an appropriate polymer composition, suitable for the encapsulation of the agents, followed by morphological modifications to the polymer, and finally incorporation of the catalyst system.

1.7 References

1 M. R. Buchmeiser and John Wiley & Sons., *Polymeric materials in organic synthesis and catalysis*, Wiley-VCH, 2003.

2 A. D. Jenkins, *Polym. Int.*, 1992, **28**, 95–95.

3 J. M. G. (John M. G. Cowie and V. (Valeria) Arrighi, *Polymers : chemistry and physics of modern materials.*, CRC Press, Scotland, 3rd edn., 2008.

4 H. R. Allcock and F. W. Lampe, *Contemporary polymer chemistry*, Prentice Hall, 1990.

5 J. M. G. (John M. G. Cowie, *Polymers: chemistry and physics of modern materials*, Blackie, 2nd edn., 1991.

6 R. J. (Robert J. Young and P. A. (Peter A. . Lovell, *Introduction to polymers*, Chapman & Hall, 1991.

7 J. M. G. (John M. G. Cowie and V. (Valeria) Arrighi, *Polymers : chemistry and physics of modern materials.*, CRC Press, 2008.

8 H.-G. Elias, *An introduction to polymer science*, VCH, 1997.

9 K. S. Anseth, C. M. Wang and C. N. Bowman, *Macromolecules*, 1994, **27**, 650–655.

10 in *IUPAC Compendium of Chemical Terminology*, IUPAC, Research Triagle Park, NC.

11 J. E. Mark, B. Erman and F. R. (Frederick R. Eirich, *Science and technology of rubber*, Elsevier Academic Press, 2005.

12 in *IUPAC Compendium of Chemical Terminology*, IUPAC, Research Triagle Park, NC.

13 H. Stutz, K.-H. Illers and J. Mertes, *J. Polym. Sci. Part B Polym. Phys.*, 1990, **28**, 1483–1498.

14 Y. Diamant, S. Welner and D. Katz, *Polymer (Guildf).*, 1970, **11**, 498–506.

15 H. D. Heinze, K. Schmieder, G. Schnell and K. A. Wolf, *Rubber Chem. Technol.*, 1962, **35**, 776–793.

16 K. J. Lissant, *Emulsions and emulsion technology. Pt. 1*, Dekker, 1974.

17 M. Yahaya Khan, Z. A. Abdul Karim, F. Y. Hagos, A. R. A. Aziz and I. M. Tan, *Sci. World J.*,

2014, **2014**, 1–15.

18 J. Sjöblom, *Emulsions and emulsion stability*, Taylor & Francis, 2006.

19 W. D. Bancroft, *J. Phys. Chem.*, 1914, **19**, 275–309.

20 W. C. Griffin, *J. Soc. Cosmet. Chem.*, 1949, **1**, 311–326.

21 M. Aulton, *Pharmaceutics : the science of dosage form design.*, Churchill Livingstone, Edinburgh, 2nd edn., 2002.

22 K. Shinoda and H. Saito, *J. Colloid Interface Sci.*, 1969, **30**, 258–263.

23 K. Shinoda and H. Sagitani, *J. Colloid Interface Sci.*, 1978, **64**, 68–71.

24 M. K. Sharma and D. O. Shah, 1985, pp. 1–18.

25 T. Werz, M. Baumann, U. Wolfram and C. E. Krill, *Mater. Charact.*, 2014, **90**, 185–195.

26 C. S. Chern, *Prog. Polym. Sci.*, 2006, **31**, 443–486.

27 G. G. Odian, *Principles of polymerization*, .

28 D. Urban and K. Takamura, Eds., *Polymer Dispersions and Their Industrial Applications*, Wiley-VCH Verlag GmbH & Co. KGaA, Weinheim, FRG, 2002.

29 N. R. Cameron and D. C. Sherrington, Springer, Berlin, Heidelberg, 1996, pp. 163–214.

30 N. R. Cameron, *Polymer (Guildf).*, 2005, **46**, 1439–1449.

31 M. S. Silverstein, *Prog. Polym. Sci.*, 2014, **39**, 199–234.

32 N. R. Cameron, D. C. Sherrington, L. Albiston and D. P. Gregory, *Colloid Polym. Sci.*, 1996, **274**, 592–595.

33 A. Y. Sergienko, H. Tai, M. Narkis and M. S. Silverstein, *J. Appl. Polym. Sci.*, 2002, **84**, 2018–2027.

34 J. Pinto, A. Athanassiou and D. Fragouli, *J. Phys. D. Appl. Phys.*, 2016, **49**, 145601.

35 Y. Wan, Y. Feng, D. Wan and M. Jin, *RSC Adv.*, 2016, **6**, 109253–109258.

36 H. He, W. Li, M. Zhong, D. Konkolewicz, D. Wu, K. Yaccato, T. Rappold, G. Sugar, N. E. David and K. Matyjaszewski, *Energy Environ. Sci.*, 2013, **6**, 488–493.

37 S. Kovačič and M. S. Silverstein, *Macromol. Rapid Commun.*, 2016, **37**, 1814–1819.

38 Q. Wang, H. Ma, J. Chen, Z. Du and J. Mi, *J. Environ. Chem. Eng.*, 2017, **5**, 2807–2814.

39 M. S. Silverstein, *Polymer (Guildf).*, 2014, **55**, 304–320.

40 N. R. Cameron and D. C. Sherrington, *J. Mater. Chem.*, 1997, **7**, 2209–2212.

41 M. S. Silverstein and N. R. Cameron, in *Encyclopedia of Polymer Science and Technology*, John Wiley & Sons, Inc., Hoboken, NJ, USA, 2010.

42 R. Butler, C. M. Davies and A. I. Cooper, *Adv. Mater.*, 2001, **13**, 1459–1463.

43 R. Butler, I. Hopkinson and A. I. Cooper, *J. Am. Chem. Soc.*, 2003, ***125***, 14473–14481.

44 N. R. Cameron and D. C. Sherrington, *J. Chem. Soc. Faraday Trans.*, 1996, **92**, 1543.

45 J. M. Williams and D. A. Wrobleski, *Langmuir*, 1988, **4**, 656–662.

46 H. Xu, X. Zheng, Y. Huang, H. Wang and Q. Du, *Langmuir*, 2016, **32**, 38–45.

47 A. Menner and A. Bismarck, *Macromol. Symp.*, 2006, **242**, 19–24.

48 J. M. Williams, A. J. Gray and M. H. Wilkerson, *Langmuir*, 1990, **6**, 437–444.

49 V. Rajagopalan, C. Solans and H. Kunieda, *Colloid Polym. Sci.*, 1994, **272**, 1166–1173.

50 A. Barbetta, N. R. Cameron and S. J. Cooper, *Chem. Commun.*, 2000, **0**, 221–222.

51 N. R. Cameron and A. Barbetta, *J. Mater. Chem.*, 2000, **10**, 2466–2471.

52 A. Barbetta and N. R. Cameron, *Macromolecules*, 2004, **37**, 3188–3201.

53 M. T. Gokmen and F. E. Du Prez, *Prog. Polym. Sci.*, 2011, **37**, 365–405.

54 M. Bokhari, R. J. Carnachan, S. A. Przyborski and N. R. Cameron, *J. Mater. Chem.*, 2007, **17**, 4088.

55 C. Zhao, E. Danish, N. R. Cameron and R. Kataky, *J. Mater. Chem.*, 2007, **17**, 2446.

56 H. Zhang, A. I. Cooper and R. Robinson Laboratories, *J. Macromol. Sci., Rev. Macromol. Chem. Phys*, 1991, **24**, 4017–4020.

57 H. Zhang, G. C. Hardy, Y. Z. Khimyak, M. J. Rosseinsky and A. I. Cooper, *Chem. Mater.*, 2004, **16**, 4245–4256.

58 D. Štefanec and P. Krajnc, *React. Funct. Polym.*, 2005, **65**, 37–45.

59 H. Zhang, A. I. Cooper and R. Robinson Laboratories, *J. Macromol. Sci., Rev. Macromol. Chem. Phys*, 1991, **24**, 4017–4020.

60 F. Lapierre, N. R. Cameron and Y. Zhu, *J. Micromechanics Microengineering*, 2015, **25**, 035011.

61 M. T. Gokmen, W. Van Camp, P. J. Colver, S. A. F. Bon and F. E. Du Prez, *Macromolecules*, 2009, **42**, 9289–9294.

62 N. R. Cameron, D. C. Sherrington, I. Ando and H. Kurosu, *J. Mater. Chem.*, 1996, **6**, 719–726.

63 C. Saiwan, P. Muchan, D. deMontigny and P. Tontiwachwutikul, *Energy Procedia*, 2014, **63**, 2317–2322.

64 E. H. Mert, M. A. Kaya and H. Yıldırım, *Des. Monomers Polym.*, 2012, **15**, 113–126.

65 M. S. Silverstein, *Prog. Polym. Sci.*, 2014, **39**, 199–234.

66 R. T. Woodward, A. Jobbe-Duval, S. Marchesini, D. B. Anthony, C. Petit and A. Bismarck, *Polymer (Guildf).*, 2017, **115**, 146–153.

67 M. Ovadia and M. S. Silverstein, *Polym. Int.*, 2016, **65**, 280–289.

68 A. Katchalsky, S. Lifson and H. Exsenberg, *J. Polym. Sci.*, 1951, **7**, 571–574.

69 W. Kuhn, B. Hargitay, A. Katchalsky and H. Eisenberg, *Nature*, 1950, **165**, 514–516.

70 F. L. Buchholz, *J. Chem. Educ.*, 1996, **73**, 512.

71 US. Pat., US3229769 (A), R. N. Bashaw and B. G. Harper

72 F. L. Buchholz, *J. Chem. Educ.*, 1996, **73**, 512.

73 K. Kabiri and M. J. Zohuriaan-Mehr, *Iran. Polym. J.*, 2008, **17**, 451–477.

74 K. Kabiri, H. Omidian, S. A. Hashemi and M. J. Zohuriaan-Mehr, *Eur. Polym. J.*, 2003, **39**, 1341–1348.

75 S. Reinicke, S. Döhler, S. Tea, M. Krekhova, R. Messing, A. M. Schmidt and H. Schmalz, *Soft Matter*, 2010, **6**, 2760.

76 K. Peng, A. Kros and I. Tomatsu, *Adv. Drug Deliv. Rev.*, 2011, **63**, 1257–1266.

77 K. Varaprasad, G. M. Raghavendra, T. Jayaramudu, M. M. Yallapu and R. Sadiku, *Mater. Sci. Eng. C*, 2017, **79**, 958–971.

78 V. K. Thakur and M. K. Thakur, *Int. J. Biol. Macromol.*, 2015, **72**, 834–847.

79 E. Caló and V. V. Khutoryanskiy, *Eur. Polym. J.*, 2015, **65**, 252–267.

80 V. P. Silva Nykänen, A. Nykänen, M. A. Puska, G. G. Silva and J. Ruokolainen, *Soft Matter*, 2011, **7**, 4414.

81 L. A. Errede and S. C. Hanson, *J. Appl. Polym. Sci.*, 1994, **54**, 619–647.

82 S. Kiatkamjornwong, S. Traisaranapong and P. Prasassarakich, *J. Porous Mater.*, 1999, **6**, 205–215.

83 G.-R. Shan, P.-Y. Xu, Z.-X. Weng and Z.-M. Huang, *J. Appl. Polym. Sci.*, 2003, **89**, 3309–3314.

84 M. H. Zhou and W.-J. Cho, *J. Appl. Polym. Sci.*, 2002, **85**, 2119–2129.

85 D. Ceylan, S. Dogu, B. Karacik, S. D. Yakan, O. S. Okay and O. Okay, *Environ. Sci. Technol.*, 2009, **43**, 3846–3852.

86 H. Bi, X. Xie, K. Yin, Y. Zhou, S. Wan, L. He, F. Xu, F. Banhart, L. Sun and R. S. Ruoff, *Adv. Funct. Mater.*, 2012, **22**, 4421–4425.

87 H. X. Jin, B. Dong, B. Wu and M. H. Zhou, *Polym. Plast. Technol. Eng.*, 2012, **51**, 154–159.

88 T. Ono, T. Sugimoto, S. Shinkai and K. Sada, *Nat. Mater.*, 2007, **6**, 429–433.

89 D. K. and and M. Satoh, *Macromolecules*, 1999, **32**, 7828–7835

90 N. Yasumoto, Y. Hata and M. Satoh, *Polym. Int.*, 2004, **53**, 766–771.

91 T. Ono, M. Ohta and K. Sada, *ACS Macro Lett.*, 2012, **1**, 1270–1273.

92 T. Ono, T. Sugimoto, S. Shinkai and K. Sada, *Adv. Funct. Mater.*, 2008, **18**, 3936–3940.

93 K. Iseda, M. Ohta, T. Ono and K. Sada, *Soft Matter*, 2011, **7**, 5938.

94 T. Ono, S. Shinkai and K. Sada, *Soft Matter*, 2008, **4**, 748.

95 Y. Nishikori, K. Iseda, K. Kokado and K. Sada, *Polymers (Basel).*, 2016, **8**, 148.

96 K. Sada, *Polym. J.*, 2018, **50**, 285–299.

97 A. Pourjavadi, M. Doulabi and S. H. Hosseini, *Polymer (Guildf).*, 2012, **53**, 5737–5742.

98 M. J. Muldoon and C. M. Gordon, *J. Polym. Sci. Part A Polym. Chem.*, 2004, **42**, 3865–3869.

99 S. G. Roy, U. Haldar and P. De, *ACS Appl. Mater. Interfaces*, 2014, **6**, 4233–4241.

100 S. Sunaga, K. Kokado and K. Sada, *Soft Matter*, 2018, **14**, 581–585.

101 P. J. Flory, *Principles of polymer chemistry*, Cornell University Press, 1953.

102 F. Horkay, I. Tasaki and P. J. Basser, *Biomacromolecules*, 2000, **1**, 84–90.

103 L. E. Nielsen, *J. Macromol. Sci. Part C*, 1969, **3**, 69–103.

104 R. Wong, M. Ashton, K. Dodou, R. S. H. Wong, M. Ashton and K. Dodou, *Pharmaceutics*, 2015, **7**, 305–319.

105 M. Mahkam and L. Doostie, *Drug Deliv.*, 2005, **12**, 343–347.

106 K.-J. Kim, S.-B. Lee and N. W. Han, *Polym. J.*, 1993, **25**, 1295–1302.

107 *J. Soc. Chem. Ind.*, 1936, **55**, 665–665.

108 L. J. Hughes and G. E. Britt, *J. Appl. Polym. Sci.*, 1961, **5**, 337–348.

109 C. Hansen, 1967.

110 C. M. Hansen, *J. Paint Techn.*, 1967, **39**, 104–117.

111 R. F. Blanks and J. M. Prausnitz, *Ind. Eng. Chem. Fundam.*, 1964, **3**, 1–8.

112 C. M. Hansen and K. Skaarup, *J Paint Technol.*, 1967, **39**, 511–514.

113 C. M. Hansen and A. Beerbower, *Kirk-Othmer Encycl. Chem. Technol.*, 1971, 889–910.

114 D. Karst and Y. Yang, *J. Appl. Polym. Sci.*, 2005, **96**, 416–422.

115 A. Forster, J. Hempenstall, I. Tucker and T. Rades, *Int. J. Pharm.*, 2001, **226**, 147–161.

116 C. M. Hansen, *Hansen solubility parameters : a user's handbook*, CRC Press, 2007.

117 K. Ganesan, S. K. Raza and R. Vijayaraghavan, *J. Pharm. Bioallied Sci.*, 2010, **2**, 166–78.

118 J. Bajgar, *Adv. Clin. Chem.*, 2004, **38**, 151–216.

119 F. R. Sidell and W. A. Groff, *Toxicol. Appl. Pharmacol.*, 1974, **27**, 241–52.

120 A. Forsberg and G. Puu, *Eur. J. Biochem*, 1984, **140**, 153–156.

121 M. Pohanka, *Biomed. Pap. Med. Fac. Univ. Palacky. Olomouc. Czech. Repub.*, 2011, **155**, 219–29.

122 A. Polavarapu, J. A. Stillabower, S. G. W. Stubblefield, W. M. Taylor and M.-H. Baik, *J. Org. Chem.*, 2012, **77**, 5914–5921.

123 S. L. Hoenig, *Compendium of chemical warfare agents*, Springer, 2007.

124 K. Kim, O. G. Tsay, D. A. Atwood and D. G. Churchill, *Chem. Rev.*, 2011, **111**, 5345–5403.

125 K. P. Sullivan, W. A. Neiwert, H. Zeng, A. K. Mehta, Q. Yin, D. A. Hillesheim, S. Vivek, P. Yin, D. L. Collins-Wildman, E. R. Weeks, T. Liu and C. L. Hill, *Chem. Commun.*, 2017, **53**, 11480–11483.

126 F. Piana, M. Facciotti, G. Pileio, J. R. Hiscock, W. Van Rossom, R. C. D. Brown and P. A. Gale, *RSC Adv.*, 2015, **5**, 12287–12292.

127 J. R. Hiscock, M. R. Sambrook, N. J. Wells and P. A. Gale, *Chem. Sci.*, 2015, **6**, 5680–5684.

128 C. Wilson, M. J. Main, N. J. Cooper, M. E. Briggs, A. I. Cooper and D. J. Adams, *Polym. Chem.*, 2017, **8**, 1914–1922.

129 B. Singh, V. V Singh, M. Boopathi and D. Shah, *Def. Life Sci. J.*, 2016, **1**, 127.

130 E. D. Davis, W. O. Gordon, A. R. Wilmsmeyer, D. Troya and J. R. Morris, *J. Phys. Chem. Lett.*, 2014, **5**, 1393–1399.

131 M. R. Sambrook and S. Notman, *Chem. Soc. Rev.*, 2013, **42**, 9251.

132 A. A. Tomchenko, G. P. Harmer and B. T. Marquis, *Sensors Actuators B*, 2005, **108**, 41–55.

133 Y. C. Yang, J. A. Baker and J. R. Ward, *Chem. Rev.*, 1992, **92**, 1729–1743.

134 V. Kumar, R. Goel, R. Chawla, M. Silambarasan and R. K. Sharma, *J. Pharm. Bioallied Sci.*, 2010, **2**, 220–38.

135 G. W. Wagner, *Ind. Eng. Chem. Res.*, 2011, **50**, 12285–12287.

136 D. Marciano, M. Goldvaser, I. Columbus and Y. Zafrani, *J. Org. Chem.*, 2011, **76**, 8549–8553.

137 S.-Y. Moon, Y. Liu, J. T. Hupp and O. K. Farha, *Angew. Chemie Int. Ed.*, 2015, **54**, 6795–6799.

138 J. E. Mondloch, M. J. Katz, W. C. Isley III, P. Ghosh, P. Liao, W. Bury, G. W. Wagner, M. G. Hall, J. B. DeCoste, G. W. Peterson, R. Q. Snurr, C. J. Cramer, J. T. Hupp and O. K. Farha, *Nat. Mater.*, 2015, **14**, 512–516.

139 E. Gershonov, I. Columbus and Y. Zafrani, *J. Org. Chem.*, 2009, **74**, 329–338.

140 Y. Liu, S.-Y. Moon, J. T. Hupp and O. K. Farha, *ACS Nano*, 2015, **9**, 12358–12364.

141 Y. Liu, A. J. Howarth, J. T. Hupp and O. K. Farha, *Angew. Chemie Int. Ed.*, 2015, **54**, 9001–9005.

142 Y. Liu, C. T. Buru, A. J. Howarth, J. J. Mahle, J. H. Buchanan, J. B. DeCoste, J. T. Hupp and O. K. Farha, *J. Mater. Chem. A*, 2016, **4**, 13809–13813.

143 P. Janoš, J. Henych, O. Pelant, V. Pilařová, L. Vrtoch, M. Kormunda, K. Mazanec and V. Štengl, *J. Hazard. Mater.*, 2016, **304**, 259–268.

144 G. W. Wagner, Q. Chen and Y. Wu, *J. Phys. Chem. C*, 2008, **112**, 11901–11906.

145 R. B. Balow, S. L. Giles, C. L. McGann, G. C. Daniels, J. G. Lundin, P. E. Pehrsson and J. H. Wynne, *Ind. Eng. Chem. Res.*, 2018, **57**, 8630–8634.

146 A. Barba-Bon, A. M. Costero, M. Parra, S. Gil, R. Martínez-Máñez, F. Sancenón, P. A. Gale and J. R. Hiscock, *Chem. - A Eur. J.*, 2013, **19**, 1586–1590.

147 F. Worek, T. Wille, M. Koller and H. Thiermann, *Arch. Toxicol.*, 2016, **90**, 2131–2145.

148 H. John, M. J. van der Schans, M. Koller, H. E. T. Spruit, F. Worek, H. Thiermann and D. Noort, *Forensic Toxicol.*, 2018, **36**, 61–71.

149 The White House, Government Assessment of the Syrian Government's Use of Chemical Weapons on August 21, 2013, https://obamawhitehouse.archives.gov/the-press-office/2013/08/30/government-assessment-syrian-government-s-use-chemical-weapons-august-21, (accessed 9 July 2018).

150 BBC News, Amesbury Novichok poisoning: Couple exposed to nerve agent, https://www.bbc.co.uk/news/uk-44719639, (accessed 9 July 2018).

Chapter 2 -

Synthesis of Styrene Based Absorbents: Polyelectrolyte Design and Development.

2.1 Introduction and aims

This chapter describes the development of a styrene based polyelectrolyte gel with significant variations in ionic content. The determination of its ability to swell in a range of organic solvents and then subsequently a range of chemical warfare agent simulants was investigated.

2.1.1 Introduction to organic polyelectrolytes

A large body of research has described the swelling of hydrogels, and how they are designed to exhibit polyelectrolyte nature to increase swelling; as seen in recent reviews regarding the generalities of hydrogel systems,[1] and more specific reviews dedicated to use of hydrogels and polyelectrolyte hydrogels for responsive biomedical applications.[2,3] One review discusses organogels for drug delivery and differentiates between gelators and polymer matrices, however does not focus mention organic polyelectrolytes.[4] A final review was found which discusses organic polymer polyelectrolytes for water treatment, however again, where the polymers presented are organic, the applications are in the majority water based.[5] In terms of the hydrogels, it was found that the increase in osmotic pressure of a polyelectrolyte hydrogel by introducing salt groups can cause a significant increase in the swelling of such polymers in water.[6,7] This was based upon the understanding that when the ion pairs dissociate, the water is brought into the matrix through the increase in free-ion concentration which increased the internal osmotic pressure of the polymer. This then moves the swelling equilibrium to a higher swelling degree.[8] This same principle of osmotic pressure increasing the swelling of a polymer can in fact be observed in organogel polyelectrolyte systems. A group led by Sada recently published various works regarding the incorporation of an electrolytic monomer into a polymer to increase the swelling of organic solvents, specifically targeting oils. Their first report in 2007 described using small amounts (5 mol%) of ionic monomers (Figure 2.1) in a crosslinked long chain acrylate system to increase the swelling of low-polarity solvents.[9] Their research was based upon the ionic monomer increasing the osmotic pressures inside the matrix, therefore increasing the swelling, similarly to what was historically seen in hydrogels.

They were able to swell some organic solvents to very high degrees (Q_{THF} = 122, $Q_{chlorobenzene}$ = 70) when compared to the non-ionic gels (Q_{THF} = 23, $Q_{chlorobenzene}$ = 35).

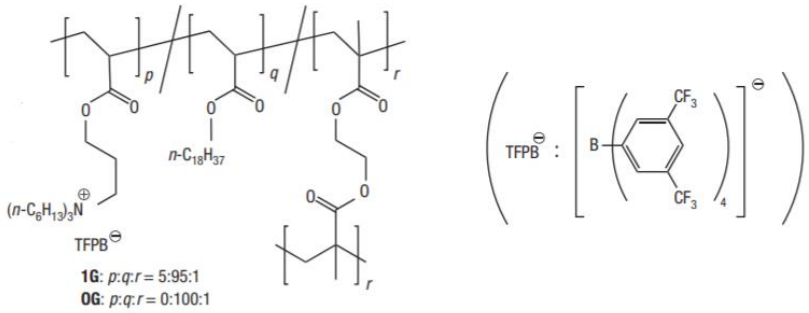

Figure 2.1 – A scheme showing the approach used by Sada *et al*.[9] to produce a lipophilic polyelectrolyte gel

A follow up paper by the same group developed the previous acrylate system and varied the ionic content up to 10 mol% with different chain length acrylates and proposed that the increasing swelling of the low polarity solvents was due to the increasing content of the lipophilic electrolyte species.[10] A final notable work by the group was along very similar lines, except that they utilized a styrene based network, again with a quaternary ammonium ionic monomer with BARF anion at only 3 mol%. They observed large swelling increases as with the acrylate systems such as octanone from Q = 9 to Q = 75.[11] Whilst Sada's group looked into working with small amounts of quaternary ammonium chloride electrolytic monomers in the gel, different work by Jeffrey Horne *et al.* looked at wholly ionic polymer systems based upon poly(ionic liquid) electrolyte systems such as poly(methyl imidazolium) species. These polymers were able to swell polar solvents to over Q =200 in DMSO.[12] The research into this type of poly(electrolyte) based upon ionic liquids has developed significantly in recent years.[13] The important factor which was taken from both of these contrasting works is that whilst some state swelling is proportional to ionic content, as seen in the ionic liquid systems, some others say overly high concentrations of ionic functionality can cause reduced swelling in certain solvents due to ion aggregation.[14,15]

2.1.2 Development of a styrene based polyelectrolyte

The work with polyelectrolytes in acrylates and styrene based systems by Sada *et al*. did not examine the swelling effects of the polymers with vastly increased ionic content past 10% ionic monomer, with any of the polyelectrolyte systems they reported.[16,17] Additionally, they only made brief correlations between the dielectric constant and polarity of the solvents with respect to understanding the swelling. For these reasons it was decided that there would be an investigation into the swelling performance of a styrene based system, weakly crosslinked with divinylbenzene, where the styrene based electrolytic monomer was implemented at increasing feed ratio. The ionic monomer used by Sada et al. mostly utilized the 'BARF' anion which they proposed to be highly lipophilic and weakly coordinating, but for this work the chloride anion would be investigated: trihexyl (vinylbenzyl) ammonium chloride (THVBAC) (Figure 2.2). This monomer was to be introduced up to 100% of the total monomer fraction.

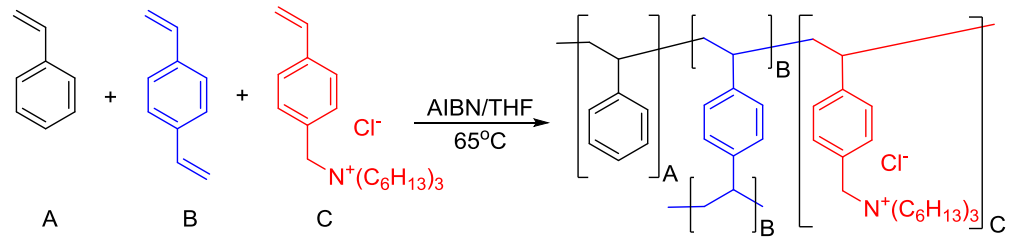

Figure 2.2 – A scheme showing the polymerisation including the ionic monomer THVBAC (C). The ionic monomer would be balanced against the styrene (A), maintaining a constant crosslinking density of divinylbenzene (B)

The swelling performance of these terpolymers was then tested in a range of solvents which covered a range of functional groups and properties. The twenty-two solvents chosen for the swelling experiments comprised of methanol, ethanol, propan-1-ol, butan-1-ol, pentan-1-ol which would represent increasing lipophilicity in the alcohol series. Dichloromethane (DCM) and 1-bromopropane were chosen as low polarity halogenic solvents. Hexane and dodecane, xylene and toluene, were selected to represent the simple aliphatic and aromatic solvents respectively. Acetone, tetrahydrofuran (THF), dimethyl sulfoxide (DMSO), dimethylformamide

(DMF) and acetonitrile were picked to show the increasing polarity of small polar aprotic solvents. Triethylamine, benzyl amine and acetic acid were chosen to add functional group diversity and hydrogen bonding comparison. Finally, diethyl ether, ethyl acetate, ethoxyethyl acetate were selected for the ethers and esters.

2.1.3 Analysis of the swelling behaviour

Once the swelling performances of the polymers were known, the degrees of swelling would be correlated with the dielectric constant of each solvent. This would prove inconclusive and so further analysis would be carried out to try to understand what influenced the swelling of the various solvents as the ionic content of the polymers was varied. The Hansen solubility parameters of the polymers and subsequent Ra values would be determined so that they could be used to try to show a relationship between the increasing ionic content and the swelling performances. The HSPs would be gathered by use of specific software designed for determining HSPs known as HSPiP (explained further in 2.1.4). The swelling of the polymers with respect to the HSP data showed correlations but exhibited flaws. A model would ultimately be developed which would aim to clarify the swelling of all the solvents in this polymeric system by utilizing both the dielectric of the solvent, ionic content of the matrix and Ra between the solvent and polymer. The ability of the model to predict the swelling of a further set of four solvents (dioxane, propylene carbonate, butanone, methyl benzoate) and three chemical warfare agents (VX, Sarin, sulfur mustard) was tested. The experimental swelling of these agents and solvents was determined and correlated to the prediction. The swelling of the chemical warfare agents in the polymers of varying ionic content would be used to observe if any of the polymers with varying ionic weighting presented good absorbency towards these chemicals. The CWA swelling was compared with potential physical simulants which were selected based on HSP matching. An appropriate simulant would be used in place of the agents for use in future work in this thesis.

2.1.4 Determination of Ra

The Ra, a measure of similarity between two sets of HSPs, for each of the combinations of polymer and solvent were calculated as;[18]

$$Ra = \sqrt{4\left(\delta d_{poly} - \delta d_{solv}\right) + \left(\delta p_{poly} - \delta p_{solv}\right) + \left(\delta h_{poly} - \delta h_{solv}\right)}$$

(Equation 2.1)

2.1.4.1 Introduction to HSPiP

A piece of specialized software for examining HSPs was found and purchased. This software; HSPiP (*Hansen solubility parameters in practice*), contained a database of thousands of sets of HSPs from experimental and modelled sources.[19] For compounds and polymers which were not included, the software had a range of computational options for the estimation of HSPs. A commonly used example of this was the Y-MB (Yamamoto molecular break) method which estimated the HSPs from basic first order S-P group contributions which could then also be applied to find values of a small polymer chain. In the software the SMILES code of a chemical could be used for automatic calculation.[20] A similar development of the group contribution technique is the Stefanis-Panayiotou (SP) method which was claimed to be more accurate due to incorporation of conjugation theory[19] Unlike Y-MB, the SP method would require manual calculation of the group contributions. All the physical data and HSPs for the Ra calculations were to be gathered from this software for the purposes of consistency. The solvent HSPs would be taken from the database, and unknown solvents / CWAs would be predicted with the Y-MB tool. This project would look at co-polymer systems where monomers include ionic groups, heterocycles and crosslinking and therefore the computational methods would not be able to accurately derive a series of parameters for the polymers and so they would be found experimentally.

2.1.4.2 Spheres and derived HSPs

The main aspect the project would focus on being able to define the solubility parameters of the polymers which were synthesised from experimental results of swelling. The experimental data from swelling studies would be inputted to the HSPiP software. This data would instruct HSPiP on relatively how well each solvent swelled the polymer. From this swelling data and the associated solvent parameters for each of the solvents, the program is able to mathematically fit a 'solubility sphere' around the 'good' swelling solvents (Figure 2.3) and exclude the 'badly' performing solvents. The sphere was built against three axes; one for each of the dispersion (δd), polarity (δp) and hydrogen bonding (δh) components which make up the HSP's. The theory then teaches that the centre coordinate (x= δd , y= δp , z= δh) of the sphere would then correspond to the HSPs for a solvent which would swell 'perfectly' / be perfectly 'miscible' with the chosen polymer. Therefore by extension, the coordinates would be equal to the polymers' own HSPs. In terms of practicality, the sphere which is generated must have had a small radius encapsulating the correct solvents; which comes down from accurate and reproducible swelling results. Conditions which would describe an unreliable sphere include; a large radius and incorrect solvent placement (bad swelling inside/good swelling outside). The sample size must also be large. These phenomena must have been controlled as the HSPs derived from badly formed spheres would likely be incorrect. The sphere forming functionality would allow a swelling study of many solvents with known data to be used to find the parameters of the polymer that was being swollen. This would be extremely useful throughout the project for both gathering data on the bespoke polymer compositions where this cannot be achieved through computational methods. A large set of solvents (>20) with already trusted parameters and a variety of properties was imperative for an accurate sphere with a small radius to be formed. The 22 solvents described in 2.1.2 would be suitable for this task.

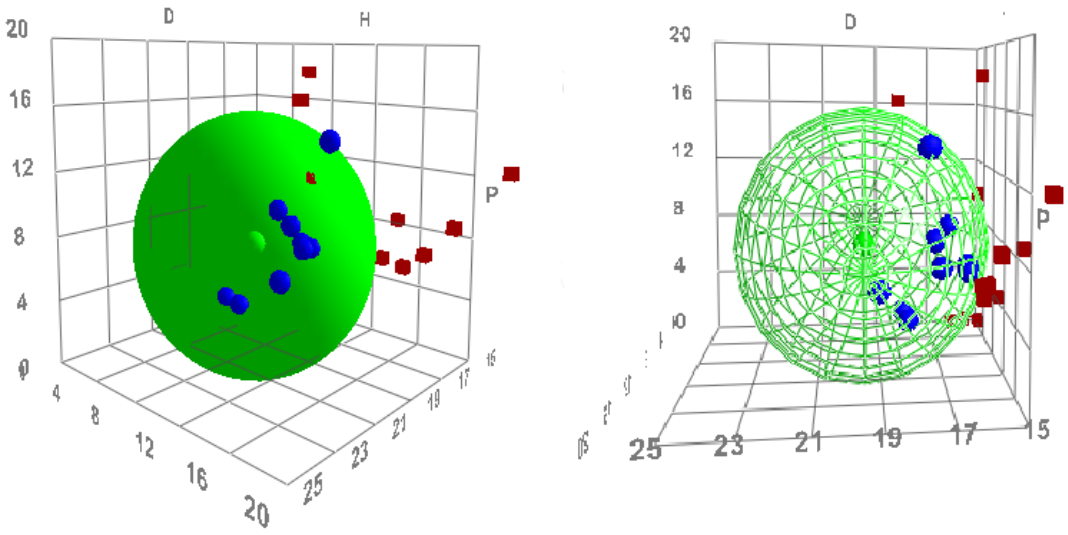

Figure 2.3 – An example of HSPiP fitting a sphere around a selection of solvents. The good swelling solvents are represented by blue circles (inside the sphere) and the bad or non-swelling solvents are shown as red squares (excluded from the sphere). The right hand image is a wireframe representation of the left hand image, rotated around the 'P' axis by 90 degrees. The centre of the sphere is represented by a green circle and for this example has the coordinates D (δd) = 19.2, P (δp) = 7.0, and H (δh) = 7.8.

2.2 Experimental

2.2.1 Materials and Equipment

4-Vinylbenzylchloride (90 %, Sigma, stabilised with 500 ppm tert-butylcatechol) was used without purification or removal of inhibitor. Styrene (99 %, Acros) was passed through an alumina column before use to remove the inhibitor. Trihexylamine (96%, Sigma), AIBN (98 %, Sigma), tetrahydrofuran (HPLC, Fisher), acetonitrile (HPLC, Fisher), and divinylbenzene (80 % mix of isomers, Sigma) were all used without further purification. All solvents used for swelling of polymers were used as received at 'HPLC grade' where available.

Nuclear magnetic resonance data was obtained on a Jeol ECS-400 spectrometer and all NMR samples were prepared in chloroform-d (d-99.8 atom%, CIL). Spectra were obtained at room temperature (22 °C). Samples of the crosslinked polymer networks with varying ionic content

were prepared for NMR by grinding the dry samples to a powder with a pestle and mortar. The powders were then transferred to NMR tubes and deuterated chloroform was added to swell the polymers in situ. These gel NMR samples were run with an extended relaxation delay of 60 seconds.

Elemental analysis was performed by Mr S. Boyer at the London Metropolitan University elemental analysis service.

2.2.2 Synthesis of the ionic monomer – trihexyl (vinylbenzyl) ammonium chloride (THVBAC)

Trihexyl (vinylbenzyl) ammonium chloride (THVBAC) was synthesised following slight modifications to a previously published procedure by Sada et al.[11] 4-vinylbenzylchloride, 18.3 g (120 mmol), and trihexylamine, 16.2 g (60 mmol), were placed into a round bottom flask with 120 ml acetonitrile and a magnetic stirrer. The flask was covered with foil and reacted with stirring at 50 °C for 48 hours after which time the acetonitrile was removed by rotary evaporation. The remaining yellow oil containing the product and excess 4-vinylbenzylchloride was poured slowly into 250 ml of vigorously stirring cold hexane, and the product precipitated as a white flaky powder. The product was collected by vacuum filtration, then dissolved into tetrahydrofuran and reprecipitated into hexane. The final product was collected and dried in vacuo to leave a white fluffy powder (21.35 g, 84 %). ^{1}H NMR 400 MHz, $CDCl_3$, room temperature) found ppm δ: = 0.91 [t, **9H** ($\mathbf{CH_3}CH_2CH_2CH_2CH_2)_3N$, J = 6.18 Hz], 1.35 [s, **18H** ($CH_3\mathbf{CH_2CH_2CH_2}CH_2CH_2)_3N$], 1.75 [s, **6H**($CH_3CH_2CH_2CH_2\mathbf{CH_2}CH_2)_3N$], 3.31 [t, **6H** ($CH_3CH_2CH_2CH_2CH_2\mathbf{CH_2})_3N$, J = 8.28 Hz], 5.01 [s, **2H** $N\mathbf{CH_2}C_6H_4CHCH_2$], 5.37 [d, **1H alkene,** J = 11.49 Hz] 5.85 [d, **1H alkene,** J = 17.46 Hz], 6.70 [dd, **1H alkene,** J_1 = 11.01 Hz, J_2 = 6.52 Hz], 7.50 [dd, **4H phenyl,** J_1 = 8.13 Hz, J_2 = 23.31 Hz]. ^{13}C NMR (Figure 2.5) found ppm δ: = 13.95, 22.51, 22.74, 26.19, 31.29, 58.93, 63.29, 116.32, 127.00, 132.91, 135.64, and 139.89. Elemental analysis: expected; **C** 76.82 %, **H** 11.46 %, **N** 3.32 %, found; **C** 76.68 %, **H** 11.35 %, **N** 3.24 %.

2.2.3 Synthesis of polyelectrolyte gels

AIBN/THF solution (2 ml, 0.1 M) was placed into a boiling tube. To the boiling tube was then added 0.2500 g of a divinylbenzene/THF stock solution (divinylbenzene, 0.7 M; 0.506 g, in 5 g THF) and 2 g styrene (19 mmol). The final ratio of the divinylbenzene, to initiator, to styrene was 1:1:100. The tube was then sealed with a rubber septum and degassed with nitrogen for 20 minutes. The polymerisation was then carried out at 65 °C for 24 hours without stirring. After the polymerisation was complete the polymer was removed from the tube and cut into pieces of approximately 100 mg each. The gels were crudely washed: chunks were swollen in an excess of THF and after 2 hours the supernatant liquid was removed. Further THF was added and the gel was left to sit for another hour after which the supernatant was again removed. Finally the gel was left to de-swell slowly in ambient conditions. To prepare the gel for swelling studies, the chunks were further dried under a slowly increasing vacuum at 65 °C for 24 hours. All the polymers formed brittle gels. For the synthesis of a polyelectrolyte styrene based gel; the ionic species (ion) was introduced into the boiling tube before degassing and completely dissolved. The quantity of ionic monomer was adjusted against the quantity of the styrene to allow for a variation in ionic component, whilst maintaining the same overall initiation and crosslinking density across the series of gels. The overall ratio for a polyelectrolyte gel consisting of: divinylbenzene, initiator, styrene and ionic component (ion) was 1: 1: 100-Ion: Ion.

2.2.4 Swelling procedure

A glass vial was tared on a 100 g x 0.0001 g balance and a single small chunk of pre dried polymer (typically 0.1 g) was added and the mass was recorded. The polymer was then submerged in a vast excess of the chosen solvent. The vial was capped and left for 72h. On completion of the swelling, the excess solvent was decanted off and the polymer carefully removed in its entirety where it was then weighed on a tared balance. This was repeated two further times with fresh chunks of polymer to give a minimum of three results for each

polymer/solvent combination. The swelling degree by mass (Q) was then calculated from equation 2.1.

$$Q = \frac{(mass\ swollen\ gel - mass\ dry\ gel)}{mass\ dry\ gel}$$

(Equation 2.2)

The volume change (Q_v) could not be directly measured due to the irregular forms of the polymer samples. Q_v was therefore calculated when needed from the mass swelling degree according to equation 2.2;

$$Q_v = Q\ \frac{1}{\rho}$$

(Equation 2.3)

where ρ is the density of the solvent.

2.3 Results and Discussion

2.3.1 NMR of the ionic monomer

The proton and carbon NMR of the ionic monomer (Figure 2.4 and Figure 2.5) confirmed the synthesis was successful, and the styrenic vinyl group was retained.

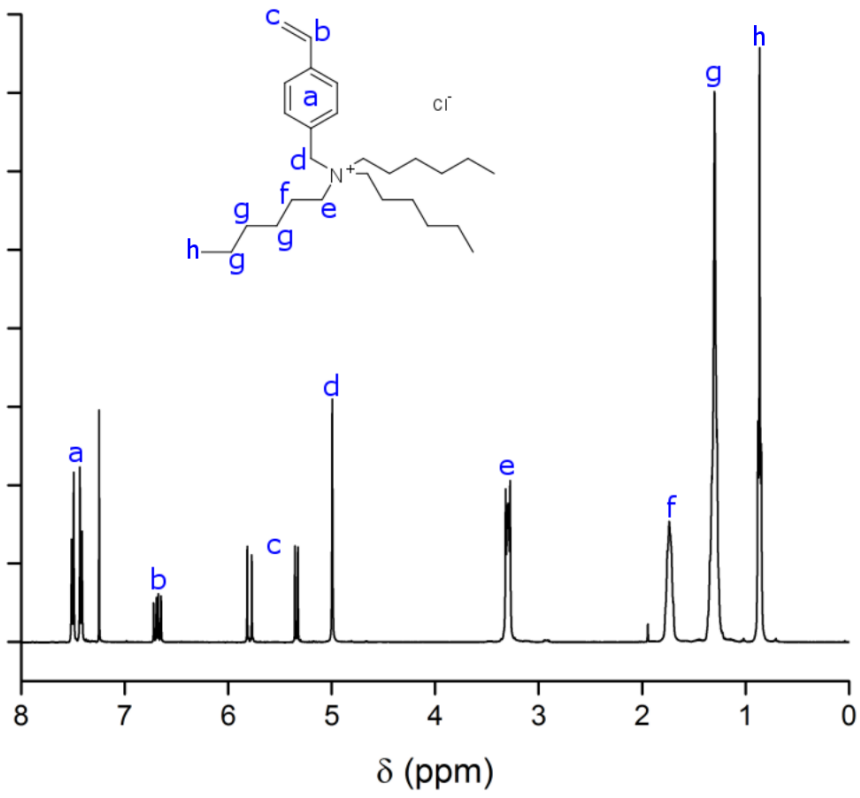

Figure 2.4 – ^{1}H NMR of the ionic monomer THVBAC.

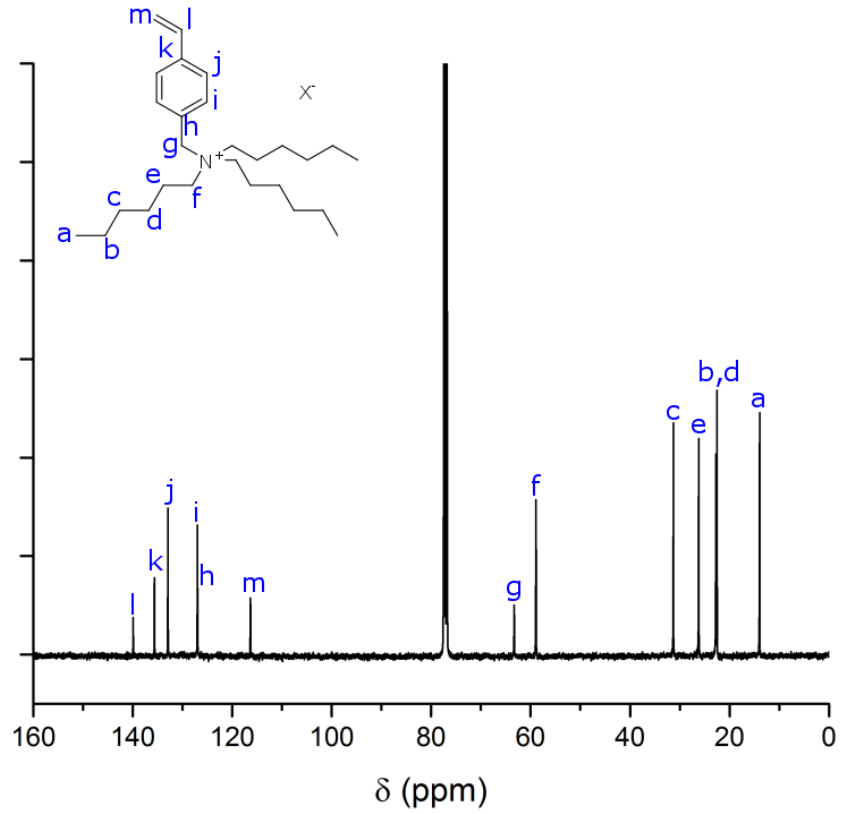

Figure 2.5 – ^{13}C NMR of the ionic monomer THVBAC.

2.3.2 Determination of the ionic content of the polymers

A sample of each of the gels was ground up in a pestle and mortar and then re-dried thoroughly. These samples were then each swollen to their maximum into a standard NMR tube using deuterated chloroform. Careful attention was paid to the swollen mass to ensure that there were minimal amounts of free solvent around the swollen gel. The swollen polymers were then run on a standard solution state NMR, running at 400 MHz, with an extended relaxation delay of 60 seconds. The acquisition of the spectra was good, although significant line broadening was observed in all samples, stereotypical of polymer spectra. A comparison of the 6 NMRs can be seen in Figure 2.6.

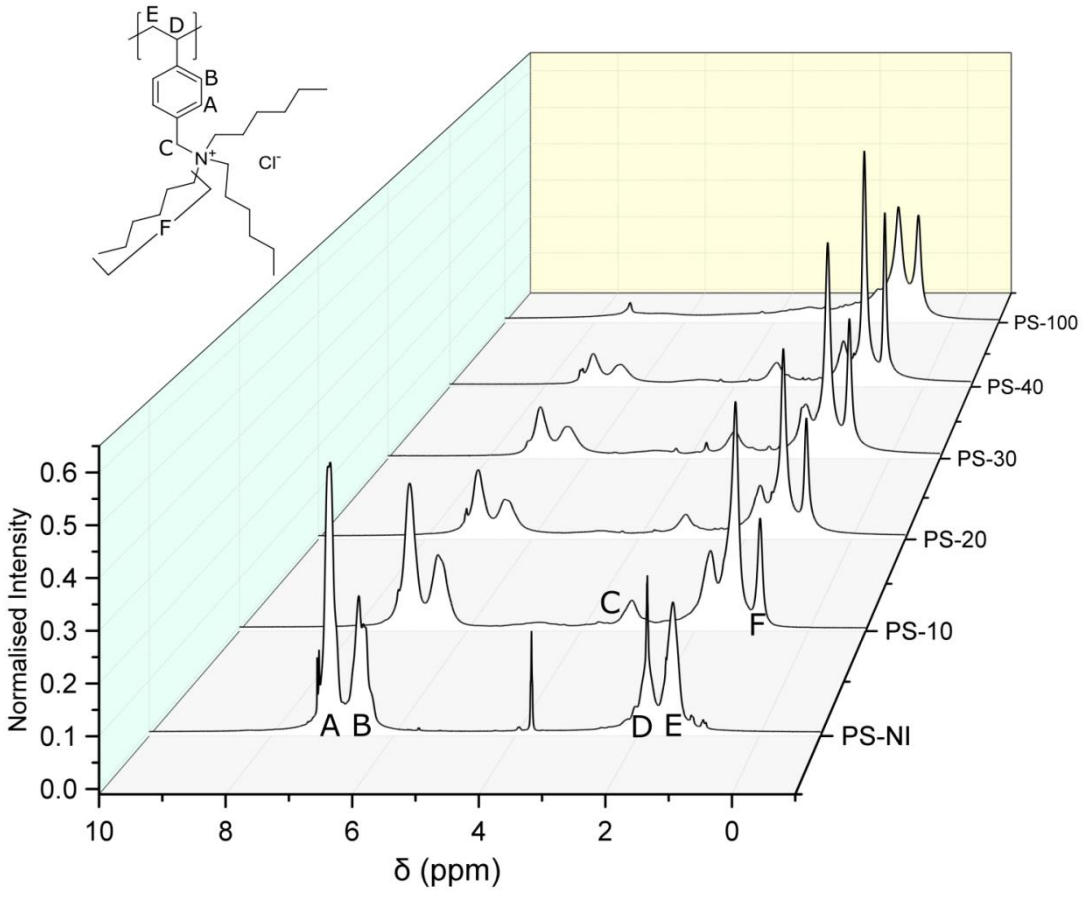

Figure 2.6 – A cascade overlay of the ^{1}H NMR spectra for each of the polymers synthesised with varying ionic content. The assignment of the peaks due to styrene is made against PS-NI, and the assignments due only to the ionic monomer are made against the PS-10 sample.

The integrals for the hexyl chains on the quaternary ammonium group, and the methylene between the nitrogen and the benzene were compared against those of the styrenic benzene and polymer backbone to give an indication of the monomer compositions of the final samples. The samples were also sent off for elemental analysis, and the values for the NMR and elemental analysis can be seen below in Table 2.1.

Table 2.1 – The elemental analysis values for each of the polymers. Estimates by monomer feed ratio are presented alongside measurements from the NMR integral data. The experimental results which are within an acceptable range (0.3 %, Polymer Chemistry RSC)[21] of the NMR estimates are presented in bold.

Polymer (ionic % by design)	*Estimated according to the polymer design*			***Ionic % calc. from NMR integration***	*Estimated based upon the NMR integrals*			*Found experimentally*		
	C (%)	***H (%)***	***N (%)***		***C (%)***	***H (%)***	***N (%)***	***C (%)***	***H (%)***	***N (%)***
PS-NI (0 %)	91.96	7.77	0.26	**0 %**	91.96	7.77	0.26	**91.73**	**7.86**	**0.37**
PS-10 (10 %)	87.33	8.90	1.21	**12 %**	86.65	9.07	1.35	84.14	**9.44**	**1.52**
PS-20 (20 %)	84.43	9.60	1.81	**21 %**	84.20	9.66	1.86	82.28	**9.86**	**2.03**
PS-30 (30 %)	82.44	10.09	2.22	**31 %**	82.27	10.13	2.25	77.36	**10.51**	**2.18**
PS-40 (40 %)	80.99	10.44	2.51	**39 %**	81.11	10.41	2.49	78.80	11.25	**2.66**
PS-100 (100 %)	76.85	11.45	3.36	**96 %**	76.85	11.45	3.36	74.58	11.89	**3.53**

Table 2.1 shows the predicted elemental analysis results based upon the gel NMR calculations, as well as the estimates from the original feed ratio and the experimentally obtained values. There was generally a larger difference in elemental analysis results between the experimental values and the estimates based upon the ionic content by design, compared to the estimates based upon the ionic content calculated through NMR integration. The elemental analysis results diverged from either of the estimates as the ionic content increased. This was likely due to stoichiometric bound solvent from the synthesis interfering with the analysis. The NMR analysis estimations of the monomer composition were slightly more reliable than the designed feed ratio. This was because the NMR estimations would take into account what was actually incorporated into the polymer, rather than just what was placed into the reaction.

Ideally the NMR would have been carried out on a semi-solid, or even better, a full magic-angle probe but this was not accessible during the study. The polymers were prepared for NMR as gels (semi-solids) however the probe was only designed for solution state NMR. The analyses showed that the syntheses were effective for the most part, giving polymers with ionic content close to that of the design.

2.3.3 Swelling results

The swelling of each of the polymers in each of the solvents was carried out in triplicate. The results are presented in Figure 2.7 with the textual data version for all of the data points presented in appendix 2A. Very large errors were observed in the 100 % ionic polymer with good swelling solvents. It was suspected that the higher ionic content polymers may have been crosslinking irregularly due to the lack of stirring, hindered nature of the DVB, or a potential incompatibility/phase separation between the ionic monomer and the low polarity DVB. A more consistent route to crosslinking in the high ionic fraction polymers would be to use a crosslinker where both reactive groups are more mobile and accessible in a crowded system, such as ethylene glycol dimethacrylate (EGDMA). A variety of trends were observed as the ionic content was increased from 0 % ($St_{100}Ion_0$) to 10 % ($St_{90}Ion_{10}$), 20 % ($St_{80}Ion_{20}$), 30 % ($St_{70}Ion_{30}$), 40 % ($St_{60}Ion_{40}$), and 100 % (St_0Ion_{100}) of the polymer.

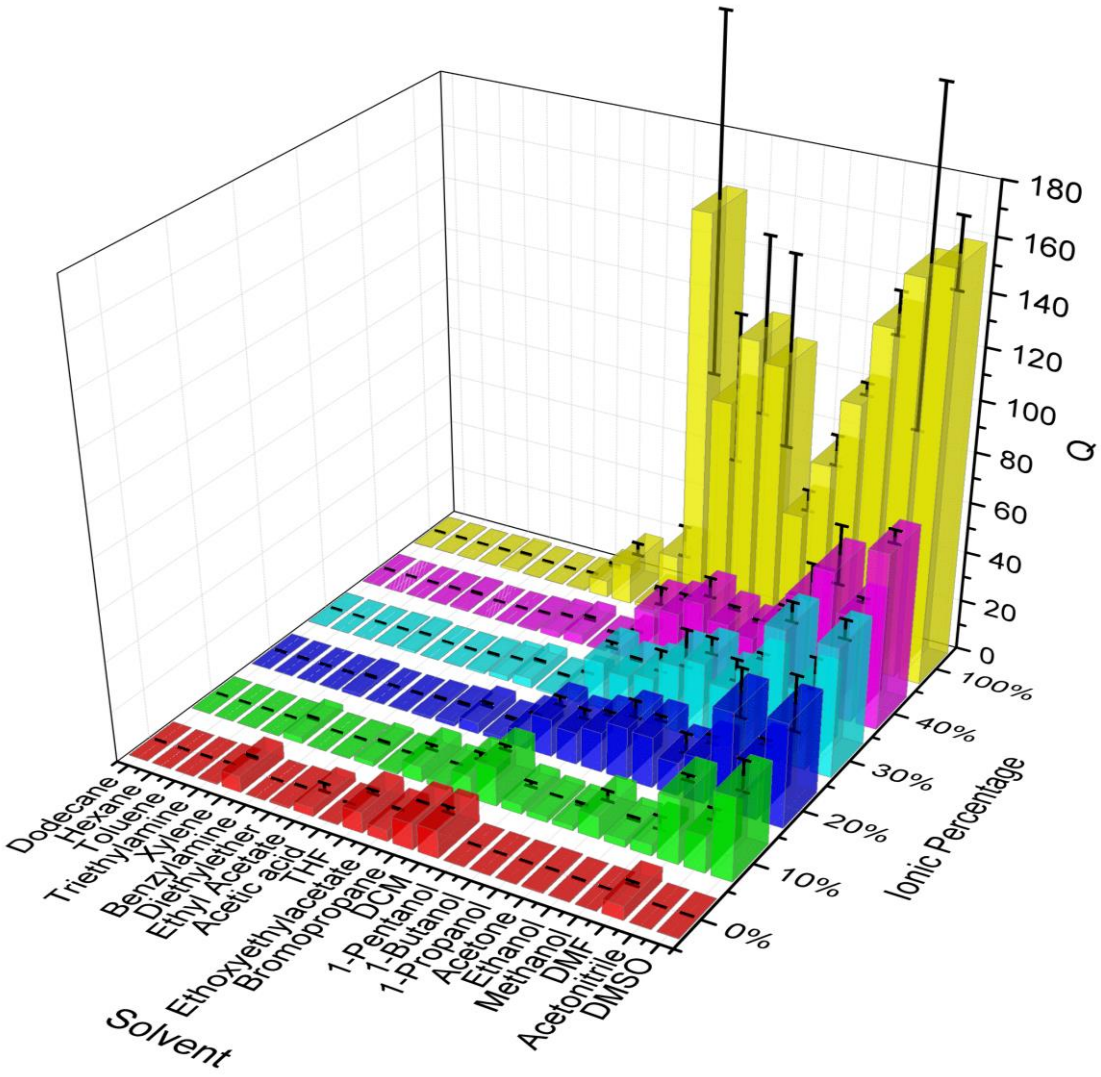

Figure 2.7 – The swelling of each of the 22 solvents in each of the 6 polymers. The solvents are arranged in order of increasing dielectric constant from left to right.

For some solvents, such as the alcohols, the swelling increased steadily. Polar aprotic solvents - especially DMF, DMSO and acetonitrile showed a significant increase in swelling performance up to maxima of Q = 133, Q = 159, and Q = 154 respectively, as the ionic content increased. In contrast, the less polar solvents decreased or maintained their low swelling performance with increasing ionic fraction. A notable example; DCM, which possesses low polarity and dielectric constant, managed to show the highest swelling potential in the 100% ionic polymer of Q = 161 which was an unexpected result. It was decided to attempt to correlate the degree of swelling of the polymers with some known solvent properties.

2.3.4 Correlation of swelling with dielectric

The first approach was to correlate the swelling of the system with the dielectric constant of the solvents. As the ionic content increased, the osmotic pressure inside the system should also increase; which would improve the swelling in high dielectric solvents. The swelling against the dielectric is presented in Figure 2.8. There appeared to be a general trend where increased dielectric lead to increased swelling degree in the higher ionic samples.

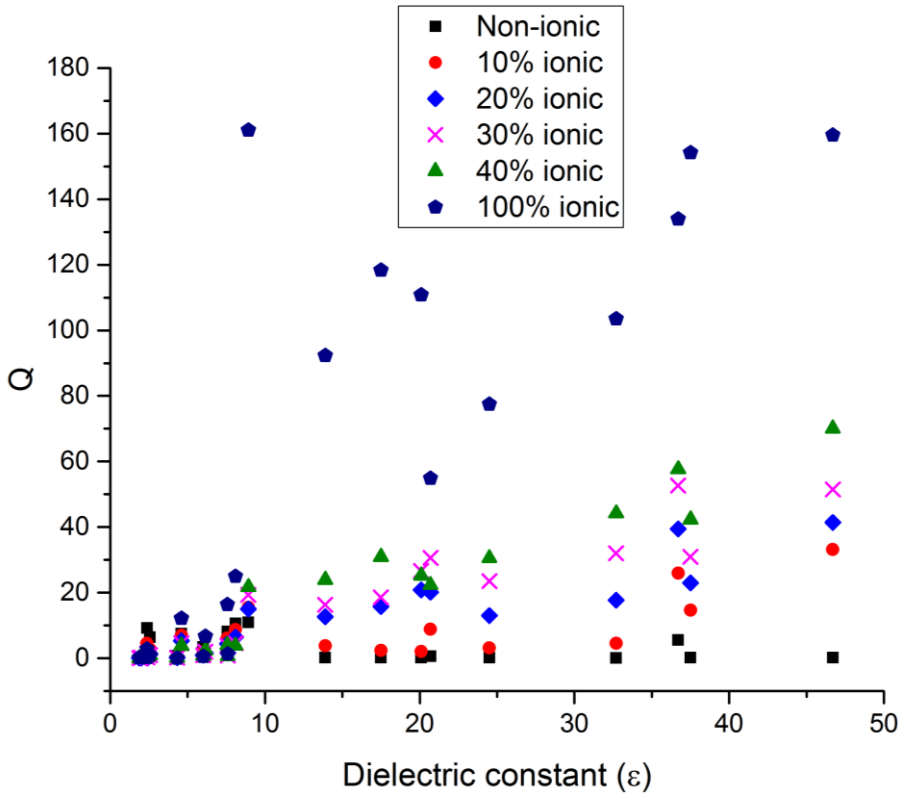

Figure 2.8 - The Q value for all the solvents in each of the 6 polymers plotted against the dielectric constant of the solvents.

When the 100 % and 40 % ionic polymers were observed in more detail (Figure 2.9), it was clear that the increase in dielectric is not so proportional to the swelling degree. These two polymers showed high swelling in solvents across the mid-range of dielectric as well as the high. This was especially pronounced in the 100 % sample.

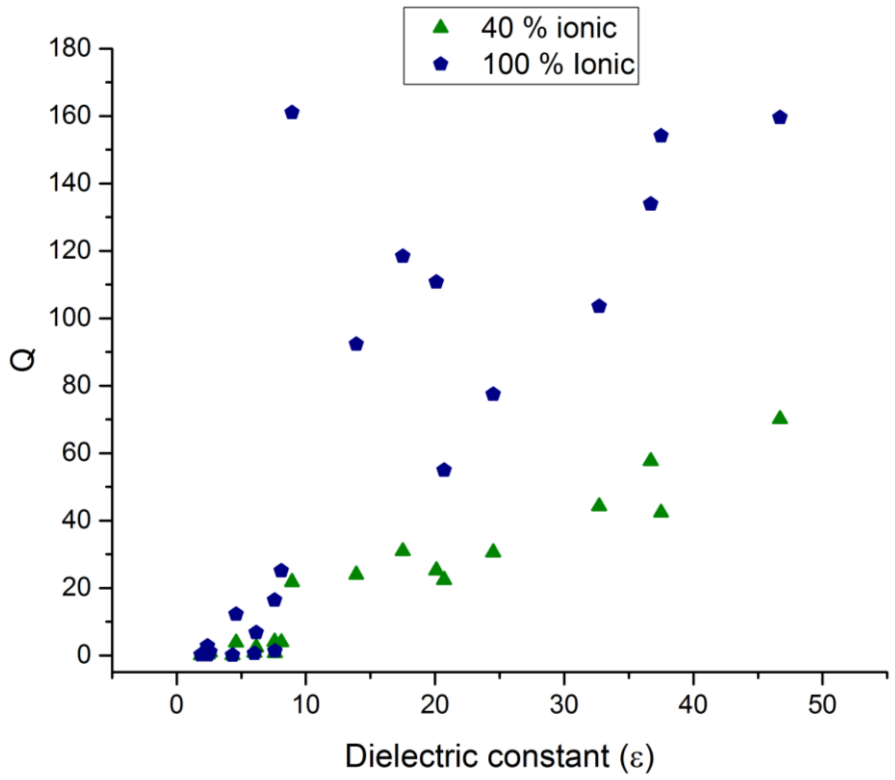

Figure 2.9 – An expansion of the dielectric constant vs swelling performance for the 40 % and 100 % ionic polymers.

Estimating swelling magnitude based upon dielectric alone may be useful for solvents at the far ends of the dielectric scale, but less useful in the middle where the swelling differences are less distinct.

2.3.5 Determination of the polymer HSPs

Gathering of the HSPs of the polymers in this system required the swelling of each solvent to be graded for each polymer. The solvents were designated as 'good' or 'bad' for the HSPiP software so that it could generate a solubility sphere. The software was coded so that it could be instructed in a binary fashion with the solvents designated 'good' or 'bad', or instructed with a grading system (1 to 6) which would take into account the relative 'goodness' of each solvent in a specific data set. Using the binary system would lead to a less accurate solubility sphere. The swelling abilities for this work were graded relative to the other solvents for the chosen polymer. The full range of values for the grading (1 to 6, 1 = best) were calculated as;

$$Grade = 6 - \left(\frac{Q}{Q_{max}}\ x\ 5\right)$$

(Equation 2.4)

Where Q was the degree of swelling of the solvent in question, and Q_{max} was the swelling degree of the highest swelling solvent in the dataset of the chosen polymer. The grade was then rounded to the closest integer value. For example: the grade for ethanol (Q = 23) in the 20 % ionic content polymer, where the highest swelling degree achieved was DMSO (Q = 51.5), would be 2 (2.23). Following the grading of the swelling performance of each solvent, the data for each polymer was plotted as a sphere in HSPiP. The polymers swelled (or didn't) based upon the compatibility between the matrix and the solvent. Therefore plotting a sphere would mean that the centre of the sphere represented the coordinates of a perfectly compatible solvent: and in turn, the solubility parameters of the polymer itself. The centre coordinates of the spheres were extracted to give an experimentally derived set of HSPs for each of the 6 polymers (Table 2.2). There was a significant increase in hydrogen bonding and polarity component weighting as the ionic content increased. The increase in polarity component was a natural expectation of adding the ionic moiety. The increase in hydrogen bonding component was unanticipated as the quaternary nitrogen species does not strictly contain any hydrogen bond accepting site. The δh value increase was simply an artefact of the system having absorbed solvents with high hydrogen bonding ability, such as ethanol and methanol, causing the sphere to form with significant weighting towards the δh parameter. It was important to note that the HSP values for the polymers did not change after 20 % ionic monomer addition which suggest that either the solubility characteristics of the polymers did not change with increasing ionic content or that another factor was influencing the degree of swelling beyond solvent compatibility. The observation that the swelling magnitudes continued to change, yet the solubility parameters of the polymers remained the same past 20 % ionic content was concerning. This demonstrated a potential flaw in prediction capability with respect to swelling magnitude when utilizing solubility parameter data.

Table 2.2 – The solubility parameters for each of the polymers synthesised which were extracted from the spheres generated in HSPiP using the graded swelling data.

Polymer ID	δd	δp	δh
$St_{100}Ion_0$	19.5	7.1	7.7
$St_{90}Ion_{10}$	19.3	14.6	6.2
$St_{80}Ion_{20}$	19.2	15.6	14.8
$St_{70}Ion_{30}$	19.2	15.7	14.8
$St_{40}Ion_{60}$	19.2	15.6	14.9
St_0Ion_{100}	19.2	15.6	14.9

2.3.6 Relationship between swelling and Ra

The sphere derived HSP parameters for the polymers were used to calculate the Ra value of each polymer against each of the solvents. HSP values for the solvents were either taken from the internal solubility parameter database found in the *Hansen solubility parameters in practice* (HSPiP) software or, if data did not exist, calculated using the Y-MB solubility parameter estimation tool in this software. The data for all the Ra values and the parameters used for each solvent are given in Appendix 2B. The Ra was then plotted against each set of polymer Q values to determine if there was a relationship between swelling and Ra (Figure 2.10).

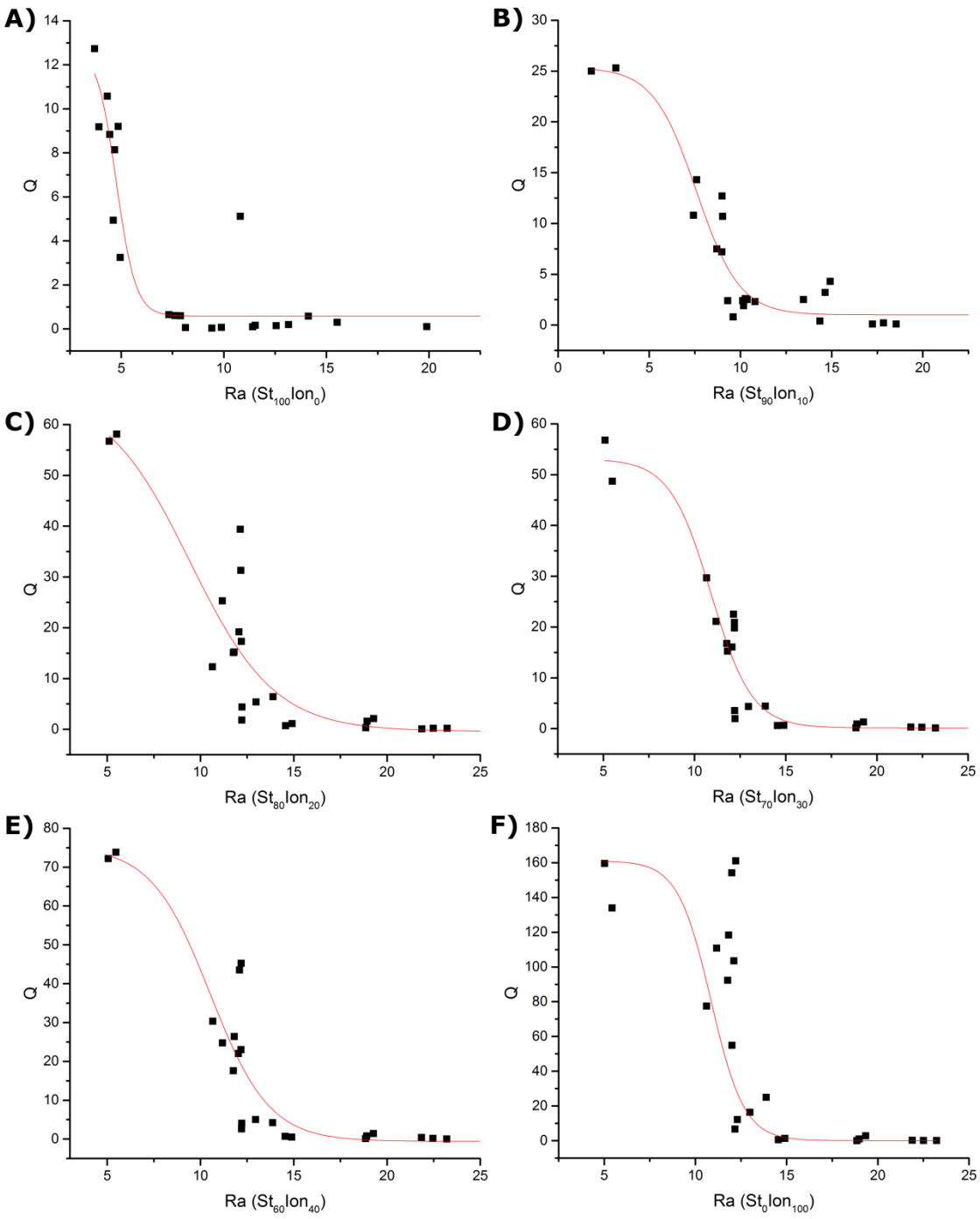

Figure 2.10 – A) Ra vs Q for the non-ionic polymer, B) Ra vs Q for the 10 % ionic polymer, C) Ra vs Q for the 20 % ionic polymer, D) Ra vs Q for the 30 % ionic polymer, E) Ra vs Q for the 40 % ionic polymer, F) Ra vs Q for the 100 % ionic polymer.

The graphs of Ra vs. swelling were fitted each with a Boltzmann function which showed good fitting ($R^2_{0\ \%\ ion}$ = 0.8466, $R^2_{10\ \%\ ion}$ = 0.8831, $R^2_{20\ \%\ ion}$ = 0.7535, $R^2_{30\ \%\ ion}$ = 0.9018, $R^2_{40\ \%\ ion}$ = 0.7937, $R^2_{100\ \%\ ion}$ = 0.6901). The graphs showed that as the Ra decreased, the swelling

increased. This was expected when using the experimental data to form the polymer solubility parameters. One obvious drawback was that there seemed to be a very narrow band of Ra values across which a solvent would exhibit swelling at either extreme of the range. The exponential nature of the relationship was an issue for any practical applications of the model. For example, a solvent which may have showed an Ra of 12.5 against the 100% ionic polymer could be reasonably expected to show swelling anywhere between Q = 5 and Q = 180.

2.3.7 Correlation of swelling against dielectric and Ra

The HSP's showed no dramatic shift for the copolymer networks after 20 %, yet there were significant and continued changes in swelling magnitude. It was believed that there was therefore a deficit in the information, and subsequent predictions, which could be obtained from the Hansen parameters alone. Figure 2.8 showed how correlating the swelling with dielectric exhibited a reasonably good relationship. Plotting both the dielectric and Ra against the swelling degree was considered as a way to better understand the swelling of the system, and overcome the weaknesses of their respective correlations. Further to this, the ionic content of the polymer needed to be accounted for. The concentration of free ions, and therefore the all-important osmotic pressure in the polymer gel, was directly proportional to the concentration of ionic monomer. A suitable term to take into account the effects of the dielectric and the ionic fraction was developed. This was known as 'ε x n' where ε was the dielectric constant of the solvent and n was the ionic fraction of the polymer (0, 1, 2, 3, 4, 10, for the 0 %, 10 %, 20 %, 30 %, 40 % and 100 % polymers respectively). This term was expected to give the correct weighting to the swelling contribution from the osmotic pressure, with respect to the polymer/solvent combination. The Q_v and Ra was subsequently plotted against $-\log_{10}$ (ε x n) (Figure 2.11). The Ra would continue to represent the compatibility of all solvents with the polymers. The volume swelling data (Q_v) was used for this correlation as it provided a better fitment than the mass (Q) swelling.

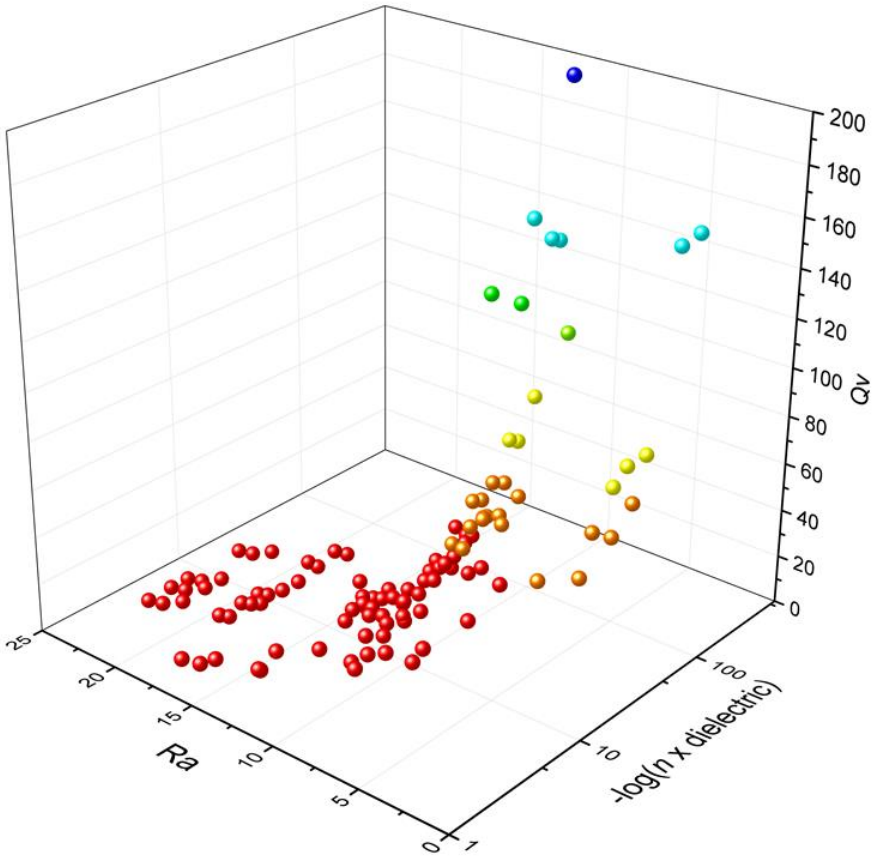

Figure 2.11 – A plot of all the polymer swelling data, where the Q_v is plotted against both the Ra and (n x ε).

The correlation was also presented in Figure 2.12 as a 2D heat map of the swelling performance. These two representations demonstrated that for a polymer to swell the system to a very high degree there must be a low Ra (good compatibility) in addition to the solvent having a high dielectric, especially when the swelling is to be improved by utilization of an ionic monomer. The compatibility allows diffusion of the solvent into the matrix, and the high dielectric permits dissociation of the ion pair, leading to a higher concentration of free ions in the gel. The increase in free ions increases the osmotic pressure and drives the high swelling in the polyelectrolyte.[22] The perturbation in the centre of the heat map was due to the anomalously high swelling performance of the dichloromethane.

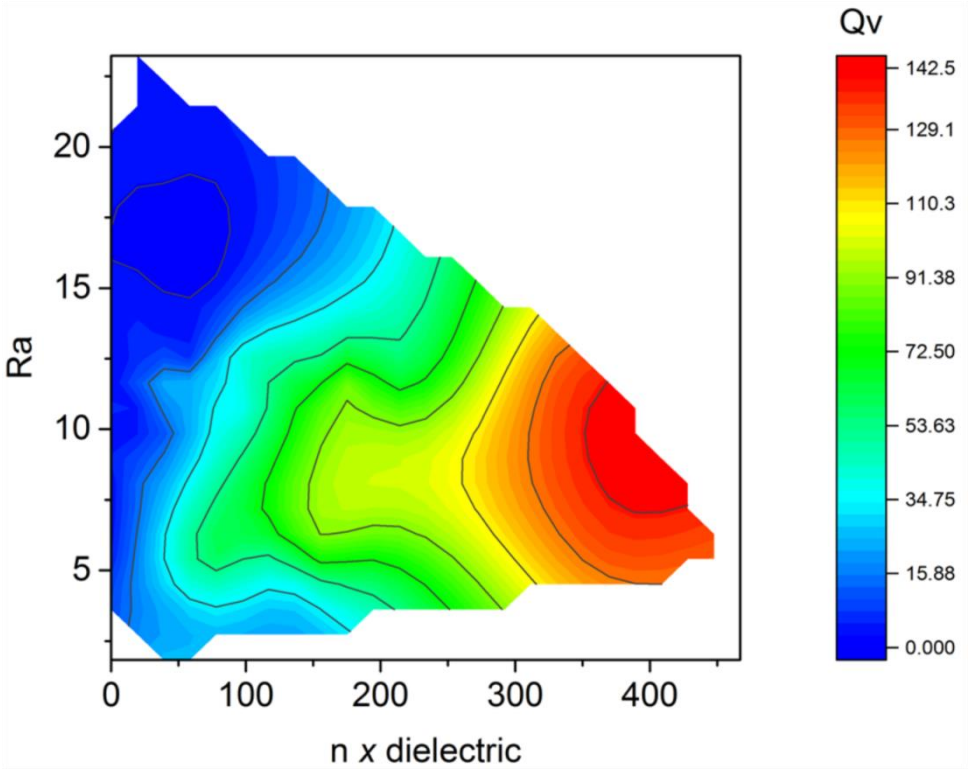

Figure 2.12 – A 2D colour mapped representation of the Q_v, Ra and (n x ε) correlation results.

2.3.8 Prediction of solvent swelling

The purpose of the correlation of the swelling with HSPs and dielectric was not only to demonstrate the correlation, but also to see whether the data could be fed back into a mathematical model to generate accurate predictions of swelling behaviour in this system. To form a predictive model, linear regression analysis was carried out of the Q_v for all of the data gathered (each of the solvents in each polymer) against both the Ra and $n \; x \; \varepsilon$ (**Figure 2.13**). The regression analysis was performed using Microsoft Excel's data processing function. The Q_v was then predicted for solvents of unknown swelling performance by using the formula;

$$Q_v = I + (a \; x \; Ra) + (b \; x \; n\varepsilon)$$

(Equation 2.5)

Where I = 8.037317, a = -0.57503 and b = 0.411456, which were calculated from the regression analysis. A linear fit between the predicted Q_v from the regression and the experimental Q_v presented an R^2 = 0.8308.

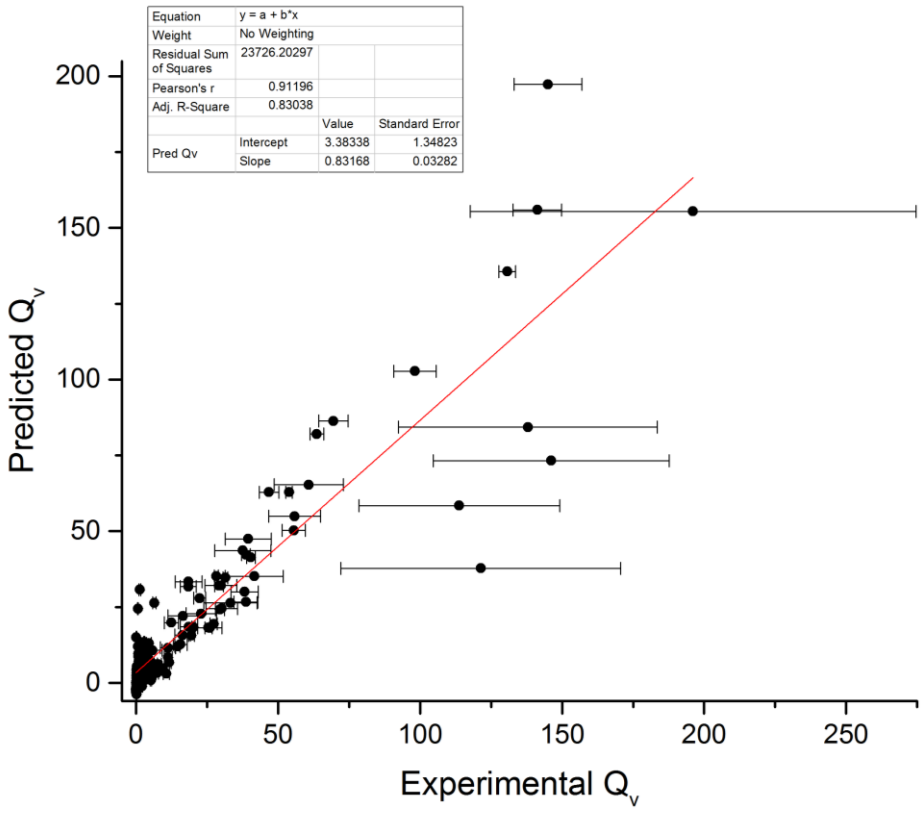

Figure 2.13 – The predicted Q_v plotted against the experimental Q_v with error, for all 132 polymer / solvent combinations. The predicted Q_v for each polymer and solvent combination was obtained through utilizing equation 2.5. The red line represents the linear fit of the data with an R^2 = 0.8308.

Ra would be calculated from the solvent parameters of the unknown solvent and the polymer from the data in section 2.3.5.

2.3.9 Testing the predictive model

The predicted swelling was calculated from equation 2.5 for four solvents which had not previously been studied in this work. These were propylene carbonate (ε = 64.9); a highly polar high melting point solvent, 1-4,dioxane (ε = 2.25); a low polarity heterocycle, methyl benzoate (ε = 6.6); a CWA physical simulant candidate and butanone (ε = 18.5) which has intermediate dielectric constant value. The values for the Ra and nε in each of these solvent are presented in Table 2.3.

Table 2.3 – All of the values for nε, Ra, and the subsequently predicted Q_v for the 4 solvents.

Solvent	Polymer ionic %	Calculated Ra	nε	Predicted Qv
Propylene carbonate	0	11.5	0	1.4
	10	4.23	64.9	32.3
	20	11.1	129.8	55.1
	30	11.1	194.7	81.8
	40	11.2	259.6	108.4
	100	11.2	649	268.6
Dioxane	0	6.77	0	4.1
	10	13.6	2.25	1.1
	20	15.4	4.5	1.1
	30	15.4	6.75	1.9
	40	15.4	9	2.9
	100	15.4	22.5	8.4
Methyl Benzoate	0	3.41	0	6.1
	10	6.62	6.6	6.9
	20	12.5	13.2	6.3
	30	12.6	19.8	8.9
	40	12.6	26.4	11.6
	100	12.6	66	27.9
Butanone	0	7.71	0	3.6
	10	8.73	18.51	10.6
	20	13.4	37.02	15.6
	30	13.4	55.53	23.2
	40	13.4	74.04	30.8
	100	13.4	185.1	76.5

Across the board, the predicted swelling was found to be in line with the experimental swelling to a good standard, with a correlation between the two sets of data having an $R^2 = 0.9825$ (Figure 2.14).

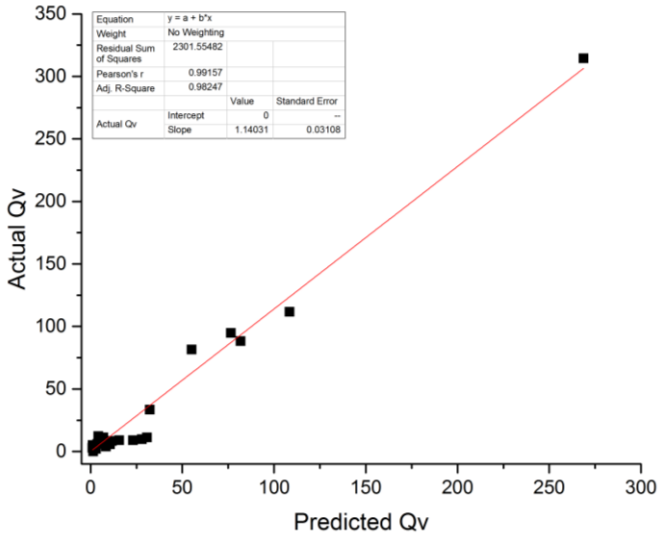

Figure 2.14 – Predicted and experimental Qv values for the four solvents tested in the 6 polymers. The correlation showed an adjusted R^2 value = 0.9825.

The results for each of the individual solvents are presented in Figure 2.15. Exceptional swelling ability was shown for the propylene carbonate, nearly reaching Qv = 300 in the 100 % ionic polymer. The trend and magnitudes of the predicted swelling were extremely closely aligned in this solvent. The predictions for methyl benzoate showed good similarity to the experimental results in trend and magnitude, with exception to the 100 % ionic network where the predicted swelling value (Q = 27) was nearly three times that of the experimental value. The model predicted the trends and magnitudes of the swelling for both propylene carbonate and butanone well when compared to the experimental results. The experimental swelling of dioxane presented a unique trend where the swelling decreased from (Q = 12) 0 % to (Q = 2) 30 % ionic content, where it then increased slightly back up to 100 % ionic content (Q = 4). The predictions were able to show this trend. An explanation for this swelling behaviour was that dioxane was incompatible in terms of Ra with the ionic monomer. This incompatibility caused the decrease in swelling to 30 % ionic content at which point the Ra stabilized at 15.4. After 30 % ionic content, the $n \times \varepsilon$ (osmotic effects) term became dominant which caused the swelling to increase slightly with increasing ionic content. The dioxane experiment showed how important the combination of Ra and $n \times \varepsilon$ were in understanding the swelling behaviour.

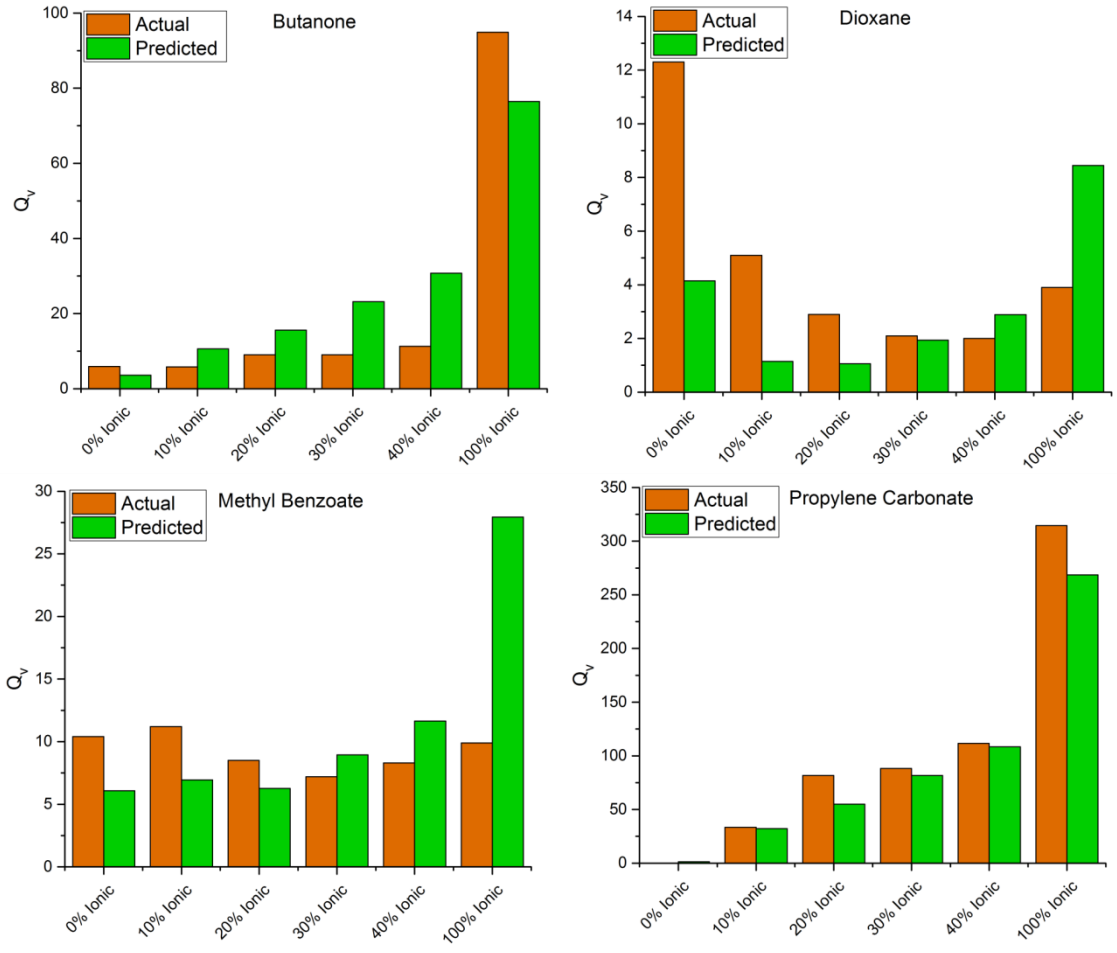

Figure 2.15 – The predicted and experimental volume swelling of each of the 4 additional solvents; propylene carbonate, dioxane, butanone and methyl benzoate. The orange bars represent the experimental swelling and the green the predicted values.

2.3.10 Prediction of CWA swelling behaviour

Using the same process as in section 2.3.9, the predicted swelling of VX, sulfur mustard, and sarin were calculated. The dielectric constant for each of the CWAs was gathered from a literature source (ε_{VX} = 10.0, ε_{HD} = 10.7, and ε_{sarin} = 13.2).[23] The Ra of the agents and polymers was calculated using HSP values which were estimated using the Y-MB tool of the HSPiP software, as none were available in literature (Table 2.4).

Table 2.4 – A table showing the predicted Q_v, calculated Ra and *n x ε* for sarin, VX and HD (sulfur mustard). The HSPs for each agent used to calculate the Ra against each polymer are shown beside their name.

CWA (δd, δp, δh)	Polymer Ionic (%)	Calculated Ra	N x ε	Predicted Q_v
Sarin (16.4, 12.6, 6.1)	0	8.36	0	3.2
	10	6.15	13.2	9.9
	20	10.37	26.4	12.9
	30	10.4	39.6	18.4
	40	10.45	52.8	23.8
	100	10.45	132	56.3
VX (17.5, 11.0, 6.1)	0	5.81	0	4.7
	10	5.09	10	9.2
	20	10.41	20	10.3
	30	10.46	30	14.4
	40	10.5	40	18.5
	100	10.5	100	43.1
Sulfur Mustard (18.8, 8.4, 5.1)	0	3.23	0	6.2
	10	6.38	10.7	8.8
	20	12.11	21.4	9.9
	30	12.17	32.1	14.2
	40	12.19	42.8	18.6
	100	12.19	107	45.1

The data from the predictions anticipated that in general, the swelling of all agents would increase as the ionic content of the polymer was increased. The swelling magnitudes of each would also be similar.

2.3.11 Swelling results of the polymers in CWAs

The predictive ability of the swelling model was demonstrated on laboratory solvents, and the predicted Q_v of three CWAs was calculated with the same model. The penultimate task was to test the swelling ability of these polymers in the CWAs. The experimental swelling of the agents could then be compared to the predicted values. The measurements were not repeated in triplicate due to the costs and safety considerations involved in testing the agents. Tests were performed using the polystyrene and 10, 20, 30 and 40 % ionic content polymers. The

agents tested were VX, sarin and sulfur mustard and were contrasted with the predicted values (Figure 2.16).

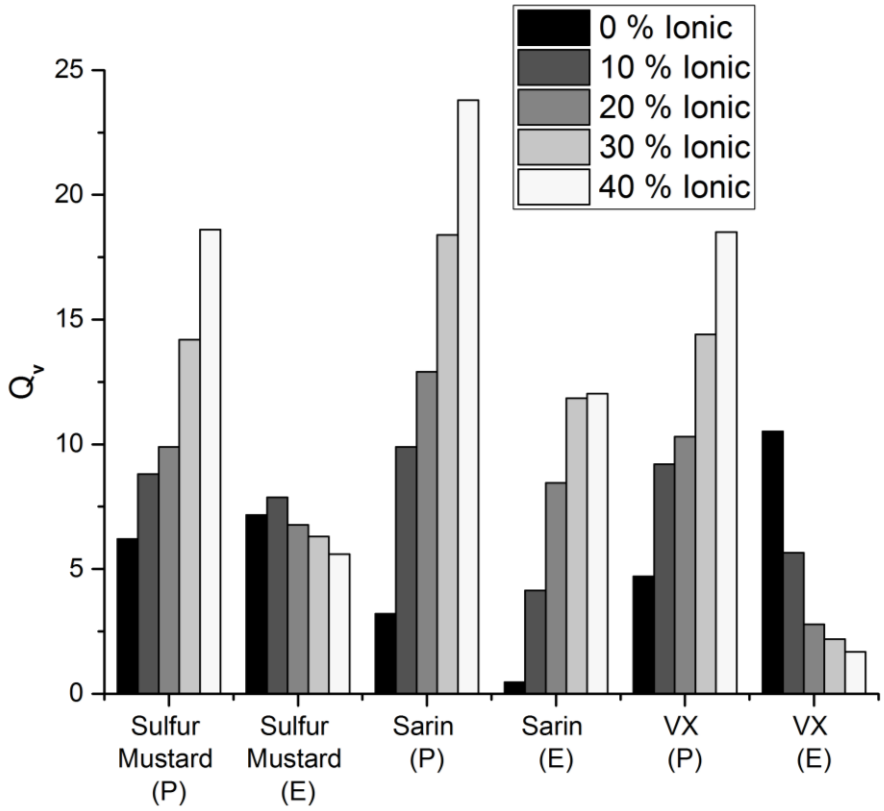

Figure 2.16 – The experimental (E) and predicted (P) swelling performance of sulfur mustard (HD), sarin (GB) and VX in the 0-40 % ionic polymers.

The sulfur mustard showed a slight decrease in swelling with increased ionic content. The VX also showed a decrease in swelling with increased ionic content, although more sudden than the sulfur mustard. The predictions were distinctly incorrect for these two agents. Sarin displayed an increase in swelling with ionic content which was also displayed by the predictions however the actual magnitudes of the swelling varies wildly. Figure 2.17 demonstrates the lack of correlation between the predicted and experimental Q_v for the CWAs. Section 2.3.7 demonstrated that for high swelling, high dielectric of the solvents was required. Because of the low dielectric of all the agents, it was unlikely that extremely high swelling would be achieved as the agents would not be able to dissociate the ionic pairs, to increase the osmotic pressure inside the matrix. The predictions for Ra were gathered using

the Y-MB tool and were likely the most unreliable aspect of the process. The complex functionalities around the phosphorus in sarin and VX may have been especially inaccurate as the function has not been documented with phosphorus centres.[24] The Ra was likely one of the largest faults in the prediction of the CWA swelling.

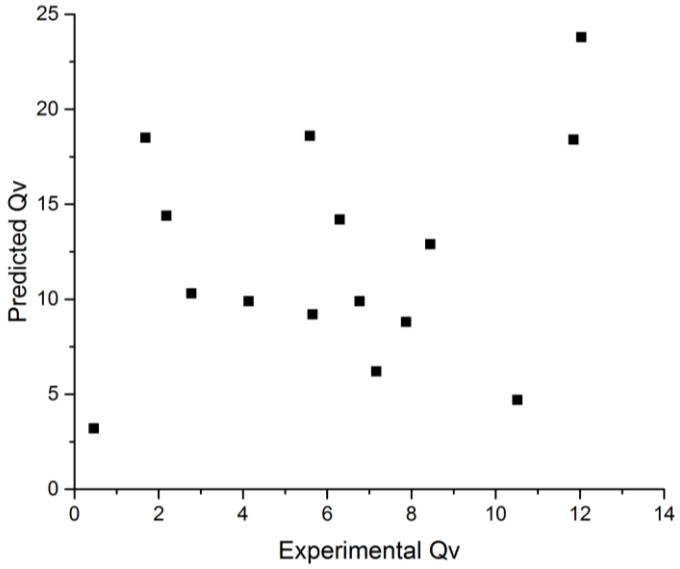

Figure 2.17 – The predicted and experimental Q_v for the CWA swelling.

In general, none of the agents were appreciably absorbed by any of the polymer samples. These results show that not only were all the agents restricted to relatively low magnitudes of swelling for this system, but also that the sarin showed vastly different swelling trend to the VX and sulfur mustard. Due to the different swelling trends of the CWAs, a polymer able to absorb all three agents equally would likely not be a viable target. An effective VX, and sulfur mustard absorbent may however be possible based upon this data as these two agents showed similar trends with respect to ionic content.

2.4 Simulant selection

Armed with the results obtained from the swelling of real CWAs in the polymers, it was then decided to use this data to determine a set of simulants which would be physically suitable for the examination of swelling performance in later trials. The results obtained on the CWAs gave

not only a magnitude of swelling, but also a trend in swelling which would be matched in order to determine the ability of a simulant to represent an agent effectively. The work started by probing the HSP's of the CWAs through HSPiP using the Y-MB prediction tool and then the solvent database was searched to obtain a selection of solvents which may be suitable for each of the CWA's. The closest matches (Figure 2.18) were selected for testing in this polymer system. Methyl benzoate was selected as a simulant for sulfur mustard. 2-chhloroethyl ethyl sulfide (also known as half mustard) is a common simulant for sulfur mustard but it was found it was not as closely matched with HSP's as methyl benzoate. 2-CEES is also quite toxic and very expensive to use. N-N-Diethylacetamide was selected for sarin based purely on the HSP matching, similarly to 5-phenyl-1-penatanol for the VX.

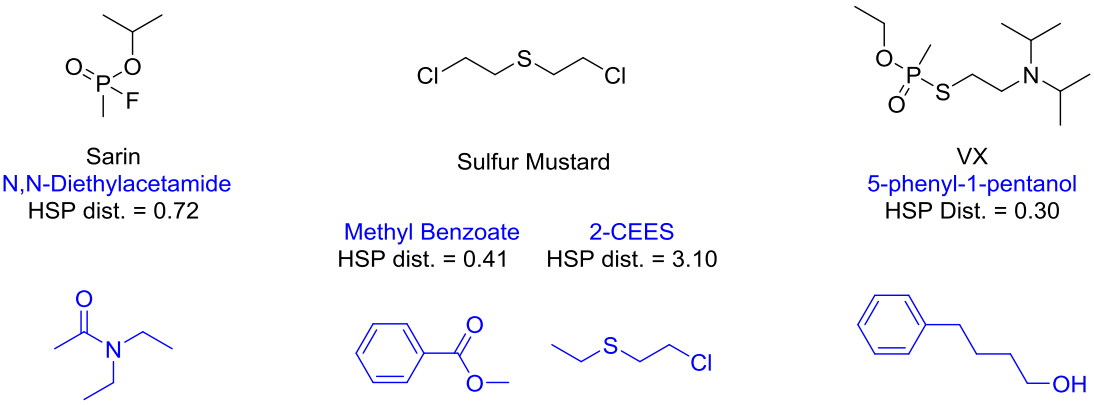

Figure 2.18 – Sarin, HD and VX (black) along with a proposed physical simulant (blue) for each based upon the HSP matching of the agents and potential simulants. The Ra between the agent and simulants is presented.

The simulants were tested in the same manner as that of the agents, and the swelling of each is presented against the respective simulant below (Figure 2.19).

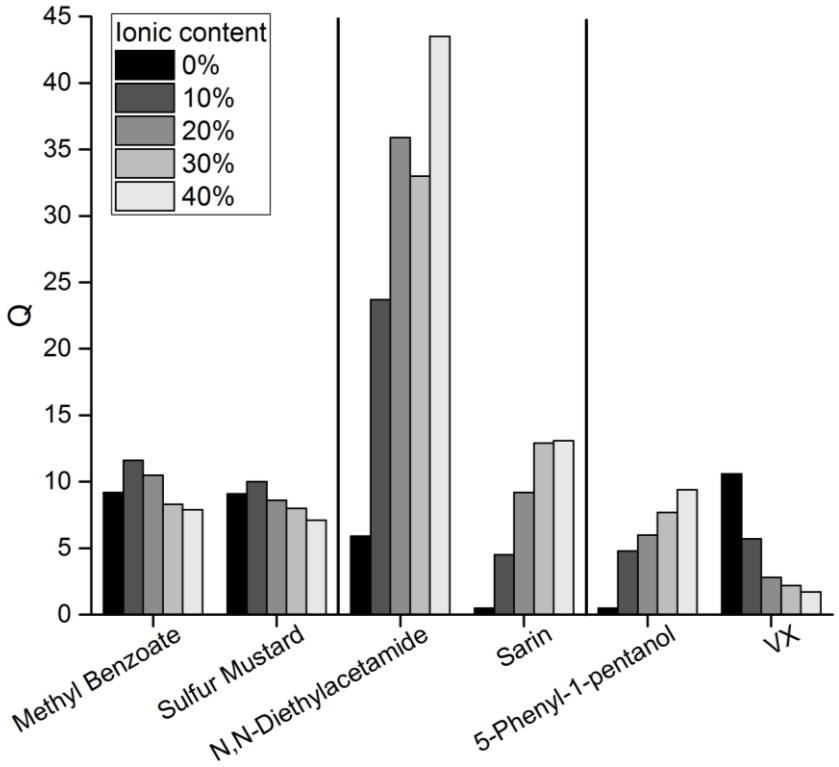

Figure 2.19 – The swelling of HD, sarin and VX alongside the simulant chosen to represent them. Swelling was conducted in 5 of the polymers (0 % ionic to 40 % ionic).

It was evident from the graph that the simulant for VX, 5-phenyl-1-pentanol, was completely unsuitable for the simulation of VX. Not only was the swelling trend wrong (Q = 1 to Q = 10 instead of the inverse in VX), but the magnitude of the increase relative to the polymer composition was also wrong. The simulant for sarin, N,N-diethylacetamide, exhibited the correct trend, yet the magnitude of the swelling vastly exceeded the swelling of the sarin. Of the proposed simulants, only methyl benzoate showed similar swelling characteristic to its target compound. Not only was the correlation more than acceptable, but the availability of this solvent as a much cheaper system with very low hazard would allow testing on kilogram scales to be carried out with little risk. It was hoped that this simulant may also have been useful as a VX simulant, due to the similar swelling magnitude and trends, especially in the low ionic systems.

2.5 Conclusions

In this chapter, the swelling of 6 polymers in a range of common laboratory solvents was observed. Swelling maxima was observed in fully ionic polyelectrolyte gels with the highest swelling being seen in the most polar / highest dielectric solvents (acetonitrile Q = 150 and DMSO Q = 155). The lowest swelling performance was shown by the least polar solvents, such as hexane and diethyl ether. When the swelling was correlated with dielectric of the solvent, general trends were observed, but at 40% and 100% ionic content, the correlation was weak. The solvent parameters for each of the 6 polymers were extracted from the swelling data through use of the HSPiP software, and it was found that the values did not change after the inclusion of 20% ionic content. The deficit in available information which could be extracted with the HSPs of the polymers was observed when the Ra was plotted against swelling. There was a very small fringe of Ra values for which the swelling would be either good or bad. By combining the Ra with the dielectric of the solvent, and taking into account the ionic fraction of the polymer; a model was developed for the prediction of swelling in this system. These terms in the model utilized both the compatibility of the components, as well as the osmotic effects of having an ionic monomer in the polymer. The model was able to predict the swelling of 4 other solvents with varying dielectric and Ra values. For these predictions, the trends for swelling against ionic content were seen to be correct, and the magnitudes were within respectable boundaries. This showed that the model was effective at predicting the swelling of solvents where only the Ra and dielectric was known. The final part of this chapter looked at the swelling of CWAs. The swelling of VX, sarin and HD was predicted from literature dielectric constants, and Ra values calculated from HSPiP. The agents only swelled experimentally small amounts, and did not correlate with the predictions. The low swelling was likely due to the agents' low dielectric constants and low levels of compatibility with the ionic portion of the matrix. The low dielectric of the agents prevented them from being able to exploit the ionic content of the polymers. More specifically, they were unable to dissociate the ion pairs which

would lead to higher free ions in solution, and therefore higher osmotic pressure inside the polymer gel, increasing the swelling. The swelling did show that the mustards and V agents prefer low polarity systems and the G agents prefer higher ionic content. From the agent swelling results, a good physical simulant (methyl benzoate) was chosen to represent both the V agents and mustards in any further work.

2.6 References

1 E. M. Ahmed, *J. Adv. Res.*, 2015, **6**, 105–121.

2 E. Caló and V. V. Khutoryanskiy, *Eur. Polym. J.*, 2015, **65**, 252–267.

3 S. Lankalapalli and V. R. M. Kolapalli, *Indian J. Pharm. Sci.*, 2009, **71**, 481–7.

4 A. Vintiloiu and J.-C. Leroux, *J. Control. Release*, 2008, **125**, 179–192.

5 B. Bolto and J. Gregory, *Water Res.*, 2007, **41**, 2301–2324.

6 I. Ohmine and T. Tanaka, *J. Chem. Phys.*, 1982, **77**, 5725–5729.

7 A. El Halah, J. Contreras, L. Rojas-Rojas, M. Rivas, M. Romero and F. López-Carrasquero, *J. Polym. Res.*, 2015, **22**, 233.

8 F. Ganji, S. Vasheghani-Farahani and E. Vasheghani-Farahani, *Theoretical Description of Hydrogel Swelling: A Review*, 2010, vol. 19.

9 T. Ono, T. Sugimoto, S. Shinkai and K. Sada, *Nat. Mater.*, 2007, **6**, 429–433.

10 T. Ono, T. Sugimoto, S. Shinkai and K. Sada, *Adv. Funct. Mater.*, 2008, **18**, 3936–3940.

11 K. Iseda, M. Ohta, T. Ono and K. Sada, *Soft Matter*, 2011, **7**, 5938.

12 W. J. Horne, M. A. Andrews, K. L. Terrill, S. S. Hayward, J. Marshall, K. A. Belmore, M. S. Shannon and J. E. Bara, *ACS Appl. Mater. Interfaces*, 2015, **7**, 8979–8983.

13 J. Yuan, D. Mecerreyes and M. Antonietti, *Prog. Polym. Sci.*, 2013, **38**, 1009–1036.

14 S. G. Starodoubtsev, A. R. Khokhlov, E. L. Sokolov and B. Chu, *Macromolecules*, 1995, **28**, 3930–3936.

15 A. R. Khokhlov and E. Y. Kramarenko, *Macromol. Theory Simulations*, 1994, **3**, 45–59.

16 K. Iseda, M. Ohta, T. Ono and K. Sada, *Soft Matter*, 2011, **7**, 5938.

17 T. Ono, T. Sugimoto, S. Shinkai and K. Sada, *Adv. Funct. Mater.*, 2008, **18**, 3936–3940.

18 C. M. Hansen, *Hansen solubility parameters : a user's handbook*, CRC Press, 2007.

19 E. Stefanis and C. Panayiotou, *Int. J. Thermophys.*, 2008, **29**, 568–585.

20 S. Abbott, C. Hansen and H. Yamamoto, Yamamoto-Molecular Break (Y-MB) in HSPiP, http://www.pirika.com/NewHP/Y-MB/Y-MB.html, (accessed 15 September 2018).

21 Polymer Chemistry, Guide to the presentation of experimental data, http://www.rsc.org/journals-books-databases/journal-authors-reviewers/prepare-your-article/experimental-data/#data-presentation, (accessed 27 July 2018).

22 F. Horkay, I. Tasaki and P. J. Basser, *Biomacromolecules*, 2000, **1**, 84–90.

23 L. L. Szafraniec and W. J. Shuely, *Dielectric constant measurement employing an NMR technique and an onsager calculation of dipole moment: organophosphorus and organosulfur liquids*, Maryland, USA, 1988.

24 S. Abbott, C. Hansen and H. Yamamoto, Hansen Solubility Parameters in Practice e-Book, https://www.pirika.com/ENG/HSP/E-Book/index.html, (accessed 15 September 2018).

2.7 Appendix 2A

Table 2.5 – The Q values for each of the swollen polymer/solvent combinations

Solvent	**Q 0%**	**Error 0%**	**Q 10%**	**Error 10 %**	**Q 20%**	**Error 20%**	**Q 30%**	**Error 30%**	**Q 40%**	**Error 40%**	**Q 100%**	***Error 100%***
DCM	11.0	1.27	15.5	0.95	15.0	1.84	19.3	1.20	21.7	3.62	161.0	65.34
THF	8.2	0.78	6.2	1.02	4.4	0.75	3.9	0.31	4.0	0.68	16.4	2.52
Bromopropane	10.6	0.16	8.7	1.49	6.5	0.25	4.6	0.17	3.9	0.29	25.0	6.34
Xylene	6.4	0.36	2.7	0.38	1.3	0.24	1.0	0.09	0.9	0.26	1.0	0.14
Ethoxyethylacetate	4.5	0.26	2.6	0.09	1.6	0.37	0.9	0.19	0.7	0.16	1.3	0.36
Toluene	9.3	0.98	4.6	0.25	1.9	0.17	1.4	0.08	1.3	0.08	2.8	0.59
Benzylamine	7.5	1.28	7.0	0.14	5.3	0.74	4.6	0.75	3.8	0.14	12.2	2.39
Ethyl Acetate	3.4	1.68	2.0	0.33	1.0	0.25	0.9	0.22	0.8	0.08	0.6	0.08
Diethyl ether	0.7	0.09	0.3	0.08	0.2	0.08	0.2	0.08	0.1	0.08	0.1	0.09
Acetone	0.6	0.05	8.9	2.08	20.2	1.03	30.6	3.33	22.4	0.59	54.9	4.11
triethylamine	0.5	0.05	0.1	0.05	0.1	0.05	0.3	0.05	0.3	0.08	0.2	0.08
Dodecane	0.1	0.05	0.2	0.05	0.1	0.08	0.2	0.05	0.2	0.05	0.2	0.05
Hexane	0.0	0.05	0.1	0.05	0.1	0.08	0.0	0.05	0.0	0.00	0.2	0.09
Pentanol	0.2	0.09	3.8	1.02	12.7	1.96	16.4	0.47	23.9	1.29	92.3	28.64
DMF	5.6	0.71	25.9	1.20	39.5	9.68	52.7	3.88	57.6	11.59	133.9	8.12
Acetic acid	0.3	0.05	0.9	0.09	1.6	0.33	2.1	0.09	2.4	0.17	6.7	0.61
Butanol	0.2	0.05	2.4	0.05	15.8	0.85	18.6	4.34	30.9	3.89	118.4	33.65
DMSO	0.2	0.05	33.2	6.15	41.4	10.9	51.5	3.77	70.1	2.60	159.6	13.13
1-Propanol	0.2	0.05	2.0	0.60	20.9	3.41	26.7	7.57	25.2	0.68	110.8	36.58
Acetonitrile	0.2	0.05	14.6	2.39	23.0	1.19	31.0	6.36	42.3	0.94	154.1	61.64
Ethanol	0.2	0.08	3.1	0.57	13.0	4.15	23.6	4.43	30.5	1.20	77.5	5.90
Methanol	0.1	0.05	4.6	2.71	17.7	1.68	32.0	1.18	44.2	7.22	103.5	2.34

2.8 Appendix 2B

Table 2.6 – The HSP for each solvent and the Ra values for each solvent/polymer combination. Hansen solubility parameters are measured in $Mpa^{1/2}$.

Solvent	δd	δp	δh	Ra $St_{100}Ion_0$	Ra $St_{90}Ion_{10}$	Ra $St_{80}Ion_{20}$	Ra $St_{70}Ion_{30}$	Ra $St_{40}Ion_{60}$	Ra St_0Ion_{100}
DCM	17.0	7.3	7.1	5.04	8.68	12.15	12.22	12.21	12.21
THF	16.8	5.7	8.0	5.59	10.37	12.93	13.01	12.99	12.99
Bromopropane	16.4	7.9	4.8	6.89	8.97	13.81	13.86	13.88	13.88
Xylene	17.8	1.0	3.1	8.36	14.27	18.92	19.00	18.98	18.98
Ethoxyethylacetate	15.8	5.5	6.3	7.70	11.48	14.85	14.92	14.91	14.91
Toluene	18.0	1.4	2.0	8.60	14.09	19.27	19.34	19.33	19.33
Benzylamine	19.0	4.6	9.4	3.18	10.52	12.26	12.35	12.30	12.30
Ethyl Acetate	15.8	5.3	7.2	7.63	11.68	14.49	14.57	14.55	14.55
Diethyl ether	14.5	2.9	4.6	11.28	15.22	18.81	18.87	18.86	18.86
Acetone	15.5	10.4	7.0	8.68	8.72	11.94	11.99	12.01	12.01
Triethylamine	15.5	0.4	1.0	12.40	16.92	21.82	21.89	21.89	21.89
Dodecane	16.0	0.0	0.0	12.60	17.18	22.44	22.51	22.50	22.50
Hexane	14.9	0.0	0.0	13.94	18.14	23.16	23.23	23.22	23.22
1-Pentanol	15.9	5.9	13.9	9.58	13.46	11.77	11.85	11.77	11.77
DMF	17.4	13.7	11.3	8.61	6.42	5.37	5.40	5.43	5.43
Acetic acid	14.5	8.0	13.5	11.60	13.75	12.16	12.22	12.17	12.17
1-Butanol	16.0	5.7	15.8	10.80	14.66	11.83	11.91	11.82	11.82
DMSO	18.4	16.4	10.2	9.88	4.74	4.94	4.92	5.03	5.03
1-Propanol	16.0	6.8	17.4	11.97	15.16	11.19	11.27	11.16	11.16
Acetonitrile	15.3	18.0	6.1	13.85	8.69	11.93	11.91	12.00	12.00
Ethanol	15.8	8.8	19.4	13.95	16.03	10.66	10.72	10.62	10.62
Methanol	14.7	12.3	22.3	18.23	18.69	12.17	12.20	12.11	12.11

Chapter 3 -
Chemical Modification of a *net*-Styrene-*co*-Divinylbenzene-*co*-QAS Polyelectrolyte: Towards a Better Swelling Performance in CWAs and Low Polarity Solvents

3.1. Introduction and aims

3.1.1. Introduction

Chapter 2 described research into the influence of ionic moieties on the swelling of polystyrene based ionic networks and how these influences were rationalised by use of Hansen similarity parameters and dielectric constants. This chapter will describe research attempting to optimize the swelling of a set of polymers based upon these learned principles. Two approaches are described for the design of absorbent polymers for chemical warfare encapsulation. Whilst these two approaches diverge in terms of design; the end targets for both were the same. One approach was to examine the effects of the exchange of the counter ion for the previously discussed ionic monomer incorporated into the styrene networks. The second aspect was to modify the polymer by balancing the non-ionic monomer (styrene) with alternative low-polarity monomers. This was carried out with the aim of reducing the Ra between the resulting polymers and CWAs which would ideally lead to increased swelling. The alternative monomers were chosen by exploring the Hansen solubility parameters of a range of common monomers, and those with HSPs which matched closely with the methyl benzoate were chosen for the polymerisation either partially or wholly replacing styrene in the networks. These approaches were designed to look at the swelling effect of different anion dissociation for the more high swelling polar solvents, and the importance of compatibility matching for the less polar solvents respectively. Both design processes would be approached with an aim of quickly screening monomers, and combinations of monomers, both ionic and non-charged. Copolymers with good swelling performance in the simulant were then considered for further modification in following areas of the project.

3.1.2. Modification of the ionic moiety

3.1.2.1. History of the BARF polyelectrolyte system

The first part of the chapter, regarding the modification of the anion on the ionic monomer was inspired by the work of Sada *et al*. This group claimed that the modification of the ionic

monomer by introducing a 'weakly coordinating anion'[1] could significantly increase swelling compared to non-ionic gels, especially in low polarity solvents such as DCM. The anion they chose to represent use was the 'weakly/non-coordinating' anion; BARF.

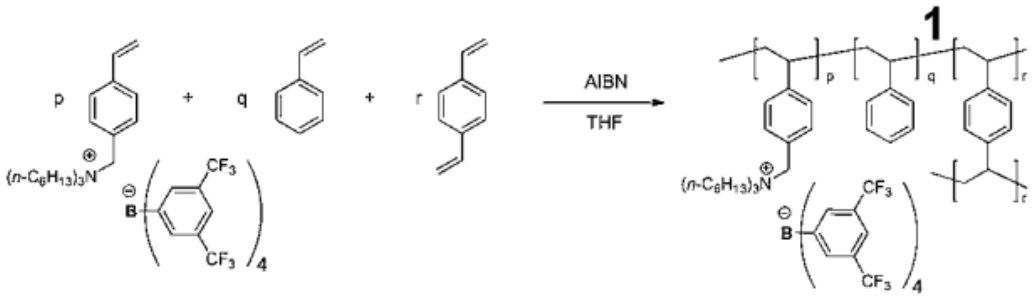

Figure 3.1 – A reaction scheme describing the use of the BARF anion quaternary ammonium monomer in the co-polymerisation of styrene, divinylbenzene and this ionic group. This scheme was taken from the work by Sada et al.

They reported that by introducing this version of the ionic monomer into a styrene based polymer network at low concentrations (3 %) and low crosslinking density (1 mol%), they could increase the swelling drastically when compared to a non-ionic gel.[2] For example, they reported a swelling increase from Q = 39 to Q = 109 in dichloromethane in this system.

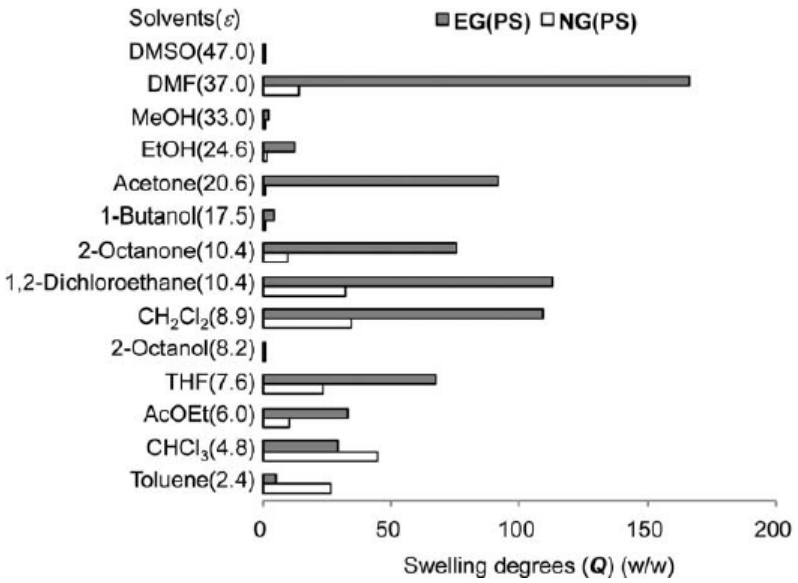

Figure 3.2 – Swelling degrees of a polyelectrolyte gel containing 3 % BARF monomer (grey bar), and a non-ionic polystyrene gel (open bar) in various organic solvents at room temperature (23 °C). In parentheses, their dielectric constants are shown. Taken from Sada et al.[2]

This swelling was maintained at low temperatures (-80 °C). The same group went on to develop these systems further with long chain alkyl methacrylate based gels in place of styrene, where they increased the content of this anion in various polymers up to 5 %[3,4], and 10 %[5] against the other monomers. They reported to be able to swell the polymers in dichloromethane to over Q = 325 in the best of these systems, with an increase in swelling observed as ionic content increases. One report was made by Sada into alternative anions to the BARF, these were a dodecyl sulfate anion and a pentafluorophenylborate imidazolium based anion. The lowest swelling across the board was seen in the dodecylsulfate gel, followed by the BARF with the imidazolium system coming out slightly on top. The highest swelling was seen in DCM (Q = 35, Q = 125 and Q > 200 for the anions respectively).[6]

3.1.2.2. The anion exchange process

The reports from Sada's group discussed in detail the swelling changes specific to the BARF anion. The project presented in this chapter was designed to look at a range of other anions

which could also be considered 'less coordinating' than chloride, and how they affected swelling performance in a styrenic polymer. The objectives for this work were to first test the reproducibility of the work done by the Sada group with regards to the swelling of the BARF containing polymer. The work would then move to exchanging the chloride for different anions whilst maintaining the same cationic moiety. The anions chosen for this work were selected to include different physical sizes, hydrophobicity and hydrophilicity amongst other aspects. Many of the anions chosen are considered to be weakly or non-coordinating anions.[7] This term means that the anion is so sterically hindered by the structure around the formally charged atom, such as the boron in tetraphenyl borate, that it is vastly dissociated from the cation and this in theory, would increase the swelling capacity of the polymer. This is believed to occur due to the lower association between the ion-pairs causing higher osmotic pressure inside the system. The osmotic pressure in the system is increased due to the increased fraction of free ions in the solution/gel.[8] The anions chosen for the comparison with the chloride (Cl^-) were: tetrakis [(3,5-trifluoromethyl)phenyl] borate ($BARF^-$), hexafluoro phosphate (PF_6^-), tetraphenyl borate(BPh_4^-), tetrafluoro borate(BF_4^-), bromide (Br^-), perchlorate (ClO_4^-) and dodecylsulfate (SDS^-) (Figure 3.3). In their quaternary ammonium monomer forms they will be referred to as QAS-Cl, QAS-BARF, QAS-PF_6, QAS-BPH_4, QAS-BF_4, QAS-Br, QAS-ClO_4, and QAS-SDS respectively. Where THVBAC was used in chapter 2, this is equivalent to QAS-Cl.

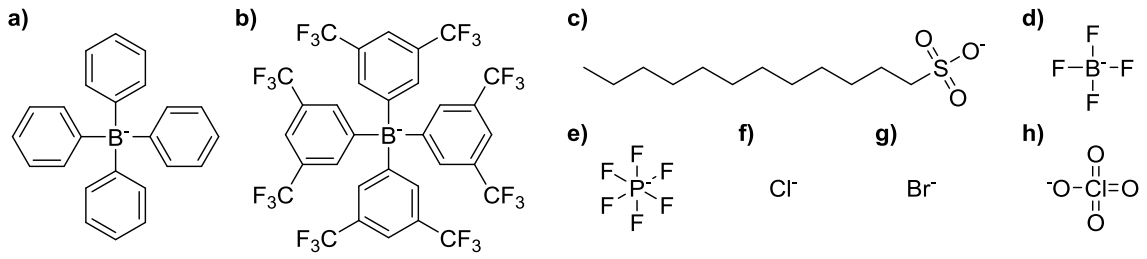

Figure 3.3 - The structures of the anions used in this study; a) tetraphenyl borate, b) tetrakis [(3,5-trifluoromethyl)phenyl] borate, c) dodecylsulfate, d) tetrafluoro borate, e) hexafluoro phosphate, f) chloride, g) bromide, and h) perchlorate.

Initially, the BARF containing polymer was synthesised at 10 % ionic content with 90 % styrene, and swelled in a range of solvents to mimic the increase in ionic content in methacrylate gels presented by Sada *et al.*[5] The rest of the anions were then introduced to the polymers at 20 % molar content relative to 80 % styrene. This configuration was selected as the results from the previous chapter showed that the Hansen solubility parameters of the polymer network plateaued at 20 mol% inclusion of this ionic monomer. After the HSP values of the polymer stabilised at 20 mol%, the biggest changes in swelling were then due to the dielectric of the solvent and the ionic fraction of the polymer. Additionally 20 mol% ionic monomer was higher loading than any of the tests undertaken by Sada *et al*. It was predicted that at this level of ionic inclusion, the swelling may not be optimal, but the swelling differences caused by the anions would be visible, which was the main aim of this aspect of work. The final justification for synthesis at 20 % ionic monomer was that in chapter 2, it was observed that the swelling in the 'good' swelling solvents continued to increase all the way to 100 %, a trend which is shared in other works.[9] Sada stopped introducing the ionic monomer at 10 % due to the fear of ion pair aggregation; however the poly(ionic liquid reports) and chapter 2 suggest this is not a concern and that the swelling increases in good solvents are proportional to the ionic fraction of the polymer.

3.1.3. Modification of the non-ionic content

The second part of the chapter will focus on the rapid synthesis and testing of many polymers which did not feature an ionic moiety but where different monomers were incorporated into the styrene networks. The monomers were chosen based upon solvent/polymer compatibility, specifically Hansen solubility parameters. The swelling of the low polarity solvents, such as oils, and CWAs could not be increased with increasing ionic content. Closer solubility parameter matched monomers based upon the principles of Hansen solubility may lead to a better swelling polymer. Earlier work in this thesis demonstrated the importance of having a polymer matrix which is chemically compatible with a solvent if a high swelling degree is to occur. The

previous search for a polymer system which was effective at swelling CWAs revealed two major trends. The first is that G-agents, represented with sarin (GB), swell better with increasing ionic content in terms of our specific electrolytic system of chapter 2, and secondly, that the V-series and sulfur mustard do not respond well to increasing ionic content, and conversely, prefer to be absorbed into a matrix which is of very low polarity. These two agents are of special interest to us due to the fact they are both very persistent in the environment and harder to degrade than sarin.[10] This means that encapsulating these agents will be a worthy target as the V-series and sulfur mustard will still remain intact and active much past the time frame of the swelling process, whereas the sarin may have broken down significantly by the time the absorption and retention is considered useful. The monomers were chosen to increase the dispersion parameter (δd) of the polymer absorbent. It was important to avoid increasing the polarity (δp) and hydrogen bonding (δh) components which have been shown to be obstructive in the swelling of these agents. The work process for this section was to screen an array of monomers which presented HSP values which showed promise when compared to the simulant, methyl benzoate. The polymers would be synthesised in line with the previous methodology and tested in the simulant.

3.2. Experimental

3.2.1. Materials and Equipment

The sodium salts of the anions PF_6^-, BPh_4^-, BF_4^-, Br^-, ClO_4^- and SDS^- were all obtained from sigma Aldrich and used without further purification. The method for the synthesis of the NaBARF is described in section 3.2.2 below.

The starting material, QAS-Cl, was synthesised following an identical procedure to that described in chapter 2. The synthesis of the subsequent ionic monomers was conducted following the similar procedure proposed by Sada for the synthesis of the QAS-BARF. Many of

the syntheses had slight variations to the following general procedure and are listed in their relevant section.

3.2.2. Synthesis of NaBARF

The NaBARF was synthesised using a slight modification of a method described by Reger *et al*.[7] as follows:

A 750 ml two necked round bottom, with dropping funnel and condenser, was charged with freshly ground magnesium shavings (3.03 g, 125 mmol). To this was then added dry diethyl ether (450 ml), sodium tetrafluoroborate (2.1 g, 19.2 mmol) and stirred. The dropping funnel was then loaded with dry diethyl ether (150 ml) and 1,3-bis(trifluoromethyl)-5-bromobenzene (18.6 ml, 108 mmol). To begin the reaction, 1,2-dibromoethane (1.5 ml, 17 mmol) was added down the condenser and mild heating was applied until the reaction initiated. Initiation occurred when with slight effervescence and self-heating of the reaction mix was observed. After initiation, the contents of the dropping funnel were added with continued stirring over approximately 25 minutes. The drop rate was managed to ensure gentle self-reflux. Nearing the end of the addition, the solution turned a yellow colour. After the contents of the dropping funnel were added, the reaction was placed into an oil bath preheated to 45 °C for 30 minutes. The reaction turned a brown cloudy colour, was allowed to cool, and then was poured into deionized water (600 ml) containing sodium carbonate (48 g) with vigorous stirring. This was left to stir for a further 60 minutes to ensure there were no reactive species left. This mixture was then filtered to remove any large particles and magnesium, separated, and the aqueous extracted three times each with diethyl ether (150 ml). The combined organic layers were stirred with activated charcoal and sodium sulfate to decolour and dry the solution. The mixture was gravity filtered and reduced under vacuum to leave a thick yellow oil. This was then triturated with hexane (200 ml) overnight where the yellow product precipitated. The solid was collected by filtration. It was then suspended with stirring in 10 ml of DCM which had been cooled to – 20 °C. After 5 minutes of washing, the mixture was then filtered to remove

the DCM containing the coloured impurities. This was repeated once further to leave a white powder, 10.1 g (59 %).

^{1}H NMR (400 MHz, $CDCl_3$, room temperature) found δ: = *7.65* [s, **4H** (B-Ph (**para**)], *7.76* [s, **8H** (B-Ph (**ortho**)]. ^{13}C NMR ($CDCl_3$, room temperature) found δ: = 76.71, 77.04 and 77.36. ^{11}Boron NMR showed a single peak at -7.7 ppm, and ^{19}flourine NMR showed a single peak at -64 ppm (both also in chloroform-d).

3.2.3. Synthesis of the anion exchanged monomers

3.2.3.1. General anion exchange procedure

A solution of the chosen sodium salt (6 mmol, 1.5 eq.) was dissolved in 10 ml of methanol. This was added dropwise with stirring to a conical flask which contained 2 g (4 mmol) of the ionic monomer starting material (QAS-Cl) which was pre-dissolved in 10 ml of methanol. The solutions were stirred for 10 minutes at room temperature. Deionised water (30 ml) was then added slowly with continued stirring to the solution to precipitate a fine white powder. This was then left to stir for 2 more hours, after which it was filtered. The filtrate was washed at the pump with excess water, removed and dried in vacuo at room temperature overnight to yield the anion exchanged QAS which presented itself as a white powder in all occasions.

3.2.3.2. QAS-BARF

^{1}H NMR (400 MHz, $CDCl_3$, room temperature) found δ: = *0.91* [t, **9H** ($\mathbf{CH_3}CH_2CH_2CH_2CH_2CH_2)_3N$, J = 6.20 Hz], *1.35* [s, **12H** ($CH_3\mathbf{CH_2CH_2}CH_2CH_2CH_2)_3N$], *1.75* [s, **12H** ($CH_3CH_2CH_2\mathbf{CH_2CH_2}CH_2)_3N$], *2.98* [t, **6H** ($CH_3CH_2CH_2CH_2CH_2\mathbf{CH_2})_3N$, 8.14 Hz], *4.21* [s, **2H** $N\mathbf{CH_2}C_6H_4CHCH_2$], *5.41* [d, **1H** alkene, J = 11.96 Hz] *5.85* [d, **1H** alkene, J = 16.66 Hz], 6.65 [dd, **1H** alkene**,** J_1 = 10.98 Hz, J_2 = 6.65 Hz], *7.16* [m, **2H** phenyl (cation)], *7.50* [m, **2H** phenyl (cation)] and [m, **4H** phenyl (anion)], 7.68 [m, **8H** phenyl (anion)]. ^{13}C NMR ($CDCl_3$, room temperature) found δ: = 13.67, 22.05, 22.15, 25.77, 35.01, 58.43, 62.38, 117.49, 117.85, 120.57, 123.28, 123.61, 125.99, 127.78, 128.91(multiplet), 131.83, 134.89, 141.58, and 161.70(multiplet). Elemental analysis: estimates; **C** 56.70 %, **H** 4.84 %, **N** 1.12 %, found; **C** 56.67 %, **H** 4.99 %, **N** 1.16 %. The integrals

associated with the anion (7.72 ppm) and the cation (7.21 ppm), were found to represent a ratio of 1:1. A yield of 93 % was obtained.

3.2.3.3. QAS-PF_6

^{1}H NMR (400 MHz, $CDCl_3$, room temperature) found δ: = *0.91* [t, **9H** ($\mathbf{CH_3}CH_2CH_2CH_2CH_2CH_2)_3N$, J = 6.51 Hz], *1.35* [s, **12H** ($CH_3\mathbf{CH_2CH_2}CH_2CH_2CH_2)_3N$], *1.75* [s, **12H**($CH_3CH_2CH_2\mathbf{CH_2CH_2}CH_2)_3N$], *3.05* [t, **6H** ($CH_3CH_2CH_2CH_2CH_2\mathbf{CH_2}$)$_3$N, J = 8.24 Hz], *4.35* [s, **2H** $N\mathbf{CH_2}C_6H_4CHCH_2$], *5.37* [d, **1H** alkene, J = 11.90 Hz] *5.85* [d, **1H** alkene, J = 16.96 Hz], 6.70 [dd, **1H** alkene, J_1 = 10.88 Hz, J_2 = 6.51 Hz], 7.50 [dd, **4H** phenyl, J_1 = 8.33 Hz, J_2 = 23.52 Hz]. ^{13}C NMR ($CDCl_3$, room temperature) found δ: = 13.92, 22.28, 22.47, 25.92, 31.13, 58.53, 62.37, 116.73, 125.80, 127.26, 132.44, 135.45, and 140.30. Elemental analysis: estimates; **C** 61.00 %, **H** 9.10 %, **N** 2.63 %, found; **C** 60.96 %, **H** 9.07 %, **N** 2.75 %. A yield of 75 % was obtained.

3.2.3.4. QAS-BPH_4

This synthesis required each of the starting material and the salt to be dissolved in 15ml of methanol. The reaction proceeded very fast with some liberation of heat on mixing the two solutions. A vast amount of white precipitate was formed which interfered with the ability of the mixture to stir when not enough solvent was used.

^{1}H NMR (400 MHz, $CDCl_3$, room temperature) found δ: = *0.91* [t, **9H** ($\mathbf{CH_3}CH_2CH_2CH_2CH_2CH_2)_3N$, J = 8.16 Hz], *1.35* [s, **12H** ($CH_3\mathbf{CH_2CH_2}CH_2CH_2CH_2)_3N$], *1.75* [s, **12H** ($CH_3CH_2CH_2\mathbf{CH_2CH_2}CH_2)_3N$], *2.26* [t, **6H** ($CH_3CH_2CH_2CH_2CH_2\mathbf{CH_2}$)$_3$N, J = 7.95 Hz], *3.03* [s, **2H** $N\mathbf{CH_2}C_6H_4CHCH_2$], *5.37* [d, **1H** alkene, J = 11.12 Hz] *5.85* [d, **1H** alkene, J = 17.15 Hz], 6.70 [dd, **1H** alkene**,** J_1 = 10.91 Hz, J_2 = 6.62 Hz], *6.89* [m, **2H** phenyl (cation)] + [m, **4H** phenyl (anion)], *6.99* [m, **8H** phenyl (anion)], 7.35 [m, **8H** phenyl (anion)], 7.48 [m, **2H** phenyl (cation)]. ^{13}C NMR ($CDCl_3$, room temperature) found δ: = 13.98, 22.18, 22.52, 25.83, 31.22, 57.80, 61.51, 116.93, 122.03, 125.40, 125.79, 127.16, 132.26, 135.41, 136.30, 140.35, 164.08 (multiplet). Elemental analysis: estimates; **C** 86.77 %, **H** 9.71 %, **N** 1.98 %, found; **C** 86.60 %, **H** 9.60 %, **N** 2.05 %. The integrals associated

with the anion (7.35 ppm) and the cation (7.48 ppm), were found to represent a ratio of 1:1. A yield of 78 % was obtained.

3.2.3.5. QAS-BF_4

This synthesis was tricky and required the use of a 1:1 mixture of DCM: methanol for the salts to properly dissolve due to the low solubility of the sodium tetrafluoroborate. Each of the two starting materials required 15 ml of this mixture to dissolve. The product naturally precipitated from the solution over 3 hours and water was not added until the washing stage. Once the synthesis was completed, the product had low solubility in many common solvents which made it difficult to work with.

^{1}H NMR (400 MHz, $CDCl_3$, room temperature) found δ: = *0.91* [t, **9H** ($\mathbf{CH_3}CH_2CH_2CH_2CH_2CH_2)_3N$, J = 6.32 Hz], *1.35* [s, **12H** ($CH_3\mathbf{CH_2CH_2}CH_2CH_2CH_2)_3N$], *1.75* [s, **12H** ($CH_3CH_2CH_2\mathbf{CH_2CH_2}CH_2)_3N$], *3.07* [t, **6H** ($CH_3CH_2CH_2CH_2CH_2\mathbf{CH_2})_3N$, J = 8.16 Hz], *4.47* [s, **2H** $N\mathbf{CH_2}C_6H_4CHCH_2$], *5.37* [d, **1H** alkene, J = 10.88 Hz] *5.85* [d, **1H** alkene, J = 17.06 Hz], 6.70 [dd, **1H** alkene, J_1 = 11.11 Hz, J_2 = 6.58 Hz], 7.50 [dd, **4H** phenyl, J_1 = 8.31 Hz, J_2 = 23.39 Hz]. ^{13}C NMR ($CDCl_3$, room temperature) found δ: = 13.95, 22.24, 22.49, 25.99, 31.36, 58.56, 62.42, 116.54, 126.20, 127.15, 132.58, 135.54, and 140.10. Elemental analysis: estimates; **C** 68.47 %, **H** 10.24 %, **N** 2.96 %, found; **C** 69.65 %, **H** 11.19 %, **N** 3.04 %. The differences between the carbon and hydrogen values on these elemental analysis results are outside of the commonly accepted range (±0.3 % difference). A yield of 75 % was obtained.

3.2.3.6. QAS-Br

^{1}H NMR (400 MHz, $CDCl_3$, room temperature) found δ: = *0.91* [t, **9H** ($\mathbf{CH_3}CH_2CH_2CH_2CH_2CH_2)_3N$], J = 6.34 Hz, *1.35* [s, **12H** ($CH_3\mathbf{CH_2CH_2}CH_2CH_2CH_2)_3N$], *1.75* [s, **12H** ($CH_3CH_2CH_2\mathbf{CH_2CH_2}CH_2)_3N$], *3.60* [t, **6H** ($CH_3CH_2CH_2CH_2CH_2\mathbf{CH_2})_3N$, J = 8.21 Hz], *4.68* [s, **2H** $N\mathbf{CH_2}C_6H_4CHCH_2$], *5.37* [d, **1H** alkene, J = 10.91 Hz] *5.85* [d, **1H** alkene, J = 17.04 Hz], 6.70 [dd, **1H** alkene, J_1 = 10.91 Hz, J_2 = 6.62 Hz], 7.50 [dd, **4H** phenyl, J_1 = 8.19 Hz, J_2 = 23.39 Hz]. ^{13}C NMR ($CDCl_3$, room temperature) found δ: = 13.97, 22.53, 22.65, 26.18, 31.29, 58.94, 63.11, 116.31, 126.77, 126.99, 132.91,

135.63, and 139.90. Elemental analysis: estimates; **C** 69.50 %, **H** 10.37 %, **N** 3.00 %, found; **C** 69.42 %, **H** 10.54 %, **N** 3.13 %. A yield of 72 % was obtained.

3.2.3.7. QAS-ClO_4

^{1}H NMR (400 MHz, $CDCl_3$, room temperature) found δ: = *0.91* [t, **9H** ($\mathbf{CH_3}CH_2CH_2CH_2CH_2)_3N$], J = 6.18 Hz, *1.35* [s, **12H** ($CH_3\mathbf{CH_2CH_2}CH_2CH_2)_3N$], *1.75* [m, **12H** ($CH_3CH_2CH_2\mathbf{CH_2CH_2}CH_2)_3N$], *3.15* [t, **6H** ($CH_3CH_2CH_2CH_2\mathbf{CH_2})_3N$, J = 8.12 Hz], *4.50* [s, **2H** $N\mathbf{CH_2}C_6H_4CHCH_2$], *5.37* [d, **1H** alkene, J = 11.01 Hz] *5.85* [d, **1H** alkene, J = 17.029 Hz], 6.70 [dd, **1H** alkene**,** J_1 = 11.31 Hz, J_2 = 6.63 Hz], 7.50 [dd, **4H** phenyl, J_1 = 8.13 Hz, J_2 = 23.44 Hz]. ^{13}C NMR ($CDCl_3$, room temperature) found δ: = 13.97, 22.24, 22.48, 26.12, 31.17, 58.51, 62.27, 116.51, 126.19, 127.14, 132.56, 135.54, and 140.06. Elemental analysis: estimates; **C** 66.71 %, **H** 9.95 %, **N** 2.88 %, found; **C** 66.58 %, **H** 9.88 %, **N** 2.93 %. A yield of 62 % was obtained.

3.2.3.8. QAS-SDS

Due to the apparent ability for the starting material and product to dissolve in nearly every single combination of solvents which were tested, the work up for this QAS was very difficult, and not all the impurities or associated solvent could be removed. This is represented especially in the elemental analysis results which were significantly different from the expected values. The product was extracted from the methanol/water with DCM and then reduced in a rotary evaporator before being precipitated into cold hexane (-10 °C).

^{1}H NMR (400 MHz, CDCl3, room temperature) found δ: = 0.91 [m, **9H** ($CH_3CH_2CH_2CH_2CH_2$)3N] and [m, **4H** (anion)], 1.35 [s, **12H** ($CH_3CH_2CH_2CH_2CH_2$)3N] and [m, **22H** (anion)], 1.70 [m, **2H** (anion)], 1.75 [s, **12H** ($CH_3CH_2CH_2CH_2CH_2$)3N], 3.13 [t, **6H** ($CH_3CH_2CH_2CH_2CH_2$)3N, J = 8.42 Hz], 4.61 [s, **2H** $NCH_2C_6H_4CHCH_2$], *5.32* [d, **1H** alkene, J = 12.01 Hz] *5.79* [d, **1H** alkene, J = 17.16 Hz], 6.70 [dd, **1H** alkene**,** J_1 = 10.99 Hz, J_2 = 6.65 Hz], 7.38 [s, **4H** phenyl]. ^{13}C NMR ($CDCl_3$, room temperature) found δ: = 13.97, 14.20, 22.43, 22.53, 22.76, 26.10 (doublet), 29.43, 29.59, 29.72, 31.28, 31.98, 58.63, 62.69, 67.41, 116.27, 126.77, 126.99, 132.79, 135.62, and 139.83. Elemental analysis: estimates; **C** 73.64 %, **H** 11.57 %, **N**

2.20 %, found; **C** 70.59 %, **H** 9.63 %, **N** 2.14 %. The NMR shows an excess of 3 protons in the environments associated with the SDS anion. A yield of 46 % was obtained.

3.2.4. Calculation of HSPs and subsequent Ra values

The HSP values for the monomers used in this study, as well as those relating to the simulant and the sulfur mustard, were gathered from the HSPiP software. This software is written by the groups of Prof. Steven Abbott, Dr. Charles Hansen and Dr. Hiroshi Yamamoto. The HSP values for all of the monomers used were gathered primarily through the database attached to the software. For the chemicals which weren't available from the database (sulfur mustard, *t*-butyl styrene and MCR-M17), these were acquired by using the Y-MB estimation tool included with the software as described in chapter 2 (section 2.2.5). The Ra values for the polymers which would have a varying amount of two monomer species (for example 25 % ODMA, 75 % styrene) were calculated from a weighting of the HSPs for each of the two monomers. The Ra between the monomers and sulfur mustard and methyl benzoate was calculated from;

$$Ra = \sqrt{4\,(\delta d_{poly} - \delta d_{solv})^2 + (\delta p_{poly} - \delta p_{solv})^2 + (\delta h_{poly} - \delta h_{solv})^2}$$

(Equation 3.1)

3.2.5. Synthesis of ionic network polymers

The free radical polymerisation was carried out similarly for each of the QAS's following the procedure set out in Chapter 2. The molar ratios for the initiator, crosslinker, styrene and QAS were set at 1:1:80:20. The amount of each salt used is given in Table 3.1 below.

Styrene (1.62 g, 15.5 mmol), was placed in a boiling tube. To this was then added the appropriate QAS (3.9 mmol), 0.25 g of the DVB stock solution (Eq. to 0.0253 g, 0.19 mmol DVB) and finally 2 ml of a 0.1 M AIBN in THF solution. The tube was sealed and the contents were mixed by bubbling nitrogen through for 15 minutes. The tubes were then placed into a preheated oil bath set at 65 °C for 24 hours to complete the polymerisation. After the

polymerisation was complete the polymer was removed from the tube and cut into pieces of approximately 50 mg each. The gels were crudely washed: chunks were swollen in an excess of THF and after 2 hours the supernatant was removed. Further THF was added and the gel was left to sit for another hour after which the supernatant was again removed. Finally the gel was left to de-swell slowly in ambient conditions. To prepare the gel for swelling studies, the chunks were further dried under a slowly increasing vacuum at 65 °C for 24 hours. All the polymers formed brittle gels.

Table 3.1 – The quantities of each anion exchanged salt required for the subsequent synthesis of the 20% ionic polymers. The molecular mass of each of the salts is also presented.

QAS Sample	Molecular mass (g/mol)	Mass for polymerisation (g)
QAS-Cl	421.35	1.6433
QAS-Br	465.30	1.8147
QAS-ClO_4	469.33	1.8304
QAS-BARF	1249.44	4.8728
QAS-BPH_4	705.54	2.7516
QAS-PF_6	531.34	2.0722
QAS-SDS	635.53	2.4786

3.2.6. Synthesis of non-ionic polymers

The non-ionic polymers were synthesised following the same method as in 3.2.5 for the ionic polymers. They were processed in the same way to maintain consistency throughout the series of tests. The compositions and quantities used for the polymers can be found below in Table 3.2. All polymers were synthesised at 65 °C using 2 ml of a 0.1 M AIBN in THF solution and 0.2500 g of a 0.7 M DVB in THF solution (0.0253 g DVB) for initiation and crosslinking, respectively.

Table 3.2- Showing the quantities of styrene and the alternate monomer, for all of the homo- and co-polymerisations with the non-ionic monomers

Polymer	Composition	Styrene (g)	Alt. Monomer (g)
Methyl styrene	100 % methyl styrene	n/a	2.113
***t*-Butyl styrene**	100 % *t*-Butyl styrene	n/a	3.114
5 % ODMA	5 % ODMA, 95 % Styrene	1.923	0.329
10 % ODMA	10 % ODMA, 90 % Styrene	1.821	0.658
25 % ODMA	25 % ODMA, 75 % Styrene	1.518	1.645
50 % ODMA	50 % ODMA, 50 % Styrene	1.012	3.290
5 % VBC	5 % VBC, 95 % Styrene	1.923	0.148
10 % VBC	10 % VBC, 90 % Styrene	1.822	0.297
15 % VBC	15 % VBC, 85 % Styrene	1.720	0.445
20 % VBC	20 % VBC, 80 % Styrene	1.619	0.593
VBC	100 % VBC	n/a	2.966
1 % MCR-M17	1 % MCR-M17, 99 % Styrene	2.004	0.854

3.2.7. Reactivity ratios of the non-ionic co-polymerisations

The reactivity rates of each of the polymerisations were examined from the literature to ensure the polymerisations would be random. Forming gradients or blocks could cause anomalous swelling performance. The reactivity ratios of VBC and styrene are known to be R_1 = 1.32 (styrene) and R_2 = 0.72 (VBC) which gives random copolymerisations.[11] ODMA / styrene shows R_1 = 0.58 (styrene) and R_2 = 0.45 (ODMA) which would also leads to a random copolymerisation.[12] Regarding the 1 % MCR-M17, this reaction was assumed to follow similar (or slightly slower) kinetics to that of a long chain methacrylate such as ODMA. No literature values were found for this specific monomer or similar siloxane monomers. The *p*-methyl styrene and *p*-*t*-butyl styrene were both copolymers only with the crosslinker DVB. No sources could be found for the reactivity ratios of these monomers with the crosslinker. A source was found for the copolymerisation of *p*-isopropyl styrene, where; R_1 (styrene) = 1.22, and R_2 (p-isopropyl styrene) = 0.89.[13] This would form a random copolymer and suggests that the *p*-*t*-butyl styrene and *p*-methyl styrene would likely also react similarly to this. It was inferred from this that these monomers would react similarly to styrene with regards to the crosslinking agent DVB. In terms of crosslinking; R_1 (styrene) = 0.77 and R_2 (*p*-DVB) = 2.08, which suggested that the crosslinker would be incorporated into the matrix faster than that of the styrene.[14]

This may have caused significant amounts of micro phasing with monomers which are even slower than styrene in this crosslinking system.

3.2.8. Swelling procedure

A carefully weighed chunk of polymer (~50 mg) was added to a vial containing the selected solvent. The polymer was left to swell for 72 hours and then removed from the solvent, dabbed to remove the excess liquid and then reweighed. This was repeated two further times on fresh sections of polymer to give triplicate results. The 7 solvents chosen for the trials with the anion modified polymers at 20 % were acetonitrile, THF, xylene, DCM, hexane, ethanol and methyl benzoate. This selection of solvents was chosen to represent a range of different properties. The polymer containing BARF at 10 % loading was tested in the full 22 solvents, similarly to chapter 2, for comparison with the work by Sada. The solvent tested on the non-ionic polymers was the VX and HD simulant methyl benzoate.

3.3. Results and discussion

3.3.1. Analysis of the starting QAS monomers

Due to the nature of the synthesis it was difficult to determine the purity of the synthesised monomers. The main concern was that the target products would be a mixture of both the starting material (QAS-Cl) and the product. This would obviously affect the results significantly and so it was of upmost importance to show the products contained simply one anion. The ^{1}H NMR for each product was examined for the chemical shifts of the protons nearest to the cationic nitrogen, and the shifts of these protons were compared to that of the starting material QAS-Cl (Figure 3.4). These two peaks are represented by ‘A’ and ‘B’, a singlet representing two protons and a triplet representing 6 protons, respectively. Where the peaks did not align with the starting material, it could be inferred that the exchange had occurred. This effect was due to the difference in electronegativity around the cationic nitrogen caused by the change in anion.

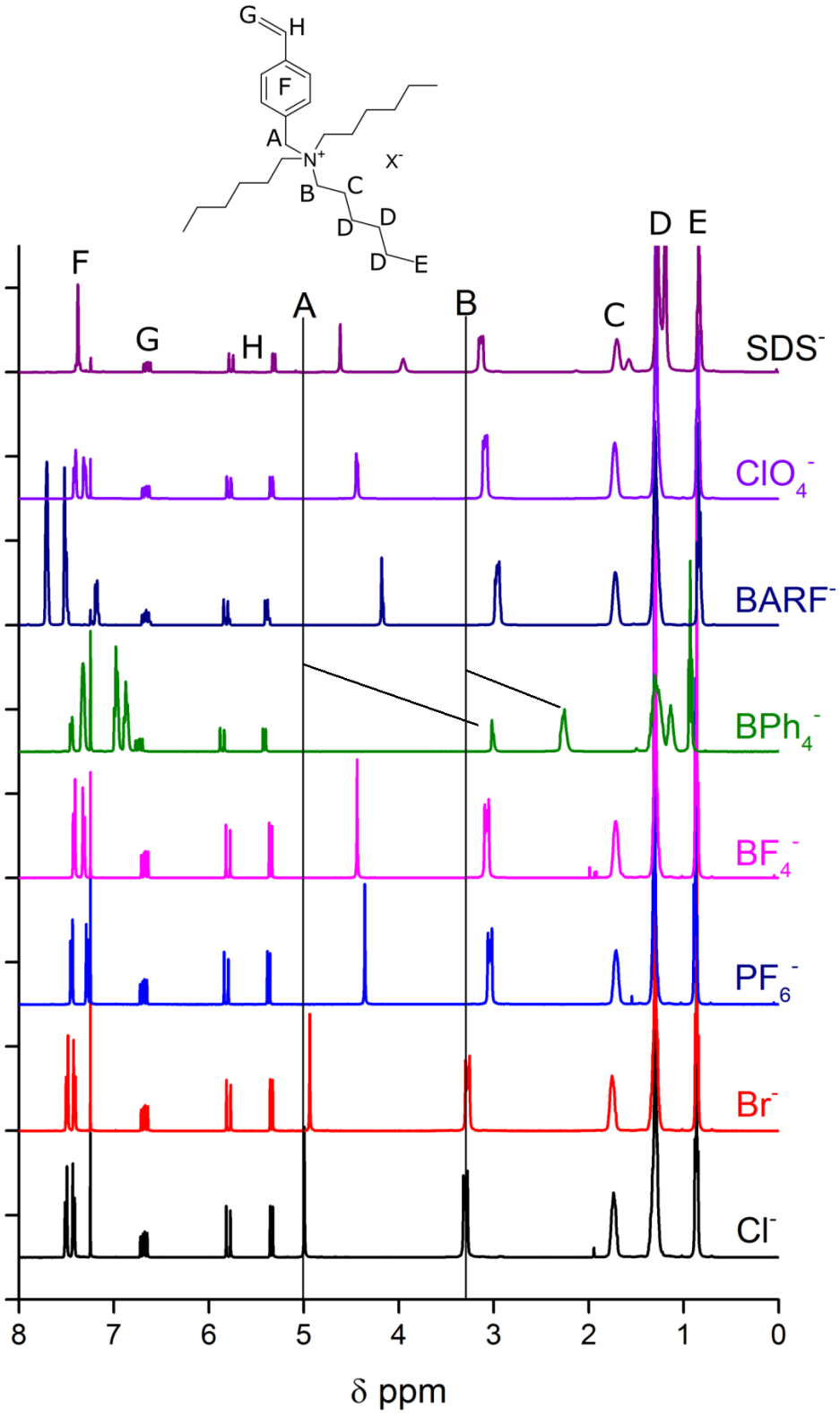

Figure 3.4 - The ^{1}H NMR spectra for each of the anion exchanged salts compared to the reference starting salt QAS-Cl at the bottom. The structure of the salt (without anion) is presented at the top. The lines labelled A and B mark the chemical shift of the CH_2 groups closest to the nitrogen for which a shift is observed as the anion is exchanged.

The ^{13}C NMR spectra for each of the synthesised salts are also shown as a comparison in Figure 3.5. This comparison does not show variation in carbon environment as clearly as is seen in the H^1 spectra. There is a presence of extra carbon environments for the BARF (around 158 ppm and 129 ppm), BPh_4 (around 162 ppm and 128 ppm) and SDS (around 68 ppm and 30 ppm) which is expected of these anions which contain additional carbon atoms in the anion structure. For these samples and the remaining anions which do not have extra carbon environments, a similar approach was taken to the H^1 spectra, where the shift of the carbons closest to the nitrogen cation was examined. This can be seen in the zoomed in image in Figure 3.6, where 'A' and 'B' both represent the same environments as of those in the proton comparison. Each anion has slightly shifted carbon environments when compared to the QAS-Cl. Where one of the peaks may align with that of the chloride, the other peak will not, for example in the QAS-Br, which helps to support that the exchanges have occurred well in all cases.

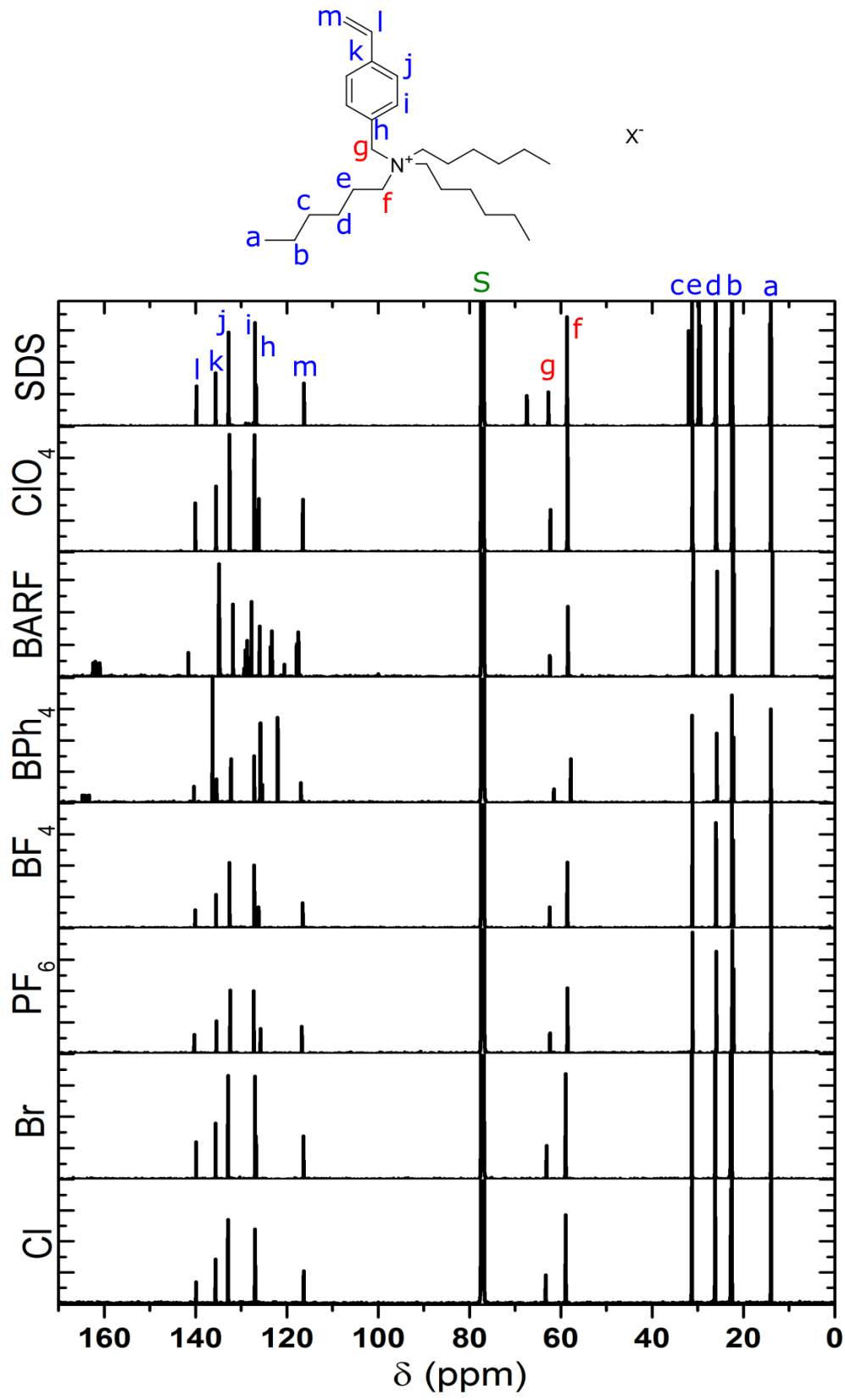

Figure 3.5 - The ^{13}C NMR spectra of each of the anion metastasized salts overlaid against the starting chloride salt.

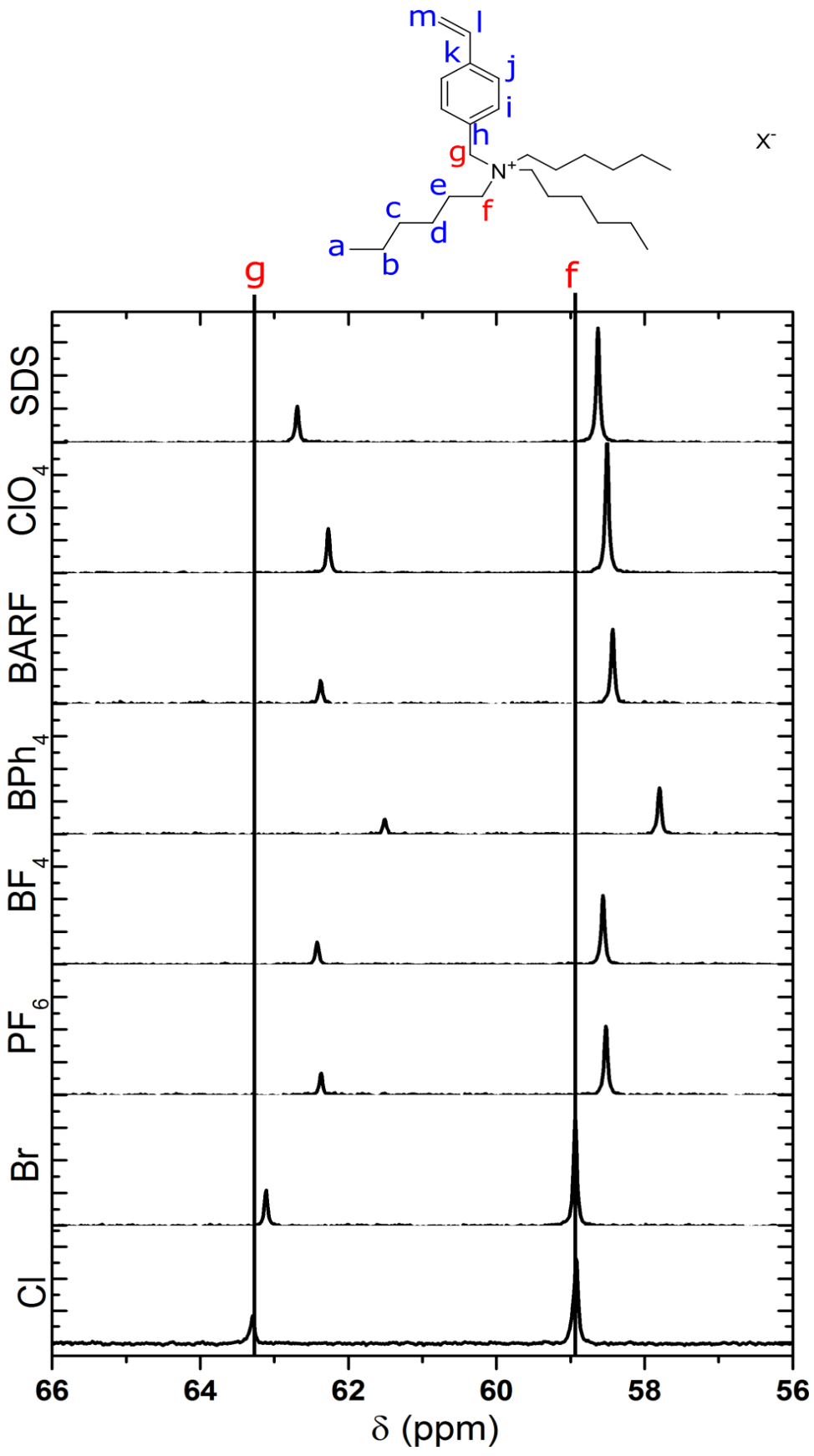

Figure 3.6 - An expansion of the ^{13}C NMR spectra of the anion exchanged salts. The lines represent the carbon environments closest to the nitrogen.

An initial concern was that salts with only small variations in chemical shift such as Cl^- and Br^- would present only one set of peaks in the NMR, where in actual fast there could be a mixture of starting material and product. The first method to determine the purity of the products, as opposed to the presence of a product, was also to use NMR. In the 3 products which contained anions bearing protons, the integrals of these could be directly compared to the body of the cationic monomer to determine ionic equivalence and therefore if there was any mixing and this is noted in the experimental section. For all the products, and especially important for the QAS-ClO_4, QAS-Br, QAS-PF_6, and QAS-BF_4, which do not possess additional proton environments to the QAS-Cl, confirmation of the synthesis was done by examining the elemental analysis results (Table 3.3).

Table 3.3 - Elemental analysis data for each of the anion exchanged salts produced. The estimates, experimental results (average of two runs) and the difference between these two are presented for each. The results where the differences are outside of acceptable ranges (0.3% difference) are shown in bold.

Anion	*C (est.)*	*H (est.)*	*N (est.)*	C (act.)	H (act.)	N (act.)	*C (Diff.)*	*H (Diff.)*	*N (Diff.)*
QAS-PF_6	*61.00*	*9.10*	*2.63*	*60.96*	*9.07*	*2.75*	*-0.04*	*-0.03*	*0.12*
QAS-BARF	*56.70*	*4.84*	*1.12*	*56.67*	*4.99*	*1.16*	*-0.03*	*0.15*	*0.04*
QAS-BPh_4	*86.77*	*9.71*	*1.98*	*86.60*	*9.60*	*2.05*	*-0.17*	*-0.11*	*0.07*
QAS-ClO_4	*66.71*	*9.95*	*2.88*	*66.58*	*9.88*	*2.93*	*-0.13*	*-0.07*	*0.05*
QAS-Br	*69.50*	*10.37*	*3.00*	*69.42*	*10.54*	*3.13*	*-0.08*	*0.17*	*0.13*
QAS-Cl	*76.82*	*11.46*	*3.32*	*76.68*	*11.35*	*3.24*	*-0.14*	*-0.11*	*-0.08*
QAS-SDS	*73.64*	*11.57*	*2.20*	*70.59*	*9.63*	*2.14*	***-3.05***	***-1.94***	*-0.06*
QAS-BF_4	*68.47*	*10.24*	*2.96*	*69.65*	*11.19*	*3.04*	***1.18***	***0.94***	*0.08*

The elemental analysis results for all of the salts except the QAS-BF_4 and QAS-SDS were within the acceptable range of ±0.3 % (Polymer Chemistry (RSC) guidelines)[15] which supported the NMR results showing good exchange of the anion. The QAS-SDS and QAS-BF_4 had large errors with respect to the estimations. QAS-SDS showed a deficit in carbon and hydrogen which suggests a lack of exchange relative to the nitrogen, and the QAS-BF_4 showed an excess of

carbon and hydrogen, which could be due to excess solvent present, or simply incomplete exchange.

3.3.2. Swelling of the QAS-BARF polymers

The first task was to try to replicate the work of Sada by synthesising a styrene based system containing the QAS-BARF at initially 3 % loading relative to styrene, and 1 mol% DVB crosslinking relative to the total monomers. The swelling ability of this polymer was tested in DCM for two batches of polymer, made with two batches of starting salt. Original data by Sada reported Q = 109 in DCM, up from Q = 35 in a non-ionic gel. Surprisingly Q was only observed to equal 5 ± 1.56, compared to Q = 11 ± 1.27 for the non-ionic equivalent. A 10 mol% loading of QAS-BARF in the polymer was then tested. Sada *et al*. previously demonstrated the increased Q in DCM, from 35 in a non-ionic gel to over 300 in a gel containing 10 mol% BARF, supported in a poly (octadecylmethacrylate) based system, where the BARF was coordinated to a quaternary ammonium methacrylate monomer, again with 1 % crosslinking. Their work showed a linear increase in swelling with an increase in BARF content.[16] It was decided this concentration of ionic monomer would be much more useful for examining the swelling change, as they had reported a 100 fold increase at this level. Therefore a 10 % QAS-BARF polymer composition was tested in the same range of solvents as from chapter 2 and this composition was compared against the QAS-Cl polymer at the same loading, and the non-ionic counterpart (Figure 3.7).

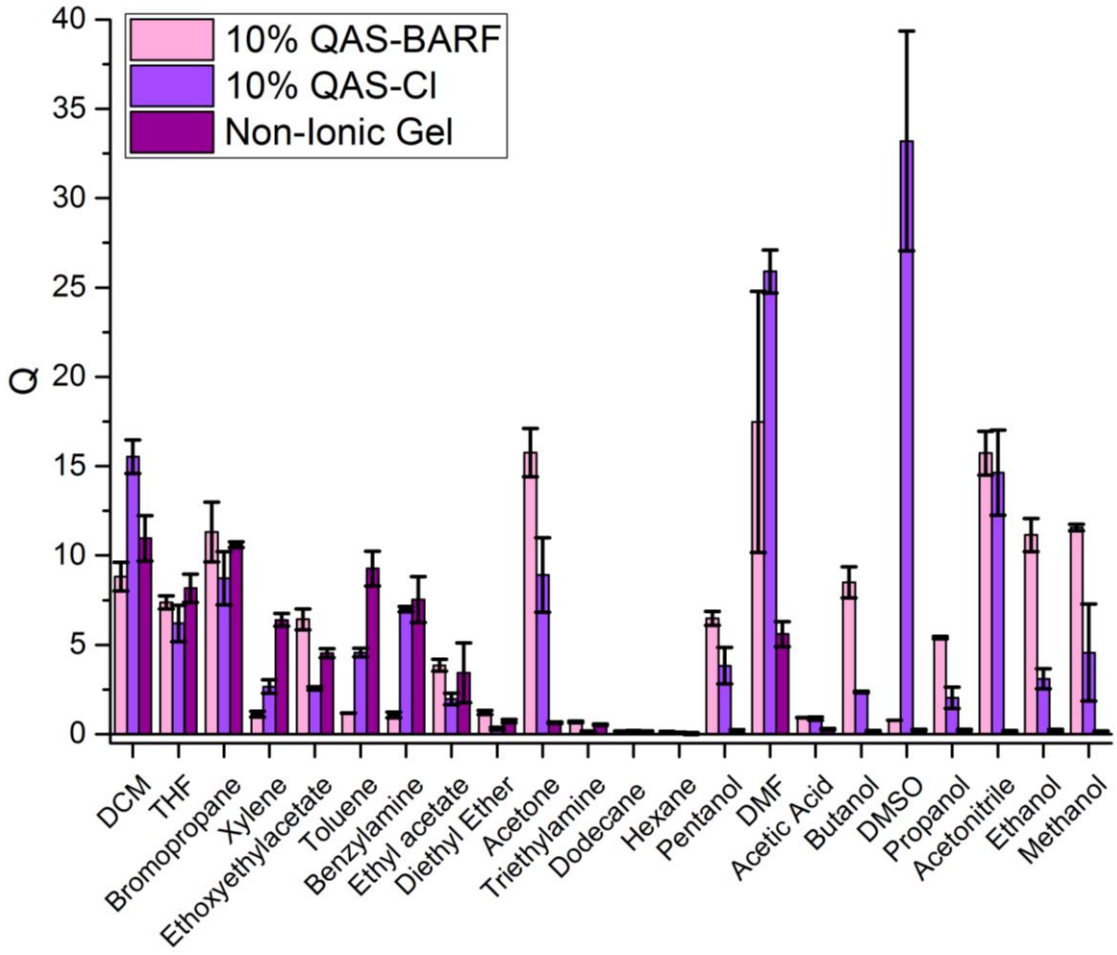

Figure 3.7 - The swelling performance of the 10% BARF polymer, against both the 10% chloride polymer and the non-ionic counterpart in a range of 22 common solvents.

Across the range of results it was apparent that the BARF containing polymer did not exceed the swelling of the chloride polymer to any significant degree, with exception of the alcohols (methanol, ethanol, propanol and butanol) where the swelling was higher (Q = 12, 12, 6, 8) compared to the chloride (Q = 5, 3.5, 2, 2) and non-ionic polymers (Q = 0). It most certainly also did not reach the swelling degrees reported by Sada et al. with our polymers displaying an order of magnitude lower swelling ability. The maximum swelling of any of our polymers at this stage in any solvent did not even manage to reach the swelling quoted for the non-ionic polymer in the previous study of Q (DCM) = 35. These disappointing results support the conclusion that adding QAS-BARF into the polymer matrix does not increase the swelling of this system to the excessive scales which were previously reported. The reason for the

improved swelling of the alcohols is unknown though it is notable that these compounds have the highest hydrogen-bond donor strengths of the solvents.

3.3.3. Swelling of anion exchanged polymers

3.3.3.1. General swelling results

QAS-BF_4 failed to polymerise in the majority of cases. Where it did polymerise, the low solubility of the starting salt in THF forced the reaction to require much more solvent (4 times greater than QAS-Cl) than was suitable for maintaining clear comparisons between this and the other QAS-polymers. This increased solvent led to the polymer swelling inconsistently, likely due to disrupted crosslinking. For these reasons, as well as the low solubility in many solvents, it was decided that a polymer consisting of this monomer would likely not swell many solvents regardless, and so was not included in the following swelling studies.

It would be unlikely for swelling to be acquired at levels which were previously reported based upon the results at this point, yet it remained important to test the smaller swelling differences which may be exhibited by changing the anion of the ionic monomer in this system. The 20 % ionic polymers were each swollen in triplicate in each of the 7 solvents and the results of the swelling behaviours are presented in Figure 3.8 below.

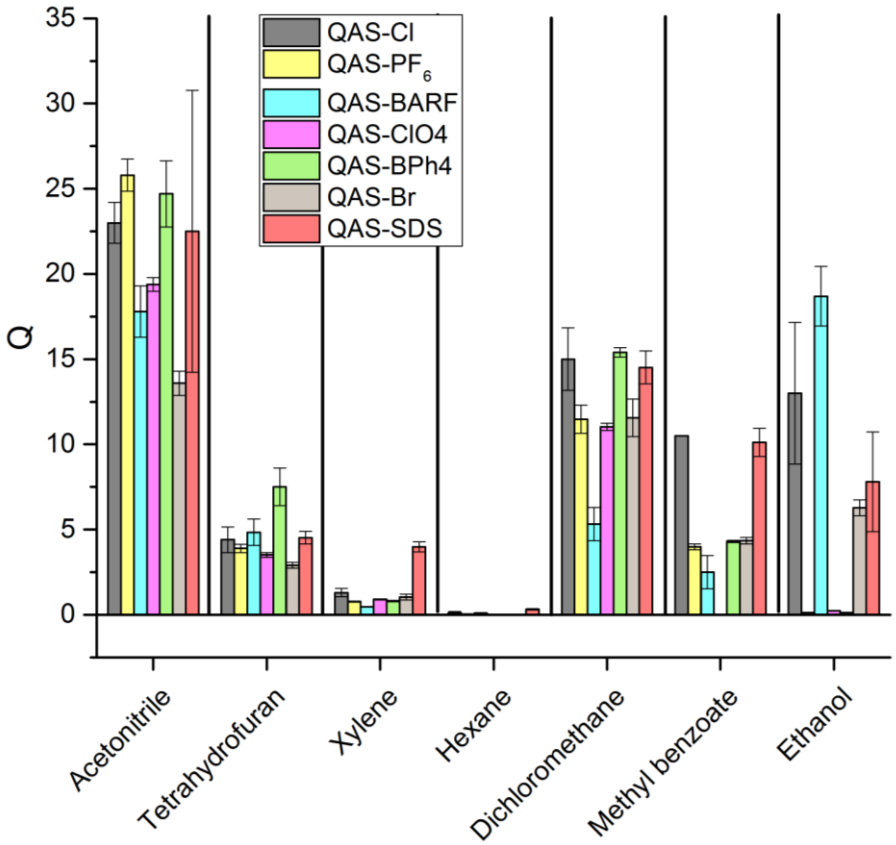

Figure 3.8 - The swelling performance of the polymers containing 20 % (of the total moles of monomer) of each of the anion exchanged ionic monomers. Each polymer was swollen in the seven solvents in triplicate.

The graph only showed limited differences in the degrees of swelling between with the different anions. For the solvents acetonitrile, THF, hexane and xylene, there appeared to be no extreme swelling magnitude variations between the anions for each solvent, outside of the error bars. In the case of acetonitrile and THF, this suggested that these solvents were compatible with all of the anionic salts. Acetonitrile, a small aprotic molecule with a relatively high dipole moment and high dielectric constant (3.92 D and ε = 37.5) showed 3 times larger swelling magnitude compared to the THF. The lower, but also consistent across all anions, swelling of THF was due to the lower polarity and dielectric (1.75 D and ε = 7.58) compared to the acetonitrile. DCM swelled all polymers well at intermediate Q values. Little to no swelling was observed for the solvents xylene and hexane suggesting that none of the anions showed any significant improvements in swelling ability compared to Cl^- Though it is worth noting that

the inclusion of the SDS anion improved the swelling relative to the Cl^- containing polymers. This is likely simply due to the fact the SDS has a substantial alkyl/non-polar component.

3.3.3.2. Swelling of DCM

To look at the swelling in more detail, the expanded graphs of just the solvents with the largest swelling ranges (DCM, ethanol and methyl benzoate) were presented.

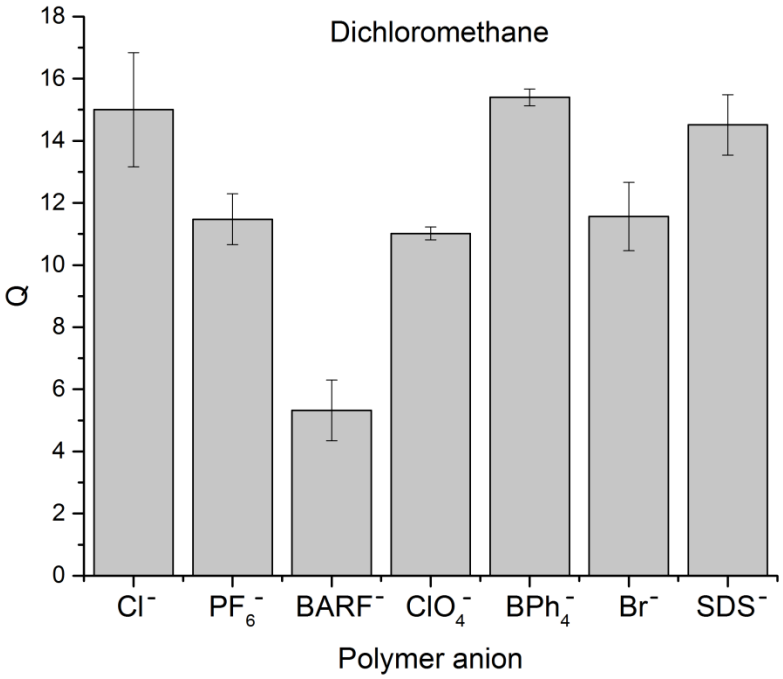

Figure 3.9 - The swelling degrees in dichloromethane (Q) of each of the polymers containing 20% of the anion exchanged ionic monomer.

The most interesting thing to note about the swelling of the dichloromethane in the polymers was that across the board the swelling did not change significantly (Figure 3.9). The only anion however which showed decreased swelling when compared to the chloride ($1/3^{rd}$ of the chloride swelling) was the BARF containing polymer. Whilst one could argue this could be attributed to low amounts of the salt in the matrix, or excess crosslinking, both of these are unlikely, as in other solvents, the BARF was equivalent to, or outperformed many of the other anions by slight margins. Disappointingly, this BARF anion was the leading choice in terms of weak coordination to the cation, and is the anion which was presented by Sada to be exceptionally good at swelling dichloromethane.

3.3.3.3. Swelling of ethanol

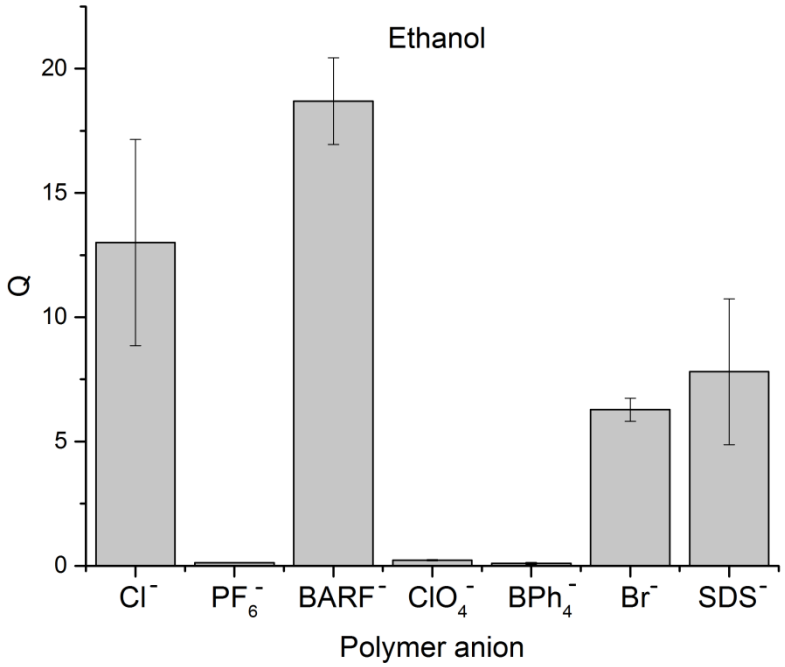

Figure 3.10 - The swelling degrees in ethanol (Q) of each of the polymers containing 20% of the anion exchanged ionic monomer.

The swelling in ethanol showed the largest degree of variation in swelling magnitude. The results presented in chapter 2 demonstrated that ethanol favours an ionic network, and therefore would be expected to swell all the polymers well. Unlike acetonitrile and THF, ethanol is a strongly protic hydrogen bond donating solvent. Knowing this, the hydrogen bonding character of the anions was considered. Research by Hunter *et al.*[17] calculated the hydrogen bonding acceptor (HBA) and donating abilities of various anion species. In terms of the polymers herein, their report provided HBA values (unitless) for Cl^- (12.1 ± 0.3), Br^- (10.6 ± 0.2), PF_6^- (8.3 ± 0.4) and ClO_4^- (7.0 ± 0.3). The HBA values were plotted against the swelling degree in ethanol (Figure 3.11).

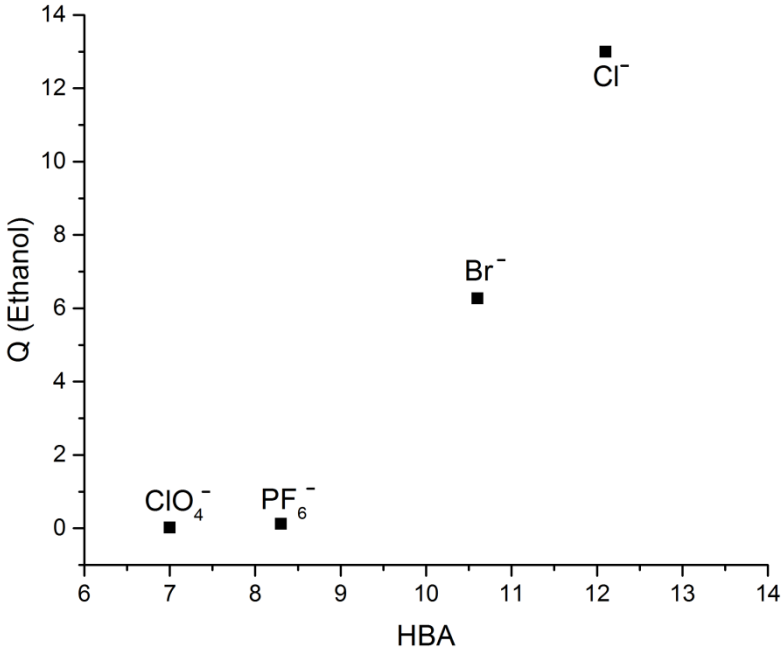

Figure 3.11 – The hydrogen bond acceptor (HBA) values from literature[17] plotted against the swelling in ethanol of the polymers containing ClO_4^-, PF_6^-, Cl^-, and Br^- anions.

The relationship between the swelling and HBA capacity of the various anions was distinct. It was clear that the low swelling of the ClO_4^- and PF_6^-, as well as the intermediate swelling of the Br^- compared to the Cl^-, was directly caused by the inability of these anions to accept the hydrogen bonds donated by the ethanol. The low hydrogen bond interactions caused only little dissociation of the ion pair in the polymer; leading to low osmotic pressure and low swelling. It could be inferred from this data that the BARF anion possesses good HBA ability, and the BPh_4, a low HBA ability. The observed relationship between the anion's hydrogen bond accepting ability and resultant swelling would likely be similar in the majority of protic solvents such as methanol, propanol and acetic acid.

3.3.3.4. Swelling of methyl benzoate

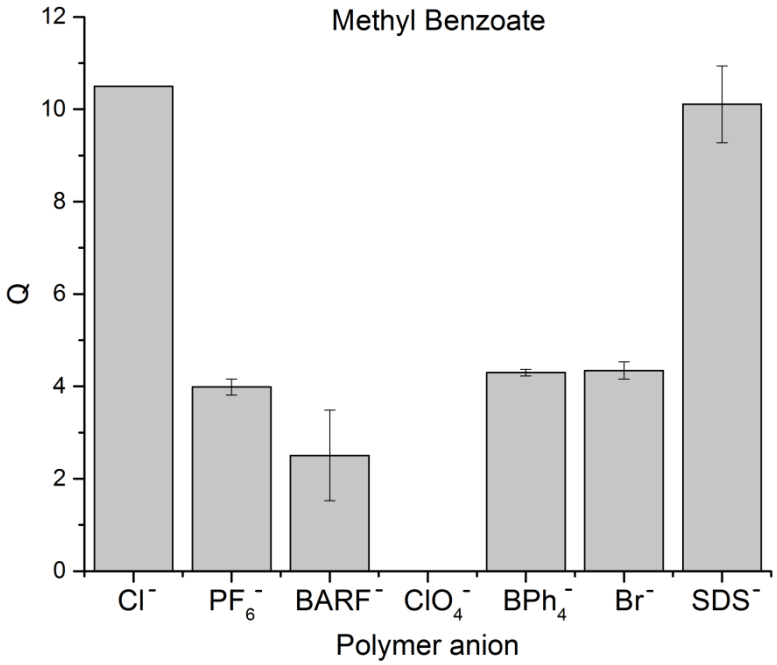

Figure 3.12 - The swelling degrees in methyl benzoate (Q) of each of the polymers containing 20% of the anion exchanged ionic monomer.

Methyl benzoate was the most important liquid for the investigation in the hunt for an anion which would improve the swelling of the low polarity simulant, HD, and V-series agents. Unfortunately, none of the anions improved the swelling ability of the polymer significantly past that of the chloride, and all but SDS decreased swelling (Figure 3.12).

3.3.4. Swelling and ion dissociation

From looking at the results, it was clear that the dielectric of the solvents and the ionic content were determining the major portion of swelling performance (as opposed to solvent compatibility). The smaller swelling magnitude differences between the various anions for each solvent must therefore have been related to the varying osmotic pressures which were directly related to the strength of each ion-pair.

3.3.4.1. Correlation of swelling to NMR chemical shift

DCM showed moderately similar Hansen solubility parameters to chloroform (Ra = 4.71), as well as similar dipole moments (D = 3.1 and 4.1) and reasonably close dielectrics (ε = 8.9 and

4.8). The swelling of the networks in DCM was plotted against the shift of the benzylic CH_2 in d-chloroform to determine if there was any correlation (Figure 3.13). The theory behind this was that the relative peak locations in the NMR can be directly related to the strength of the ionic interaction between the anion and cation. The association between the ions determines the electron density around the cationic nitrogen, and the adjacent CH_2 groups which are monitored. The ability of the d-chloroform to dissociate the ion pairs and modify the electron densities is related to the relative peak positions in NMR, and gives a guideline to the relative strength of the ionic association. Therefore, the osmotic potential inside a polymer network (and resulting swelling ability) could be correlated to the NMR peak positions. The shifts and Q values are shown in Figure 3.13.

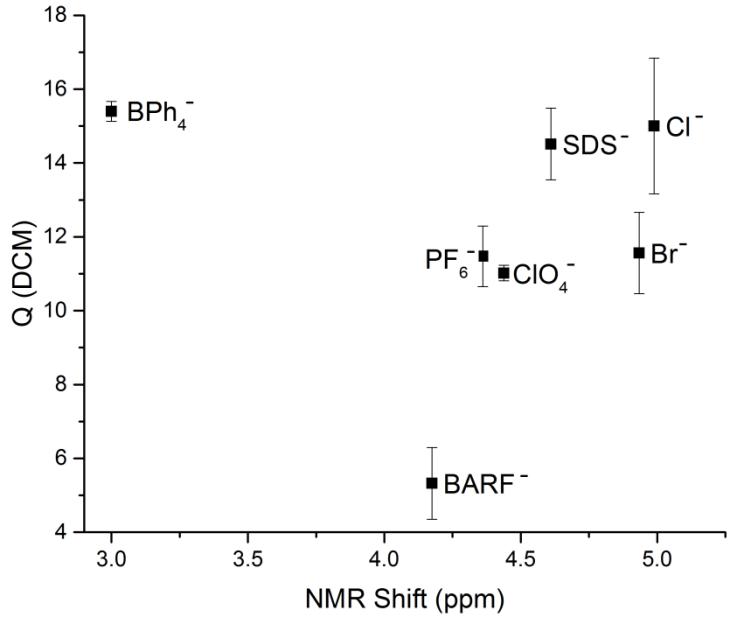

Figure 3.13 – The chemical shift of the benzylic CH_2 proton environment for the QAS salt monomers in $CDCl_3$, plotted against the swelling in DCM which was observed in the polymer containing the QAS.

With exception to the BPh_4, there did appear to be a minor correlation between the swelling ability and the up-field shift of the CH_2 protons. The peaks for the anions which were observed at lower frequencies showed decreased swelling. The polymers containing anions which swell the best (chloride, bromide) are dissociating more in the solution than the low swelling anions

(BARF, PF_6). This increased dissociation causes a higher internal osmotic pressure, which leads the higher swelling, but also reduces the electron density near the benzylic CH_2 which causes these peaks to appear further downfield.

3.3.4.2. Correlation of swelling with ion dissociation values

Previous work by Fry *et al*. has reported a compiled selection of experimental and theoretically derived ion association constants for a range of anions.[18] The model used for most of this work was a tetraalkylammonium salt onto which various anions were tested. The computational values from Fry *et al*. were gathered through a density functional theory procedure, with structural optimization being carried out with a PM6, followed by a B3LYP (6-31G+d) optimization. The energies of the atoms were then calculated with a natural population analysis method and solvation effects with a polarized continuum model.[19] The subsequent K_{ass} was calculated from the free energies:

$$\Delta G_{assoc} = G_{assoc_{computed}} - \left(G_{cation_{computed}} + G_{anion_{computed}}\right) \ [\text{kcal mol}^{-1}]$$

(Equation 3.2)

And,

$$ln\ K_{ass} = \frac{\Delta G_{ass}}{RT} \ \ [Unitless]$$

(Equation 3.3)

Experimental values are generally derived from electrical conduction measurements, which is a function of electrolyte concentration.[20] The issue with most of these data sources was they only presented association values for certain anions in certain solvents. Table 3.4 gives a range of values for the ion dissociation values of anions in specific solvents appropriate to this work, and the references from where they originated.

Table 3.4 - Showing the calculated and measured ion association constants in acetonitrile for some of the anions presented in this chapter, in various solvents. The experimental values chosen represent the highest and lowest values for each anion, demonstrating the wide range of experimental values in the literature.

Anion	K_{ass} (computational)[18]	K_{ass} (acetonitrile)
ClO_4^-	26	8[21], 38[22]
Cl^-	10	24[23]
BPh_4^-	5	5[24], 33[25]
PF_6^-	20	n/a

Across these sources only 4 anions were suitable for comparison with respect to our experimental swelling results. The computationally derived K_{ass} values for ClO_4^-, Cl^-, PF_6^- and BPh_4^- were plotted against the Q value for the subsequent polymers in acetonitrile and DCM; both good swelling solvents (Figure 3.14).

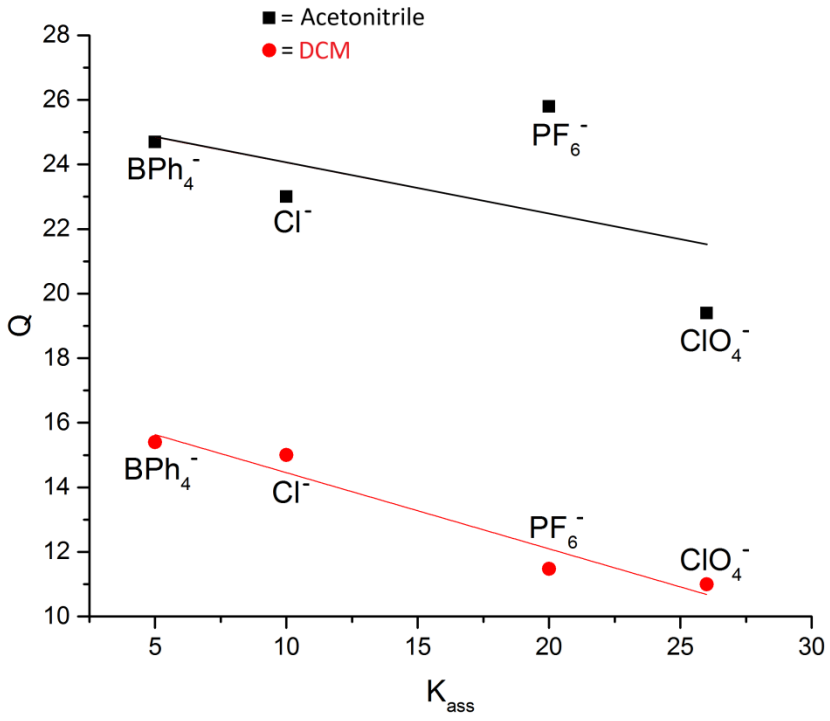

Figure 3.14 – Computed ion association constant (K_{ass}) plotted against Q for 4 of the anions whose association constants were pulled from literature. Red markers represent the swelling in DCM whilst the black represents the acetonitrile.

There did appear to be a correlation between the association constant and the swelling of the anions tested. The PF_6 containing polymer was an obvious outlier in the acetonitrile swelling (r^2 = 0.537). In DCM the PF_6 appeared to fit the trend better with an r^2 of 0.973. This data suggested that the weaker the association of the anion and cation, the higher the swelling, which is what would be expected. By this logic the swelling in a system may now be described well as a function of ion dissociation, ionic fraction/dielectric of solvent, and compatibility of the components. As opposed to just the latter two as presented in chapter 2.

3.3.5. Non-ionic polymerisations

3.3.5.1. Calculation of Ra

To enable the selection of possible monomers compatible with methyl benzoate and HD but also with the HIPE synthetic process, the Hansen solubility parameters for a range of monomers were obtained and the Ra values were calculated against both HD and methyl benzoate (Table 3.5). Initially derivatives of styrene were targeted due to the improved chemical stability of styrene over some other monomers, such as acrylates and methacrylates, which are susceptible to hydrolysis in solution over the long term.

Table 3.5 - The selection of homopolymers and co-polymers investigated alongside their HSP values and Ra values against both HD and methyl benzoate.

Polymer	δd ($MPa^{0.5}$)	δp ($MPa^{0.5}$)	δh ($MPa^{0.5}$)	Ra_{HD} ($MPa^{1/2}$) (18.8, 8.4, 5.1)	Ra_{MeBenz} ($MPa^{1/2}$) (18.9, 8.2, 4.7)
Methyl styrene	18.0	2.9	3.6	5.92	5.70
t-Butyl styrene	16.8	1.6	2.3	8.37	8.18
5 % ODMA	16.0	1.8	2.4	9.07	8.94
10 % ODMA	18.5	1.0	4.0	7.47	7.24
25 % ODMA	18.3	1.1	3.9	7.47	7.24
50 % ODMA	18.0	1.2	3.7	7.51	7.30
5 % VBC	17.3	1.4	3.3	7.83	7.64
10 % VBC	18.6	1.2	4.1	7.28	7.05
15 % VBC	18.6	1.4	4.1	7.08	6.85
20 % VBC	18.6	1.6	4.1	6.88	6.65
VBC	18.6	1.8	4.1	6.69	6.46
1 % MCR-M17	18.7	5.2	4.2	3.33	3.07
Methyl styrene	18.6	1.0	4.1	7.48	7.25
t-Butyl styrene	18.6	1.0	4.1	7.48	7.25

From looking at a range of vinylic monomers, it was seen that some of the homopolymers, and subsequent copolymer combinations did show lower Ra values against HD and the simulant when compared to styrene (Ra = 7.48 and 7.25 respectively). VBC and methyl styrene showed a good decrease in Ra, whereas *t*-Bu-styrene showed a slight increase. Given the low Ra values for VBC it was decided to synthesise a range of styrene-VBC networks for testing against the methyl benzoate simulant. ODMA was chosen due to the excellent results observed by Sada *et al.* where astonishingly high degrees of swelling for a number of relatively non-polar solvents were observed using this monomer.[3-5]

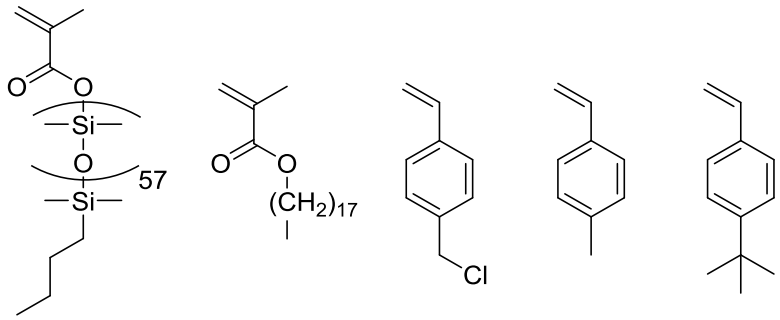

Figure 3.15 - The structures of the monomers used in an attempt to reduce the Ra and therefore increase the swelling of the non-ionic polymers. From left to right; MCR-M17 (methacrylate terminated PDMS), octadecyl methacrylate, VBC, *p*-methyl styrene, *t*-butyl styrene.

MCR-M17 (Figure 3.15) is a methacrylate terminated polydimethylsiloxane (PDMS) with a degree of polymerisation of 57 and polysiloxanes show high compatibility with non-polar solvents.[26,27] The synthesis of all the non-ionic networks containing ODMA, VBC, butyl styrene and methyl styrene led to the formation of brittle polymers. Each synthesis employed the same crosslinking density as previous networks of 1 mol%. The synthesis with MCR-M17 was carried out with only 1 % loading due to the high molecular mass of the monomer, and also formed a brittle gel.

3.3.5.2. Swelling of the non-ionic polymers

There was no significant increase in swelling with any of the alternative monomers (Figure 3.16).

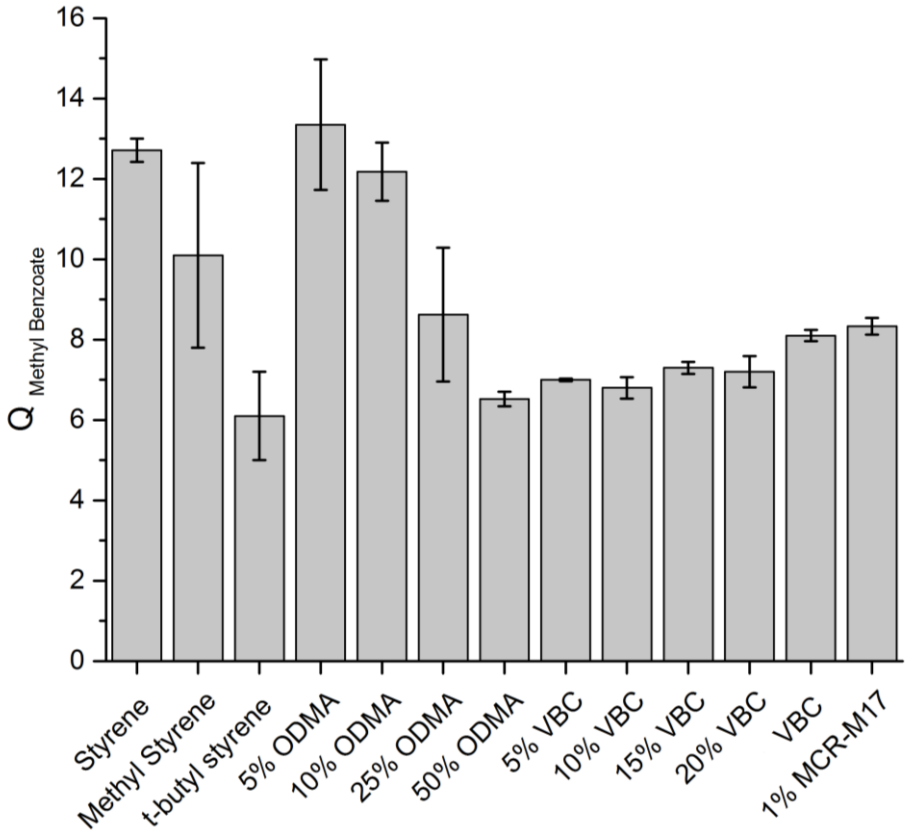

Figure 3.16 - The swelling degrees (Q) in methyl benzoate, of all of the polymer compositions which were examined with the target of improving swelling through better Ra matching.

The introduction of ODMA at 5 % of the total monomers showed slightly higher swelling (Q = 13.5), over the styrene only gel (Q = 12) the error associated could have easily negated this result. The swelling continuously decreased with additions of ODMA down to Q = 6.5 in the 50 % sample, likely due to the lack of compatibility of the solvent and this monomer. The MCR-M17 doped polystyrene also dropped in swelling capacity down to just over Q = 8. Addition of VBC reduced the swelling ability of the polymer significantly down to Q = 7 at 5 % VBC, after which increased insignificantly up to Q = 8 at 100 % VBC. Neither the methyl, nor *t*-butyl styrene, came close to that of the styrene.

3.3.5.3. Correlation of Ra to swelling performance

Comparison of the swelling and the Ra from the development process (Figure 3.17) showed that there was no value in using the Ra to determine whether the swelling of this system would be improved by adding certain monomers.

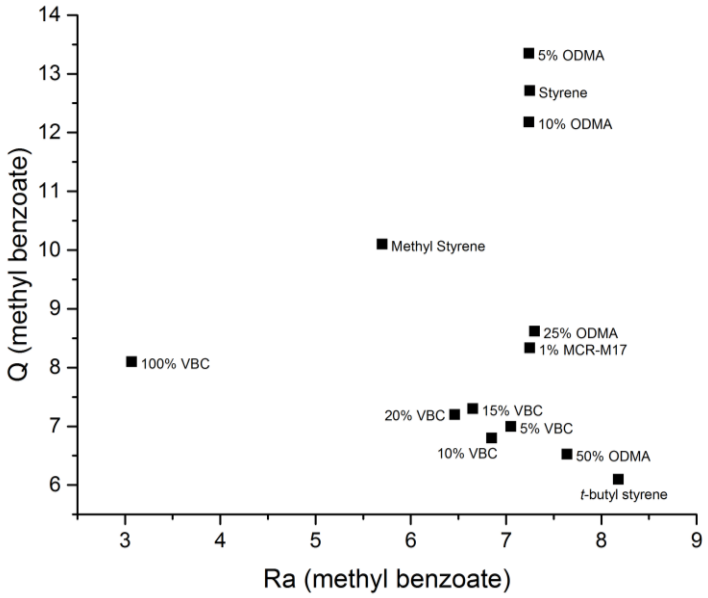

Figure 3.17 – A graph of the swelling degree in methyl benzoate (Q) against the Ra (methyl benzoate) of all of the polymers trialled in this section with respect to increasing the swelling through reducing the Ra.

As a screening process to try to identify polymers which are both easily accessible, cheap, and polymerise in a similar fashion to that of the styrene, this exercise was fruitless. For the swelling of the low polarity methyl benzoate, and therefore the sulfur mustard and VX, a simple styrene organogel was still the best performing solution. Using HSPs to improve the swelling was not useful due to the small range of Ra values over which the various monomers were arranged.

3.4. Conclusions

The work throughout this chapter, despite being based upon two lines of testing, converged with very similar results. With regards to the anionic exchange tests, it was disappointing to see that the results presented by Sada could not be replicated in any of our tests. Across all of the solvents tested with each of the BARF salt based polymers, none came even close to the values reported in the literature, despite vigorous repetitive study, both matching their synthesis and modifying it. Increasing the ionic content of BARF still did not allow us to reach swelling degrees near the quoted values in the literature, and the trend seemed to follow that of the ionic increases seen in chapter 2, just with slight magnitude changes. Despite this setback, the work continued to test the other anions with an aim to compare them to our previous work with the chloride anion. Whilst the swelling results were not as high as was had hoped, it showed that the swelling changes observed after anion exchange were directly related to the osmotic pressure of the system, which was modified by each anion. The association constants which could be gathered for Cl^-, PF_6^-, ClO_4^- and BPh_4^-, showed a relationship between swelling and association of the ion pair. Weaker association led to higher swelling likely through relatively increased free ion in the polymer matrix. Polymers swollen in ethanol were shown to have a strong relationship with the anions' ability to accept hydrogen bonds, due to the hydrogen bond donating effect of the ethanol which played a large part in its solubility. There was little discernible difference in swelling performance in this system between compact ions such as Cl^- and Br^-, were corroborated with the hydrogen bond accepting ability of these anions. The results have shown that if a targeted swelling system for a specific high polarity solvent is required, then an alternate anion may well improve the swelling a noticeable amount, for example BARF for ethanol absorption and PF_6^- or BPh_4^- for acetonitrile. With respect to the screening of non-ionic monomers for increasing the dispersion component of the system, a similar trend was observed: where none of the monomer systems examined, either homo-, or co-polymers, showed a notable increase in

swelling behaviour in most solvents when compared to the styrene only polymer. Whilst some polymers did show a slight increase in swelling, they were not distinguishable outside of the errors. Ra was not effective at predicting the swelling of the polymers formed of alternate monomers due to the very small range of Ra values involved.

Improving the swelling of a V-series or mustard chemical warfare agent, through the modification of the anion or the non-ionic monomers in a weakly ionic polyelectrolyte, was not possible; and the most effective sorbent for these CWAs at this stage remained to be a majority styrene polymer gel.

3.5. References

1 S. H. Strauss, *Chem. Rev.*, 1993, **93**, 927–942.

2 K. Iseda, M. Ohta, T. Ono and K. Sada, *Soft Matter*, 2011, **7**, 5938.

3 T. Ono, T. Sugimoto, S. Shinkai and K. Sada, *Adv. Funct. Mater.*, 2008, **18**, 3936–3940.

4 T. Ono, T. Sugimoto, S. Shinkai and K. Sada, *Nat. Mater.*, 2007, **6**, 429–433.

5 T. Ono and K. Sada, *J. Mater. Chem.*, 2012, **22**, 20962.

6 T. Ono, M. Ohta, K. Iseda and K. Sada, *Soft Matter*, 2012, **8**, 3700.

7 S. H. Strauss, *Chem. Rev.*, 1993, **93**, 927–942.

8 I. Ohmine and T. Tanaka, *J. Chem. Phys.*, 1982, **77**, 5725–5729.

9 W. J. Horne, M. A. Andrews, K. L. Terrill, S. S. Hayward, J. Marshall, K. A. Belmore, M. S. Shannon and J. E. Bara, *ACS Appl. Mater. Interfaces*, 2015, **7**, 8979–8983.

10 A. F. Kingery and H. E. Allen, *Toxicol. Environ. Chem.*, 1995, **47**, 155–184.

11 S. Kondo, T. Ohtsuka, K. Ogura and K. Tsuda, *J. Macromol. Sci. Part A - Chem.*, 1979, **13**, 767–775.

12 E. Hrvatsko kemijsko društvo., K. Hrvatsko prirodoslovno društvo. and Z. Sveučilište u Zagrebu., *Croatica chemica acta = Arhiv za kemiju.*, [Hrvatsko kemijsko društvo], 1956, vol. 75.

13 R. H. Wiley and J.-I. Jin, *J. Macromol. Sci. Part A - Chem.*, 1969, **3**, 835–843.

14 R. H. Wiley, W. K. Mathews and K. F. O'driscoll, *J. Macromol. Sci. Part A - Chem.*, 1967, **1**, 503–516.

15 Polymer Chemistry, Guide to the presentation of experimental data,

http://www.rsc.org/journals-books-databases/journal-authors-reviewers/prepare-your-article/experimental-data/#data-presentation, (accessed 27 July 2018).

16 T. Ono and K. Sada, *J. Mater. Chem.*, 2012, **22**, 20962.

17 S. J. Pike, J. J. Hutchinson and C. A. Hunter, *J. Am. Chem. Soc.*, 2017, **139**, 6700–6706.

18 A. J. Fry, *J. Org. Chem.*, 2015, **80**, 3758–3765.

19 J. Tomasi, B. Mennucci and R. Cammi, *Chem. Rev.*, 2005, ***105*** (8), 2999–3094.

20 G. Moumouzias and G. Ritzoulis, *J. Solution Chem.*, 1996, **25**, 1271–1280.

21 J. F. Coetzee and G. R. Padmanabhan, *J. Am. Chem. Soc.*, 1965, **87**, 5005–5010.

22 R. J. LeSuer, C. Buttolph and W. E. Geiger, *Anal. Chem.*, 2004, **76**, 6395–6401.

23 M. S. Z. Syal, V. K.; Chauhan, S.; Chauhan, *Phys. Chem.*, 1988, **159**, 49.

24 D. S. Gill, N. Kumari and M. S. Chauhan, *J. Chem. Soc. Faraday Trans. 1 Phys. Chem. Condens. Phases*, 1985, **81**, 687.

25 D. K. Das, B.; Saha, N.; Hazra, *J. Chem. Eng. Data*, 2000, **45**, 343.

26 C. V. Rumens, M. A. Ziai, K. E. Belsey, J. C. Batchelor and S. J. Holder, *J. Mater. Chem. C*, 2015, **3**, 10091–10098.

27 N. L Jessamine., P. Cheolmin., and G. M. Whitesides, *Anal. Chem*., 2003, **75**, 6544-6554.

Chapter 4 -

Synthesis of a Poly(styrene-*co*-vinylbenzylchloride-*co*-divinylbenzene) Poly High Internal Phase Emulsion with Exceptional Swelling Ability in Chemical Warfare Agents

A large part of the research presented in this chapter has been peer-reviewed and published in; *ACS Appl. Mater. Interfaces,* 2017*, 9*, 31335-31339.[1]

4.1. Introduction and Aims

4.1.1. Introduction to pHIPEs as sorbents

The aims presented in this chapter were to investigate the impacts which a morphological change in the polymer structure would have on the swelling performance in the chemical warfare agent simulants. Specifically, the morphology change examined would be a movement from a bulk network, as presented in the previous two chapters, towards a polymerised high internal-phase emulsion (pHIPE). This polymeric morphology was chosen due to its proven versatility across a wide range of research areas. Recent works, of which there is a limited selection, have shown that this morphology is effective at producing hydrogel sorbents of various compositions. Silverstein *et al*. utilized an o/w pHIPE with an internal phase of 78 % to produce monoliths of poly (2-hydroxyethyl methacrylate) which showed good swelling behaviour in water of with maximum swelling of Q = 6.6 in less than 10 minutes.[2] Functionalised glycidyl methacrylate o/w pHIPEs has also been used for similar purposes by Kovačič *et al*. and resulted in improved water swelling in an 80 % internal phase system of Q = 15.[3] Hydroxyethyl methacrylate and methacrylic acid copolymer based pHIPEs have also been developed with swelling which responds to pH changes. From pH 2 to 10, the water swelling of the polymers changed from Q =7.8 to Q = 18.2 due to the formation of the sodium salt of the methacrylic acid at high pH, effectively forming a weak polyelectrolyte (Figure 4.1).[4]

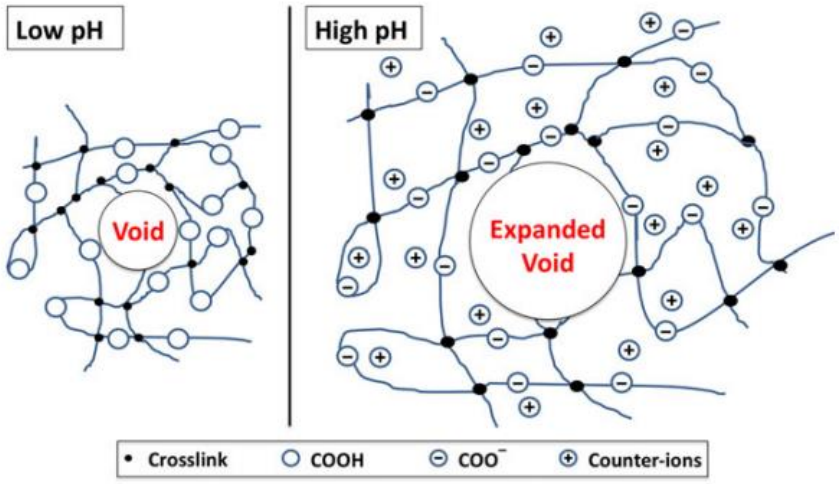

Figure 4.1 - A figure taken from reference[4] which shows how the water swelling of a methacrylic acid based pHIPE is affected by pH. The figure also demonstrates how as the polymer network swells; the voids (pores) increase in size, allowing further absorption.

In terms of the swelling and absorption of organic materials, a few reports were found in literature. Jiang *et al*. developed a Fe_3O_4 doped styrene/DVB based monolith which could absorb oils from the surface of water at up to Q = 16. The monoliths swelling could be cycled and were also able to be removed with a magnet from the water due to the supported iron oxide particles.[5] Guo *et al*. utilized waste polystyrene by-products as a stabilizer, which could then produce pHIPE monoliths in a continuous film production for oil spill remediation. They claimed a Q = 15 in diesel with the ability to cycle the polymers over 20 times, each time reclaiming over 85 % of the oil.[6] Truly superabsorbent pHIPEs were first reported in 2016 by Silverstein *et al*. where a poly(2-acrylamido-2-methyl-1-propanesulfonic acid) pHIPE with low crosslinking and 85 % internal phase showed impressive water absorption of over Q = 300.[7] A very recent paper also by Silverstein *et al*. demonstrated how forming an amphiphilic pHIPE from a methacrylate terminated triblock copolymer and high internal phase (85 %) allowed them to absorb to very high levels water (45 ml g^{-1}), Ethanol (40 ml g^{-1}), toluene (55 ml g^{-1}) and DCM (95 ml g^{-1}) in a single system.[8] Many of the reports on pHIPE swelling attribute the absorption to the swelling-driven void expansion of the polymers. This is an advantageous effect of using a pHIPE as an absorbent material which allows the voids to increase as the

supporting polymer swells. In comparison to absorption with pHIPEs, one group has directed research towards other morphologies for the absorption of CWAs. One such example is a collaboration with DSTL in Porton Down, UK, where they developed functional hypercrosslinked styrene/DVB systems with absorption capacities in sulfur mustard and sarin reaching nearly Q = 20.[9] At the time of writing there was no literature where pHIPEs were utilized only for CWA absorption.

4.1.2. The approach and design

The best performing polymer composition from chapter 2 (St_{100}), would be used in this chapter, and modified into a pHIPE. The synthesis of pHIPEs forms a sponge like structure which is hoped to have good static uptake ability for liquids; however an overly crosslinked / rigid sponge would not be able to exploit the network swelling aspects of the bulk polymers. The crosslinking density of the pHIPEs was therefore chosen to remain at 1 mol% against the other monomers so that as the pHIPE sponge absorbs the liquid; the polymer network can also swell, and in turn increase the internal volume of the pores, allowing for more liquid uptake in a dynamic fashion through the void-expansion effect.

The pHIPE was then modified with respect to monomer choice and internal phase. This would change the chemical compatibility and total internal pore volume, respectively. The resulting open-cell polymer foams would be analysed for their; porosity (through SEM), swelling ability, ability to retain a chemical agent simulant over time, and ability to swell from a compressed state. The characteristically low density/large volume form factors in a pHIPE would be a barrier to aspects of practical use such as transport. For this reason, the polymer would need to be able to be compressed to make it more logistically viable, without loss of the microstructure and swelling ability. Starting with a direct comparison of a pHIPE version of St_{100}, small amounts of vinylbenzyl chloride (VBC) would be introduced to the composition. This would be done to add a labile functional group which could be utilized in further work to

modify the chemistry of the polymer. With respect to compatibility, chapter 3 showed that adding VBC would likely reduce the swelling of the polymer in the simulant slightly.

Previous work by Kondo *et al.* has determined the reactivity ratio for the copolymerization of styrene and VBC to be $r_1 = 0.72$ and $r_2 = 1.32$ respectively.[10] The $r_1r_2 = 0.95$ favours the formation of a statistically random copolymer. This should lead to minimal composition drift in the polymerisation. Composition drift to gradient copolymers or discreet homopolymers could be disadvantageous. Furthermore, the VBC has been shown previously to be hydrophobic enough to not interfere with the delicate formation of the HIPE foam.[11,12] In fact it has been shown to be effective at forming pHIPEs which could be functionalised with amines for tailored carbon dioxide uptake.[13]

The final modifications to the pHIPEs in this chapter would be with regards to the internal-phase fraction. An emulsion with an internal phase of anything over 74 % is considered a HIPE, but to increase the swelling performance, the polymers would be synthesised with an internal phase fraction much higher, starting at 92 %. The volume percentage of internal phase of the emulsion determines the resulting density and interconnectivity of the pHIPE, and therefore the solvent uptake ability. To optimize the internal volume and interconnectivity of the polymers, the internal phase was increased from the original 92 %, up to 95 %, 96 % and 97 %, to observe how this would affect the swelling performance. If a composition and morphology could be identified which absorbs CWAs to over Q ~ 25, the polymer was to be tested for scalability of both the swelling behaviour, and the production.

4.2. Experimental

4.2.1. Materials and Equipment

All the chemicals used for this work were purchased from Sigma Aldrich. Styrene (99.9 %), 4-vinylbenzyl chloride (VBC) (90 %) and divinylbenzene (technical grade, >80 %) were all passed through a short column of basic alumina immediately before use to remove the inhibitors. The

Span 80 (1000-2000 mPa) and potassium sulfate (99.0 %) were used without further modification. Water for the internal phase was laboratory deionised water (pH 7.0, 0.5 mS cm^{-1}).

Electron micrographs were obtained using a Hitachi S-3400 scanning electron microscope. The chamber was set to full vacuum, with an electron beam voltage of 20 kV and an emission current of 80 mA. Detections were carried out with the backscatter electron detector. The pHIPE samples were prepared for SEM by drying thoroughly and then cutting into thin slices using a fresh scalpel blade, and with care taken to not disrupt or damage the surface of the sample. Samples were analysed directly in the SEM without any further preparation.

Pore distributions of the samples were determined from the electron micrographs of samples of freshly sliced pHIPEs. Analysis of the pores was carried out with ImageJ software. Each sample had a minimum of 350 pore measurements randomly measured from three slices to achieve a reasonable statistical distribution for analysis.

^{1}H NMR spectra were acquired on a Bruker Avance Neo NMR at 400MHz at room temperature (22 °C). The samples were examined using an HR-MAS semi-solids probe, utilizing magic angle (54.736 °) spinning at a moderate frequency of 5000 Hz. To ensure more reliability regarding integration of the samples, the relaxation delay was set to 60 seconds for all NMR which was expected to be more than suitable for these samples based upon previous literature in crosslinked polymer samples.[14,15] The pHIPE samples were swollen in d-chloroform inside Bruker disposable inserts (poly(triflurorochloroethylene). These were then placed in a 4mm zirconium spinner with plastic rotor designed for the 4mm probe.

Infra-red spectroscopy was carried out on a Shimadzu IRAffinity-1S, with an ATR gate, a sweep of 500 - 4000 cm^{-1}, a resolution of 2 cm^{-1} and 64 scans.

4.2.2. PHIPE Synthesis

A general procedure for the synthesis of the pHIPEs based on that reported by Williams *et al*.[16] was followed.

Styrene, divinylbenzene, 4-vinylbenzyl chloride, AIBN, and span-80 (sorbitan monooleate) were added into a 250 ml conical flask. The flask was stirred at 250 rpm with a 4 cm hemispherical PTFE overhead stirred paddle for 5 minutes to homogenise the oil phase. A solution of potassium sulfate in deionized water was then prepared. The stirring speed of the organic mixture was increased to 750 rpm and the aqueous solution was dropped in at rate of around 1.5 drops per second. After all the aqueous phase was added, the stirring speed was increased further to 900 rpm and left to homogenise for 10 minutes. The formed HIPEs all exhibited a texture similar to that of mayonnaise and were prone to irreparably splitting if the water was added too fast. The HIPE was placed into a plastic cylinder, sealed and cured in an oven at 65 °C for 24 hours. After curing, the pHIPE monolith was cooled and removed from the cylinder and cut into disks of around 1 cm thick. It was then dried under vacuum at 65 °C for 48 hours minimum. Complete dryness was determined by observation of the point at which mass reduction ceased and coincided with the expected polymer mass. The surfactant was not removed prior to any experiments. Quantities of monomer, stabilisers, water and initiator for the different samples are given in Table 4.1. The 97 % internal phase sample was run at half the scale of the other samples due to the extremely large mixing volume which would have been required at 97 % internal phase.

Table 4.1 – Quantities used for the synthesis of each of the pHIPE samples.

Sample	DVB	Styrene	VBC	AIBN	SMO	Water/ K_2SO_4
$St_{100}VBC_0IP_{92}$	0.0988 g	7.900 g	-	0.015 g	1.65 g	92 ml / 0.5 g
$St_{95}VBC_5IP_{92}$		7.509 g	0.579 g			
$St_{90}VBC_{10}IP_{92}$		7.114 g	1.158 g			
$St_{85}VBC_{15}IP_{92}$		6.718 g	1.737 g			
$St_{95}VBC_5IP_{95}$		7.509 g	0.579 g			155 ml / 0.5 g
$St_{95}VBC_5IP_{96}$						196 ml / 0.5 g
$St_{95}VBC_5IP_{97}$	0.0494 g	3.754 g	0.290 g	0.0075 g	0.825 g	132 ml / 0.25 g

4.2.3. Determination of solvent absorption by pHIPE samples

The absorption of the pHIPE samples was determined by immersing a small cube of the dry pHIPE of pre-determined weight (typically around 50mg) into the chosen CWA simulant, methyl benzoate, for 24 hours. After the elapsed time, the polymer was removed from the solvent and excess solvent dabbed off. The absorption capacity, Q, was calculated from;

$$Q = \frac{(Mass\ swollen\ polym. - Mass\ dry\ polym.)}{(Mass\ of\ dry\ polym.)}$$

(Equation 4.1)

For the pHIPE which was crushed before swelling, this was done by placing a cube of the pHIPE (c. 12 mm x 12 mm x 10 mm) in a press and applying 220 N of force with the polymer between two small steel plates. The compressed cube was then immediately weighed and then placed in solvent for swelling in the same fashion. This value for compression was chosen as it represented the highest compression that could be achieved before the matrix started to show visible cracking.

Swelling studies on the chemical agents were carried out to the same methodology and similar scales at: DSTL Porton down, Wiltshire, United Kingdom, by Dr. Marcus Main and Dr Nicholas Cooper.

4.2.4. Scaled up synthesis of $St_{95}VBC_5IP_{95}$

The following outlines the procedure for the production of 1 kg of dry $St_{95}VBC_5IP_{95}$. To a 20 litre glass round bottom reaction vessel with a 100 mm ground glass rim, was added divinylbenzene (10.868 g, 0.08 mol), styrene (825.9 g, 7.93 mol), 4-vinylbenzyl chloride (63.7 g, 0.42 mol), sorbitan monooleate (SPAN-80) (181.5 g), and AIBN (1.65 g, 0.01 mol). A 100mm wide paddle stirrer was placed into the vessel and multiport ground glass lid was then arranged around the shaft and clamped closed. The shaft was attached into an IKA Eurostar 100 digital overhead stirrer. At this point, the organic external phase was mixed for 20 minutes at 300 rpm. Three portions of the internal, aqueous phase was prepared; each by mixing 5 L of deionised water with potassium sulfate (16.13 g) and a final portion made up consisting of 2050 ml of deionised water containing 6.63 g of potassium sulfate. The stirring was then increased to 850 rpm and the internal phase was slowly added over the course on an hour and a half to form the emulsion foam. During the addition of the internal phase, the stirrer paddle needed to be increased in height incrementally to ensure there was not a layer of standing aqueous phase at the top of the foam. This was due to the stirrer choice not being sufficient to satisfactorily move the emulsion around as the volume and viscosity increased, in the future it would be advantageous to modify the stirring apparatus to include a lower shear attachment such as a propeller to force the emulsion to circulate. Once the internal phase had been added the stirring was increased to 1000 rpm and the overhead stirrer was moved manually in a pattern such that the mixture was homogenised to a satisfactory extent (Figure 4.2). The mixture was then poured into four rectangular plastic containers, each with a total volume of 5.5 L (c. 29 cm x 23 cm x 11 cm). The surface of the foam was then smoothed out and the boxes were sealed and placed into a 65 °C oven for 36 hours to cure.

Figure 4.2 – Left; the set up for the mixing of the large scale pHIPEs (20 L reactor), centre; mixing for the emulsion after addition of the first 25 % internal phase, right; the emulsion after addition of all internal phase.

After curing the monoliths of polymer were cut into strips 1 inch deep (Figure 4.3) and were arranged in the fume cupboard to cool. They were then placed into a 55 L thermos scientific vacuum oven. The oven was set to 55 °C and 100 mbar pressure with gas ballast to carry the water vapour. In these conditions the polymer took over a week to dry completely.

Figure 4.3 – Left; the HIPE in the trays used for curing, centre; the cured monolith of $St_{95}VBC_5IP_{95}$, right; the cured monolith after having been sliced for drying in vacuum oven.

4.3. Results and Discussion

4.3.1. NMR analysis of the pHIPE VBC content

To determine the VBC content of each of the pHIPEs, analysis was attempted through proton NMR. Due to the crosslinked nature of the polymers, solution state NMR was not possible, as the broadening of the peaks rendered the spectra useless. Limited selections of samples were run on MAS semi-solids probe which the department acquired late into the project. The polymers were swollen in chloroform-d inside the MAS spinner at magic angle. Spinning the samples as a gel allowed observation of significant line sharpening to a point where compositional analysis could be carried out to a reasonable degree. The NMR analyses were carried out on the $St_{95}VBC_5$, $St_{95}VBC_5IP_{92}$, $St_{90}VBC_{10}IP_{92}$, $St_{85}VBC_{15}IP_{92}$, and $St_{95}VBC_5IP_{95,}$ and were compared to a solution state NMR of the VBC monomer (Figure 4.4).

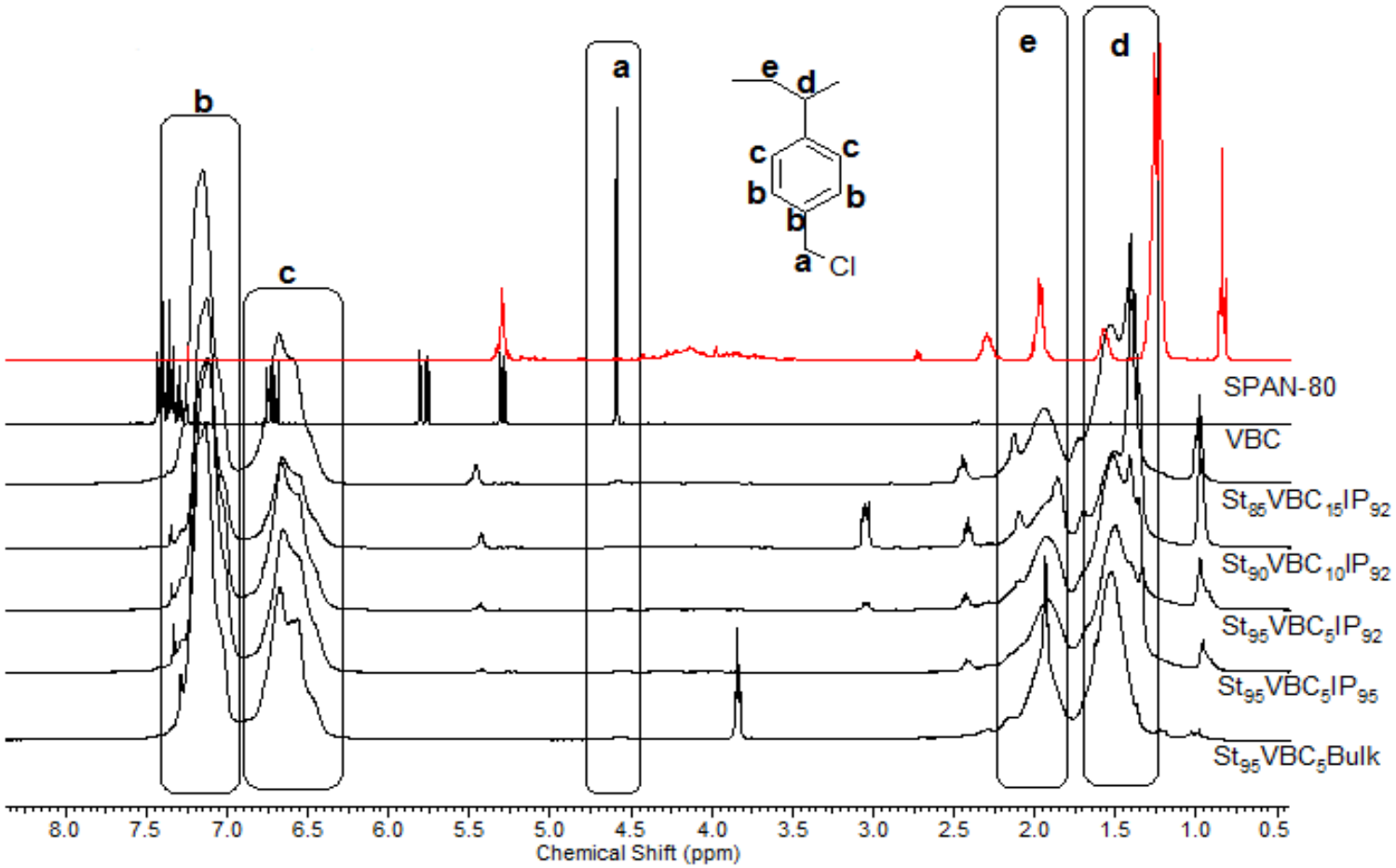

Figure 4.4 - H^1 MAS-NMR of the pHIPEs with varying VBC content (5 % - 15 %), compared to that of a non HIPE sample, the monomer VBC and the surfactant SPAN-80 (red). The peaks of importance are encased with rectangles and are correlated to the structure of VBC in the top image.

The peaks marked (a) on the spectra represented the CH_2 unique to the VBC in the polymer. This region was the only region unique to VBC. The surfactant presented large signals in the regions of (e) and (d) and a broad set of multiplets between 3.5 and 4.5 ppm. All pHIPE samples showed signals at 1.0, 2.2 and 5.5 ppm which were derived from the surfactant which remained in the matrix. Contrasting the surfactant peak (CH_3) at 1.0 ppm to the polymer backbone peaks of (b) and (c) showed the surfactant remaining in the polymer was constant throughout all pHIPEs, with exception to $St_{80}VBC_{10}IP_{92}$ which showed double the relative amount of surfactant than all the others. An abnormality to note was that a multiplet was present at 3.0 ppm in both $St_{95}VBC_5IP_{92}$, and $St_{90}VBC_{10}IP_{92}$ which could not be identified. Integration of the VBC CH_2 signal at 4.5 ppm (a) against the benzene region of the polymer (b) and (c) showed a decreasing ratio of these groups to the VBC which is what would be expected as the VBC content increases (Table 4.2).

Table 4.2 - Relative integration values for the peaks in the MAS-NMR of the pHIPEs with VBC variation

Sample	**Benzene** Integral (*b* + *c*)	**VBC** Integral (*a*)	**% VBC** in the polymer
$St_{95}VBC_5$	238	2	2.1
$St_{95}VBC_5IP_{95}$	172	2	2.9
$St_{95}VBC_5IP_{92}$	169	2	2.9
$St_{90}VBC_{10}IP_{92}$	142	2	3.5
$St_{85}VBC_{15}IP_{92}$	145	2	3.4

Comparison could not be accurately made against the backbone protons (Figure 4.1 signals d and e) due to the presence of the surfactant which shared the same proton environment. Due to this, accurately deducing the amount of VBC in the networks in these systems was not possible. The preliminary results obtained suggested that there was very similar amounts of VBC incorporated into each of the polymers, not the 5 % increases designed to be present.

4.3.2. Swelling related analysis of the pHIPEs

4.3.2.1. Comparison of $St_{100}VBC_0IP_{92}$ with the non-HIPE polymers

Initially, the $St_{100}VBC_0IP_{92}$ sample was swollen in a range of laboratory solvents for comparison against the 'bulky' versions from the previous work known as St_{100} (Figure 4.5). The swelling of the pHIPE equivalent was much larger than that of the non HIPE polymers in all solvents.

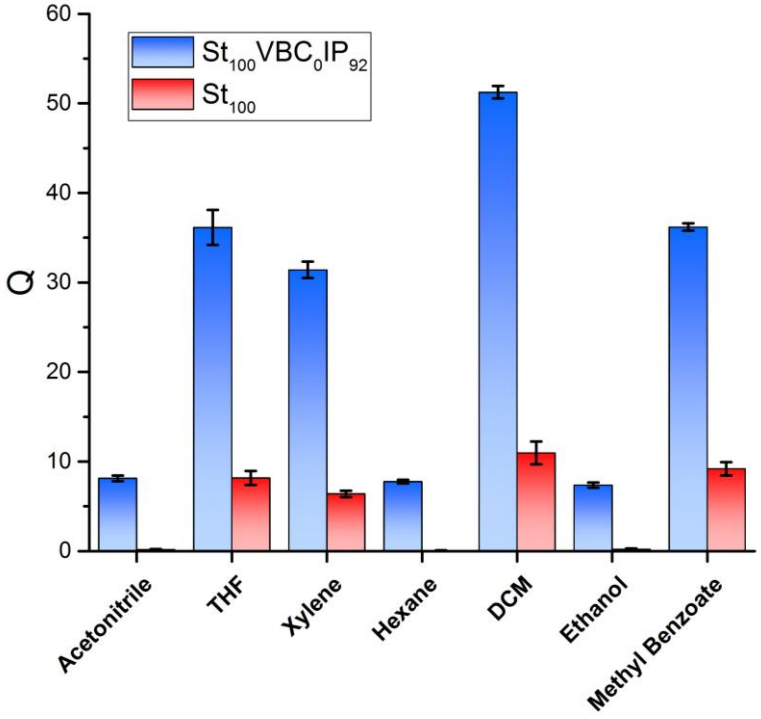

Figure 4.5 - A comparison of the swelling of the 100% styrene bulk gel, with its pHIPE counterpart at 92% internal phase.

Interestingly, the solvents which had originally showed little or no swelling ability in the St_{100}, all showed a mass uptake of around Q = 7.5 in the pHIPE version. This equated to an average volume swelling of Q_{vol} = 10.4 ± 1.02. This was a demonstration of swelling purely because of adsorption into the voids in the matrix and suggests that that free volume in the polymer is 91.2 % of the total volume. This is in line with the 92 % by design. The compatibility of the solvents and the matrix was not important for this uptake because it was likely the solvent was sitting only in the pores, taken in by capillary action. There may also have been a propensity for some solvents to be drawn in due to the intermolecular forces between the surfactant and

the solvent which was not removed after the synthesis. When the adsorption capacity of a non-compatible solvent in the pHIPE ($Q_{ethanol}$ = 7.5) was added to the swelling performance of a good solvent in the bulky St_{100}, for example in DCM (Q = 11), the result is only Q = 18.5. This value represents the potential for the matrix to swell a good solvent, added to the pore adsorption capacity of the pHIPE. This value was much lower than the swelling of DCM in the pHIPE which exhibited Q = 52. This shows that the swelling of the pHIPE was much larger than the sum of the static pore volume and matrix swelling. This is a good example of the swelling driven void-expansion effect. This shows that as the polymer matrix in a pHIPE swells the pores increase in volume which dynamically increases the total solvent absorption capability of the material. The swelling of DCM in the pHIPE was over two and a half times better than the sum of the bulk swelling ability of the matrix and static uptake potential of the pHIPE. This was the case across the board, and shows just how effective the dynamic swelling of these networks can be at increasing the resulting void volume and total swelling degree in a well optimized system.

4.3.2.2. Swelling of all the polymers in the CWA simulant

The polymer samples were each swollen in triplicate in methyl benzoate as the chosen CWA simulant (Figure 4.6). The initial change in morphology from a simple bulk polymer (St_{100}) to a 92 % internal phase pHIPE of equivalent chemical composition ($St_{100}VBC_0IP_{92}$) showed an impressive increase in swelling performance of nearly 4 times; from Q = 9.2 ± 0.75 to Q = 36.2 ± 0.41. This swelling represented one of the highest pHIPE swelling capacities in organic liquids observed to date and comparable to the absorption capacity of non-HIPE materials such as porous (spongy) graphene[17] and carbon nanofiber aerogels.[18] Following this morphologically based change, the pHIPE compositions were modified to include a small amount of VBC in place of the styrene. On the addition of 5 % VBC ($St_{95}VBC_5IP_{92}$), the swelling was seen to improve again by around 20 % up to Q = 42.9 ± 1.4. The swelling of the subsequent 10 % ($St_{90}VBC_{10}IP_{92}$), and 15 % VBC ($St_{85}VBC_{15}IP_{92}$) pHIPEs did not show any further increase in swelling performance outside of the error. Due to the lack of discernible swelling performance

observed when including a higher fraction of VBC, the 5% VBC polymer sample was chosen as the most appropriate for taking forward for use with the increased internal phase fraction. The internal phase was increased through the introduction of more water into the emulsion to 95 % ($St_{95}VBC_5IP_{95}$), 96 % ($St_{95}VBC_5IP_{96}$), and 97 % ($St_{95}VBC_5IP_{97}$). These systems could therefore have been considered hyper-internal phase emulsions.[19] On exposure to the chemical agent simulant, the swelling increased proportionally with the increasing internal phase fraction (95 %; Q = 55.6 ± 3.1 and 96 %; Q = 69.1 ± 1.07) to a maximum of Q = 89 ± 6.18 in the 97 % internal phase polymer.

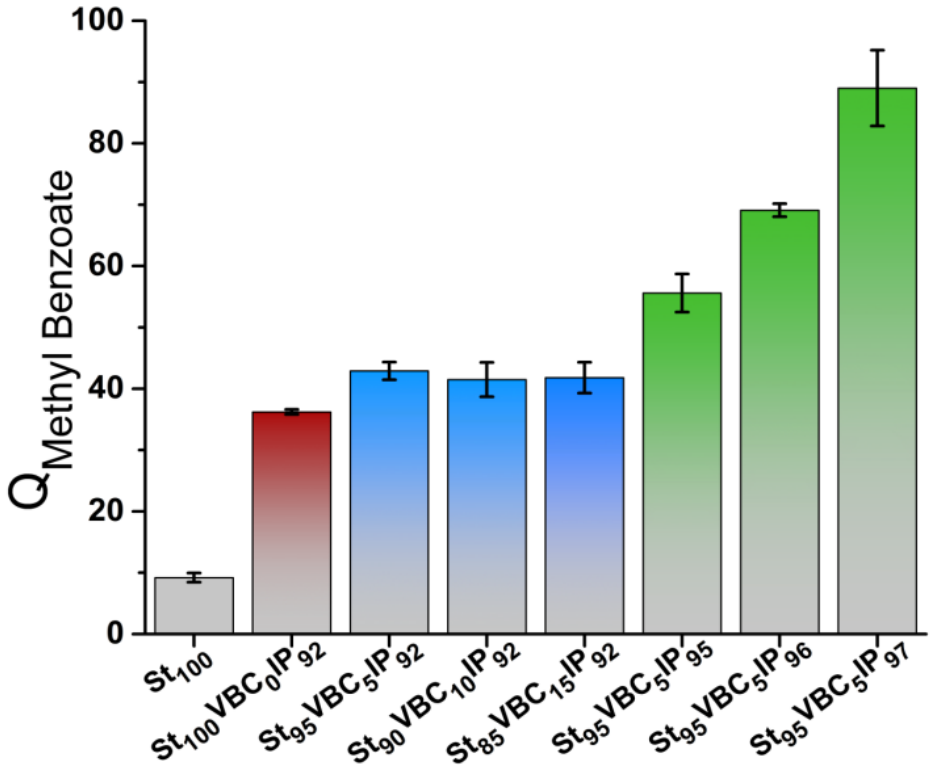

Figure 4.6 - The swelling performance in methyl benzoate of the 100% styrene bulk gel, in comparison to all of the subsequent pHIPE versions, with both increasing VBC content and internal phase.

4.3.2.3. Scanning electron micrographs of the pHIPEs

SEM was also undertaken on all of the samples (Figure 4.8), to show that the correct morphology had been achieved. This was also useful for determining the void/pore distributions of the polymers to see the pore features could be related to the swelling ability

changes. This was especially important in $St_{95}VBC_5IP_{92}$, $St_{10}VBC_{10}IP_{92}$ and $St_{85}VBC_{15}IP_{92,}$ where the swelling did not vary much with increased VBC content. The micrographs showed that all of the polymers formed morphologies typical of a cured HIPE.[20] The initial impression from viewing the micrographs showed that it was hard to differentiate between what is referred to in other literature[21] as the voids (pores) and the windows (interconnections), in these hyper-internal phase polymers. A traditional morphology would comprise of pores, with smaller connecting windows visible in the walls. In these polymers however, the windows were extremely large in diameter which made them indistinguishable from the pores. The composition appeared more alike a three dimensional spiders web, as shown in Figure 4.7. This was likely due to the extremely high internal phase fraction, causing large windows to form.

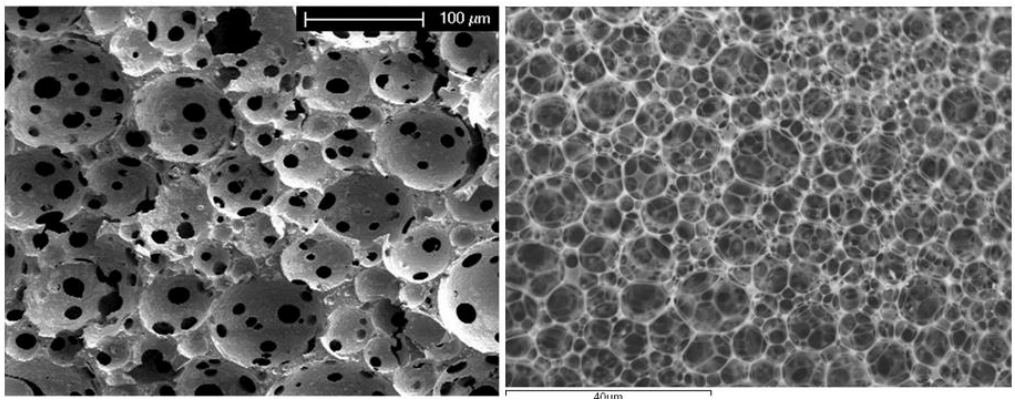

Figure 4.7 – A comparison of micrographs of pHIPEs; left) an 85 % internal phase pHIPE taken from reference,[22] and right) of $St_{95}VBC_5IP_{95}$. The left hand image exhibits clearly the large pores with distinct, small, interconnecting windows. The right hand image shows how the windows are indistinguishable from the pores.

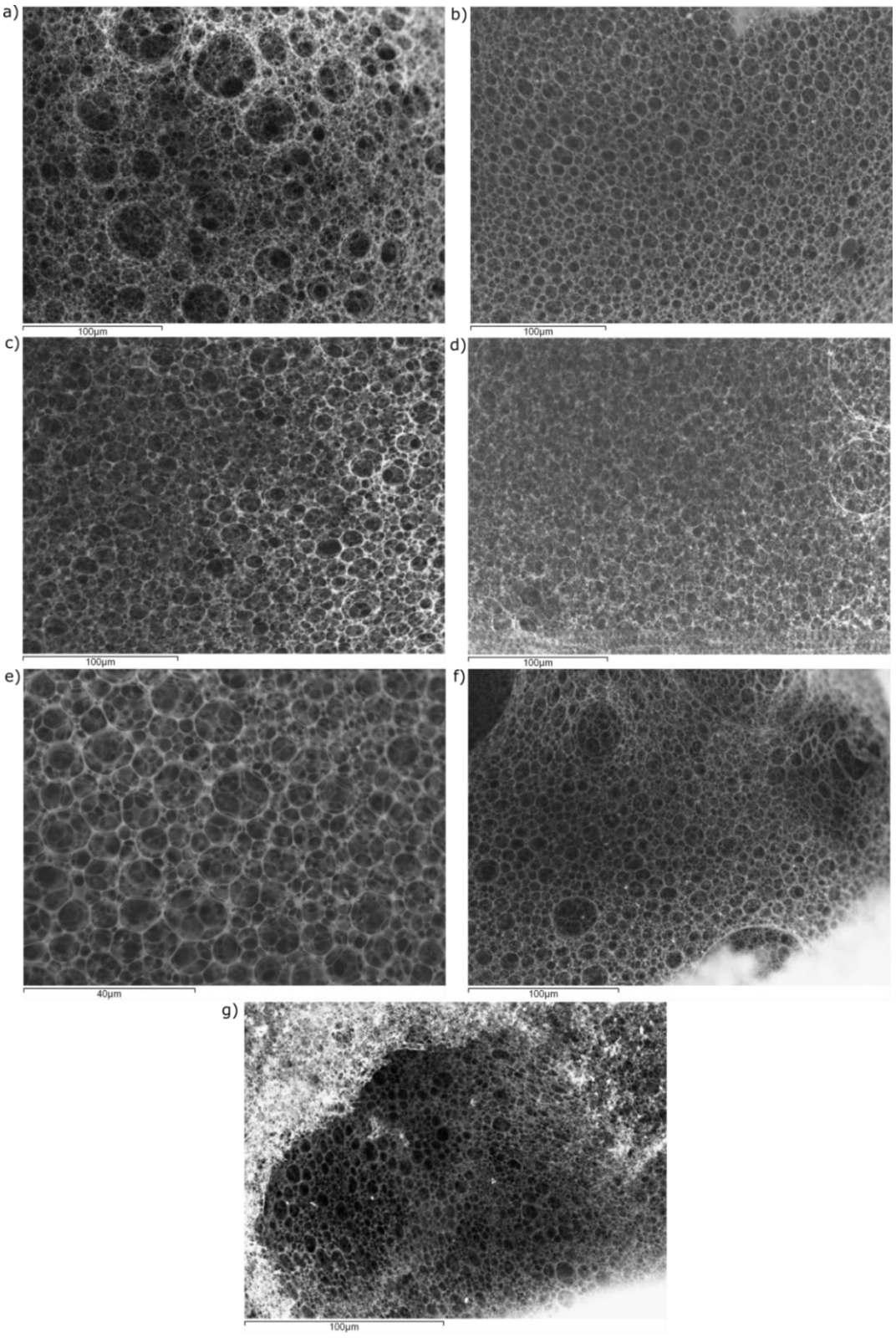

Figure 4.8 - Scanning electron micrographs demonstrating the internal morphology of the 7 pHIPEs; a) $St_{100}VBC_0IP_{92}$, b) $St_{95}VBC_5IP_{92}$, c) $St_{90}VBC_{10}IP_{92}$, d) $St_{85}VBC_{15}IP_{92}$, e) $St_{95}VBC_5IP_{95}$, f) $St_{95}VBC_5IP_{96}$, g) $St_{95}VBC_5IP_{97}$.

4.3.2.4. Analysis of the pore data to explain swelling results

An explanation of the swelling changes due to the addition of VBC and then the internal phase increase can be found from examining the pore data gathered from the SEM images (Figure 4.9 and appendix 4A). Analysis of the $St_{100}VBC_0IP_{92}$ and $St_{95}VBC_5IP_{92}$ gave average pore sizes of 8.6 µm and 6.8 µm respectively. Work by Barbetta *et al*. reported pore size reduction with the introduction of VBC to a 90 % internal phase DVB pHIPE of 10 µm, down to less than 5 µm. This effect was observed as VBC was introduced up to 100 % of the monomers, but most dramatically up to 30 %.[23]Increasing the VBC content in $St_{95}VBC_5IP_{92}$ to 15 % in $St_{85}VBC_{15}IP_{92}$ did not agree with this report; as the pHIPEs showed an increase in pore diameter back to 9 µm on increasing VBC content. The NMR data however showed there was only very slightly increasing VBC content from 2.9 % to 3.5 % in the polymers as opposed to the 5 % to 15 % by design. This suggested that the variations in pore sizes were more likely to be due to synthetic variations between the three samples rather than the incorporation of the VBC into the polymer.

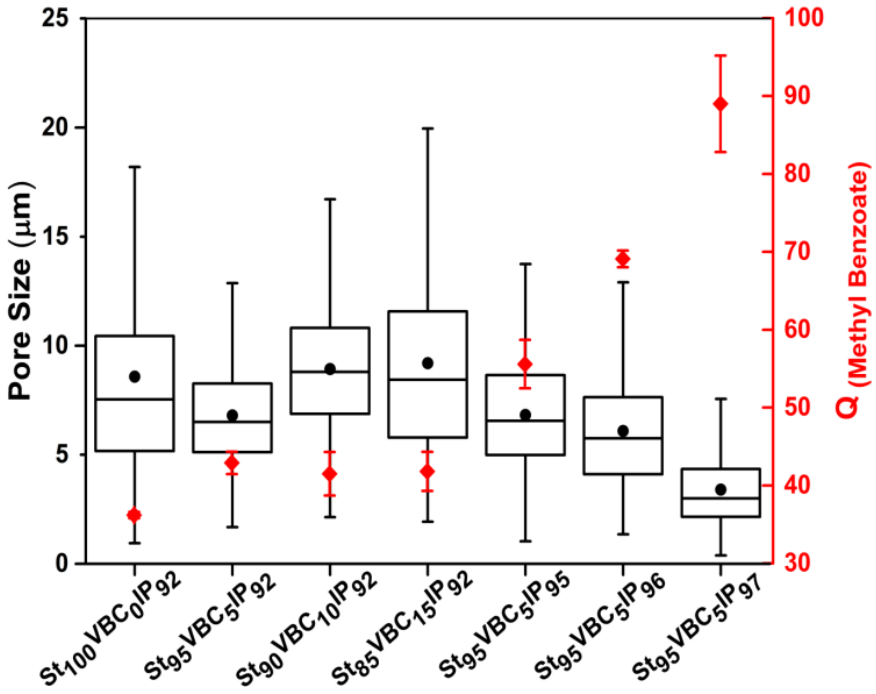

Figure 4.9 – The absorption capacities (Q) of each of the pHIPEs (red), contrasted with the respective pore size distributions (black), gathered from SEM images. The boxes represent the median and interquartile ranges and ● represents the mean pore size.

For the mechanics of absorption, especially when looking at fraction of solvent which does not swell the physical polymer matrix, it was assumed that capillary action was the driving force for filling the voids. Furthermore, the capillary pressure was inversely proportional to the pore radius, [24] and therefore the increase in absorption could be attributed to the decrease in pore radius according to the approximation:

$$\Delta P = \frac{2\gamma \cos\theta}{r}$$

(Equation 4.2)

Where ΔP=capillary pressure, γ= surface tension of liquid, Θ = contact angle of liquid and polymer and r = pore radius.'[25] It was also possible that the increased absorption was a result of an increase in the contact angle for the methyl benzoate with the polymer surface, rather than the decrease in pore radius. Since the surface energies were very similar (38-39 mJ m^2 for polystyrene and 40-43 mJ m^2 for poly(vinylbenzyl chloride)) it was not likely that the contact angles should differ significantly.[26] Previous work however has claimed that the VBC will gather at the interface of the water and oil phases in the system due to the more hydrophilic chloride group on the VBC.[27] Whilst this may favour increased VBC content on the surface of the pores, and therefore the higher surface tension, it was still likely that the pore radius changes were the largest contributing factor to the swelling. The pore sizes were further reduced by increasing the internal phase of the emulsions from 92 % to 95 %, 96 % and 97% internal phase. These reductions in pore diameter directly correlate with the increase in swelling of the system.

4.3.2.5. Leakage from the high internal phase samples

Unfortunately, it was observed that for the polymers which exhibited larger internal phase fractions; specifically the 96% and 97% samples, that they would not retain the simulant as efficiently as was hoped. When samples of the swollen system were left in an empty vial, a portion of the liquid would be expelled from the network over time. The ability of the

polymers to statically retain liquid over time was tested by leaving samples of the polymers after full absorption of the liquid in fresh vials and measuring the liquid loss gravimetrically after three days. From the equilibrium state $St_{95}VBC_5IP_{97}$ showed a mass loss of 31 ± 4.5 %, $St_{95}VBC_5IP_{96}$ showed a loss of 16 ± 3.4 %, $St_{95}VBC_5IP_{95}$ showed a loss of 4 ± 0.7 %, and the 92% internal phase sample ($St_{95}VBC_5IP_{92}$) showed no measurable mass loss over the time period. The increase in loss found in the higher internal phase samples was a logical consequence of having polymer morphologies where the porosity and degree of interconnected space is so high that the surface and interfacial tensions of the liquid and polymer struggles to overcome external forces such as gravity in this case. It was decided that $St_{95}VBC_5IP_{95}$ would be a suitable candidate for moving forward with further testing as the swelling degree of Q = 55 was high and the liquid release levels were deemed acceptable.

4.3.2.6. Comparison of the swelling of $St_{95}VBC_5IP_{95}$ with a non-HIPE polymer

Similarly to in section 4.3.2.1, the swelling of the best performing pHIPE was compared to that of the non-HIPE polymer (Figure 4.10). Across all solvents, the swelling was greater than that of the non-HIPE polymer and $St_{100}IP_{92}$. The average volume adsorption of the solvents which did not swell the bulk polymer (acetonitrile, ethanol and hexane) was Q_{vol} = 15.3 ± 0.66. This equated to a free volume inside the polymer of 93.8 %, larger than that of the $St_{100}IP_{92}$, but lower than the volume by design of 95 %.

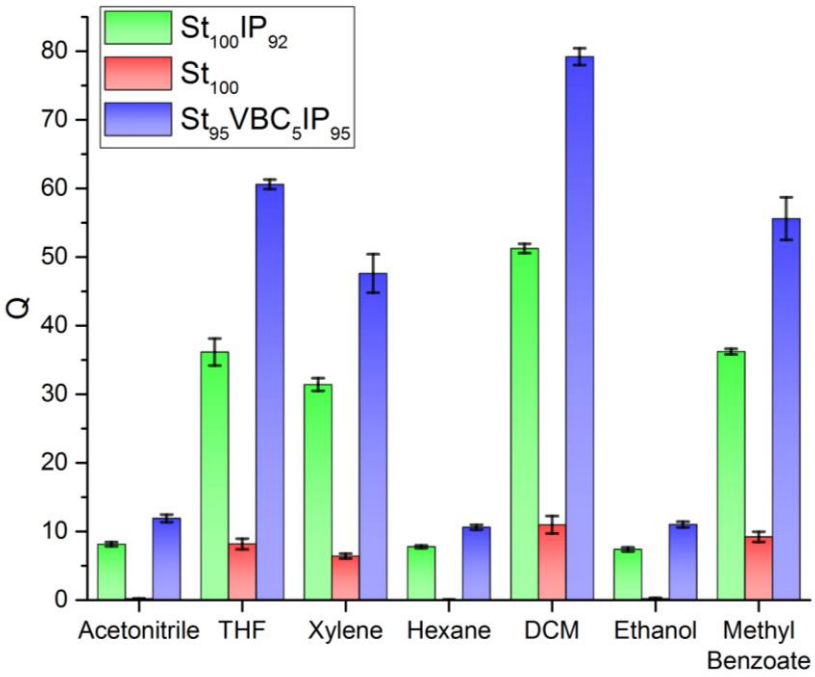

Figure 4.10 – A comparison of the swelling of the 100% styrene bulk gel, with its pHIPE counterpart at 92% internal phase, and the best performing pHIPE $St_{95}VBC_5IP_{95}$.

4.3.2.7. Swelling rate of $St_{95}VBC_5IP_{95}$

The absorption rate of the pHIPE sample $St_{95}VBC_5IP_{95}$ in methyl benzoate was extremely rapid with the swelling of a cube of approximately $1cm^3$ complete within around 5 minutes (Figure 4.11). The rapid absorption rate of $St_{95}VBC_5IP_{95}$ compared to bulk sample such as St_{100} is a consequence of the porous nature of the polymer.

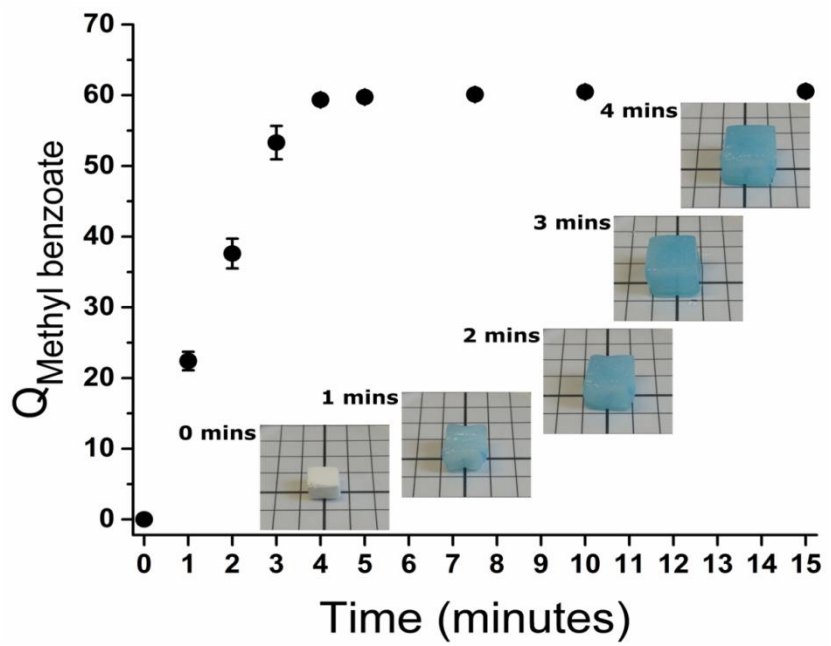

Figure 4.11 - The rate of swelling of a 10 x 10 x 10mm cube of $St_{95}VBC_5IP_{95}$ submerged in dyed methyl benzoate. Pictures to the right demonstrate the volume increase in the first 4 minutes.

In a bulky polymer sample the matrix will swell only as the solvent is absorbed from the surface inwards. The complex interconnected structure of the pHIPE enables the liquid to be driven through the pores via capillary action, at which point the polymer/solvent interface is orders of magnitude larger than that of a bulk polymer of equivalent volume. Where the swelling mechanics of the actual polymer network are the same as that for a bulky sample; it is the high surface area to volume ratio, paired with the solvent mobility through the system, allowing faster access throughout the system, which were the controlling factors to the swelling rate.

4.3.2.8. Compression tests with $St_{95}VBC_5IP_{95}$

An important consideration for the potential use of the polymer in a practical situation would be its final form factor. For this reason it was important to test if the large, low density monoliths could be compressed down to a smaller volume and higher density, yet still retain their swelling ability. Samples of $St_{95}VBC_5IP_{95}$ were compressed and then compared to their as-synthesised counterparts. After compression the volume of the polymer was reduced to

around 17 % of the original value (from 0.685 ± 0.032 cm^3 to 0.116 ± 0.004 cm^3) and the density was increased proportionally from 0.064±0.001 g cm^{-3} to 0.377±0.004 g cm^{-3}. The ability of the compressed polymers to swell is shown in Figure 4.12 and the compressed polymer not only swelled to the same value as the control, but exceed its swelling ability (Q = 55 versus Q = 65). The increase was however only slightly outside of the error. One proposed reason for the slightly increased performance after compression was because of the formation of fractures and damage to the microstructure of the polymer. This may have reduced the elastic potential and increased the interconnectivity of the polymer. These features were not visible through SEM due to the resolution requirements needed to see this potential effect, and so could not be validated.

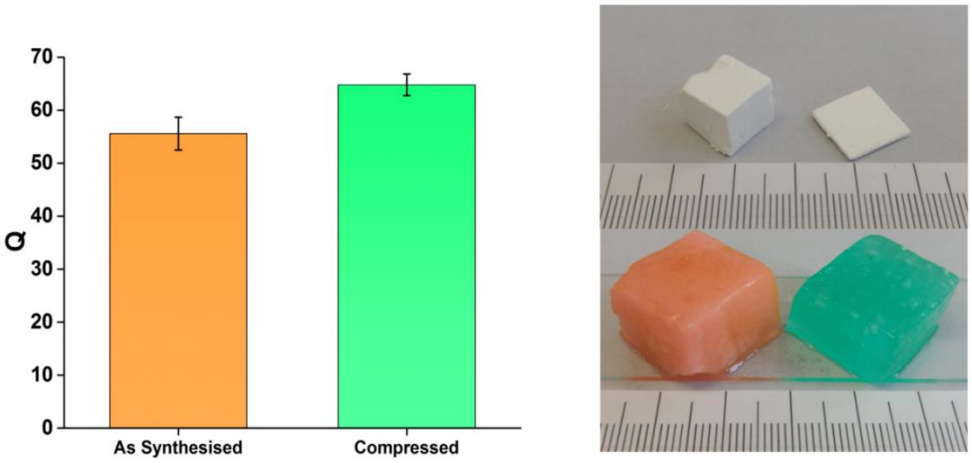

Figure 4.12 – Left; swelling degree (Q) of cubes of $St_{95}VBC_5IP_{95}$ both as synthesized and after having been compressed at 220N. Right, above; images of the two samples before swelling, below; the swollen pHIPEs after being exposed to coloured methyl benzoate.

4.3.3. Absorption of chemical warfare agents

The final feature of the area of the study into the application of the HIPE morphology to chemical warfare encapsulation was naturally; to test the chosen pHIPE samples on the real CWAs. Samples of $St_{95}VBC_5IP_{95}$ were swollen in GB (sarin) (isopropyl methyl phosphonofluoridate; VM (diethylaminoethyl O-ethyl methylphosphonothioate); *i*-Bu-VX (diethylaminoethyl O-isobutyl methylphosphonthioate); n-Bu-VX (diethylaminoethyl O-nbutyl

methylphosphonothioate); VX (diisopropylaminoethyl O-ethyl methylphosphonothioate); and HD (bis (2-chloroethyl) sulfide), whose structures are shown in Figure 4.13 below.

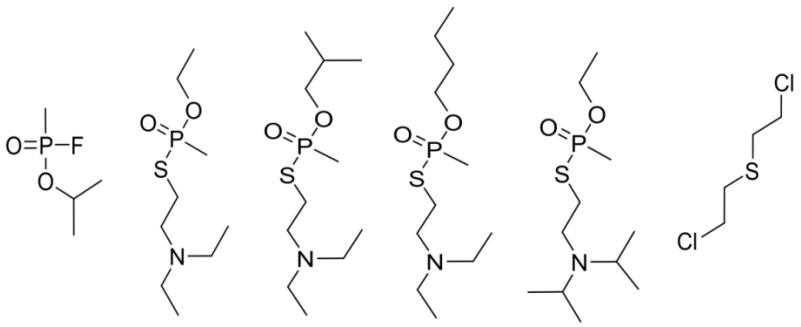

Figure 4.13 - The structures of CWAs; (from left to right) sarin (GB), VM, i-Bu-VX, n-Bu-VX, VX and sulfur mustard (HD)

The results for the swelling studies are presented in Figure 4.14. The swelling performance of the agents did compare to the simulant. With exception to sarin, which was not a direct target for this specific line of work, all the agents showed swelling degrees of over Q = 40.

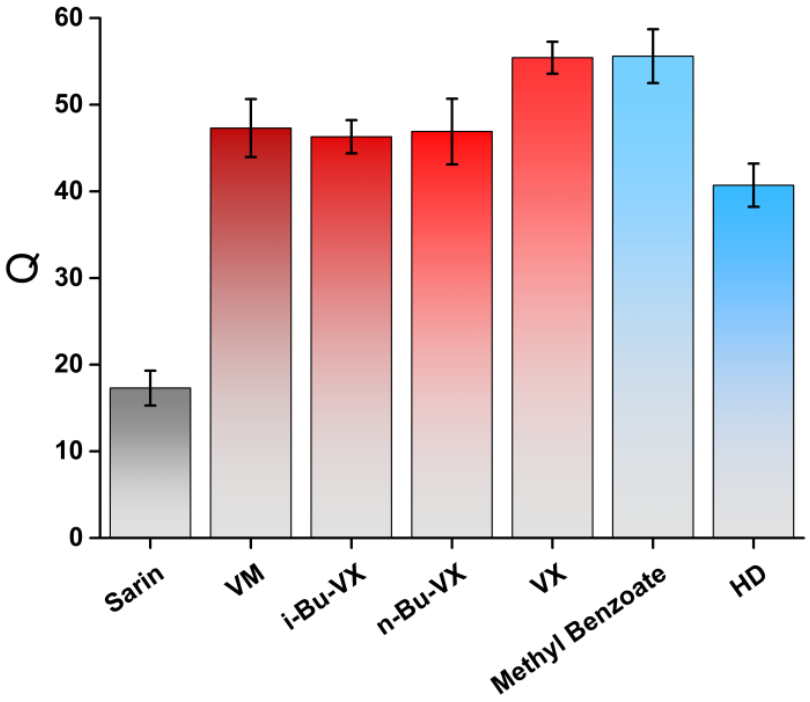

Figure 4.14 - Swelling performance of the $St_{95}VBC_5$ IP_{95} pHIPE in the CWAs: sarin (GB), VM, i-Bu-VX, n-Bu-VX, VX and HD, shown alongside the original simulant result.

All agents in the V-series performed better than was expected with a minimum of Q = 45 across the board. Sulfur mustard was absorbed to Q = 40 which was less than what was expected, based upon the previous simulant swelling of Q = 55. Whilst sarin was not expected to perform to a notable extent, as it previously did not swell in a mostly polystyrene matrix, the HIPE morphology still produced absorption values of Q = 17.5 in this agent.

4.4. The scaled up synthesis and swelling of $St_{95}VBC_5IP_{95}$

4.4.1. Absorption of large volumes of liquid

Knowing that the swelling performance of the simulant was very similar to that of the V-agents, a large scale swelling test was undertaken. This was done to show that the polymer could be easily added to a bulk volume of solvent and the material would swell to a sufficient degree to absorb and encapsulate the liquid. For this test 1000 g of the simulant, methyl benzoate (925 ml, ρ = 1.08), was placed in a 1 L glass bottle. The polymer was presented as disks (Θ = 2 cm x 0.5 cm) which had been compressed from a cylinder to the earlier compression specifications. Each of the disks had a mass of around 0.75 g, giving a total of 23 g. This was to give an average Q = 42; near the maximum (Q = 55) shown previously. The swelling was observed without any agitation and pictures at the most significant time periods from the video are presented in Figure 4.15 below.

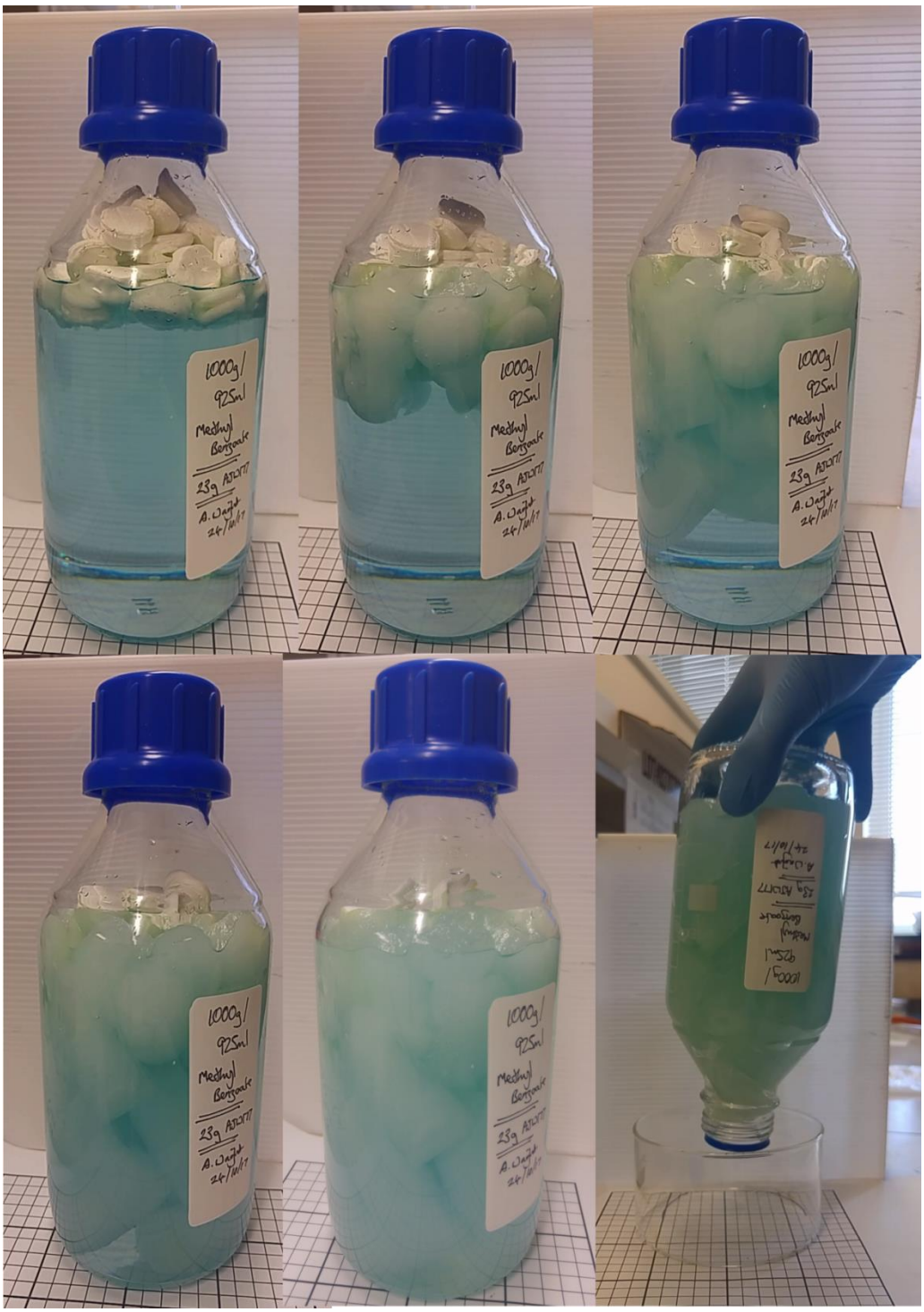

Figure 4.15 - Images taken from the large scale swelling study of $St_{95}VBC_5$ IP_{95} in dyed methyl benzoate (from top left to bottom right) immediately after addition of the polymer [T=0 mins], T = 10 mins, T = 30 mins, T = 90 mins, T= 16 hours, T= 16 hours (inversion).

The first important observation to note was that the polymer floated on the surface of the simulant. Whilst this is a trivial demonstration of the density differences it proved to be

important in the later stages of the absorption process. As the polymer swelled the simulant, it did so in a downward fashion. This meant that in the first ten minutes, the bottom layer of disks had already swollen sufficiently to mostly plug the surface of the liquid with a layer of polymer. The first fully swollen disk was observed to liberate itself from the plug in after 30 minutes. After 90 minutes most of the volume of simulant was taken up by the polymer. There was however still some completely dry disks on the top of the plug. The absorption was allowed to continue for 16 hours further at which point there was only very small voids of liquid left and the swelling had mostly equilibrated. These small voids were due to the bad packing of the cylinders. The bottle was inverted and none of the liquid escaped the bottle. This was in part due to the neck diameter, but also as the voids of liquid moved, they were prevented from escaping due to the top layer of the plug absorbing them. The top layer had not reached anywhere near maximum Q and was acting as an active absorption layer – a side effect of the polymer floating on the surface throughout. Even after multiple inversions and vigorous shaking, nothing was released from the bottle. This was a promising result which also served to show that the disk form factor was effective in preventing movement out of a container when the swollen dimensions of the disk were greater than that of the opening, yet small enough in compressed state to be placed in easily.

4.4.2. Scaled up synthesis of $St_{95}VBC_5IP_{95}$

Due to the extremely successful swelling performance of the $St_{95}VBC_5IP_{95}$ pHIPE for all of the CWAs and the positive results from the larger scale swell test from a compressed state, it was decided that it would be worth proving that the synthesis and work up could be carried out on much larger scales. It was therefore decided to scale up the synthesis and produce 10 Kg of polymer. A batch of 10 kg of polymer would have the swelling capacity to absorb in excess of 400 litres of v-agent, equivalent to nearly two 55 US gallon oil drums. Demonstrating that these synthetic scales were practical would be the final assurance that this polymer had met the targets set out at the start of the project.

4.4.2.1. Logistical issues experienced with the scale up

Due significant increase in the scale, the biggest problem initially encountered was that of volume. Due to the high internal phase fraction of $St_{95}VBC_5IP_{95}$, the mixed mass was significantly higher than the mass of the final dry polymer sample. The original syntheses would typically generate around 10 g of polymer from a total mixed volume of around 165 ml; scaling this up to a single 10 Kg batch would require a total mixed volume of nearing 165 litres. Scaling the reaction to 10 x 1 kg batches reduced the mixed volume to a scale which was manageable in a university fume cupboard, and also be safe to move under normal manual handling conditions. Before synthesis of the 1kg batches, smaller trial scales of 500 g and 750 g were carried out, and these were seen to mix and cure without issue. The total volume for each batch for a final 1 kg of dry polymer was 17.5 litres. The second issue which was encountered follows on from the problem of the large mixing volume, and relates to the drying of the cured polymer. Normally the polymer would be dried under vacuum, with the original scale requiring the 155 ml of water to be removed. As the majority of the mixed volume was water (95 %), the 1 Kg scales required the removal of 16.5 litres of water each. The mixing of these large quantities of relatively viscous emulsion proved to be problematic. As the emulsion increased in viscosity, the bulk developed regions of water which were not incorporated. These had to be mixed in with manual movement of the stirrer apparatus. The ability of the stirrer paddle to both cause enough shear on the mixture to form the HIPE, but also circulate the mass was not sufficient with the 100 mm anchor bar which was used. In hindsight, a high shear paddle should have been used in conjunction with a propeller to assist the circulation of material.

4.4.2.2. Quality control of the scaled up polymers

Quality assurance tests were carried out which involved swelling samples from each batch in the methyl benzoate. The swelling performance was in line with the trial scale polymers across all of the batches (Table 4.3 and Figure 4.16). The variation in absorption (Q) values between the batches was likely due to the quality of the mixing with the less than ideal stirrer paddle.

Regardless, the swelling of any of the systems never dropped below Q = 50. The total mass of polymer formed was 9.5 kg.

Table 4.3 - The scaled up synthesis batches of $St_{95}VBC_5IP_{95}$, along with their respective reaction scale and swelling degree in methyl benzoate.

Sample ID	Reaction Scale (g)	Q (methyl Benzoate)
PB-1	500	69.8 ± 3.1
PB-2	500	70.6 ± 1.2
PB-3	750	61.9 ± 1.7
PB-4	500	68.2 ± 1.7
PB-5	1000	50.3 ± 8.3
PB-6	1000	55.9 ± 2.6
PB-7	1000	66.3 ± 2.8
PB-8	1000	59.4 ± 7.5
PB-9	1000	54.6 ± 5.5
PB-10	1000	58.0 ± 4.1
PB-11	1000	58.3 ± 1.5
PB-12	750	60.6 ± 3.3

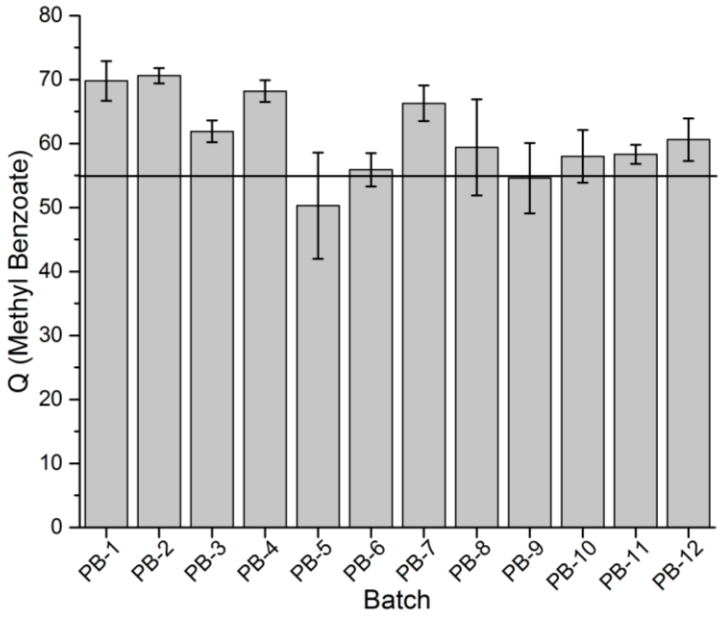

Figure 4.16 – The swelling performance in methyl benzoate of the production scale batches of $St_{95}VBC_5IP_{95}$. The horizontal black line represents Q = 55 which was the swelling observed in the first small batch.

4.5. Modifications of the PHIPE

4.5.1. Removal of the surfactant from the polymer

The effect of removing the surfactant from the sample was then investigated. By removing the surfactant the pendant chloride on the VBC and other functional areas could be utilized without the surfactant interfering with any of the potential reactions which would be used. It was also hoped that removing surfactant would make the polymer completely hydrophobic, as with the surfactant the polymer would adsorb water into the matrix as seen in Figure 4.17. Batches of $1cm^3$ chunks of $St_{95}VBC_5IP_{95}$ were washed in a 20 ml of ethanol. The polymer was left to stir in the ethanol for 3 hours and then the ethanol was changed for a fresh 20 ml volume. This was left for a further 3 hours after which the polymer was removed and dried in under vacuum at 45 °C overnight. The removal of surfactant by monitoring the reduced mass of the batch compared to the starting mass, which would equate to loosing 16.7 % of the total mass (surfactant = additional 20 % of the total polymer mass). The water contact angle of the washed sample in comparison to a surfactant included sample was examined (Figure 4.17). From these results it was clear that the removal of the surfactant had occurred sufficiently through simply washing the polymer with the non-swelling ethanol. The samples containing surfactant adsorbed water immediately upon contact, whereas the surfactant free sample was able to maintain a contact angle of 127 ° with the water with no change in angle over 10 minutes. This contact angle classed the polymer as hydrophobic, however it was not large enough (> 150 °) to class it as super hydrophobic.[23]

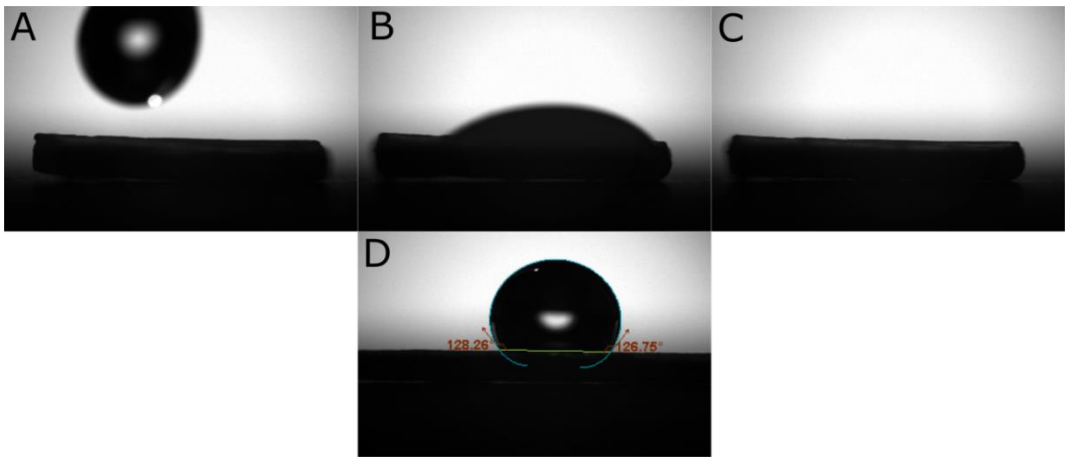

Figure 4.17 - Pictures taken from contact angle measurements of the surfactant included (A to C) and surfactant free pHIPE sample (D). A) Picture taken just before a drop of water was added to the sample, B) the sample four frames after addition of the water T = 0.25 s, C) eight frames after picture B showing the adsorption of the water into the matrix (T = 0.75 s). D) Demonstrating the contact angle (127 °) of the water on the surfactant free polymer after 10 minutes.

The swelling of the surfactant free sample, known as $St_{95}VBC_5IP_{95}$(-S), was tested and compared to the original polymer results (Figure 4.18).

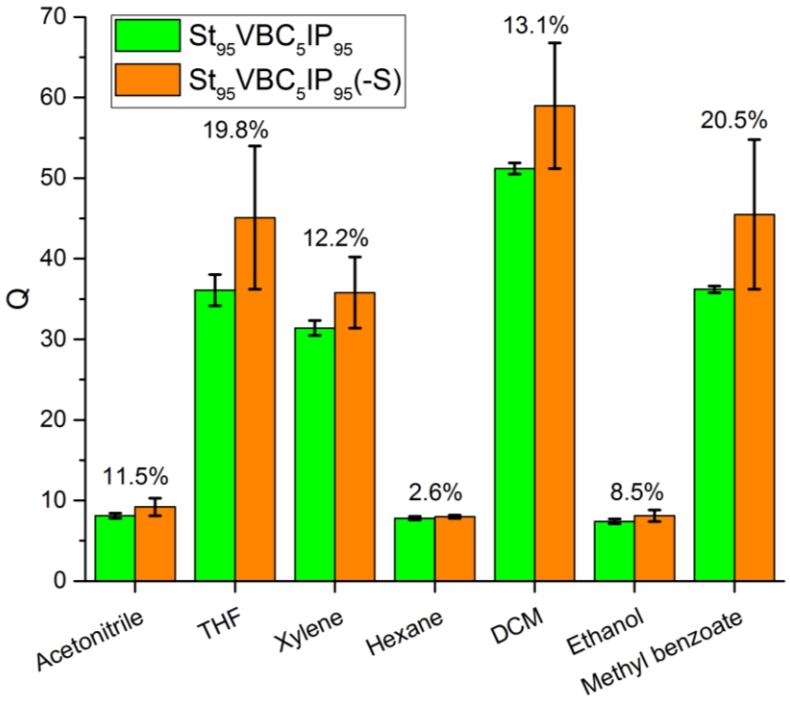

Figure 4.18 - The swelling degrees of 7 solvents in both the surfactant included sample (green) and the surfactant free sample (orange). The values above the bars represent the percentage increase in swelling between the original polymer and the polymer without surfactant.

Across the board, all of the surfactant free polymers showed increased absorption when compared to the original sample. This swelling increase was most likely a feature of the starting polymer having a mass 16.6 % lower due to the lack of surfactant; thereby artificially increasing the swelling degree which was observed. This 16 % increase was only observed in the THF and methyl benzoate swelling. The greatest swelling degree differences as a percentage of the original are seen in the highest swelling solvents, although this was not mimicked in the DCM.

4.5.2. Absorption of xylene from a water surface

This section describes a short experiment which was undertaken to demonstrate the capability of the polymer to absorb low polarity solvents from the surface of water. It was known that the polymer would encapsulate xylene to Q = 30 and hexane to Q = 8 with surfactant, and then

Q = 35 and Q = 8 in these solvents respectively after removal of the surfactant. Additionally, the surfactant free polymer was hydrophobic and possessed a low density which caused it to float on water. These features not found in the polymer with surfactant, suggested the surfactant free polymer would be effective at absorbing xylene as a slick on water. Xylene (12 ml), dyed with a flake of perylene was added to the surface of 75 ml of water in a 150 ml beaker. A sample of $St_{95}VBC_5IP_{95}$(-S) (0.5 g) of the polymer was then dropped in, and the swelling of the xylene from the surface of the water was observed (Figure 4.19).

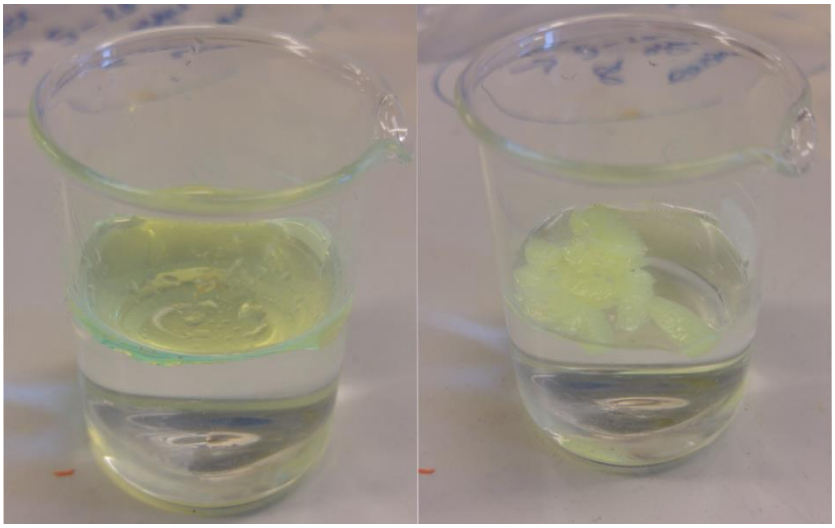

Figure 4.19 - Left) the 20 ml of xylene, dyed with perylene, on the surface of the 75 ml of water. Right) the swollen pHIPE $St_{95}VBC_5IP_{95}$(-S) after having been dropped into the surface of the liquid. The polymer has absorbed all of the xylene from the surface of the water.

The polymer appeared visually to have absorbed all of the xylene from the surface of the water within 5 minutes. The final Q value for the polymer was 23, in line with the volume of xylene on the surface of the water. During the absorption, the polymer was not stationary. The hydrophobicity combined with the attraction of the polymer to the xylene caused the polymer to linger in the shrinking puddle of xylene at all times (hydrophobic effect). Lifting of the polymer from the surface without any xylene leaking back onto the surface of the water was easily achieved. Although a simple qualitative test, this showed the ability of the polymer to be

quickly modified in a way that allowed it to be used as a spillage control measure for organics in aqueous environments.

4.5.3. Sulfonation of the $St_{95}VBC_5IP_{95}$(-S)

The final experiment was to utterly alter the swelling performance of the system by modifying the hydrophobic polymer into a hydrophilic system by way of sulfonating the matrix into polystyrene sulfonate (PSS). The transformation of polystyrene to PSS is a known and facile procedure.[28] There was a concern that the harsh reaction conditions, and repeated swelling and de-swelling during the procedure could be detrimental to the morphology of the pHIPE in a network with such low levels of crosslinking. The reaction was carried out by the simple addition of the polymer to concentrated sulfuric acid. 0.75 g of the 1 cm^3 chunks of $St_{95}VBC_5IP_{95}$(-S) which were produced in the earlier procedure were cut in half and placed into a round bottom flask with 25 ml of concentrated sulfuric acid. The mixture was heated to 80 °C and left stirring overnight. At first the polymer did not absorb the acid well, but as the polymer was slowly converted to the sulfonate, the polymer became visibly turgid with acid, helping to show the progression of the reaction. After stirring in acid, the polymer was placed into a large excess (400 ml) of saturated sodium bicarbonate solution with gentle stirring to neutralize the remaining acid. The polymer was then washed with deionized water (2 x 200 ml) and then 100 ml of 0.5M NaOH to ensure the sodium salt of the sulfonate had formed. Finally, it was washed with ethanol which caused it to gently de-swell, after which it was dried under vacuum at 45 °C. IR was carried out to qualitatively analyse if the sulfonation had occurred (Figure 4.20). Intense bands around 1250 cm^{-1}, a reduction in intensity of the aromatic –CH- at 3000 cm^{-1}, and a broad –OH peak at 3150-300 cm^{-1} show that sulfonation had occurred. These features of polystyrene sulfonation have been previously reported in literature.[29]

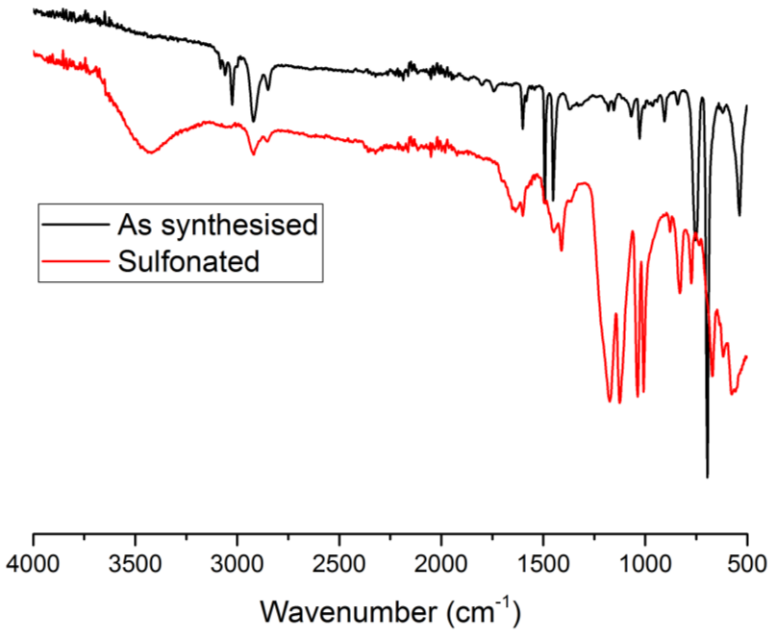

Figure 4.20 – The IR spectra of the $St_{95}VBC_5IP_{95}$ before (black) and after (red) sulfonation of the matrix with sulfuric acid.

The swelling of the polymer was carried out in the regular solvents and additionally, water (Figure 4.21). None of the organic solvents were absorbed by the sulfonated HIPE to any significant degree. It was likely that the polymer matrix had become completely incompatible with any solvents other than water. There was an extremely high swelling degree in water of over Q = 50 (Figure 4.21 and Figure 4.22). These swelling results support the IR data in that the conversion to sulfonate was successful and the polymer maintained the correct pHIPE morphology. Quantitative analysis of the degree of sulfonation was not carried out.

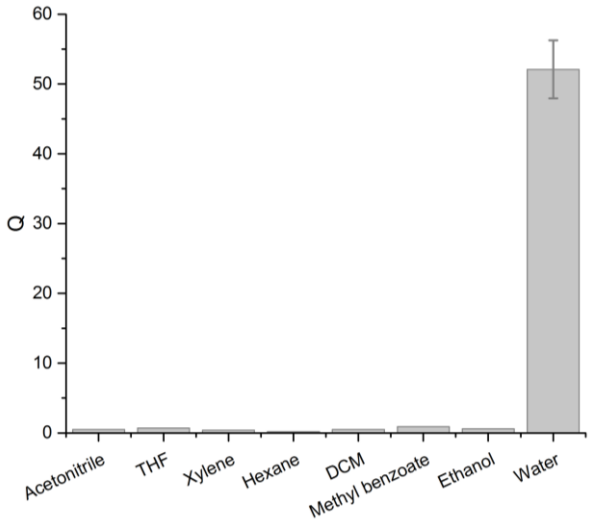

Figure 4.21 – The swelling performance of the 7 solvents in addition to water in the sulfonated pHIPE.

Figure 4.22 - On the left is a 7 ml vial showing swollen sulfonated-HIPE in water and to the right is an equivalent dry mass of the polymer on the right.

4.6. Conclusions

Overall, the movement from a bulk styrene polymer, to a high internal phase emulsion polymer with slight VBC doping showed great improvements over the swelling performance of all the previous experimentation. The swelling of all the V-series and mustards were absorbed at unprecedented levels (Q = >40), with the swelling of sarin in line with other studies (Q = 16), satisfying the primary aim of the work. Not only was the polymer a significant swelling degree

improvement of over twice the previous best; it also showed incredibly fast swelling rates, and the ability to be swollen from a compressed state which allowed it to be considered more useful in a logistical sense. The scaled up swelling test and large scale synthesis of $St_{95}VBC_5IP_{95}$ was considered a successful venture. Where the drying times seemed to be the biggest issue in terms of production rate, this could have been mitigated through changes to the drying form factor, for example from slabs to cubes, to increase the surface area to volume ratio and therefore increase the drying speeds. There are a still a small number of small engineering problems such as the drying, which after fixing could significantly reduce the difficulty of the polymer production even at larger scales. The final studies with the $St_{95}VBC_5IP_{95}$ pHIPE showed that it was versatile not only for the absorption of CWAs, but it could also be modified post synthetically to improve other properties. Removal of the surfactant was facile and left a polymer monolith which showed good hydrophobicity, allowing it to then act as an effective sorbent on the surface of water. Sulfonation of the surfactant free sample produced a completely hydrophilic polymer where water swelling of Q = 50 was observed, and the ability to swell all of the organic solvents tested was lost. The development of this pHIPE has led to an adaptable system with a multitude of possibilities for further development.

4.7. References

1 A. J. Wright, M. J. Main, N. J. Cooper, B. A. Blight and S. J. Holder, *ACS Appl. Mater. Interfaces*, 2017, **9**, 31335–31339.

2 O. Kulygin and M. S. Silverstein, *Soft Matter*, 2007, **3**, 1525.

3 D. Pahovnik, J. Majer, E. Žagar and S. Kovačič, *Polym. Chem.*, 2016, **7**, 5132–5138.

4 M. Ovadia and M. S. Silverstein, *Polym. Int.*, 2016, **65**, 280–289.

5 N. Zhang, S. Zhong, T. Chen, Y. Zhou and W. Jiang, *RSC Adv.*, 2017, **7**, 22946–22953.

6 T. Zhang and Q. Guo, *Chem. Eng. J.*, 2017, **307**, 812–819.

7 S. Kovačič and M. S. Silverstein, *Macromol. Rapid Commun.*, 2016, **37**, 1814–1819.

8 T. Zhang and M. S. Silverstein, *Macromolecules*, 2018, **51**, 3828–3835.

9 C. Wilson, M. J. Main, N. J. Cooper, M. E. Briggs, A. I. Cooper and D. J. Adams, *Polym. Chem.*, 2017, **8**, 1914–1922.

10 S. Kondo, T. Ohtsuka, K. Ogura and K. Tsuda, *J. Macromol. Sci. Part A - Chem.*, 1979, **13**, 767–775.

11 C. Saiwan, P. Muchan, D. deMontigny and P. Tontiwachwutikul, *Energy Procedia*, 2014, **63**, 2312–2316.

12 D. Štefanec and P. Krajnc, *React. Funct. Polym.*, 2005, **65**, 37–45.

13 C. Saiwan, P. Muchan, D. deMontigny and P. Tontiwachwutikul, *Energy Procedia*, 2014, **63**, 2317–2322.

14 W. T. Ford and T. Balakrishnan, *Macromolecules*, 1981, **14**, 284–288.

15 M. F. Froix, D. J. Williams and A. O. Goedde, *Macromolecules*, 1976, **9**, 354–358.

16 J. M. Williams and D. A. Wrobleski, *Langmuir*, 1988, **4**, 656–662.

17 H. Bi, X. Xie, K. Yin, Y. Zhou, S. Wan, L. He, F. Xu, F. Banhart, L. Sun and R. S. Ruoff, *Adv. Funct. Mater.*, 2012, **22**, 4421–4425.

18 H.-W. Liang, Q.-F. Guan, L.-F. Chen, Z. Zhu, W.-J. Zhang and S.-H. Yu, *Angew. Chemie Int. Ed.*, 2012, **51**, 5101–5105.

19 K. Watanabe, T. Ohmura, T. Ikeda, A. Miki and T. Teshigawara, *Int. J. Cosmet. Sci.*, 2010, **32**, 315–316.

20 A. Y. Sergienko, H. Tai, M. Narkis and M. S. Silverstein, *J. Appl. Polym. Sci.*, 2002, **84**, 2018–2027.

21 M. S. Silverstein, *Prog. Polym. Sci.*, 2014, **39**, 199–234.

22 J. Naranda, M. Sušec, U. Maver, L. Gradišnik, M. Gorenjak, A. Vukasović, A. Ivković, M. S. Rupnik, M. Vogrin and P. Krajnc, *Sci. Rep.*, 2016, **6**, 28695.

23 A. Barbetta, N. R. Cameron and S. J. Cooper, *Chem. Commun.*, 2000, **0**, 221–222.

24 P. C. Reeves and M. A. Celia, *Water Resour. Res.*, 1996, **32**, 2345–2358.

25 J. Pinto, A. Athanassiou and D. Fragouli, *J. Phys. D. Appl. Phys.*, 2016, **49**, 145601.

26 J. M. Williams, A. J. Gray and M. H. Wilkerson, *Langmuir*, 1990, **6**, 437–444.

27 A. Barbetta, N. R. Cameron and S. J. Cooper, *Chem. Commun.*, 2000, **0**, 221–222.

28 R. H. Wiley and T. K. Venkatachalam, *J. Polym. Sci. Part A-1 Polym. Chem.*, 1966, **4**, 1892–1894.

29 Y. T. and and P. Auroy, *J. Am. Chem. Soc.*, 2001, ***123*** (16), 3644–3654.

4.8 Appendix 4A

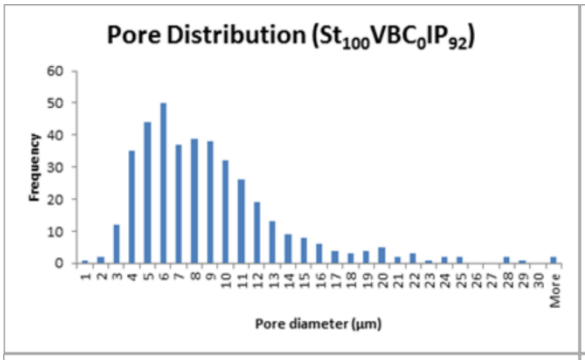

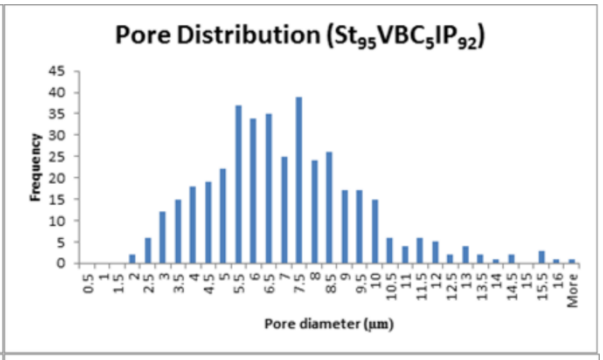

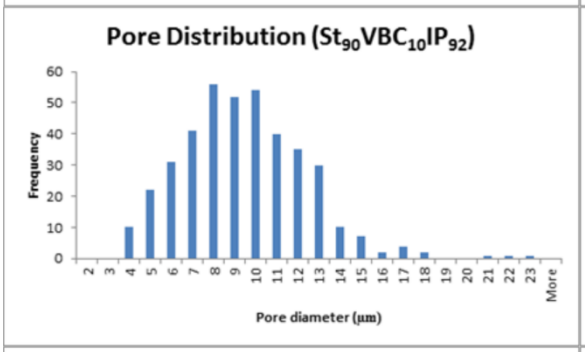

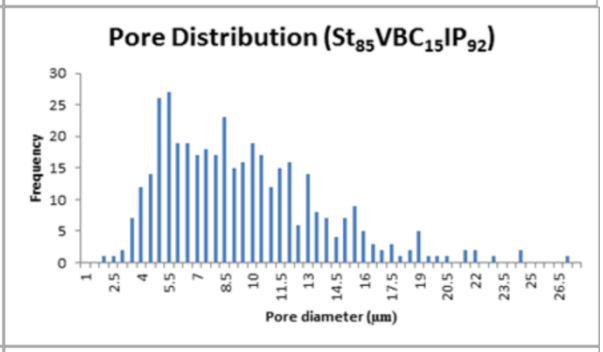

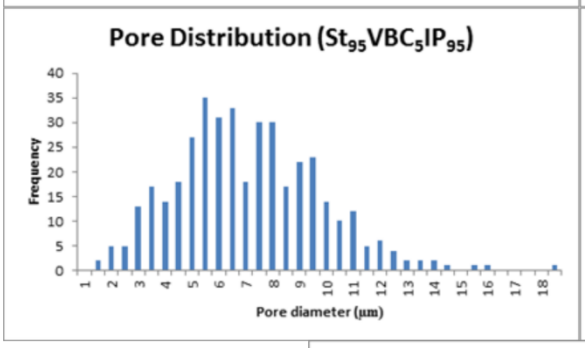

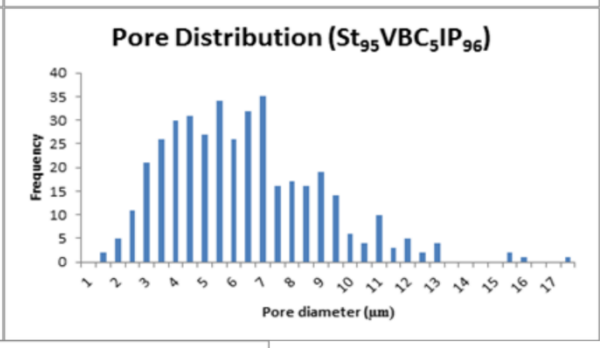

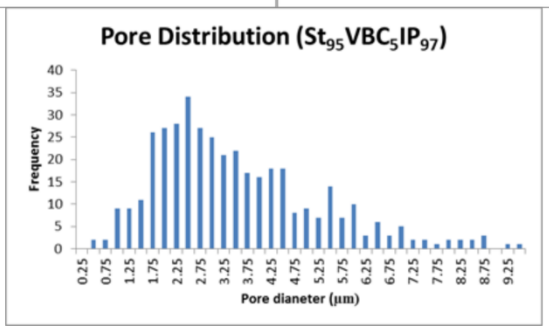

Chapter 5 -

An Internally Buffered MOF/pHIPE Composite for the Degradation of Neat Chemical Warfare Agents

5.1 Introduction and aims

This chapter was the amalgamation of two areas of work, in a collaboration which extended through the life of the project. Throughout all the preceding work, the main target was to develop a chemical warfare agent-absorbing polymer with high swelling degrees across a range of agents. The learnings from chapter two and three led to the design of a composition which was then implemented into the versatile morphology of the pHIPEs in chapter 4. The final polymer from chapter 4 showed great promise in across the board absorption of CWAs.[1] The ultimate aim and objectives which are presented in this chapter were to develop a catalyst-pHIPE composite that would simultaneously immobilise a CWA and degrade it. A catalyst which was developed by a collaborator, Yaroslav Kalinovskyy, was incorporated into a pHIPE with an internal buffer to aid the breakdown of the CWAs. The catalytic system was a metal-organic framework (MOF) material which provided hydrolysis capabilities. Merging the effective hydrolysis catalysts with the high swelling polymers lead to an effective provision for the immobilization and decontamination of V-agents in a self-decontaminating material (SDM).

5.1.1 Simulant choice

In contrast to the physical simulant for the previous work which was methyl benzoate, a new chemical simulant was required for the catalytic screening. This chemical simulant would need to accurately mimic the breakdown of CWAs. This chapter would focus on the work of breaking down VX (and other V-series agents by proxy). In the breakdown of V-agents, specifically the hydrolysis of VX, the phosphorus-sulfur bond needs to be broken in order to leave less-toxic decomposition products; ethyl methylphosphonate and 2-(diisopropylamino)ethanethiol.[2] If the hydrolysis was to occur on the less reactive phosphorus/oxygen ether, the resulting products would be the extremely toxic phosphonic thioester, and ethanol. These two pathways are shown in Figure 5.1.

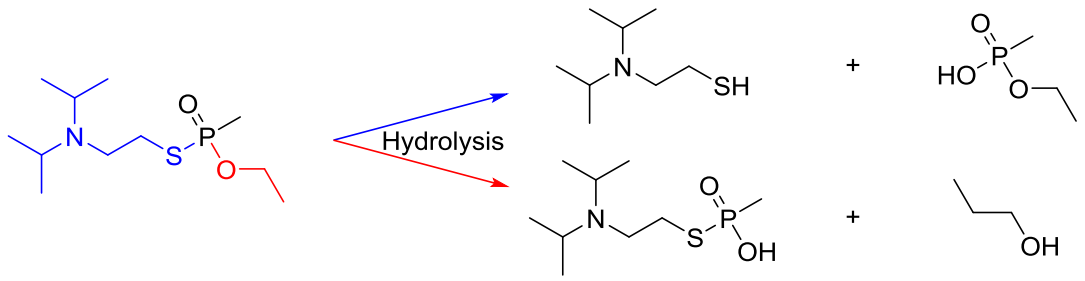

Figure 5.1 – The two potential hydrolysis routes for the breakdown of VX. The fragments from the red arrow depict the non-ideal breakdown route, and the blue arrows represent the target route.

As this phosphorus-sulfur ether bond was the major target for catalysis into less toxic products, a chosen simulant must possess a hydrolysable bond with similar energy to that of the actual agent. For these reasons, the simulant which was chosen for the catalysis aspect of this work was methyl paraoxon (Figure 5.2). This molecule does not include the P-S ether as seen in VX, however the electronic and steric effects of the nitrobenzene group cause the P-O ether to possess very similar degradation kinetics to that of the P-S bond in VX.[3]

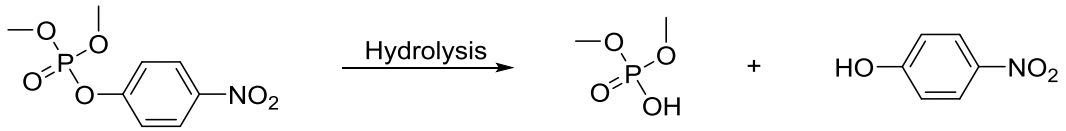

Figure 5.2 – The breakdown of DNMP (methyl paraoxon) into the two hydrolysis products.

Degradation studies would be carried out with methyl paraoxon and swelling studies would be carried out with methyl benzoate.

5.1.2 Catalyst selection

5.1.2.1 Introduction to MOFs

Metal organic frameworks (MOFs) represent a large area of research in the supramolecular community. The fundamental components of MOFs are a metal unit, or cluster, which is linked with organic linkers (Figure 5.3). These materials are generally crystalline with permanent porosity.[4]

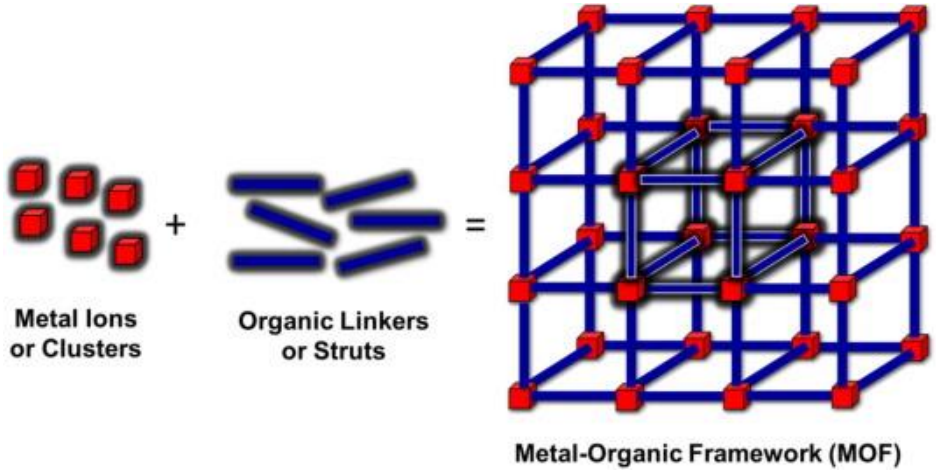

Figure 5.3 - A representation of a basic MOF showing how the metal clusters and the organic linkers form a 3D structure with clear pores.[5]

It is common for MOFs to have porosities of up to 90 % free volume, and with some resulting surface areas exceeding 6000 $m^2 g^{-1}$.[6] The subsequent porosity and pore diameters of these materials can be controlled by changing either of the two building blocks, but it is common for the organic linker to be modified.[7] Pore diameters can vary in a range of around 3 to 20 angstroms depending on the linker used and the designed usage.[8] MOFs represent versatile materials which have many potential applications. Two of the common areas are in catalysis[9] and gas capture, specifically, CO_2 capture.[10] One noteworthy work with MOFs in recent years has been in the removal of atmospheric water in deserts. A MOF-801, zirconium based MOF, was developed which could harvest 2.6 litres per 1 Kg of MOF per day with as low as 20 % relative humidity, using only heat from the sun as a driving force.[11]

5.1.2.2 Introduction to MOF-808

Kalinovskyy's work lead to the development of a selection of MOF based catalysts, specifically a zirconium based material; based on the previous work with MOF-808.[12] Kalinovskyy's work showed the MOF catalyst to be effective at degrading the simulant methyl paraoxon and VM, at a catalytic loading of just 1.25 mol%.[3] MOF-808 is a zirconium based MOF where the zirconate cluster is 12 coordinate. The zirconate clusters are connected with the tri-topic ligand benzene tricarboxylic acid (BTC) (Figure 5.4).[13]

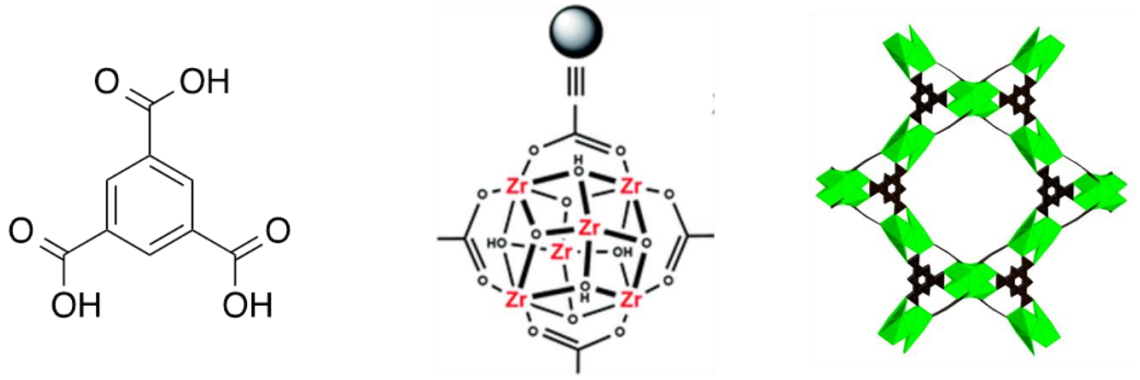

Figure 5.4 – From left to right; the structure of the linker (benzene tricarboxylic acid), a representation of the zirconate cluster in MOF-808, a representation of the MOF-808.

For the purposes of this study, the clusters would be moderated with 6 equivalents of acetic acid, which would reduce the connectivity through the organic linker from 12 to 6; leaving 6 of the catalytically active zirconate sites free of linker. MOF-808 has been used extensively in research. A versatile system with exchangeable active sites,[14] it has been produced through microwave synthesis and used for the removal of arsenic contamination in water.[15] It has also been developed as a super acid by the addition of sulfate groups to the zirconate clusters.[16] In addition to unrelated applications, it has also been used to facilitate the breakdown of Sarin simulants.[17,18,19]

5.1.2.3 Buffering of the catalyst system

The catalytic route for the degradation of VX through hydrolysis would require the use of stoichiometric quantity of water. There was also a requirement for these catalytic systems to be buffered to a slightly basic pH in methyl paraoxon (DMNP). This is required to increase the rate of exchange between zirconium node-bound water molecules and the DMNP substrate during the catalytic cycle.[20] The degradation of the DNMP forms an acidic *p*-nitrophenol by-product which increases the acidity, and reduces the exchange of water from the zirconium nodes, and therefore the hydrolysis rate. It was proposed that in the V-agents, the tertiary amine by-product would lead to the reaction to be self-buffering once initiated. This autocatalytic breakdown has been shown in literature.[21]

5.1.3 Catalytic pHIPE development

Three main objectives were identified for creation of a composite material; incorporation of the MOF catalyst in the pHIPE, buffering of the MOF catalyst in the pHIPE, and allowing the catalyst to access stoichiometric amount of water which was required for the hydrolysis. The work began by synthesising a pHIPE/MOF prototype using a DUT-52 MOF and $St_{95}VBC_5IP_{92}$ pHIPE. This first prototype was to show that by introducing the MOF into the pHIPE as a component of the aqueous phase during mixing, the polymer could be loaded with the active catalyst without loss of MOF structure, or swelling ability. A MOF loading of 25 % by mass of the monomers was chosen. This was chosen on the assumption that a swollen polymer in a v-agent should reach at least Q = 40, this would leave the catalytic loading against the mass of absorbed substrate to be around 0.5 % by mass. The project then moved onto incorporating the active MOF-808 into the remarkably swelling $St_{95}VBC_5IP_{95}$. This was then tested for its catalytic activity with methyl paraoxon in a system with external aqueous buffer. Ultimately, a bespoke pHIPE/MOF-808 composite was developed which composed of a bound buffer, based upon a piperidine containing monomer unit which was synthesised in house. This removed the requirement for external buffer to be added. All composites were tested for: the swelling ability of the polymers gravimetrically, the conservation of the MOF structure using XRD and SEM, and the homogeneity and porosity of the pHIPEs using SEM. Monitoring of the catalytic activity was carried out through various NMR methods based upon the ^{31}P isotope.

5.1.3.1 Development of the buffered pHIPE

Introducing the MOFs into the matrix was found not to be such a problem. Introducing a basic monomer presented some issues as most basic functionalities show some level of hydrophilicity which interfered with the delicate balance in the HIPE. An ideal monomer was a morpholine derivative to mimic the external aqueous buffer; N-ethylmorpholine. This was considered too hydrophilic and so the monomer chosen for the buffer was vinylbenzyl piperidine (VBPP). This monomer was introduced into the polymer at 5 % of the total moles of monomer to leave a polymer composed of VBC, VBPP, crosslinker, styrene and MOF-808

(Figure 5.5). The VBPP was not added post synthetically through risk of damage to the pHIPE or the MOF, although this route was considered.

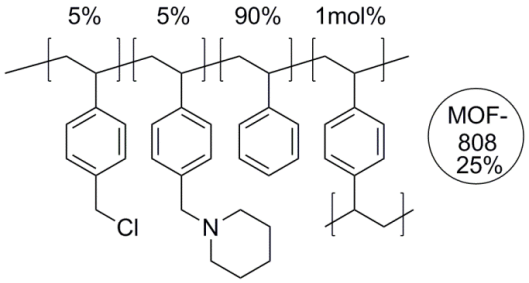

Figure 5.5 – The polymer structure of the final MOF/pHIPE composite used for the degradation of the CWAs

5.2 Experimental

5.2.1 Materials and Equipment

Electron micrographs were obtained using a Hitachi S-3400 scanning electron microscope. The pHIPE samples were prepared for SEM by drying thoroughly and then cutting into thin slices with care taken to not disrupt or damage the surface of the sample, and analysed immediately after cutting, similarly to chapter 4. The chamber was set to full vacuum, with an electron beam voltage of 20 kV and an emission current of 80 mA. Detections were carried out with the backscatter electron detector.

Infra-red spectroscopy was carried out at room temperature on a Shimadzu IRAffinity-1S, with an ATR gate, a sweep of 500 - 4000 cm^{-1}, a resolution of 2 cm^{-1} and 64 scans.

^{1}H and ^{31}P NMR was acquired on a Bruker Avance Neo NMR, running a proton frequency of 400 MHz at room temperature (22 °C). Swelling and catalytic activity studies on the CWAs were carried out at DSTL Porton down, Wiltshire, United Kingdom, by Dr. Marcus Main and Dr Nicholas Cooper. The procedures used offsite were as similar to the procedures used for the simulant studies as possible to ensure the humidity and relative concentrations inside the experiment did not vary excessively.

^{1}H NMR gel-state spectra were acquired on a Bruker Avance Neo NMR at 400MHz at room temperature (22 °C). The samples were examined using an HR-MAS semi-solids probe, utilizing magic angle (54.736 °) spinning at a moderate frequency of 5000 Hz. The relaxation delay was set to 60 seconds.

PXRD analysis was conducted by placing the powdered sample of MOF onto a zero-background sample holder and analysed in a Rigaku Miniflex 600 desktop XRD.

5.2.2 Synthesis of the MOF-808

The synthesis of the MOF-808 was carried out by Y. Kalinovskyy, and followed a previously reported preparation.[22]

$ZrCl_4$, (1.28 g, 5.5 mmol) was dissolved in DMF (60 ml) and sonicated for 10 minutes. 1,3,5 benzene tricarboxylic acid (1.12 g 5.5 mol) was then added and the solution was sonicated for a further 10 minutes. Finally, acetic acid (31 ml, 54 mmol) was added to the solution which was sonicated for another 10 minutes. The solution was sealed in a 250 ml screw top vessel and placed in a preheated oven where it was heated at 130 °C for 24 hours. The vial was removed from the oven and allowed to cool to room temperature. A white solid was observed. The resulting white solid was filtered from the supernatant, washed with DMF and acetone and then vacuum dried to yield a solid white powder. Bulk phase purity was confirmed by PXRD analysis (section 5.3.1).

5.2.3 Swelling procedure (Q and Q_{mod})

The Q swelling value referred to in previous chapters remains the same, and the swelling procedure was conducted in the same fashion;

$$Q = \frac{(Mass\ of\ swollen\ polymer - mass\ of\ dry\ polymer)}{Mass\ of\ dry\ polymer}$$

(Equation 5.1)

However where the polymer contained MOF, or extra surfactant above the standard 20%, the Q value was modified into Q_{mod}, to account for the increased starting mass of the polymer sample, such that;

$$Q_{mod} = \left(\frac{Q}{M_p}\right) * (M_p + M_e)$$

(Equation 5.2)

Where M_p represents the total % mass of the polymer and surfactant (120 for HIPE), and M_e represents the % mass of the extra components, for example 35 in MOF-HIPE-VBPP-S (25 % MOF and 10 % extra surfactant), or 25 in MOF-HIPE (25 % MOF).

5.2.4 Synthesis of DUT-HIPE

Styrene (0.751 g, 7.2 mmol), divinylbenzene (0.01 g, 0.075 mmol), 4-vinylbenzyl chloride (0.0579 g, 0.375 mmol), AIBN (0.0030 g, 0.02 mmol), and span-80 (sorbitan monooleate) (0.165 g), were added into a 50 ml conical flask. The flask was stirred at 200 rpm with a 2 cm hemispherical PTFE overhead stirred paddle for 5 minutes to homogenise the oil phase. The aqueous phase was then prepared. Potassium sulfate (0.05 g) was dissolved into 9.2 ml of deionized water. To this solution was added 0.200 g of the finely ground DUT-52 sample. The aqueous phase was then vigorously mixed to suspend the MOF. This agitation was continued throughout the addition of the aqueous phase to the organic to ensure good homogeneity of the non-dissolving MOF. The stirring speed of the organic mixture was increased to 750 rpm and the aqueous solution was dropped in at rate of around 1 drop per second. After all the aqueous phase was added, the stirring speed was increased further to 900 rpm and left to homogenise for 10 minutes. The HIPE foam formed well with and was placed into a 100 ml polypropylene cylinder, sealed and cured in an oven at 65 °C for 24 hours. After curing, the pHIPE monolith was cooled and removed from the cylinder. It was then dried under vacuum at 65 °C for 48 hours minimum.

5.2.5 Synthesis of MOF-HIPE

Styrene (1.502 g, 14.4 mmol), divinylbenzene (0.0198 g, 0.15 mmol), 4-vinylbenzyl chloride (0.116 g, 0.75 mmol), AIBN (0.0060 g, 0.04 mmol), and span-80 (sorbitan monooleate) (0.33 g), were added into a 100 ml conical flask. The flask was stirred at 200 rpm with a 4 cm hemispherical PTFE overhead stirred paddle for 5 minutes to homogenise the oil phase. The aqueous phase was then prepared. Potassium sulfate (0.1 g), was dissolved into 32 ml of deionized water. To this solution was added 0.409 g of the finely ground MOF-808 sample. The aqueous phase was then vigorously mixed to suspend the MOF. This agitation was continued throughout the addition of the aqueous phase to the organic to ensure good homogeneity of the non-dissolving MOF. The stirring speed of the organic mixture was increased to 750 rpm and the aqueous solution was dropped in at rate of around 1.5 drops per second. After all the aqueous phase was added, the stirring speed was increased further to 900 rpm and left to homogenise for 10 minutes. The HIPE foam formed well with and was placed into a 100 ml polypropylene cylinder, sealed and cured in an oven at 65 °C for 24 hours. After curing, the pHIPE monolith was cooled and removed from the cylinder. It was then dried under vacuum at 65 °C for 48 hours minimum. The surfactant was not removed prior to any experiments.

5.2.6 Synthesis of 4-vinylbenzyl piperidine (VBPP)

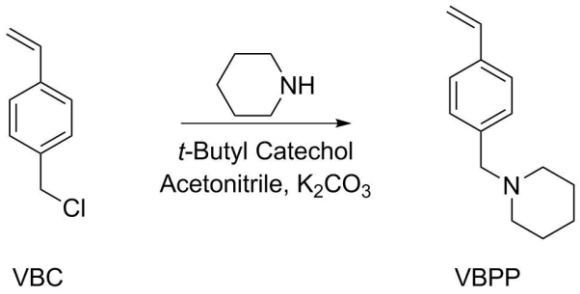

Figure 5.6 – The reaction procedure for the synthesis of the internal buffer monomer VBPP.

This synthesis was carried out by Y. Kalinovskyy. Piperidine (5.8 ml, 60 mmol) was dissolved in acetonitrile (50 ml). 4-Vinylbenzyl chloride (8.5 ml, 60 mmol) was then added dropwise to the stirring solution along with a flake of 4-tert-butylcatechol. This was followed by the addition of potassium carbonate (16 g). The mixture was refluxed at 120 °C for 2 hours. The mixture was subsequently cooled to room temperature and then chilled using an ice bowl and the white

solid was filtered off and washed with acetonitrile (25 ml). Another flake of 4-tert-butylcatechol was added to the filtrate. The filtrate was concentrated under reduced pressure to yield pale yellow oil (8.17 g, 39 mmol, 65 % yield). Before use in polymerisation, the oil was passed through a short alumina column which removed the inhibitor and subsequent yellow colouring. ^{1}H NMR (400 MHz, $CDCl_3$) found ppm (δ) = 1.37 (m, **2H**), 1.50 (m, **4H**), 2.33 (m, **4H**) 3.42 (s, **2H**), 5.18 (d, **1H**, J = 10.6 Hz), 5.69 (d, **1H**, J = 17.4 Hz), 6.67 (dd, **1H**, J = 10.9 Hz, 17.4 Hz), 7.21 (m, **4H**). ^{13}C NMR ($CDCl_3$) found ppm (δ) = 24.4, 26.0, 54.5, 63.6, 113.3, 125.9, 129.4, 136.2, 136.7, 138.3.

5.2.7 Synthesis of the internally buffered pHIPEs

The synthetic route for the internally buffered composite MOF-HIPE-VBPP-S is as follows. Styrene (1.778 g, 17 mmol), divinylbenzene (0.025 g, 0.19 mmol), 4-vinylbenzyl chloride (0.145 g, 0.95 mmol), 4-vinylbenzyl piperidine (0.191 g, 0.95 mmol), AIBN (0.0038 g, 0.02 mmol), and span-80 (sorbitan monooleate) (0.626 g), were added into a 100 ml conical flask. The flask was stirred at 200 rpm with a 4 cm hemispherical PTFE overhead stirred paddle for 5 minutes to homogenise the oil phase. The aqueous phase was then prepared. Potassium sulfate (0.125 g), was dissolved into 40 ml of deionized water. To this solution was added 0.535 g of finely ground MOF-808 sample. The aqueous phase was then vigorously mixed to suspend the MOF, but not sonicated. This agitation was continued throughout the addition of the aqueous phase to the organic to ensure good homogeneity of the MOF. The stirring speed of the organic mixture was increased to 750 rpm and the aqueous solution was dropped in at rate of around 1 drop per second. After all the aqueous phase was added, the stirring speed was increased to 1000 rpm and left to homogenise for 5 minutes. The HIPE foam was placed into two 25 ml glass vials, sealed and cured in an oven at 65 °C for 24 hours. After curing, the pHIPE monoliths were cooled and the vials destroyed to leave two samples of pHIPE. They were then dried under vacuum at 65 °C for 48 hours minimum. The complete list of polymers synthesised and their respective compositions are noted in Table 5.1 below.

Table 5.1- A table of all of the quantities required for each of the polymers and composites synthesised in this chapter.

Sample	Styrene (g)	VBC (g)	VBPP (g)	DVB (g)	AIBN (g)	SMO (g)	Water (ml) / K_2SO_4 (g)
DUT-HIPE	0.751	0.058	n/a	0.01	0.003	0.17	9.2 / 0.05
HIPE	7.509	0.579	n/a	0.099	0.015	1.65	155 / 0.5
MOF-HIPE	1.344	0.347	n/a	0.020	0.006	0.34	32.5 / 0.1
MOF-HIPE-S	1.877	0.145	n/a	0.025	0.004	0.626	38.9 / 0.13
HIPE-VBPP-S	1.778	0.145	0.191	0.025	0.004	0.626	39.8 / 0.13
MOF -HIPE-VBPP-S	1.778	0.145	0.191	0.025	0.004	0.626	39.8 / 0.13

5.2.8 DMNP Hydrolysis monitoring procedure

The majority of the hydrolysis NMR studies were carried out by Y. Kalinovskyy.

5.2.8.1 Buffered Hydrolysis procedures

The following procedure was implemented to monitor the hydrolysis rates of the polymer composite materials in a buffered simulant screening system. The selected composite or catalyst powder (3.2 mg, 0.11 µmol, 1.25 mol % MOF-808) was sliced up into small pieces (1-2 mm^3) then added to an NMR tube along with DMNP, 20 µL (0.09 mmol). A 0.6 ml mixture containing: 0.2 ml of D_2O, 0.2 ml of THF and 0.2 ml of 1.45 M *N*-ethyl morpholine (NEM) aqueous buffer (effective final concentration 0.45 M) was then added to the tube. The tube was inverted once and immediately loaded into an NMR auto-sampler and the first spectrum was obtained within 8 minutes of the reaction commencing. The sample was then cycled on the auto-sampler to collect subsequent data points. Each measurement was performed in triplicate. For the THF-free experiments, the same procedure was followed however the 0.2 ml of THF was replaced with an additional 0.2 ml of H_2O.

5.2.8.2 Unbuffered hydrolysis procedures

The following procedure was used to probe the hydrolysis of the MOF-HIPE-VBPP-S polymer composite material using a non-buffered simulant screening system. 5 NMR tubes were each charged with DMNP, 5 µL (0.02 mmol). The composites were each sliced up into small chunks (1-2mm^3). Various quantities of MOF-HIPE-VBPP-S were used (32.5 mg, 16.5 mg and 8 mg)

along with MOF-HIPE-S (32.5 mg) and MOF-808 (5.2 mg). MOF-HIPE-VBPP-S (32.5 mg) contained MOF-808 (5.2 mg, 0.18 μmol, 14.5 mol%). MOF-HIPE-VBPP-S (16.5 mg) contained MOF-808 (2.7 mg, 0.09 μmol, 7.3 %). MOF-HIPE-VBP-S (8 mg) contained MOF-808 (1.3 mg, 0.04 μmol, 3.6 mol%). For controls, MOF-HIPE-S (32.5 mg) was used which contained MOF-808 (5.2 mg, 0.18 μmol, 14.5 mol%) and powdered MOF-808 (5.2 mg, 0.18 μmol, 14.5 mol%). The polymer was then added to the corresponding NMR tube along with 0.2 ml of D_2O, 0.2 THF and 0.2 ml of H_2O. The tubes were inverted once and left to react for 20 hours. After 20 hours, the content of each tube was analysed using ^{31}P NMR spectroscopy.

5.2.9 Procedures for the catalytic studies of MOF-HIPE-VBPP-S in VX

The catalyst tests with VX were carried out by N. Cooper at DSTL. The final testing was of the internally buffered composite (MOF-HIPE-VBPP-S) and controls in VX. Two studies were carried out, the first mimicked that of the DMNP hydrolysis without external buffer, and the other was to show the effectiveness of the composites in neat agent without THF or added water. Both of these studies were carried out by Nicholas Cooper at DSTL, Porton Down.

5.2.9.1 Testing with water and THF

VX (24 mg) was placed into a standard NMR tube. The polymers were finely chopped and the appropriate amount of each composite was added into the tube. To the tube was then added 0.3 ml of a 1:1 D_2O/H_2O mixture, followed by 0.3 ml of THF. The catalytic loading was calculated to be 1.25 mol%. Immediately after the addition of the THF, the tube was capped and inverted three times to mix the solution, after which, the NMR spectra was immediately acquired. Subsequent spectra were gathered at 15 minute intervals for the first two hours and then a final spectrum at 24 hours was gathered.

5.2.9.2 Testing with neat VX

The following procedure outlines the procedure for the monitoring of the composites in neat VX. Into a vial was placed VX (250 mg) and to this was added 10 mg of the appropriate composite/control sample (MOF-HIPE-S, HIPE-VBPP-S and MOF-HIPE-VBPP-S). This represented a catalytic loading of only 0.15 % and a targeted swelling value of Q = 25 with

respect to the VX. The mixtures were left to react in an open vial with a lab relative humidity of 60 %. At 4, 7, 11 and 14 days, aliquots were taken from the reactions. This was done by gently squeezing the composite with a pipette whilst applying suction. The aliquot was diluted with chloroform-d in an NMR tube which allowed the reaction was monitored with ^{1}H and ^{31}P NMR.

5.3 Results and Discussion

5.3.1 MOF-808 PXRD analysis

Figure 5.7 shows the simulated and experimental PXRD pattern for the MOF-808 which was synthesised. The diffractogram for the synthesised MOF-808 appeared to be in good agreement with the simulated pattern for MOF-808.

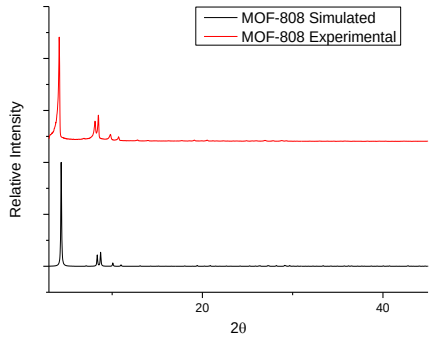

Figure 5.7 – The PXRD pattern of the synthesised MOF-808, plotted against a simulated pattern for the same structure.

5.3.2 NMR of the VBPP monomer

The proton NMR of the VBPP monomer showed that the monomer had been successfully synthesised. Importantly, the vinyl groups were retained throughout the synthesis.

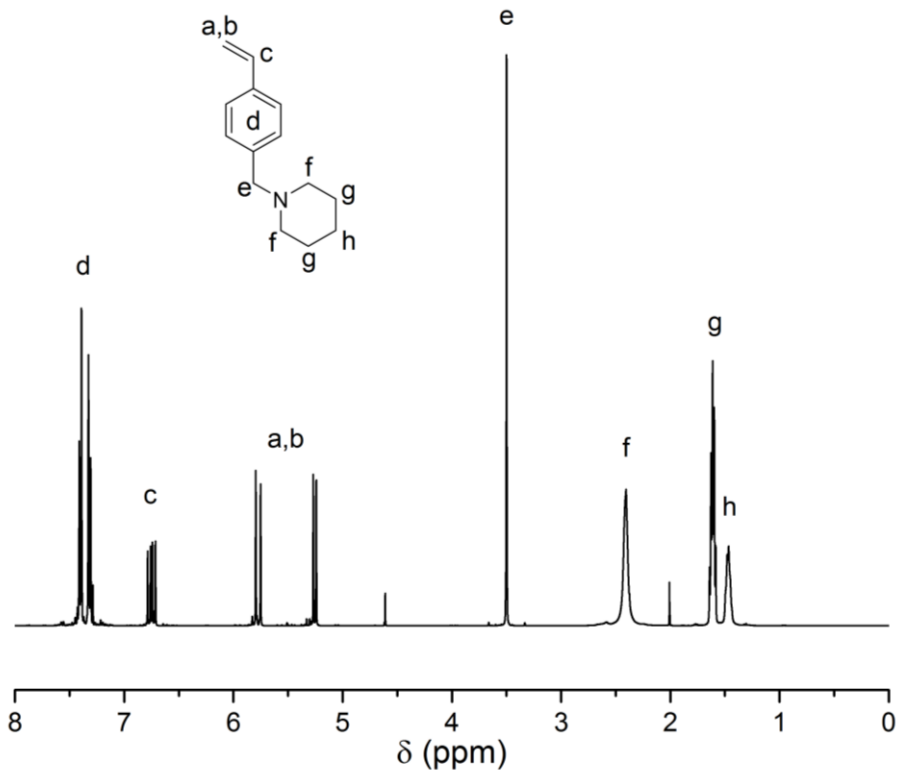

Figure 5.8 – ^{1}H NMR of the synthesised monomer VBPP.

5.3.3 Synthesis and analysis of the DUT-HIPE

The first prototype known as DUT-HIPE was synthesised containing 25 % by mass of the DUT MOF. The mixing of the 92 % high internal phase emulsion proceeded well, with no obvious perturbation in the formation of the HIPE foam. The synthesis left a solid monolith of DUT-HIPE. The monolith was examined under SEM to observe the porosity of the pHIPE and the state of the MOF, as well as the distribution of the MOF in the matrix. PXRD analysis also confirmed that the crystallinity of DUT-52 remained intact when compared to a powder sample and the pHIPE (Figure 5.9).

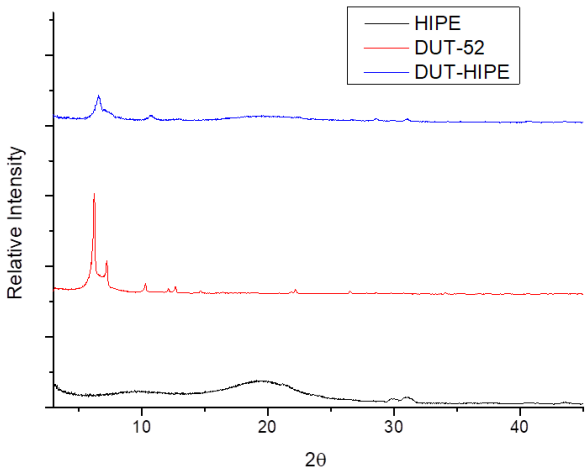

Figure 5.9 – The PXRD patters of the blank pHIPE (92% internal phase) (black) against both the DUT-52 powder (red) and the DUT-HIPE (blue).

The electron micrographs (Figure 5.10) clearly showed the MOF present in the matrix, and in many of cases the crystals appear to be distributed well. The porous nature of the pHIPE network was also visible.

Figure 5.10 – SEM images of the DUT-HIPE (A and C) with an image of the formed composite in the middle (C).

5.3.4 Synthesis and analysis of the MOF-HIPE

Encouraged by the facile synthesis of the DUT-HIPE prototype, especially when looking at the ease of incorporation of the MOF into the matrix, the active composite (MOF-HIPE) was then prepared. This composition incorporated the CWA hydrolysis catalyst MOF-808 and would be the first pHIPE/MOF system at the 95 % internal phase fraction. It was developed as an equivalent polymer to the $St_{95}VBC_5IP_{95}$ presented in chapter 4. The only difference being the

inclusion of the MOF. It was known that MOF/Zirconium MOFs were highly stable in aqueous environments so there was no concern that including it into the internal phase would disrupt its catalytic activity. When the PXRD of the composite was compared to both the starting MOF and the equivalent pHIPE ($St_{95}VBC_5IP_{95}$) it was seen that the peaks associated with the MOF had been maintained into the composite (Figure 5.11). This suggested the crystallinity had been maintained.

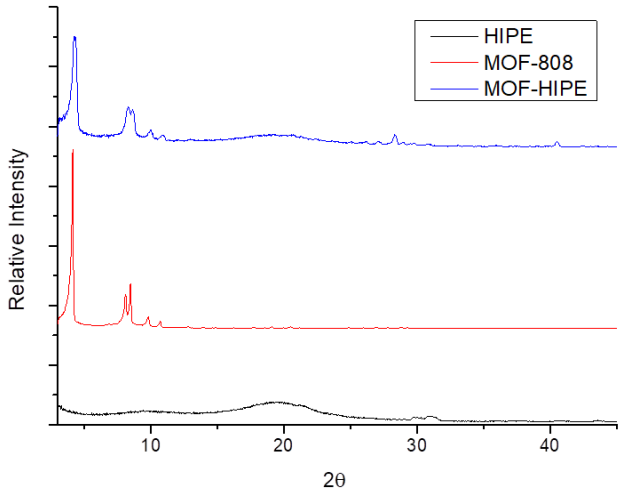

Figure 5.11 - The PXRD patters of the blank pHIPE (black) against both the MOF-808 powder (red) and the MOF-HIPE composite (blue).

The SEM images taken of this composite (Figure 5.12) were also very similar in quality to that of the DUT-MOF prototype. A good distribution of the MOF throughout the polymer matrix was observed, and the pHIPE itself appeared to be porous, although the voids and windows did not appear to be very regular in shape or size. The structure was very web-like, similar to the polymers with higher internal phases in chapter 4.

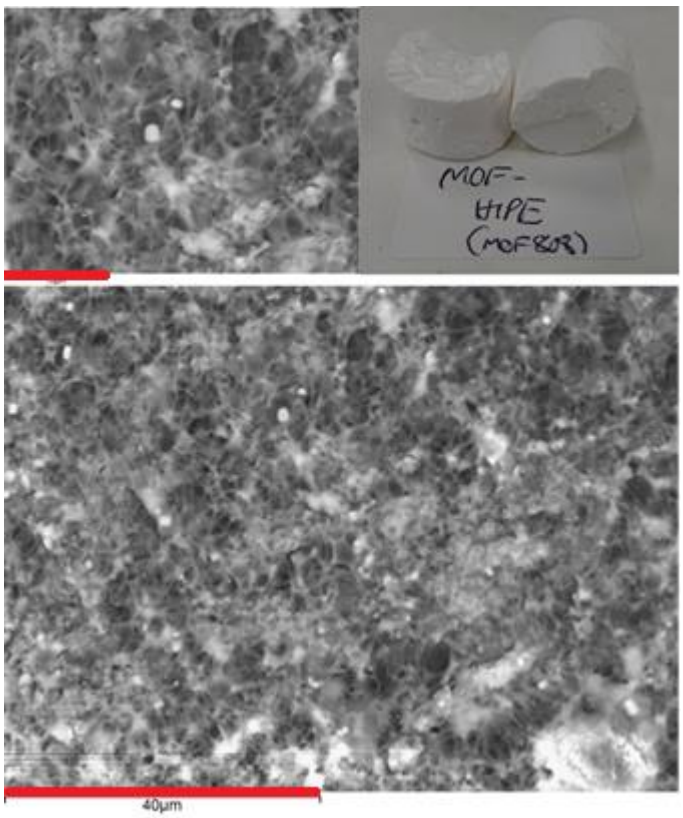

Figure 5.12 – Top left; an SEM image of the MOF-HIPE composite (red scale bar 10 microns), top right; a picture of the formed composite, bottom; SEM of the composite (red scale bar 40 microns).

5.3.5 Optimization of the synthesis of VBPP containing pHIPEs

Synthesis of the pHIPEs containing VBPP was unsuccessful when 20 % surfactant was used. 20 % weight content of surfactant was used for all previous pHIPEs in chapter 4 with good results, however with VBPP present splitting of the foam occurred during mixing and curing, resulting in complete phase separation of the emulsion. The tertiary amine of the piperidine in the VBPP was likely exhibiting enough hydrophilicity to facilitate the ripening/splitting of the foams. MOF-808 was introduced into the VBPP-HIPE with 20 % surfactant to see if the particles would help to stabilize the emulsion, similarly to a Pickering emulsion for example.[23] Stabilisation did not occur, and splitting still occurred. The work of Williams *et al*.[24,25] was consulted and it was decided that increasing the surfactant may be a simple enough solution to force the stabilization of the emulsion. The surfactant was therefore increased to 30 % with and without MOF particles to try to offset the effects of the VBPP. Increasing the surfactant to 30 % did

appear to stabilize the emulsions in both cases, allowing the synthesis of solid monoliths which presented reasonable porosity in both the final composite (MOF-HIPE-VBPP-S, section 5.3.6 and a control (HIPE-VBPP-S), section 5.3.7 . The '-s' represents that these polymers have 30 % surfactant instead of the standard 20 %.

5.3.6 Synthesis and analysis of MOF-HIPE-VBPP-S

The final composite was tested in line with the previous controls, primarily to ensure that the VBPP had not interfaced with the MOF in any way, and that the MOF had not affected the HIPE during curing (Figure 5.13).

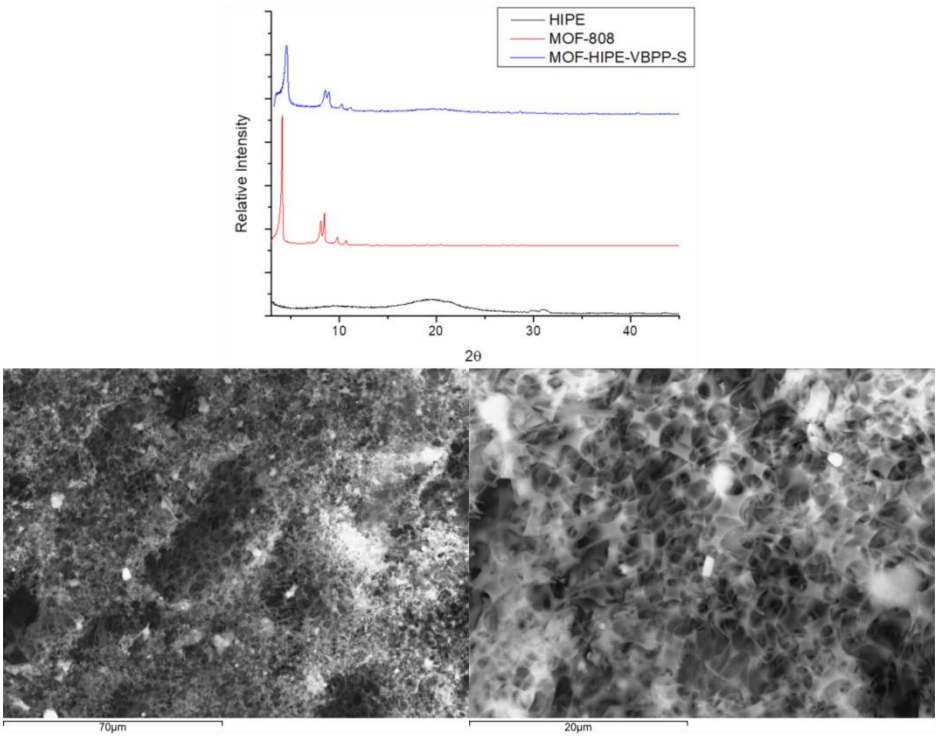

Figure 5.13 – Top; the PXRD comparison of the MOF-HIPE-VBPP-S final composite. Bottom of the figure shows SEM images of the composite. Left image scale bar is 70 microns and the right is 20 microns.

The MOF did appear to maintain its crystallinity. The porous morphology of the system was also observed, and the pores appeared to be on a much smaller scale of the VBPP-HIPE –S control.

5.3.7 Synthesis and analysis of HIPE-VBPP-S

A pHIPE with 5 % VBPP in the feed, similarly to MOF-HIPE-VBPP-S was synthesised. This polymer 'HIPE-VBPP-S' was synthesised as a control for the catalytic studies. The polymer would serve as a control by showing the rate of any hydrolysis in a polymer with both 30 % surfactant and 5 % VBPP, but with no active catalyst. This was to see if the VBPP was promoting hydrolysis in any way, regardless of the catalyst.

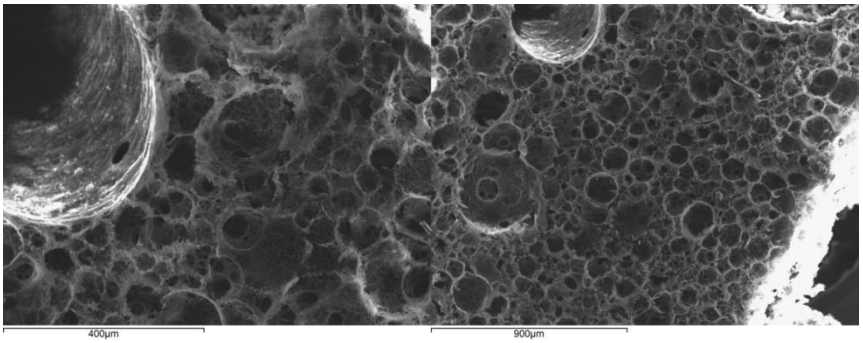

Figure 5.14 – SEM images of the HIPE-VBPP-S (left; scale bar 400 microns, right; 900 micron scale bar).

SEM was carried out on the polymer. The addition of the VBPP appeared to have not caused the porosity to be lost, however the average pore diameters were in fact extremely large (>100 µm) compared to the pore diameters in chapter 4 of around 10 µm. These large diameters suggested there may have been a ripening process still occurring during curing of the emulsion.

5.3.8 Quantification of the VBPP content

Demonstrating the presence of the VBPP in the matrix of the polymer MOF-HIPE-VBPP-S was attempted using IR spectroscopic analysis. The possibility of the VBPP not incorporating into the matrix in a regular fashion, especially due to the difficulties encountered during the HIPE synthesis, was a concern. Using the MOF-free sample for analysis (HIPE-VBPP-S) was done to reduce the noise as much as possible from the groups associated with the MOF. The IR spectra

of a powdered sample of the polymer were tested against the polymer with no VBPP in the feed (HIPE) (Figure 5.15).

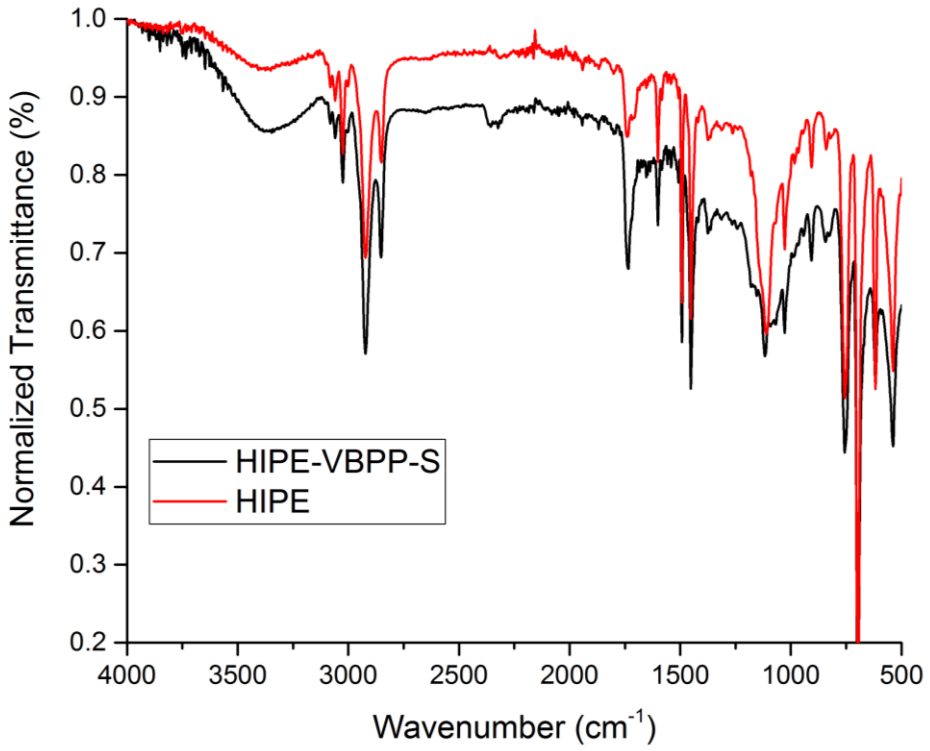

Figure 5.15 – The infrared spectra of the powdered same of HIPE-VBPP-S and the control sample HIPE.

There was no conclusive evidence of VBPP in the IR spectra for the HIPE-VBPP-S. For a tertiary amine a sharp but weak signal for C-N at 1200 cm^{-1} should have been present but could not be observed in comparison to the control. Where the VBPP should represent effectively only 3.5 % of the mass of the total sample including surfactant, it was too hard to see any evidence of this functional group. To try to observe an N-H band in a clearer region; protonation of the sample with 2M HCl, followed by drying was carried out. This approach was inspired by work which had demonstrated the appearance of a band at 2560cm^{-1} due to a protonated piperidolate group, amongst other piperidine based molecules.[26] A powdered sample of this protonated polymer was tested, but again, there was no evidence for this peak seen in the IR spectra when compared to the control HIPE.

An attempt was made for the VBPP in the matrix to be quantified using MAS-NMR. A sample of the MOF-HIPE-VBPP-S was swollen in a MAS-NMR sample holder and the spectrum was taken. This was compared to a MAS spectrum of swollen 'HIPE', the raw surfactant, and the VBPP monomer (Figure 5.16). The spectra of the final composite did not exhibit any peaks due to VBPP which were suitable for comparison. Any possible piperidine group was obstructed below the polymer matrix between 0.8 ppm and 2.8 ppm, and the bridging CH_2 'e' between the benzene and the piperidine which was clear in the monomer, was obscured by the surfactant in the composite, if present at all. The VBPP in the final composite could not be determined by integration.

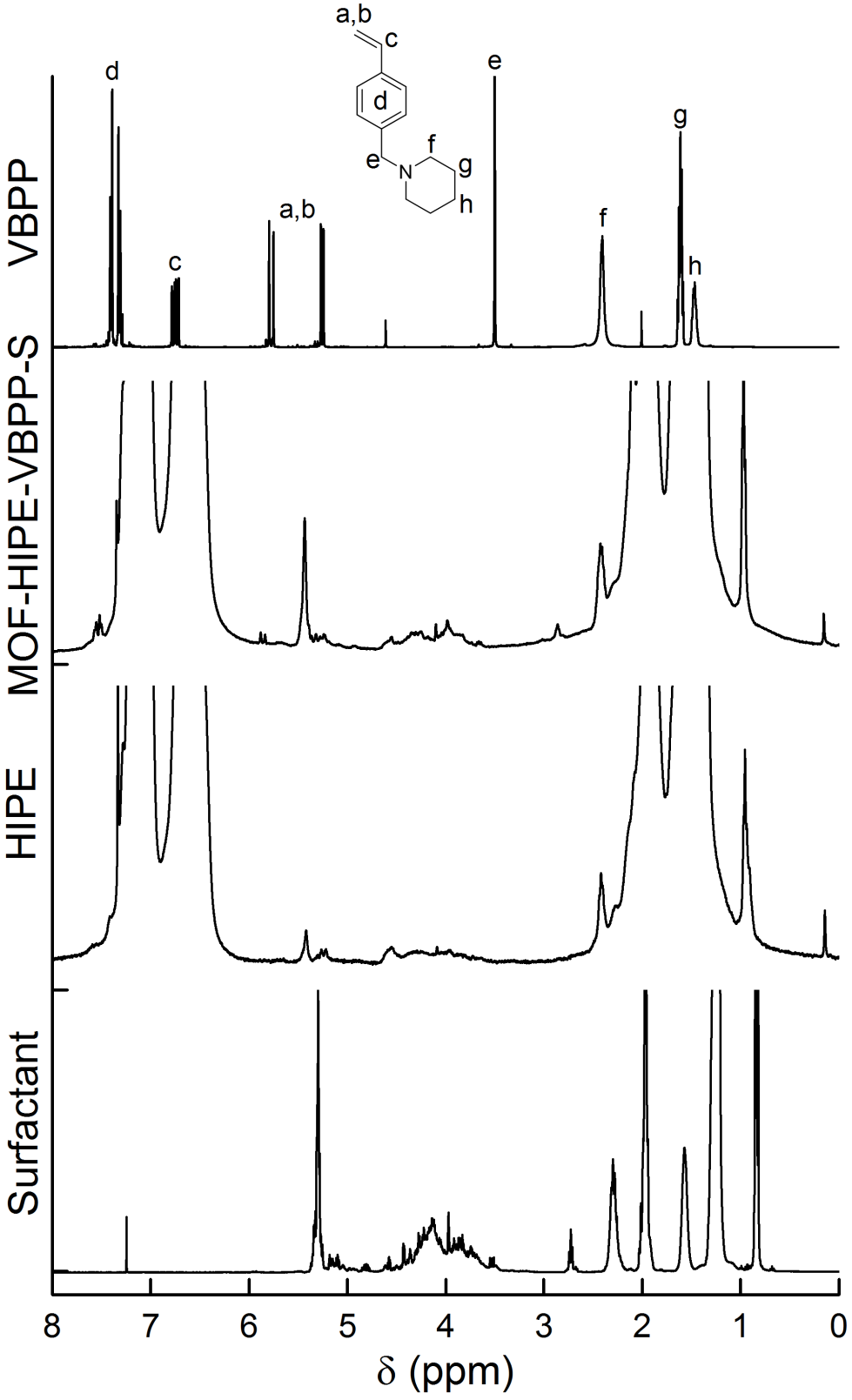

Figure 5.16 – ^{1}H NMR spectra of the (top to bottom) VBPP monomer, 'MOF-HIPE-VBPP-S' composite, 'HIPE' polymer and SPAN-80 surfactant. The two polymer spectra were obtained using MAS-NMR.

It would have likely been more probative to have compared the final composite to the 'HIPE-VBPP-S', to both show the peaks relating to the 30 % surfactant in the final composite, and to determine which regions if any were due to the MOF. This was not possible due to time constraints, and it was likely that they would have still not shown anything significant, as in the best case, the VBPP feed was only 3.5 mol%. The complications of trying to prove the presence of a low amount of a dopant in a crosslinked polymer matrix which included other materials were evident.

5.3.9 Synthesis and analysis of MOF-HIPE-S

A further sample was prepared following that of the buffered composites. The primary purpose of this synthesis was to create a catalytic control sample with 30 % surfactant, similar to the polymers MOF-HIPE-VBPP-S and HIPE-VBPP-S which both required 30 % surfactant for the synthesis rather than the 20 % in the original MOF-HIPE. The control was required for clarification that the increased surfactant required for the VBPP containing polymer synthesis was not causing increased hydrolysis. In line with the previous composites, this polymer was also examined for its MOF crystallinity, and SEM was carried out to look at the pHIPE morphology (Figure 5.17). The electron micrographs clearly showed the porous nature of the polymer, with visible voids and windows.

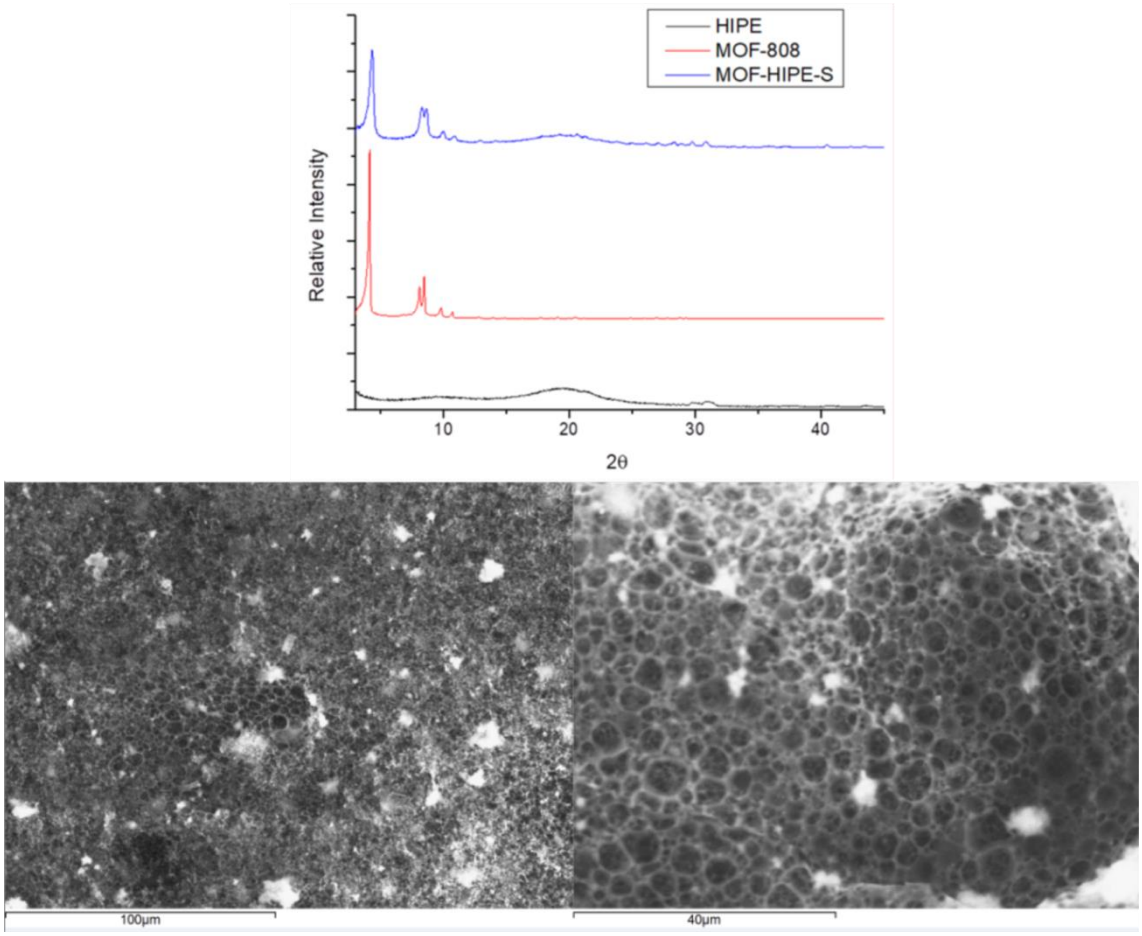

Figure 5.17 – Top; the PXRD of the MOF-HIPE-S showing the retention of crystallinity of the MOF in the composite. Bottom left; SEM image of the MOF-HIPE-S composite (scale bar 100 microns), bottom right; SEM image of the composite (scale bar 40 microns).

5.3.10 Swelling of all the composites in methyl benzoate

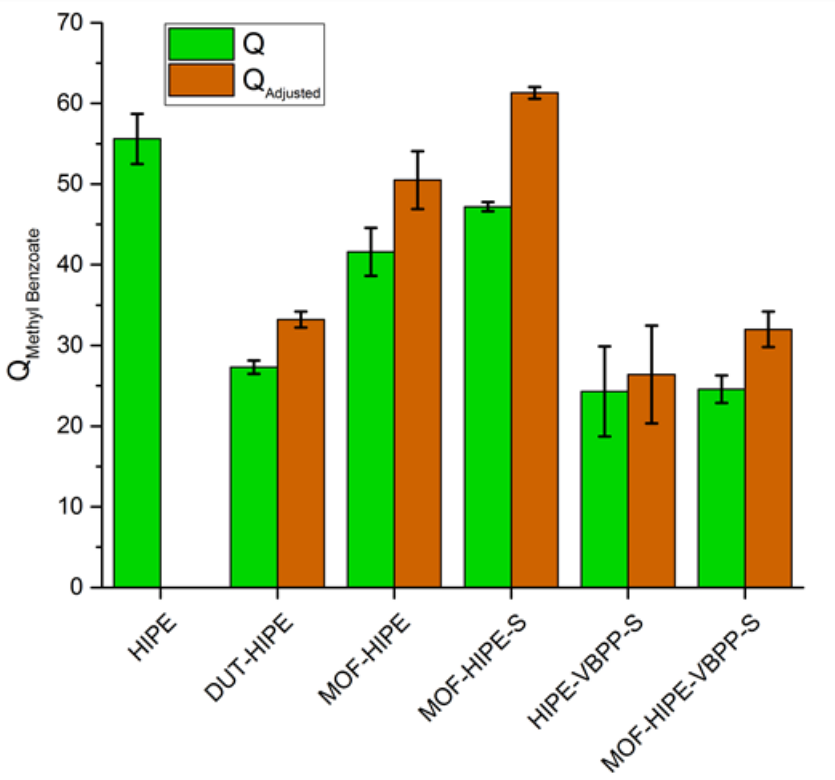

Figure 5.18 - Graph showing the swelling degrees (Q) alongside the adjusted Q for each of the samples presented in this work. HIPE does not have an adjusted value associated, as it does not contain any extra components outside of the basic synthesis.

The control sample 'HIPE' showed a Q value of 55.6 ± 3.1. When compared to this, the 'DUT-HIPE' seemed to have a dramatic reduction in swelling ability (Qmod = 33.2 ± 1.00) but it was important to note that this sample was synthesised of a 92 % internal phase and without VBC, rather than the 95 % of the control. When 'DUT-HIPE' was compared to an equivalent 92 % internal phase sample ($St_{100}IP_{92}$) Q = 42.8 ± 1.43, the swelling appears to have only dropped by around 25 % rather than 50 %. In the 'MOF-HIPE' sample containing MOF-808, the modified swelling (Q_{mod} = 50.5 ± 3.58) was much closer to that of the control. Increasing the surfactant with 'MOF-HIPE-S' further increased the swelling (Q_{mod} = 61.3 ± 0.74), which was a direct effect of having a better defined internal structure, caused by the increased surfactant. Addition of the VBPP to this system 'HIPE-VBPP-S,' then reduced the swelling by half when compared to

the control to Q_{mod} = 26.4 ± 6.04, likely due to the unstable emulsion foam, this was supported by the lack of discreet structure seen in the SEM. The final composite 'MOF-HIPE-VBPP-S' (Q_{mod} = 32.0 ± 2.20), showed increased swelling, likely due to the MOF helping to stabilize the HIPE foam somewhat. The increase however is not statistically significant compared to the 'HIPE-VBPP-S'. The final composite only swelled to 57 % of the control, which although a significant reduction, was still expected to be able to swell the V agents in excess of Q = 30 which was acceptable.

5.3.11 DMNP monitoring procedure

For all of the DMNP hydrolysis studies a standard procedure was followed as explained in section 5.2.8 and a scheme representing the procedure and showing the hydrolysis of DMNP is shown in Figure 5.19.

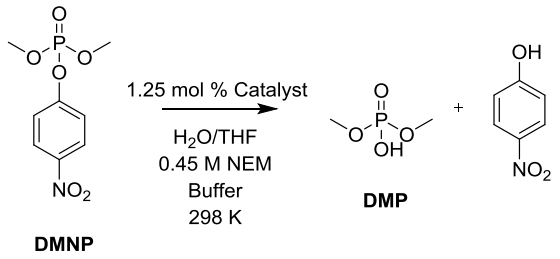

Figure 5.19 - The reaction scheme for the DMNP catalysis studies.

The phosphorus NMR spectra were examined in each case to estimate the ratio of the breakdown product dimethyl phosphonate (3 ppm), to the starting material DMNP (-5 ppm) For each study in simulant the reactions were carried out in triplicate. An example of the spectra obtained through this breakdown route is shown in Figure 5.20.

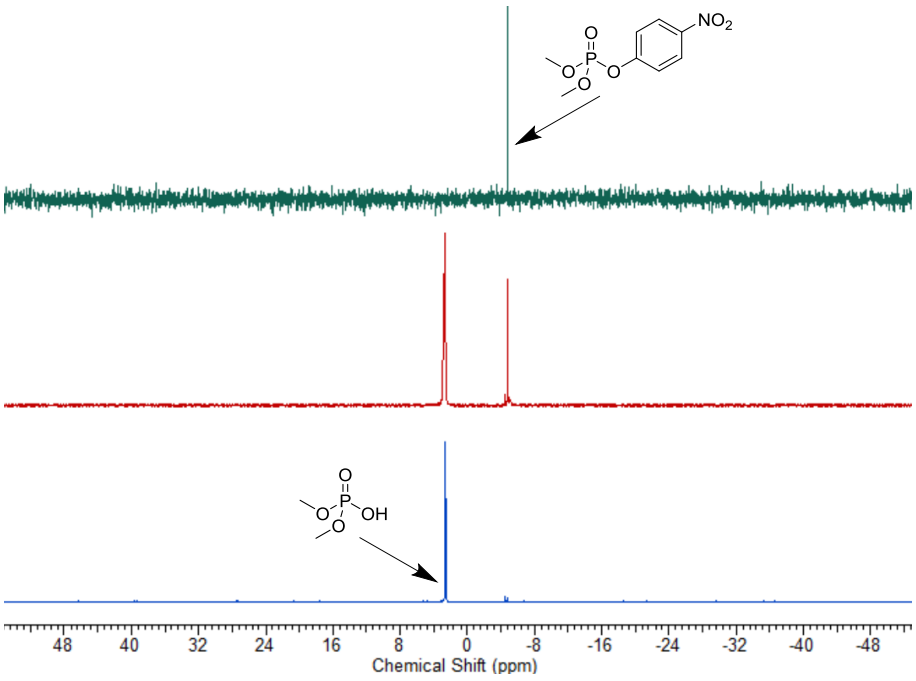

Figure 5.20 - A ^{31}P NMR overlay showing the different stages of DMNP hydrolysis. The spectra observed were for: (green) fresh DMNP, (red) DMNP 2 hours after the addition of MOF-HIPE containing 1.25 mol % MOF-808 relative to substrate, and (blue) the reaction represented by the red line after 18 more hours.

5.3.12 Catalytic activity of the MOF-HIPE

The catalytic activity of the MOF-HIPE was tested in an environment with external buffer. The quantity of catalyst was calculated from the expected total swelling of the system and therefore the amount of the substrate which would be in contact with the polymer. The activity of the composite was compared to both the lone MOF powder and the starting pHIPE (Figure 5.21). The purpose of the THF and the water was to form a binary mixture which would absorb into the matrix. Water alone would not truly swell these systems as they were intrinsically hydrophobic.

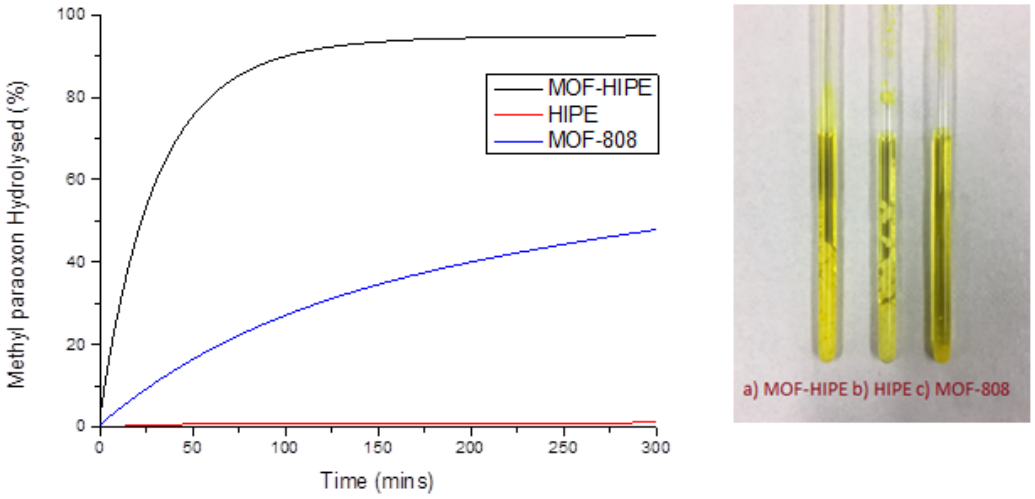

Figure 5.21 – (Left) the breakdown of DMNP in: the MOF-HIPE composite, the MOF-808 powder, and the control HIPE sample. Each set of data was obtained in triplicate. An exponential fit was calculated for each set of data. Each sample is represented as an average of the 3 exponential fits from the triplicate studies. (Right) a picture of the NMR catalyst studies, the picture shows how the MOF powder settled in the NMR tube, whereas the pHIPE composites remained more dispersed in the tubes. The yellowing is caused by the DMNP.

$St_{95}VBC_5IP_{95}$ from chapter 4 ('HIPE') was used as a blank and no DMNP hydrolysis was observed in the presence of this control. The MOF-HIPE ($k = 0.0267\ min^{-1}$) significantly outperformed MOF-808 ($k = 0.0034\ min^{-1}$). The increased reaction rate in the composite was likely due to the more dispersed nature of the MOF inside the matrix, as opposed to in the bulk form where it would aggregate at the bottom of the NMR tube (Figure 5.21).

To ensure that the catalytic activity was occurring throughout the composite sample as opposed to just on the edges where the substrate was interfacing the polymer, studies were carried out on differing areas of a pHIPE block. Firstly, a quantitative swelling study was performed on MOF-HIPE, using a 25:75 mixture of DMNP:THF. The MOF-HIPE readily swelled the test mixture of the two components to a respectable $Q = 50.6 \pm 5.41$. This suggested that the DMNP was swelling into the matrix as well as the pores. A sample of the MOF-HIPE was left

to react in the same fashion as mentioned in section 5.3.12 . This sample was then cut into sections representing the middle and edge, and the liquid from each of the two areas was removed separately by vacuum filtration. A sample of the supernatant was also taken from around the block. These three liquid samples were analysed for their DMNP content (Figure 5.22). Full conversion in both the middle and the edge of the polymer was observed, as well as only 18 % conversion in the supernatant surrounding the sample. This suggested that the experimental set up was giving a consistent result throughout the matrix. This also validated that H_2O and N-ethylmorpholine buffer were able to access the catalytic Zr_6 nodes throughout the whole material, and they weren't obstructed by the polymer matrix.

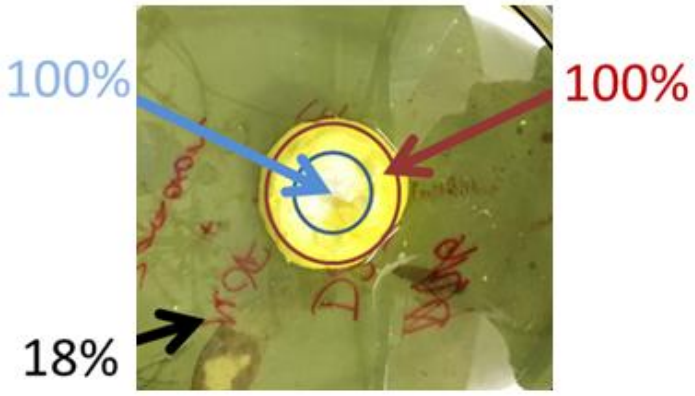

Figure 5.22 – A visual demonstration of the amount of degradation of the DNMP throughout different regions of the MOF-HIPE composite sample. The percentages represent the hydrolysis of DMNP in the middle (blue), edge (red) and supernatant (black) of the composite.

5.3.13 Catalysis of DMNP with increased surfactant

Most practical uses of a composite would be in neat V-agents. The ability of the composite to hydrolyse the DMNP in an environment where the THF was not present was tested. THF significantly improved the water influx to the polymer matrix by homogenising the components. Catalysis in the presence of only the water, buffer and simulant, would more accurately show the effect of the surfactant on the uptake of water. The 20 % surfactant polymer MOF-HIPE and the 30 % surfactant polymer MOF-HIPE-S were used (Figure 5.23).

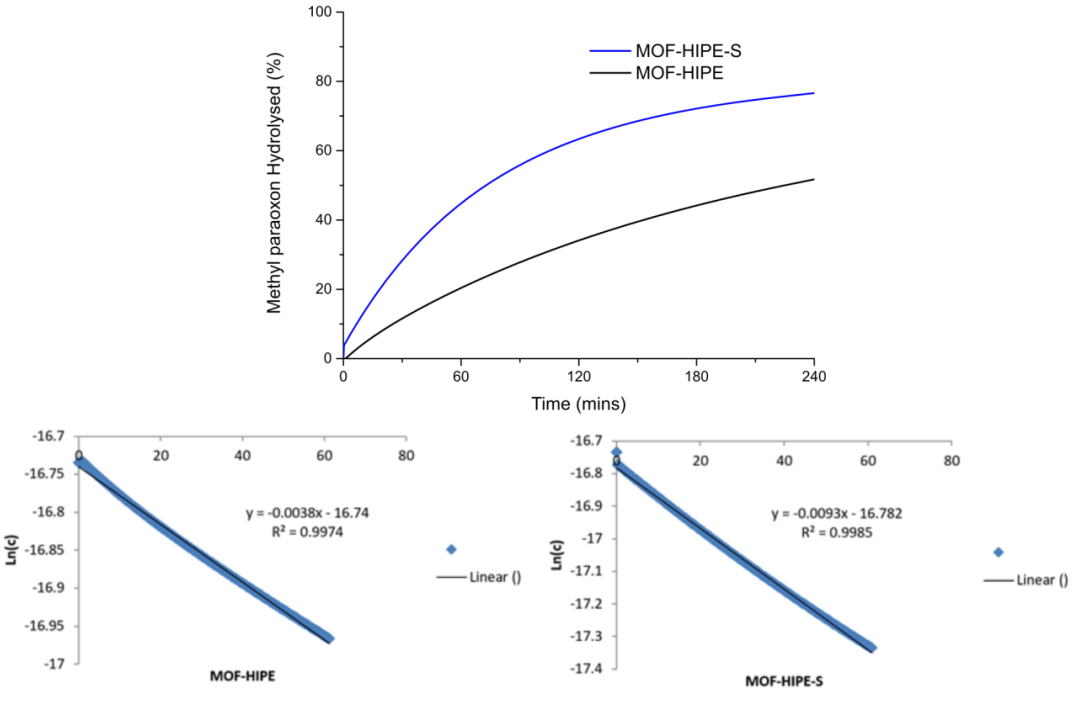

Figure 5.23 – (Top) a plot showing the hydrolysis of DMNP over time in the presence of MOF-HIPE and MOF-HIPE-S with 0.45 M NEM buffer and H_2O. Each data series is the average of three exponential fits, derived from the original data. (Bottom) Natural logarithms of the concentration of DMNP breakdown products during reactions. The first order rate constants were calculated from a linear fit through the first 60 minutes for each composite.

Slow degradation of the DMNP was observed in both composites. The 20 % surfactant composite MOF-HIPE reacted with a rate of k = 0.0023 min^{-1}, and the 30 % surfactant pHIPE composite MOF-HIPE-S showed an increased reaction rate of k = 0.0065 min^{-1}. Compared to the MOF-HIPE with THF (k = 0.0267 min^{-1}), this served to show how much of an advantage the THF played in the overall rate of hydrolysis. The rate of hydrolysis with 30 % surfactant (MOF-HIPE-S) was faster than that of the 20 % surfactant (MOF-HIPE) which means the surfactant was likely assisting in the influx of water into the polymer.

5.3.14 MOF-808 ambient catalysis of VX

The final piece of data required for the prototype development was to test the ability of the lone catalyst to degrade the neat VX in ambient conditions. In the previous tests the composite

exhibited fast degradation of the simulant; however the majority of these results were subject to artificially high levels of water and buffer. High quantities of buffer and water would not be present in a neat agent sample, and adding them would be logistically unpractical. For this reason the degradative abilities of MOF-808 with no added reagents was tested (Figure 5.24).

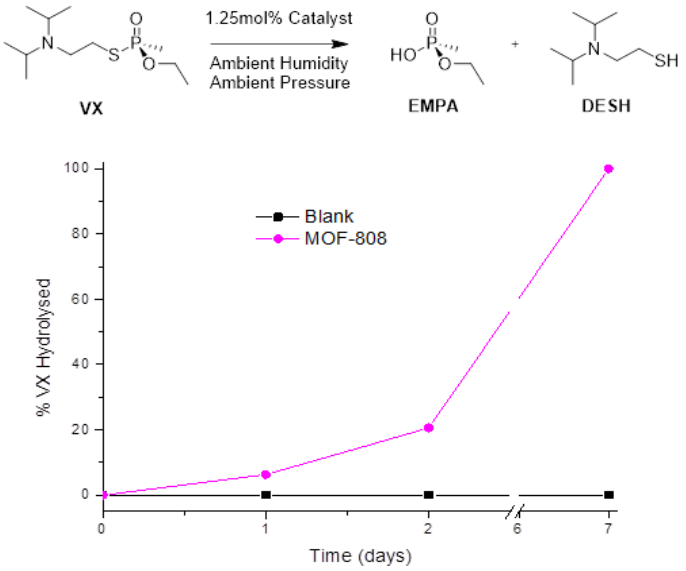

Figure 5.24 – Testing the ambient, non-buffered degradation of VX with the MOF-808 catalyst (pink) against a blank control (black). The degradation scheme is presented above the graph.

The VX was placed into an uncapped NMR tube with 1.25 mol% MOF-808, where it was monitored for degradation over 7 days. The blank sample containing only VX showed no breakdown across the timeframe, showing just how persistent and therefore dangerous this agent could be in the environment. The sample with catalyst showed a very slow breakdown of the VX, especially at the start. The conversion to the products EMPA and DESH did however reach 100 % after 7 days. The rate of reaction was likely to be limited by the water content entering the system, and also by an initiation of the hydrolysis. Once the initiation had begun, the self-buffering nature of the reaction allowed it to continue to completion, albeit slowly. To allow the hydrolysis to occur quickly in a composite without external buffer, a small kick-start would be required to start off the hydrolysis of the agent, after which it should self-buffer.

5.3.15 Catalysis of DMNP in MOF-HIPE-VBPP-S and controls with external buffer

After synthesising the composite MOF-HIPE-VBPP-S, it was tested for its catalytic activity, similarly to that of all the previous studies utilizing external buffer, THF and water. The monomeric amine (methyl piperidine pKa = 10.08) was expected to perform similarly to the N-ethylmorpholine in kicking off the hydrolysis by creating a slightly basic environment. This test is presented in Figure 5.25 alongside all the other controls.

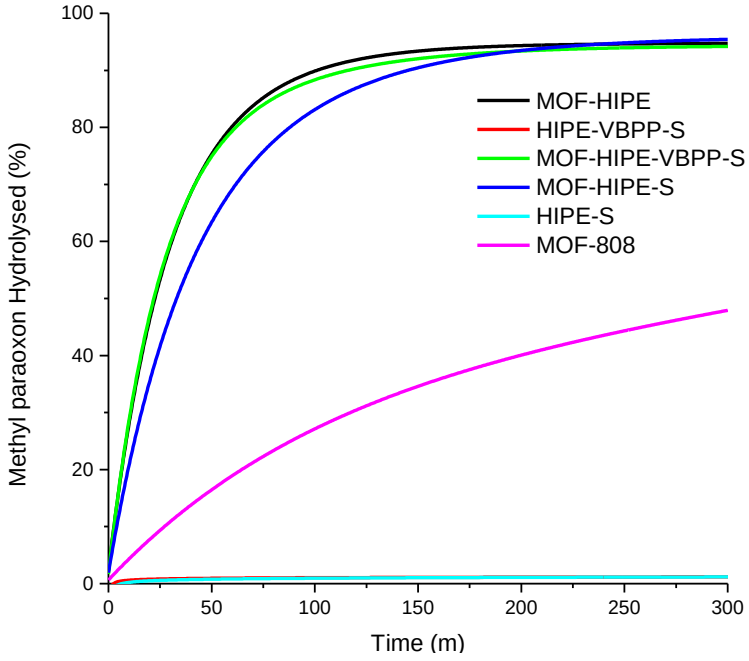

Figure 5.25 – A plot showing the hydrolysis of DMNP over time in the presence of various MOF/HIPE composites with the 0.45 M NEM external buffer, THF and H_2O. Each line is a representation of the average of the 3 exponential fits, derived from the three repeats, similar to Figure 5.21.

The rate of hydrolysis for the new composite MOF-HIPE-VBPP-S was comparably high (k = 0.0267 min^{-1}), to the MOF-HIPE and MOF-HIPE-S. This showed that the addition of the VBPP to the polymer allowed to stay hydrolytically active, and also that the VBPP had not interfered with, or degraded the MOF in any way. Despite the lower swelling ability of this composite, it

performed catalytically just as well as the previous non-buffered composites. The graphs for the calculation of the rate constants are shown in appendix 5A.

5.3.16 Catalysis with MOF-HIPE-VBPP-S with no external buffer

The activity of the composite was subsequently tested with no external buffer. The hydrolysis was tested with 3 different molar ratios (1:4, 1:8, and 1:16) of VBPP to DMNP, and also with the MOF-HIPE-S and the MOF powder. The quantities of which are shown in Table 5.2. The hydrolyses were carried out for 24 hours in all cases.

Table 5.2 – The catalytic studies of the breakdown of DNMP in the final composite MOF-HIPE-VBPP-S, and appropriate controls, with no external buffer or water.

Sample + Quantity (mg)	MOF-808 Quantity[a]	4-VBPP:DMNP Ratio[b]	DMNP Hydrolysed (%)
MOF-HIPE-VBPP-S – 32.5	4.9 mg	1:4	48
MOF-HIPE-VBPP-S – 16	2.4 mg	1:8	30
MOF-HIPE-VBPP-S – 8	1.2 mg	1:16	19
MOF-HIPE-S – 32.5	4.9 mg	No 4-VBPP	21
MOF-808 – 4.9	4.9 mg	No 4-VBPP	24

[a]The mass of MOF-808 was calculated from the mass of the composite. [b]The molar ratio was calculated from the 5 % VBPP in the polymer by design.

The hydrolysis did not go to completion in the time period for any of the trials with the final composite. As the quantity of the internal buffer increased relative to DMNP, so did the hydrolysis (Figure 5.26). The maximum degradation was seen to be 48 % with the highest polymer loading. This was due to the fact that the DMNP, unlike V-agents, was not self-buffering. The gradual production of nitrophenol during the degradation had the effect of acidifying the system and retarding the catalytic activity of the MOF.

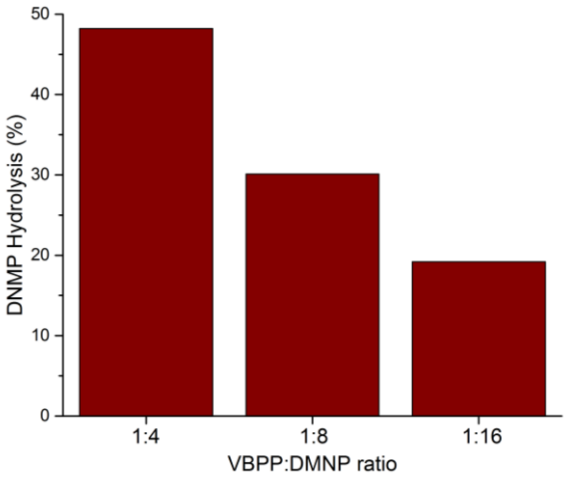

Figure 5.26 – The hydrolysis of DMNP in the presence of decreasing quantities of VBPP (achieved through reduction in the amount of total composite relative to the substrate).

Increasing the VBPP relative to the DMNP required an increase in polymer composite, and therefore more MOF. A concern was that the increase in amounts of MOF relative to DMNP was causing the increased hydrolysis in the 1:4 samples. The MOF-808 control which consisted of 4.9 mg of catalyst however only reached 24 % conversion, compared to the highest VBPP loading composite (48 % hydrolysis, 4.9 mg catalyst). This proved that the VBPP was instrumental in the improved breakdown of the DMNP.

5.3.17 Catalytic activity of MOF-HIPE-VBPP-S in VX (with water)

The first set of tests on neat VX was carried out as a replication of the work with the unbuffered simulant as described in section 5.3.16 . The reactions therefore included 1.25 mol% catalyst (20 mg of polymer), 0.3 ml H_2O/D_2O and 0.3 ml THF and 24 mg of VX. The reaction was monitored with ^{31}P NMR and an example of the monitored signals due to hydrolysis is illustrated in Figure 5.27.

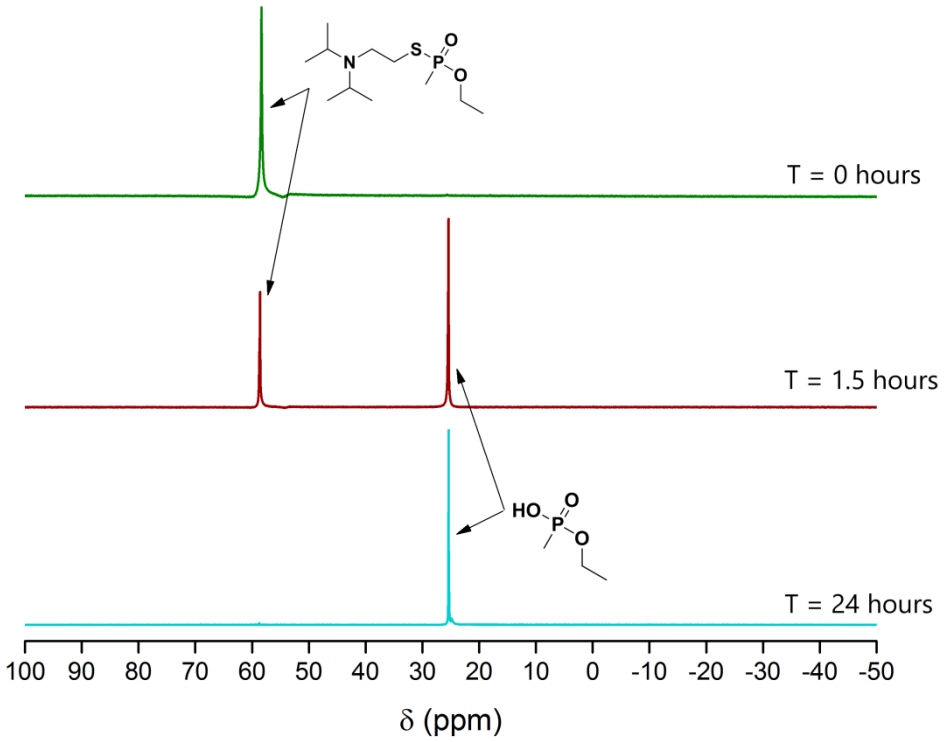

Figure 5.27 – A ^{31}P NMR overlay showing the different stages of VX hydrolysis. The spectra observed were for: (green) fresh VX, (red) VX 1.5 hours after the addition of MOF-HIPE-VBPP-S to a mixture of VX, D_2O and THF, and (blue) the reaction represented by the red line after 24 hours.

The results of the hydrolysis in VX are presented in Figure 5.28. The reaction with the final composite MOF-HIPE-VBPP-S, MOF-HIPE-S and the HIPE-VBPP-S are presented. The MOF-HIPE-VBPP-S showed the fastest rate of reaction with a k = 0.0059 min^{-1}, closely followed by the non-VBPP containing composite at k = 0.0044 min^{-1}. The reaction with no MOF showed no significant degree of hydrolysis. The rates showed that in this system with an excess of water, the VBPP did not make a significant difference in the rate of hydrolysis. Whilst degradation in the presence of VBPP was slightly higher, both composites showed very high hydrolysis performance. Also important to note was that the catalytic hydrolysis of VX in the VBPP containing composite was much higher than the near-stoichiometric hydrolysis of DMNP in the same circumstances. This shows how in reality the hydrolysis of DMNP without buffer does not hydrolyse in the same fashion as the VX.

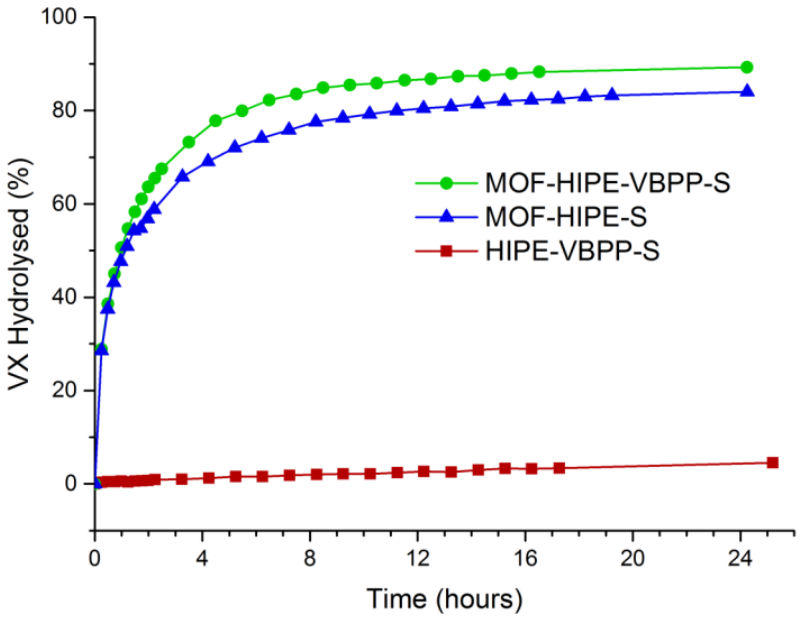

Figure 5.28 - A plot showing the hydrolysis of VX over time in the presence of three MOF/HIPE composites. The reaction was set up in an NMR tube to include 1.25 mol% catalysts relative to VX, 0.3 ml H_2O/D_2O and 0.3 ml THF.

5.3.18 Catalytic activity of MOF-HIPE-VBPP-S in neat VX (no water)

The second sets of tests of the composites in VX were carried out with no water and at a larger volume of VX (250 mg VX, 10 mg polymer) to demonstrate the practical effectiveness of solely the composite in VX with only ambient humidity. The results of these trials are presented in Figure 5.29.

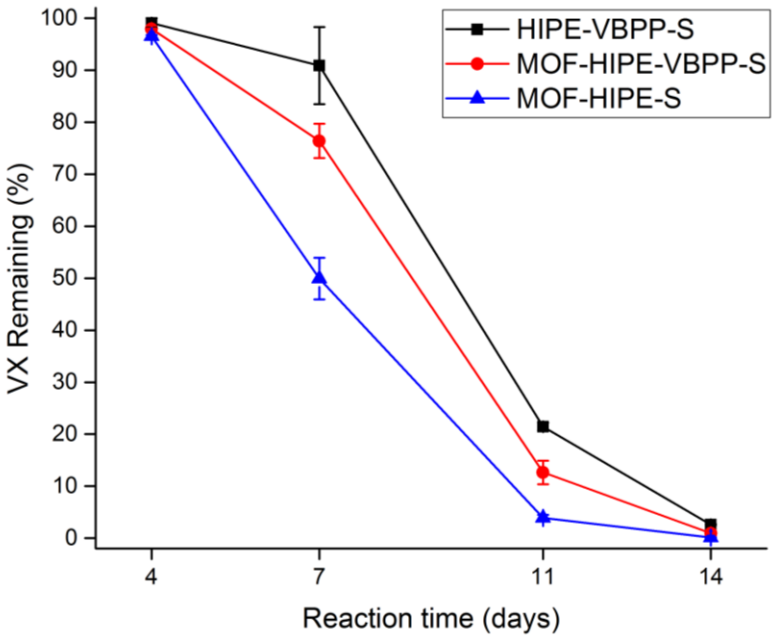

Figure 5.29 – Showing the degradation of VX (calculated from ^{31}P NMR) in the final composite MOF-HIPE-VBPP-S and two controls; MOF-HIPE-S (no internal buffer) and HIPE-VBPP-S (no MOF). The reaction consisted of only VX and the composites. The error bars represent duplicate results.

After the first 4 days, only minimal degradation was observed in any polymer. At 7 days the fastest degradation by a small fraction was seen in the MOF-HIPE-S sample which contained no VBPP. The MOF-HIPE-VBPP-S composite showed the second most progressed degradation, followed by the VBPP-HIPE-S at this point. After the full two weeks, all the tests had nearly reached completion. Across all data points the MOF-HIPE-S appeared to lead to the fastest hydrolysis. The primary theory for why the MOF-HIPE-S performed faster than that of the MOF-VBPP-HIPE-S in the initial days was because of the increased swelling potential of the MOF-HIPE-S. The increased swelling and SEM images suggested a more regular porosity throughout the pHIPE. The increased swelling capacity in the simulant (Q = 61 vs Q = 32), and therefore better swelling in the VX by proxy may have allowed for better dispersion of the VX, and consequently better contact between the VX and the catalyst. The results also suggested that the MOF-HIPE-S was able to kick start the hydrolysis which suggested the VBPP was not strictly necessary for the reaction to occur. Confirmation of either of these theories could not

be carried out due to the absence of the catalytic results in the HIPE-S sample which would have given both swelling and catalysis variance. This was due to only limited amounts of agent being available. At 7 days, the non-catalyst sample showed 7 % degradation and the MOF-HIPE-VBPP-S was at 22 %. Whilst this was only a modest increase, with only 0.15% catalyst loading in the composite, the variation was actually quite significant. Regardless of the individual rates, the composites showed that with only a catalytic loading of 0.15 % they were able to encapsulate and degrade neat VX in two weeks with only ambient water.

5.3.19 Comparison of composite effectiveness with alternative research

A paper published in 2016 led by the team of Farha *et al*. described the development of a very effective Nu-1000 Zr_6 MOF which was supported in poly(ethyleneimine) (PEI) with M_w parameters of 2500 and 25000.[24] They adsorbed this mixture onto the surface of cotton balls where they utilized the self-buffering nature of the PEI to break down VX and sarin with excess water. The important data from their VX breakdown was that they used 10.3 mol% catalyst loading, and observed a catalytic half-life of 15 minutes. When compared to our SDM, also with excess water, we observed a VX half-life of 1 hour, but with a catalytic loading of only 1.25 mol%. This equated to a turnover frequency of effectively double theirs in VX. Additionally they had no true swelling ability as the decontamination mixture was supported on cotton wool, whereas our SDM is intrinsically absorbent, and they did not test without excess water. A more recent contrasting piece of research which did have intrinsic swelling ability was that of Balow *et al*. which also utilized pHIPE morphology. This group oxidized a poly(diciclopentadiene) pHIPE in air at high temperatures generating peroxide groups on the polymer matrix. Subsequently the group showed that this system was effective for the oxidation of VX and sarin.[25] The largest disadvantage of the research was that the oxidation was stoichiometric with respect to the levels of oxidation of the polymer matrix, and therefore the material could not be classes as an SDM.

5.4 Conclusions

The collaborative efforts described in this chapter led to the development of an effective, internally buffered composite of a polymer matrix and a supported MOF catalyst. The versatility of the pHIPE morphology allowed catalytic MOF particles to be suspended in the pores of the polymer. In the first instance this composite showed increased catalytic rates for the hydrolysis of DMNP in an externally buffered environment over the lone MOF-808 powder. There was also no appreciable loss in swelling ability of the matrix in the simulant when the MOF was introduced. By modifying the matrix to include a piperidine based monomer, the hydrolysis of the simulant could be carried out without external buffering of the system, however this was seen to be stoichiometric in relation to the VBPP. Incorporation of the VBPP caused splitting of the emulsions, and this was alleviated by using increased levels of surfactant (30 %) in the synthesis. The increased surfactant not only prevented splitting of the emulsion, but also increased the rate of catalysis of DMNP in conditions without THF compared to the 20 % surfactant polymer due to the increased attraction to atmospheric water. The swelling of the final MOF-HIPE-VBPP-S composite was seen to only reach a Q_{mod} of 32, which was much lower than that of the control polymer, and could be explained from the irregular morphology and large pore size in the matrix. This suggested even with increased surfactant, that the emulsion was still ripening. Pleasingly, both the MOF-HIPE-S and MOF-HIPE-VBPP-S demonstrated that they were both effective SDMs when tested in both neat VX and VX with additional water and THF. In a scenario where excess water is available, a faster rate could be achieved with the MOF-HIPE-VBPP-S, and where the rate is not of concern, and ambient water is relied upon, the MOF-HIPE-S composite would be a more cost effective material to deploy. Utilizing MOF-HIPE-S would also be more appropriate where a larger swelling capacity is required over degradative ability. Comparing our SDMs with other leading research showed that MOF-HIPE composites were extremely competitive in their capability.

5.5 References

1 A. J. Wright, M. J. Main, N. J. Cooper, B. A. Blight and S. J. Holder, *ACS Appl. Mater. Interfaces*, 2017, **9**, 31335–31339.

2 Y.-C. Yang, *Acc. Chem. Res.*, 1999, ***32*** (2), 109–115.

3 Y. Kalinovskyy, N. J. Cooper, M. J. Main, S. J. Holder and B. A. Blight, *Dalt. Trans.*, 2017, **46**, 15704–15709.

4 H. Furukawa, K. E. Cordova, M. O'keeffe and O. M. Yaghi, *Science*, 2013, **30**, 6149.

5 Y. Liu, A. J. Howarth, N. A. Vermeulen, S.-Y. Moon, J. T. Hupp and O. K. Farha, *Coord. Chem. Rev.*, 2017, **346**, 101–111.

6 H.-C. Zhou, J. R. Long and O. M. Yaghi, *Chem. Rev.*, 2012, **112**, 673–674.

7 W. Lu, Z. Wei, Z.-Y. Gu, T.-F. Liu, J. Park, J. Park, J. Tian, M. Zhang, Q. Zhang, T. Gentle III, M. Bosch and H.-C. Zhou, *Chem. Soc. Rev.*, 2014, **43**, 5561–5593.

8 M. Eddaoudi, J. Kim, N. Rosi, D. Vodak, J. Wachter, M. O'Keeffe and O. M. Yaghi, *Science (80-.).*, 2002, **295**, 469–472.

9 J. Lee, O. K. Farha, J. Roberts, K. A. Scheidt, S. T. Nguyen and J. T. Hupp, *Chem. Soc. Rev.*, 2009, **38**, 1450.

10 K. Sumida, D. L. Rogow, J. A. Mason, T. M. McDonald, E. D. Bloch, Z. R. Herm, T.-H. Bae and J. R. Long, *Chem. Rev.*, 2012, **112**, 724–781.

11 H. Kim, S. Yang, S. R. Rao, S. Narayanan, E. A. Kapustin, H. Furukawa, A. S. Umans, O. M. Yaghi and E. N. Wang, *Science*, 2017, **356**, 430–434.

12 S.-Y. Moon, Y. Liu, J. T. Hupp and O. K. Farha, *Angew. Chemie Int. Ed.*, 2015, **54**, 6795–6799.

13 H. Furukawa, F. Gándara, Y.-B. Zhang, J. Jiang, W. L. Queen, M. R. Hudson and O. M. Yaghi, *J. Am. Chem. Soc.*, 2014, **136**, 4369–4381.

14 C. Ardila-Suárez, S. Perez-Beltran, G. E. Ramírez-Caballero and P. B. Balbuena, *Catal. Sci. Technol.*, 2018, **8**, 847–857.

15 Z.-Q. Li, J.-C. Yang, K.-W. Sui and N. Yin, *Mater. Lett.*, 2015, **160**, 412–414.

16 J. Jiang, F. Gándara, Y.-B. Zhang, K. Na, O. M. Yaghi and W. G. Klemperer, *J. Am. Chem. Soc.*, 2014, **136**, 12844–12847.

17 A. M. Plonka, Q. Wang, W. O. Gordon, A. Balboa, D. Troya, W. Guo, C. H. Sharp, S. D. Senanayake, J. R. Morris, C. L. Hill and A. I. Frenkel, *J. Am. Chem. Soc.*, 2017, **139**, 599–602.

18 S.-Y. Moon, Y. Liu, J. T. Hupp and O. K. Farha, *Angew. Chemie Int. Ed.*, 2015, **54**, 6795–6799.

19 M. C. de Koning, M. van Grol and T. Breijaert, *Inorg. Chem.*, 2017, **56**, 11804–11809.

20 H. Chen, P. Liao, M. L. Mendonca and R. Q. Snurr, *J. Phys. Chem. C*, 2018, **122**, 12362–12368.

21 Y. Yang, L. L. Szafraniec, W. T. Beaudry, D. K. Rohrbaugh, L. R. Procell and J. B. Samuel, , *J. Org. Chem.*, 1996, **61**, 8407–8413.

22 W. Liang, H. Chevreau, F. Ragon, P. D. Southon, V. K. Peterson and D. M. D'Alessandro, *CrystEngComm*, 2014, **16**, 6530–6533.

23 Y. Yang, Z. Fang, X. Chen, W. Zhang, Y. Xie, Y. Chen, Z. Liu and W. Yuan, *Front. Pharmacol.*, 2017, **8**, 287.

24 J. M. Williams, A. J. Gray and M. H. Wilkerson, *Langmuir*, 1990, **6**, 437–444.

25 J. M. Williams and D. A. Wrobleski, *Langmuir*, 1988, **4**, 656–662.

26 W. E. Thompson, R. J. Warren, I. B. Eisdorfer and J. E. Zarembo, *J. Pharm. Sci.*, 1965, **54**, 1819–1821.

27 S.-Y. Moon, E. Proussaloglou, G. W. Peterson, J. B. DeCoste, M. G. Hall, A. J. Howarth, J. T. Hupp and O. K. Farha, *Chem. - A Eur. J.*, 2016, **22**, 14864–14868.

28 R. B. Balow, S. L. Giles, C. L. McGann, G. C. Daniels, J. G. Lundin, P. E. Pehrsson and J. H. Wynne, *Ind. Eng. Chem. Res.*, 2018, **57**, 8630–8634.

5.6 Appendix 5A

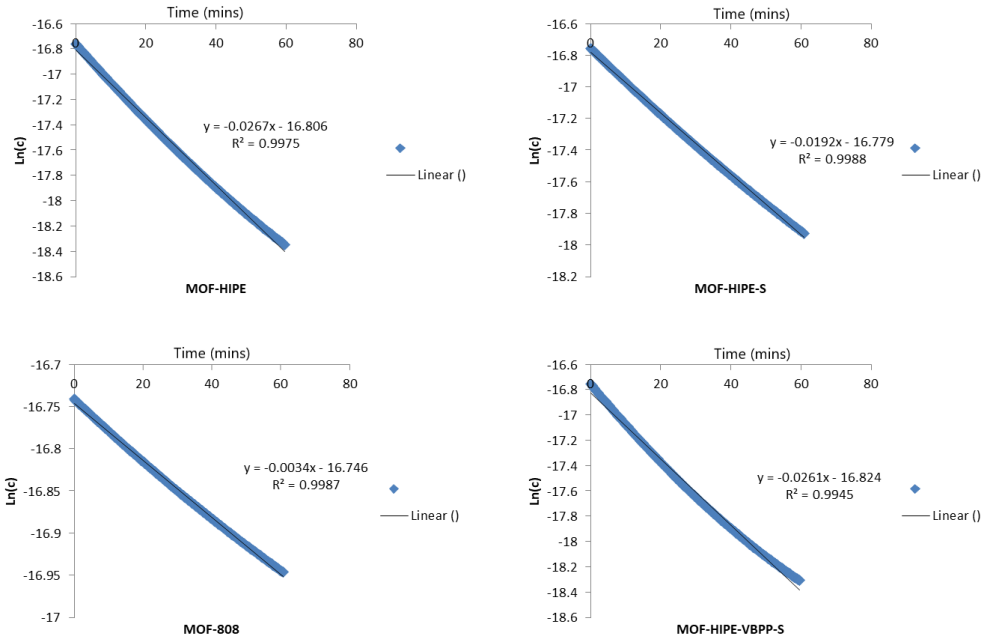

Figure 5.30 – The natural logarithms of the concentration of DMNP breakdown products during the hydrolysis reactions. The first order rate constants were calculated from a linear fit through the first 60 minutes for each composite. Top left = MOF-HIPE, top right = MOF-HIPE-S, bottom left = MOF-808 and bottom right = MOF-HIPE-VBPP-S.

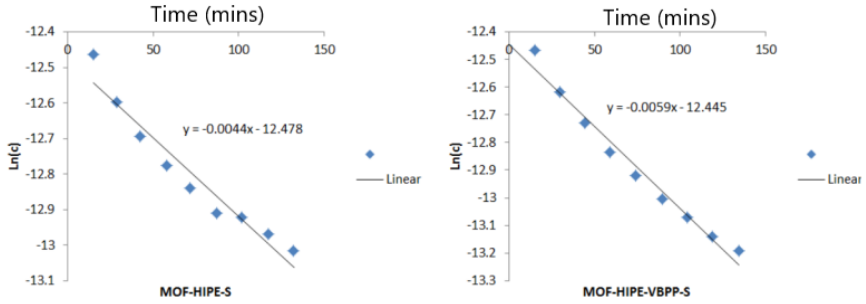

Figure 5.31 – The plots of the concentration of VX against time for the MOF-HIPE-S and MOF-HIPE-VBPP-S composites in the first hour of hydrolysis from section 5.3.17. The rate constants were derived from the gradients of the line in the bottom plots. The reactions were set up in an NMR tube to include 1.25 mol% catalysts relative to VX, 0.3 ml H_2O/D_2O and 0.3 ml THF.

Chapter 6 -

Synthesis of a Myrcene Containing Poly High Internal Phase Emulsion for a Greener Approach to CWA and Oil Encapsulation

6.1 Introduction and aims

6.1.1 Preface

The decreasing quantity of crude oil in the world coupled with the increasing public interest into the excessive use of non-renewable plastics in this age was one of the main footings for this chapter. Plastics, including polystyrene, are generally considered a serious polluting issue due to their extremely slow degradation in nature and the impact this can have on the environment. The impact of plastic pollution, specifically on marine life,[1] has become a significant area of concern in recent years and is one of the major influences for developing biodegradable polymers.[2] Whilst the use of non-renewable monomers is a necessity in many areas of materials engineering, it would be responsible to reduce their application wherever possible. This reduction in the use of non-renewable monomers must start at the design stage of research. With respect to this, the authors reflected on the use of styrene as the primary monomer for the absorptive materials designed in the previous chapters. Whilst very small amounts of styrene are found in nature in some foods,[3] the vast majority is synthesised on an industrial scale from the alkylation of benzene with ethylene and subsequent dehydrogenation of the ethylbenzene. Both starting materials involved in this synthesis are petrochemical derivatives which classes styrene, and any subsequent polystyrene, as non-renewable. This therefore meant that the CWA absorbents previously reported in this work would not be proactive at industrial scale for the reduction of crude oil usage. It was decided therefore, to attempt to design an updated absorbent, which would possess the same or improved properties as that of the pHIPEs in chapter 4 and 5, but with a central aim of synthesising around the principles of green chemistry in an attempt to reduce the impact of the absorbents on the environment. Second to this, the new absorbent would hopefully be more lipophilic, which would allow it to be used for the absorption of oils, such as for in crude oil spills.

6.1.2 Principles of green chemistry

6.1.2.1 General principles

The principles of green chemistry and environmental chemistry focus on both; reducing the use of non-renewable resources in the first instance, and reducing the formation of hazardous and polluting chemicals in all processes. To design an alternative to styrene based systems, the twelve principles of green chemistry must be understood. These principles are crucial design considerations for a chemist who wants to improve the environmental impact of their work. The principles are as follows;[4]

- **Prevention of waste**
- **Atom economy**
- **Less hazardous syntheses**
- **Designing safer chemicals**
- **Safer solvents/auxiliaries**
- **Energy efficiency**
- **Renewable feedstocks**
- **Reduce derivatives**
- **Increased use of catalysts**
- **Design for degradation**
- **Pollution prevention**
- **Accident prevention**

Most of these principles are self-explanatory, and when considered, are aspects that all chemists should consider during the design process of a chemical system.

6.1.2.2 Application of the principles to this work

With regard to the work presented in this thesis and in this chapter, it was wise to adopt a sensible amount of green principles, as opposed to trying to satisfy the majority of them. For this reason it was decided that the main principle of this work would be to try to use more renewable feedstocks primarily, and to increase the energy efficiency of the process. Due to the nature of the compounds which were targets for absorption in this work; introducing monomers which are traditionally biodegradable, and therefore contain many ether, ester and acid functionalities (Figure 6.1), would be detrimental to both the compatibility of the system and the stability of the product. For these reasons, biodegradability was not considered for

the project. The drying of the product was likely to be the most energy consuming part of the process, and so an alternative approach to the post polymerisation procedures would be ideal. The rest of the process was not extremely wasteful with respect to the rest of the green principles, and so they were not considered.

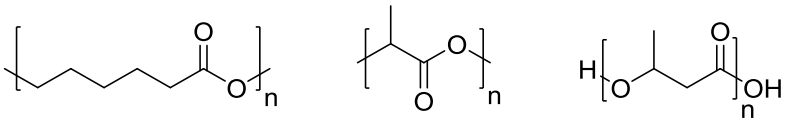

Figure 6.1 – The polymer structures of three commonly investigated bio sourced and biodegradable polymers; poly (caprolactone), poly (lactic acid) and poly (3-hydroxybutyrate).[5]

6.1.3 Choice of monomer

6.1.3.1 General requirements

Whilst searching for an appropriate monomer, factors additional to the green principles were taken into account in an attempt to improve on the properties which were established in the development of pHIPE $St_{95}VBC_5IP_{95}$ in chapter 4. The monomer must, importantly; retain good compatibility with the CWAs as to maintain similar swelling ability as seen previously, or at least be an effective sorbent for other low polarity chemicals such as oils. It would ideally also form a polymer which has elastomeric properties, as one of the large issues faces with the $St_{95}VBC_5IP_{95}$ was that the glassy nature of the polystyrene meant that it did not behave elastically. Whilst this elastic nature is not necessary for a swelling system, it may be advantageous for a system where the swollen material needs to be squeezed out from the matrix, for example in polymer supported catalysis/synthesis. This property may also allow the drying stage to have reduced energy consumption due to the ability of water to be squeezed from the pores.

6.1.3.2 Terpenes

Terpenes were chosen as a range of potential monomers for the pHIPEs. A terpene is generally considered a biosynthetic hydrocarbon with a molecular formula which is a multiple of C_5H_8.

Many terpenes can be found in nature abundantly, such as limonene from citrus, and pinene from pine trees (Figure 6.2). One advantage directly related to this project was that many terpenes are very hydrophobic in nature, due to the fact they only consist of carbon and hydrogen. This would allow them to form HIPE foams without too much modification to previous syntheses.

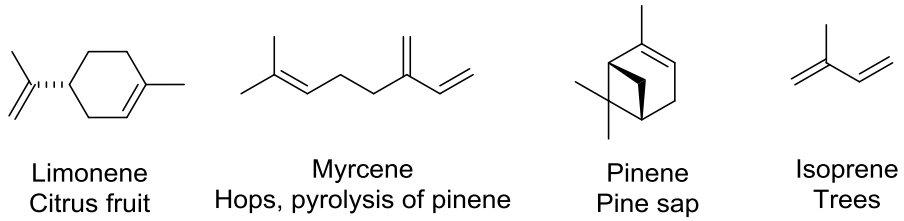

Figure 6.2 – A range of basic terpenes and their common natural sources. It is important to note the conjugated double bonds on both the myrcene and the isoprene.

Terpenes have been used as monomers for more than 75 years.[6] One of the most common poly(terpenes) is poly (isoprene), which is commonly used as a synthetic alternative to natural rubber.[7] A recent review discussed the wide range of research groups which have been utilizing terpenes in the search for more responsible monomers.[8] One approach taken has been to catalytically modify common terpenes to turn them into acrylates and methacrylates which are then easily polymerised through radical or living radical techniques, leading to industry level properties.[9,10] Some groups have utilized thio-ene click chemistry to modify the C=C bonds in terpenes to a variety of functional groups[11], leading to the formation of polymers from modified limonene and pinene.[12] Some researchers have simply opted to utilize the molecules as they are and create co-polymers through living anion methods.[13]

6.1.3.3 Myrcene

The approach undertaken in this chapter was to use a terpene without further modification. This required investigation into terpenes which were readily available and had the functionalities required for a free radical polymerisation. Whilst the most simple terpene isoprene was considered, its low boiling point (34 °C) made it too difficult to work with in conjunction with traditional radical initiators which required elevated temperatures for

decomposition. The next biggest terpene β-Myrcene showed initial promise for the project. This terpene had a boiling point of a much more reasonable 167 °C, possessed a labile alkene which would be suitable for post-polymerisation reactions, and is obtained through some industrially established green routes[14] which made it a good overall candidate. In terms of chemical compatibility, the radical polymerisation reactivity ratios of myrcene and styrene has been reported as R_1 = 1.36 (myrcene), R_2 = 0.27 (styrene) (R_1R_2=1.20)[15] which suggested there was a slight preference for the myrcene to form a block or a gradient. The conversion of radically initiated myrcene polymerisation has also been shown to reach good levels in emulsion polymerisation conditions.[16,17]

6.1.4 Previous works with elastomeric pHIPEs

No research was found which utilized terpenes in the synthesis of a pHIPE network. Other groups have however reported the synthesis of elastomeric / non-glassy pHIPE systems and some are presented herein. A report by Zimmy *et al*. described the synthesis of a silicone based porous templated polymer network for acoustic applications. This group observed archetypal pHIPE porosity (pore diameters around 9 μm, however claimed to only use upto 40 % internal phase which classed their system as a pLIPE (poly low internal phase emulsion).[18] Cameron *et al*. published research on the T_g variation in a styrene-DVB-ethyl hexyl [meth] acrylate (EHMA) set of 90 % internal phase pHIPEs. This group used soxhlet extraction to exchange the water for ethanol in the pores, before vacuum drying their monoliths. They observed no significant difference between the styrene-DVB polymers and the elastomeric (EHMA containing) polymers, except for a T_g depression. The T_g varied in a non-linear fashion compared to the EHMA content.[19] Following on from the work by Cameron, Chen *et al*. produced a similar EHMA containing pHIPE with 80 % internal phase and 10 % DVB crosslinking for use as an ion separation transport membrane. Again, this group was able to dry the polymer simply, under vacuum at 55 °C, leaving a highly porous polymer (pore size around 10 μm).[20] Another report utilizing acrylates was presented by Tunc *et al*. and utilized isobornyl, isodecyl and stearyl acrylates, balanced against styrene. They produced pHIPEs with an

internal phase fraction of 90 %, and high level of DVB crosslinking > 20%). They were able to tune the microstructure and mechanical properties by varying the monomer feed.[21] A final report which was found, presented by Moghbeli *et al*., utilized a similar EHMA/styrene/DVB system to that of Cameron *et al*., however they reinforced the monomer phase with organic clays. They observed the effect that the organic clays had on the mechanical strength of the elastomeric monoliths and found the clays acted as a co-surfactant, improving the pore diameter and porosity of the polymers.[22]

6.1.5 Development process

The synthetic approach taken in this chapter was to first attempt to synthesise a myrcene-styrene copolymer with and without 1 % DVB crosslinking. This would be to observe the effects of the polymerisation from the introduction of myrcene. Forming gels in this system would prove difficult and so an alternative crosslinker was subsequently developed. This crosslinker was to be 1-10,decanedimethacrylate and would serve three purposes. Firstly, it would consist of a long alkyl chain which would aid in the lipophilicity of the system. Secondly, it would hopefully help to increase the swelling by being more flexible and larger than the DVB previously used, and lastly, it would potentially show more efficient crosslinking due to the two labile, evenly reactive methacrylate functionalities. This new crosslinker would then be tested for its ability to gelate a 50 % styrene, 50 % myrcene copolymer. The reactions would be monitored by GPC and NMR and compared to an equivalent system with DVB. PHIPEs were then to be produced with varying concentration of myrcene with the new crosslinker at 1 % crosslinking density and 95 % internal phase, in line with the work in chapter 4. DSC would be carried out to get an idea of the glass transition of the myrcene containing polymers, and their ability to swell various solvents including the CWA simulant was tested.

6.2 Experimental

6.2.1 Materials and equipment

Nuclear magnetic resonance data was obtained on a Bruker Avance spectrometer with a proton frequency of 400 MHz. All NMR samples were prepared in chloroform-d (d-99.8 atom%, CIL) and collected at room temperature (22 °C).

Gel permeation chromatography was carried out on an Agilent PL-Gel GPC 50 system running tetrahydrofuran as the eluent at a rate of 1 ml min^{-1}. The separation media consisted of two Agilent 300mm 5 µm 'Mixed C' columns in series in a 40 °C oven. Molecular weight parameters were estimated against a poly (methyl methacrylate) standard calibration. The response was measured with a refractive index detector.

Differential scanning calorimetry (DSC) data was gathered on a Netzshe DSC 200 PC instrument. The scan temperature was run from -60 °C to 130 °C, with a 10 °C/min heat/cool rate. Cooling was achieved with liquid nitrogen. Each polymer experienced 3 cycles.

6.2.2 Synthesis of 1,10-decanedimethacrylate

The synthesis of the dimethacrylate crosslinker was based upon an acid catalysed esterification proposed by Mateo *et al*.[23]

Into a single necked 150 ml round bottom was placed *p*-toluensulfonic acid (0.25 g, 1.4 mmol), 1,10-decanediol (22 g, 125 mmol) and dry toluene (50 ml). The reaction was stirred and methacrylic acid (30 ml, 350 mmol, 250 ppm MEHQ) was added to the mixture. A dean-stark apparatus was added to the single neck of the round bottom and the graduations were prepared with extra toluene. The reaction was heated to strong reflux and left until 4 ml of water was collected (around 3 hours). The reaction was then removed from the heat and the solvent was removed by rotary evaporation to leave off-white oil with quite a large volume of waxy sludge. The mixture of crude product was eluted through a flash column packed with silica using a 1:1 mixture of hexane: diethyl ether. The product fraction was then washed with

2 x 50 ml of 0.1 M NaOH, 2 x 50 ml of $NaHCO_3$ and finally 2 x 50 ml deionized water. The organic layer was dried with sodium sulfate, filtered and reduced under vacuum to leave the product; a colourless oil (20.4 g, 52 %). For storage, 50 ppm t-butyl catechol was added to the oil. ^{1}H NMR (Figure 6.3) (400 MHz, $CDCl_3$, room temperature) found ppm δ: = *1.23* [m, **12H** $(CH_2=CCH_3)OOCH_2CH_2$**$(CH_2)_6$**$CH_2CH_2OO(CH_3C=CH_2)$], 1.*60* [q, **4H** $(CH_2=CCH_3)OOCH_2$**CH_2** $(CH_2)_6$**CH_2**$CH_2OO(CH_3C=CH_2)$, J = 7.06 Hz], *1.90* [s, **6H** $(CH_2=C$**CH_3**$)OOCH_2CH_2$ $(CH_2)_6CH_2CH_2OO($**CH_3**$C=CH_2)$], *4.09* [t, **4H** $(CH_2=CCH_3)OO$**CH_2**CH_2 $(CH_2)_6CH_2$**CH_2**$OO(CH_3C=CH_2)$, J = 6.82 Hz], *5.45 + 6.05* [s, **4H** (**CH_2**$=CCH_3)OOCH_2CH_2$ $(CH_2)_6CH_2CH_2OO(CH_3C=$**$CH_2$**$)$]. ^{13}C NMR (Figure 6.4) (CDCl3, room temperature) found δ: = 18.4, 25.9, 28.7, 29.1, 64.7, 125.2, 136.4, and 167.7.

6.2.3 Procedure for the sampling of the myrcene containing gels

The three non-HIPE polymer gels which were monitored with GPC and NMR were synthesised as follows.

Styrene (3.000 g, 28.5 mmol), myrcene (3.92 g, 28.5 mmol), AIBN (0.047 g, 0.29 mmol) and the selected crosslinker DVB (0.074 g, 0.55 mmol), DDMA (0.212 g, 0.56 mmol), or no crosslinker, were all added to a glass vial. The vial was sealed with a rubber septum and degassed with nitrogen for 15 minutes. The samples were then all put into an oil bath at 65 °C where they remained for the experiment. Samples were taken of each sample at 2.5 hrs, 4.5 hrs, 21.5 hrs, 28.5 hrs, 45.5 hrs, 69.5 hrs and 93.5 hrs by drawing a small amount (around 5 drops) out of the vessel with a needle. For GPC, these samples were diluted up to 1 ml with tetrahydrofuran. For NMR samples, a similar volume of sample was added to a vial and diluted with around 1 ml of deuterated chloroform. Yields of the non-crosslinked polymer were gathered by precipitation of a small known amount of the reaction mix into cold ethanol and subsequent drying and collection of the polymer. Additional samples at T = 0 hrs were taken for NMR to observe the

spectra of the starting mixture. All the samples were stored immediately at -10 °C until they were ready to be run on the equipment.

6.2.4 Synthesis of myrcene containing pHIPEs

A table showing the quantities for all of the pHIPEs synthesised is shown in Table 6.1 below the general synthetic procedure. All 1 % crosslinked polymers contained 0.147 g of the DDMA crosslinker, and all 5 % crosslinked polymers contained 0.737 g of DDMA. The general procedure for the synthesis of the pHIPEs is as follows.

Styrene, crosslinker, myrcene, AIBN (0.0075g), and span-80 (sorbitan monooleate) were added into a 200 ml conical flask. The flask was stirred at 250 rpm with a 4 cm hemispherical PTFE overhead stirrer paddle for 10 minutes to homogenise the oil phase. A solution of potassium sulfate (0.25 g) in deionized water was then prepared. The stirring speed of the organic mixture was increased to 750 rpm and the aqueous solution was dropped in at rate of around 1 drop per second until all was incorporated in the emulsion. After all the aqueous phase was added, the stirring speed was increased further to 900 rpm and left to homogenise for 10 minutes. The HIPE foams all mixed well under these conditions. The HIPE was placed into a plastic cylinder, sealed and cured in an oven at 65 °C for 24 hours. After curing, the pHIPE monolith was cooled and removed from the cylinder and cut into quarters along the length. It was then dried under vacuum at 45 °C for 48 hours minimum. Complete dryness was determined by observation of the point at which mass reduction ceased.

Table 6.1 - The quantities of each reagent required for all of the myrcene pHIPE syntheses.

Sample	Styrene (g)	Myrcene (g)	Water (ml)	Surfactant (g)
$St_{100}IP_{95}$	3.952	0	78	0.82
$St_{90}Myr_{10}IP_{95}$	3.557	0.517	80	0.86
$St_{80}Myr_{20}IP_{95}$	3.162	1.034	82	0.87
$St_{70}Myr_{30}IP_{95}$	2.766	1.551	84	0.89
$St_{60}Myr_{40}IP_{95}$	2.371	2.068	87	0.91
$St_{50}Myr_{50}IP_{95}$	1.976	2.585	89	0.94

6.2.5 Procedure for washing $St_{50}Myr_{50}IP_{95}$ with ethanol

The $St_{50}Myr_{50}IP_{95}$ sample was washed with ethanol in an attempt to exchange the water in the pores for the ethanol. The freshly cured pHIPE was sliced along the cross section to produce disks of monolith with a diameter of around 4 cm and a height of 1 cm. These were then cut into quarters. The polymer was dropped into a breaker of slowly stirred ethanol at room temperature overnight. The volume of ethanol used was 10 x the mass of the polymer. After washing, the polymer was removed and dried as gently as possible by placing in the vacuum oven at 150 mbar and 45 °C for 24 hours. The dry polymer appeared to have shrunk during drying to a thinner form, around a tenth of their original height.

6.3 Results and discussion

6.3.1 Analysis of the DDMA crosslinker

The reactivity ratios of methyl methacrylate (MMA) and myrcene are known as $R_1 = 0.44$ (myrcene) and $R_2 = 0.27$ (MMA) ($R_1R_2 = 0.12$),[15] which suggests a methacrylate based crosslinker should incorporate well into the polymerisation. Whilst the common crosslinker; ethylene glycol dimethacrylate (EDGMA), would likely have been more than suitable in a non-HIPE system; the relatively high hydrophilicity of the EGDMA comparison to the DVB may have been disadvantageous in the preparation of HIPE foams.

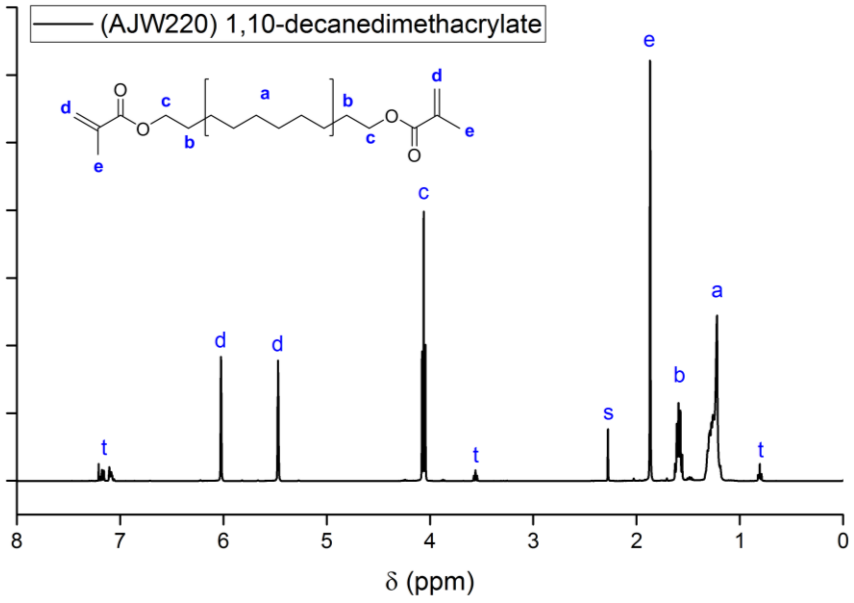

Figure 6.3 - Showing the ^{1}H NMR in chloroform for the synthesised crosslinker 1,10-decanedimethacrylate. Peaks marked as 't' refer to the *t*-butyl catechol inhibitor, and the peak marked 's' is due to the presence of 0.2 eq. toluene remaining from the synthesis.

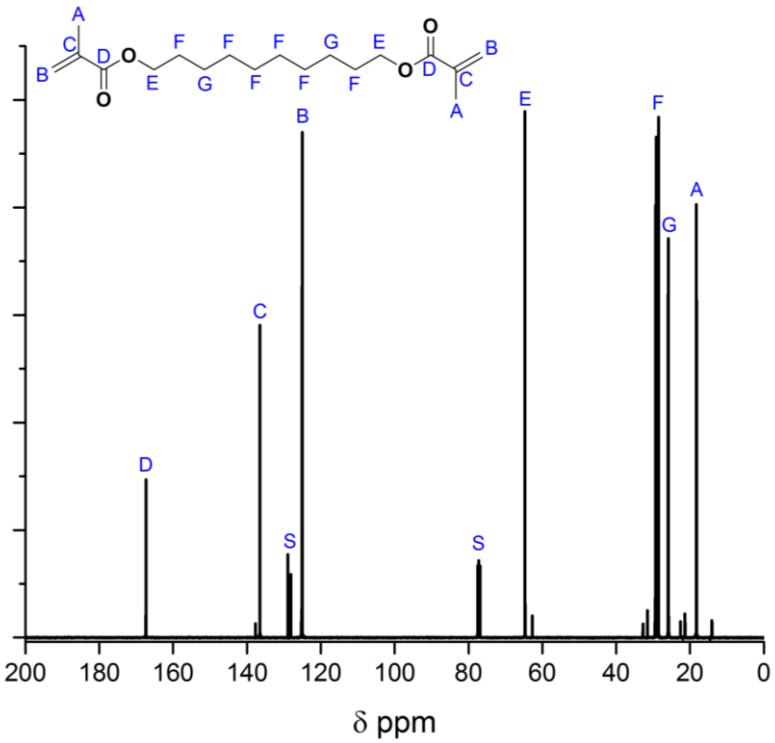

Figure 6.4 - Showing the ^{13}C NMR in chloroform for the synthesised crosslinker 1,10-decanedimethacrylate. Peaks marked 's' are due to the presence of 0.2 eq. toluene remaining from the synthesis and the small impurities are the *t*-butyl catechol inhibitor.

6.3.2 Formation of myrcene containing gels with DVB crosslinking

A gel of 50 % myrcene and 50 % styrene was synthesised with 1 % DVB crosslinking. An initial reaction time of 65 °C for 24 hours was carried out. This reaction did not lead to the formation of a gel, only a viscous liquid. The same reaction was carried out for 4 days where a gel appeared to form. To understand the polymerisation of this system, the same reaction was then monitored with GPC and NMR.

6.3.2.1 GPC monitoring

The GPC data (Figure 6.5) for the polymerisation showed little variation in M_w in the first three data points. At 28.5 hours the M_w increased non-linearly from 71200 (Đ 2.53) to M_w 130100 (Đ 3.53) at 45.5 hours. At 69.5 hours the GPC showed bimodal distribution, where one peak represented M_w 552500 (Đ 1.56) at and the slower eluting fraction representing a value for M_w of 46300 (Đ 2.12). This smaller fraction likely represented a degree of dead polymer chains which were not incorporated into the gel fraction. A sample could not be obtained at 93.5 hours due to the sample being gelated fully. From the GPC results gelling was indicated around 69.5 hours which explained why the initial reaction was a viscous liquid at 24 hours, and a gel at 4 days.

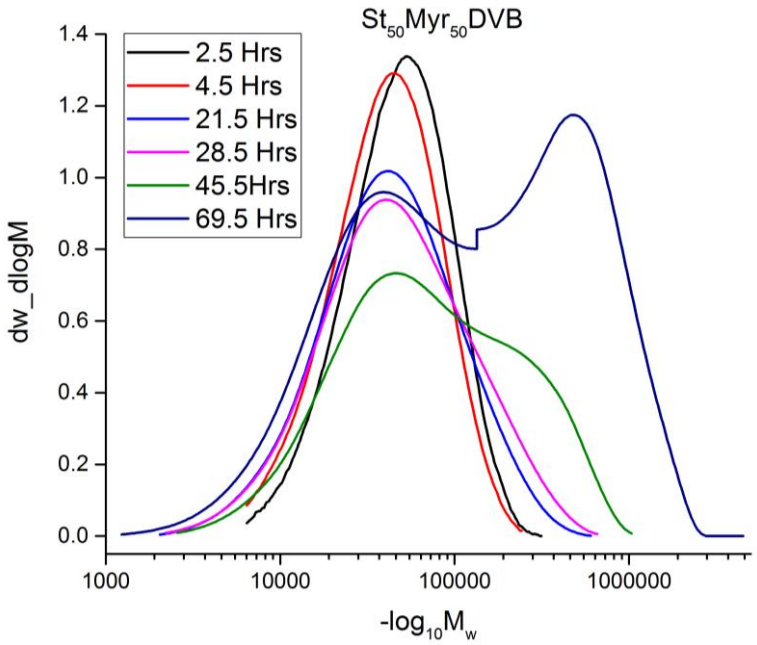

Figure 6.5 - The GPC chromatographs for the 1 % DVB crosslinked polymerisation of 50 % myrcene and 50 % styrene at 65 °C. Data could not be gathered after 69.5 hours due to gelation.

6.3.2.2 NMR Monitoring

An NMR spectrum of the reaction mix before heating was run and the spectrum is presented alongside the 69.5 hour spectrum in Figure 6.6. The spectrum showed clear peaks for both the myrcene and styrene. The peaks associated with the DVB were indistinguishable from those of the styrene in all areas apart from the peak marked 'I' which was offset from 'y' by 0.03 ppm. This made monitoring the crosslinking problematic. The polymerisation of myrcene occurs in vast majority through the 1,4 route.[24] Peaks associated with the myrcene polymerising in this manner were confirmed through comparison with literature spectra.[25] The stereo regularity of the majority 1,4-polymerisation was not confirmed as this required analysis outside the scope of this project.[26] An impurity was observed at 4.6 ppm which did not vary in relative intensity throughout the reaction.

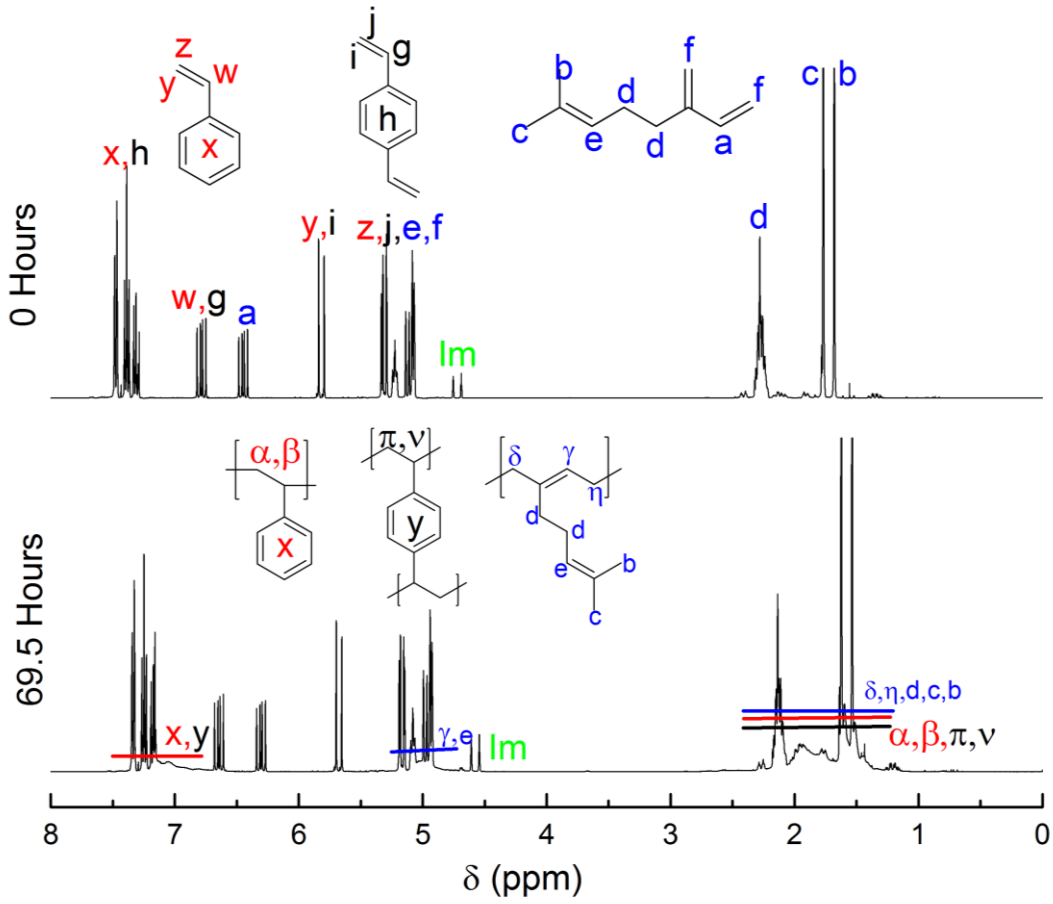

Figure 6.6 - The ^{1}H NMR spectra for (top) the 0 hour sample of the DVB crosslinked reaction and (bottom) the 69.5 hour polymerisation reaction mix.

The conversions were determined from integration and are presented in Table 6.2. The conversion of the styrene to polymer was calculated;

$$\%\ Conversion_{Styrene} = \left(\frac{Int_x - (5\ x\ Int_w)}{Int_x}\right) x\ 100$$

(Equation 6.1)

Where Int_x represented the total peak area between 6.9 ppm and 7.6 ppm, and Int_w was the area of the single proton peak 'w'. The myrcene content was calculated;

$$\%\ Conversion_{Myrcene} = \left(\frac{\left(\frac{Int_d - (10\ x\ Int_a) - \alpha}{1.4}\right)}{(Int_d - \alpha)}\right) x\ 100$$

(Equation 6.2)

Where Int_d was the total peak area between 1.4 ppm and 2.5 ppm, Int_a was the integral for the monomer peak marked 'a' and α was the relative integral value of the range 1.4 ppm to 2.5 ppm which was due to the polystyrene, calculated from Equation 6.1. The vinyl groups of the DVB (peak i) were recorded relative to the styrene as this was the only distinct region for the crosslinker.

Table 6.2- The integral values for each NMR spectra in the DVB crosslinked 50 % myrcene, 50 % styrene copolymerisation. The calculated conversions and percentage of DVB vinyl protons relative to the styrene in the mixture are shown.

Reaction Time (hours)	Int_w	Int_x	Int_a	Int_d	Styrene Conv. (%)	Myrcene Conv. (%)	Avg. Conv. (%)	DVB monomer (%)
2.5	1	5.146	0.912	10.781	3	11	7	1.7
4.5	1	5.265	0.904	11.019	5	12	9	1.9
21.5	1	5.549	0.852	13.068	10	24	17	1.8
28.5	1	5.654	0.848	13.627	12	26	19	1.5
45.5	1	5.847	0.817	14.797	14	31	23	1.5
69.5	1	6.659	0.921	20.616	25	38	31	1.7

The NMR data showed that throughout the reaction, there was higher conversion to polymer in the myrcene, than the styrene. The average conversions were also low, at no more than 50 % throughout. The quantity of DVB, calculated from the protons marked 'I' against the quantity of styrene did not vary significantly. The low conversions in NMR and slow time to reach gelation in GPC were an initial concern.

6.3.3 Monitoring the co-polymerisation of non-crosslinked myrcene and styrene

Further monitoring was carried out on the system without any crosslinking. This was to try to observe the process of the polymerisation of the two monomers in better detail. The physical yields were also determined to contrast the NMR conversion values.

6.3.3.1 GPC monitoring

The polymerisation was monitored with GPC and showed a linear increase in M_w parameter from M_w 58100 at 2.5 hours to M_w 79100 at 93.5 hours. The dispersity (Đ) also increased from 1.34 to 3.24 across the same time period.

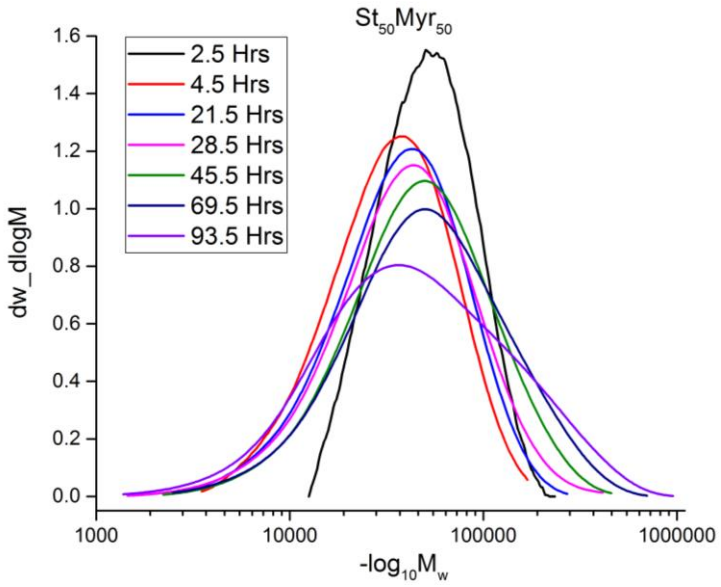

Figure 6.7- The GPC chromatographs for the non-crosslinked polymerisation of myrcene and styrene at 65 °C.

6.3.3.2 NMR monitoring

The starting and 93.5 hour proton NMR spectra for the non-crosslinked reaction are presented in Figure 6.8. The spectra were annotated with the peaks from the monomer and polymer.

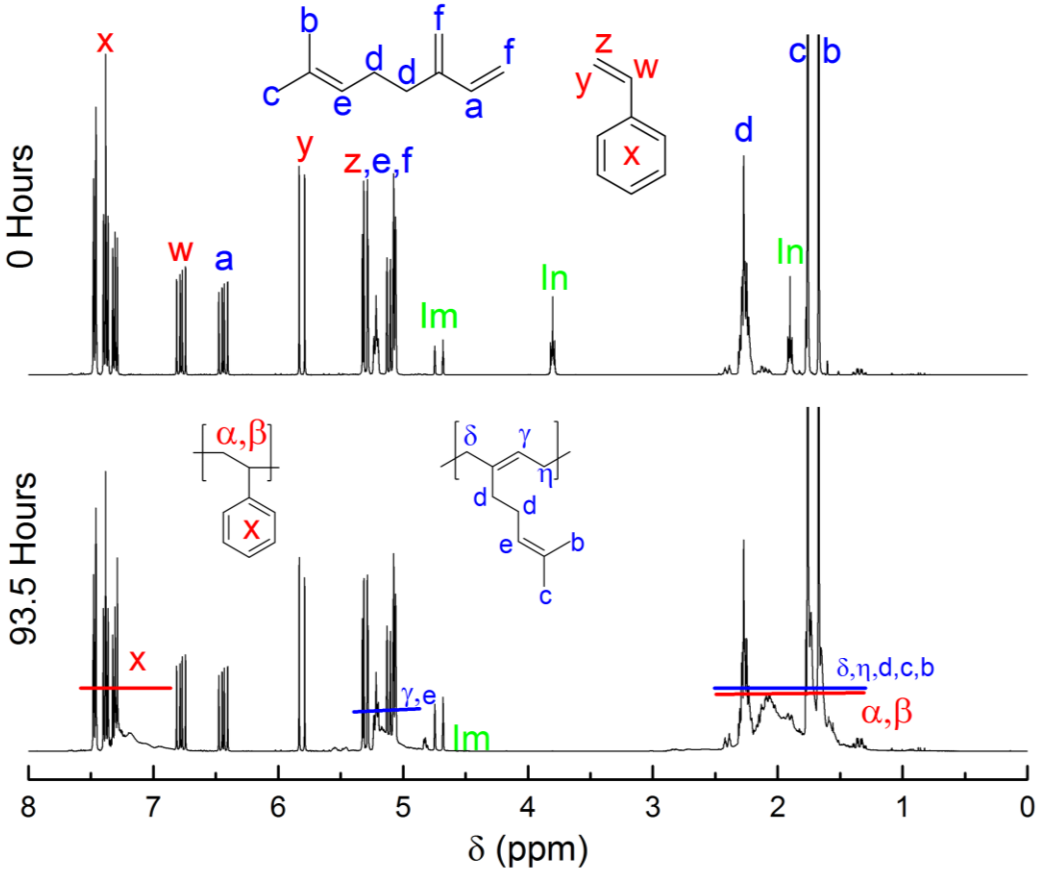

Figure 6.8 – The ^{1}H NMR spectra of the reaction mix for the 0 hour sample (top) and 93.5 hour sample (bottom) of the non-crosslinked 50 % myrcene, 50 % styrene copolymerisation. Letters in green represent an impurity (Im), and the initiator (In) AIBN.

The reaction was monitored by NMR at each data point and the conversions of each monomer in the reaction were calculated and are presented alongside the physical yield of polymer obtained in Table 6.3. The conversion of styrene to polystyrene and myrcene was calculated in the same manner as of that in 6.3.2.

Table 6.3- The yields of the non-crosslinked myrcene / styrene reaction for each time point, contrasted against the conversion calculated from NMR, and associated integral data.

Reaction Time (hours)	Physical Yield (%)	Int_w	Int_x	Int_a	Int_d	Conv. Styrene (%)	Conv. Myrcene (%)	Avg. Conv. (%)
2.5	**No solid**	1	5.142	0.947	10.341	3	5	4
4.5	**4**	1	5.163	0.94	10.546	3	7	5
21.5	**39**	1	5.462	0.895	12.421	8	19	14
28.5	**42**	1	5.642	0.886	12.961	11	21	16
45.5	**47**	1	5.867	0.883	14.84	15	27	21
69.5	**53**	1	6.155	0.873	16.852	19	33	26
93.5	**58**	1	7.728	0.889	27.978	35	47	41

It was clear that the styrene was not being converted to polymer at the same rate as the myrcene, and that the overall yields were low. The conversion by NMR showed generally a lower value than the physical yield which was obtained. These results demonstrated that regardless of crosslinking, the yields would be low.

6.3.4 Formation of myrcene containing gels with DDMA crosslinking

The new crosslinker DDMA was tested in the same way as the DVB and non-crosslinked polymerisations. This was primarily to see if the gelation was evident at an earlier stage in the reaction through GPC. The DDMA crosslinker was not expected to affect the total conversion to polymer.

6.3.4.1 GPC monitoring

The data obtained from the GPC analysis (Figure 6.9) indicated gelation had occurred in the polymer very early on. After 2.5 hours a M_w of 65600 (Đ 1.33) was observed, rising to 129000 (Đ 3.70) at 21.5 hours. At this point, the sample was already very viscous, and by 28.5 hours the sample had gelated to a point where it was difficult to obtain a sample. The results at 28.5 hours M_w 121500 (Đ 3.85) were taken from the supernatant around a sample of the gel.

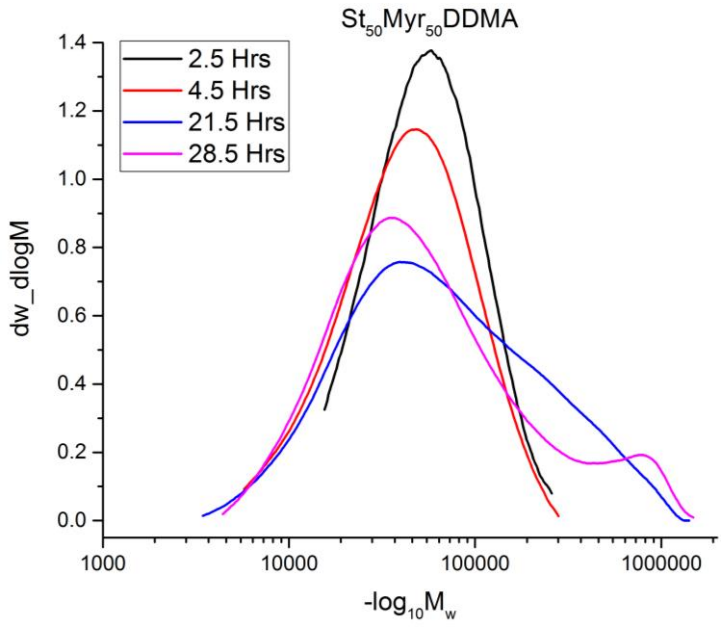

Figure 6.9 - The GPC chromatographs for the 1 % DDMA crosslinked polymerisation of 50 % myrcene and 50 % styrene at 65 °C. Gelation occurred very quickly in this reaction which explains the lack of data past 28.5 hours.

6.3.4.2 NMR monitoring

As with the previous two reactions: the starting spectrum for the NMR was analysed (Figure 6.10). The DDMA monomer in the 0 hour reaction mix was able to be differentiated from the styrene and the myrcene. The vinyl group of the DDMA marked as 'h' at 5.6 ppm and 6.2 ppm representing 2 protons was present. Part of the alkyl region of the crosslinker was also clearly separate on the spectra at 4.25 ppm, marked 'j' representing 4 protons. There were no differntiable polymer peaks howver.

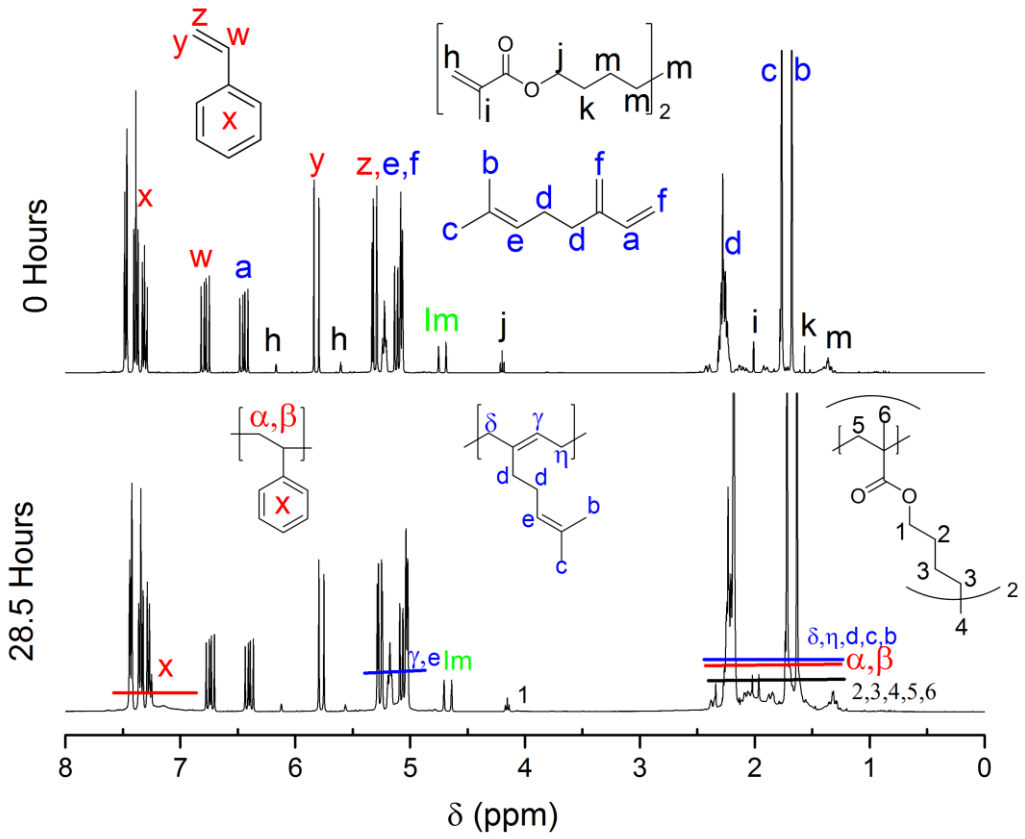

Figure 6.10 - The ^{1}H NMR spectra for the 0 hour and 28.5 hour samples of the DDMA crosslinked reaction.

The conversions were calculated the same as in both sections 6.3.2 and 6.3.3. The quantity of DDMA monomer relative to the styrene was also calculated (Table 6.4). The DDMA appeared to slowly reduce in relative abundance compared to the styrene. This suggested the DDMA was being incorporated into the polymer at a slightly faster rate than the styrene.

Table 6.4 - The integral values for each ^{1}H NMR spectra in the DDMA crosslinked 50 % myrcene, 50 % styrene copolymerisation. The calculated conversions and percentage of DDMA relative to the styrene in the mixture are shown.

Reaction Time (hours)	Int_w	Int_x	Int_a	Int_d	Conv. Styrene (%)	Conv. Myrcene (%)	Avg. Conv. (%)	DDMA (%)
2.5	1	5.21	0.947	11.185	4	10	7	2.5
4.5	1	5.247	0.938	11.465	5	12	8	2.4
21.5	1	5.826	0.935	15.336	14	26	20	2.3
28.5	1	6.013	0.939	28.208	17	47	32	2.1

Again, conversion was low, with styrene showing a smaller fraction of the total converted monomer.

6.3.5 Comparison of the GPC data for the polymer gel syntheses

The GPC data for all three polymerisations were collated and the M_w against time for each is presented in Figure 6.11. The non-crosslinked polymerisation showed a mostly linear increase in M_w which suggested that the sudden increases seen in the crosslinked reactions were due to gelation effects. The plot demonstrated how the DVB crosslinked reaction began to show features of gelation at around 45 hours, and the DDMA, around 21 hours. This indicated that the DDMA was a more effective crosslinker than the DVB in this system, with respect to the rate of gelation. The plot of Đ against time also showed a faster increase in dispersity in the DDMA crosslinked polymer compared to the DVB.

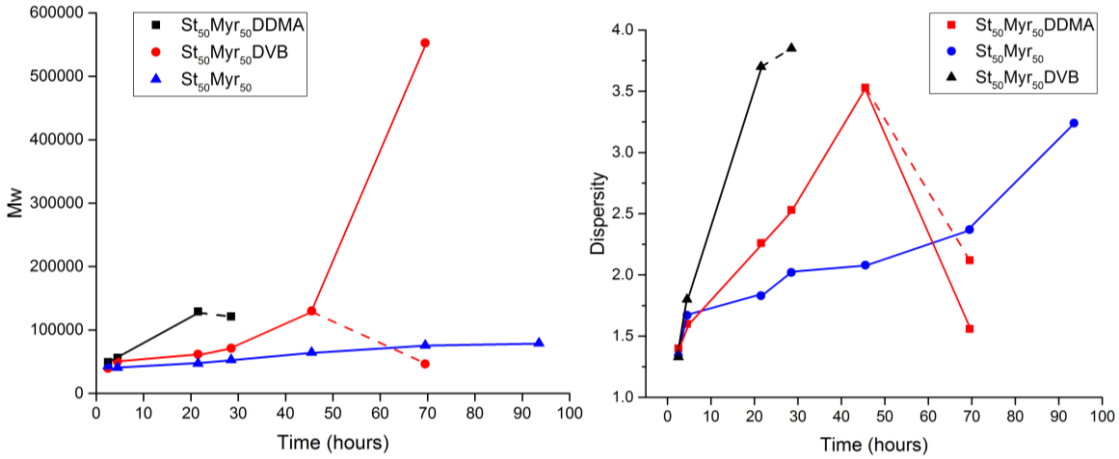

Figure 6.11 – (Left) a plot showing the M_w of each of the three reactions against the reaction time. (Right) a plot showing the *Đ* of each of the three reactions against the reaction time. The data for the DDMA reaction is cut short due to gelation occurring. The dashed line in black represents the supernatant of the gelated sample at 28.5 hours. The dashed line in red represents the second peak in the 69.5 hour sample of DVB (bimodal).

6.3.6 Vial inversion tests of the polymerisations

Photographic observations of the reaction vials having been inverted (Figure 6.12), showed that the gelation with the DVB became obvious only after 45.5 hours, and significant after the 69.5 hour sample. The gel point therefore must have fallen somewhere in the 7 hours between the last two data points. The apparent gel point of the DDMA system, both from GPC and visually, fell at least 24 hours before that of the DVB in this system. The vial inversion tests through the reaction agreed with the GPC results in that the DDMA was a faster acting crosslinking agent. Determination of gel-point through rheological techniques would have been appropriate to support these findings.

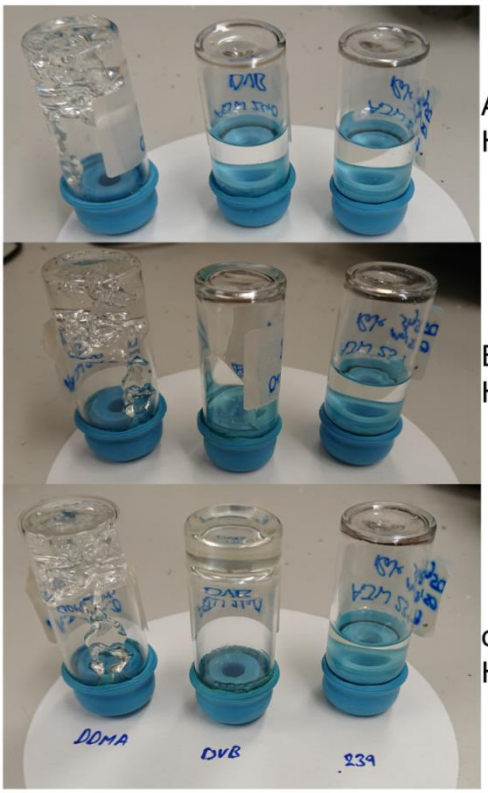

Figure 6.12 – Vial inversion tests to demonstrate the gelation of the three sampling runs. At 28.5 hours the DDMA reaction had gelated (polymer broken up in an attempt to take a sample). At 45.5 hours the DVB reaction had begun to gelate but would still flow down the vial slowly. At 69.5 hours both crosslinked reactions were gelated and the control remained a viscous liquid.

When a gel of 50 % myrcene and 50 % styrene with the DVB crosslinker was swollen in DCM, it was seen to dissolve slowly over two days. This did not occur with the DDMA crosslinked sample and it remained swollen and intact.

6.3.7 Conclusions regarding the myrcene/styrene copolymerisation monitoring

The GPC showed the DDMA caused a faster increase in molecular mass of the system, compared to the DVB. When correlated to vial inversion tests, this supported the theory that the DDMA was a faster crosslinker than the DVB. The biggest concerns from the NMR data were that there appeared to be only low amounts of conversion to polymer in the non-crosslinked run. The measured conversion and physical yields of this reaction at 93.5 hours

only reached 52 % and 58 % respectively. The physical yields of the final gels were calculated. The DDMA and DVB crosslinked gels after 4 days of reaction time were placed under strong vacuum at 75 °C. After two days the resulting yields of polymer were 84 % and 81 % respectively. These values did not correlate to the maximum conversions observed in the NMR of 40 % (DVB, 69.5 hours) and 42 % (DDMA, 28.5 hours).

6.3.8 Myrcene containing pHIPEs

6.3.8.1 Synthesis results

Despite the low polymer yields seen in 6.3.7, the attempted synthesis of the pHIPEs was carried out. The mixing of the myrcene containing HIPEs progressed well. The pHIPEs were synthesised to include 10 %, 20 %, 30 %, 40 %, and 50 % myrcene, and a control with 100 % styrene. All proceeded to retain the emulsion foam during heating and appeared visually to have the characteristics of a pHIPE in their freshly cured state (Figure 6.13). Each monolith was solid, with an increased flexibility observed as the myrcene content increased, which was expected from including myrcene. The 100 % styrene sample was not pictured but formed as expected.

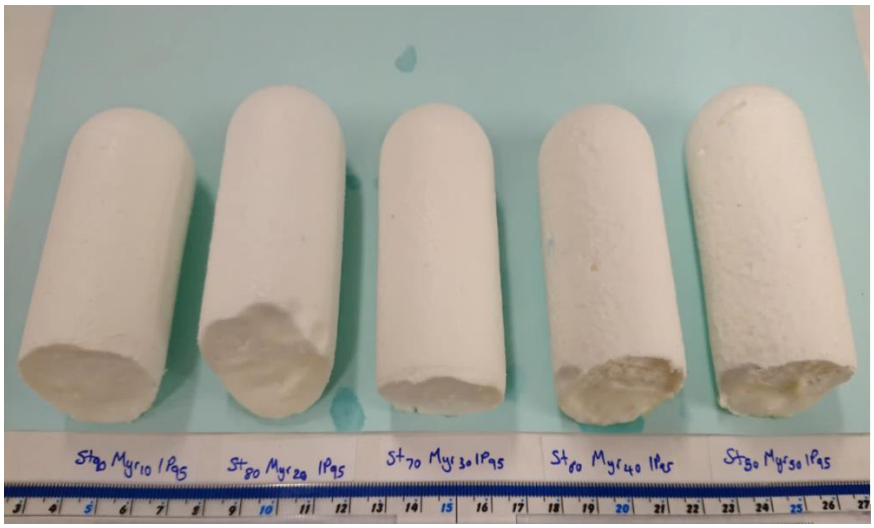

Figure 6.13 – A picture of the 5 myrcene containing pHIPEs ($St_{90}Myr_{10}1XL$, $St_{80}Myr_{20}1XL$, $St_{70}Myr_{30}1XL$, $St_{60}Myr_{40}1XL$, and $St_{50}Myr_{50}1XL$) immediately after being removed from the curing tubes.

6.3.8.2 Morphology loss during drying of the myrcene pHIPEs

On drying, the monoliths appeared to lose their morphology during removal of the internal phase. This was more pronounced with increasing myrcene content. This was seen both visually as shown in Figure 6.14. SEM was also carried out on all samples as shown in Figure 6.15. SEM analysis showed that the 50 % myrcene pHIPE after drying in vacuum at 45 °C had shrunk into a form which resembled a bulk polymer, with no distinct morphology. This was also true of the 30 % and 40 % samples which appeared as if they were a block of plastic under the microscope. The 10 % sample exhibited pores and windows which were uniform and in line with a pHIPE. The 20 % sample did not have distinct pores and windows, but the internal structure still appeared to have high surface area, as if the pores had collapsed. Increasing the myrcene content would be expected to reduce the glass transition temperature of the polymers significantly.[27,28] In doing so, the drying process could cause the polymers with sub room temperature T_g values (elastomers) to collapse in the observed fashion, losing their morphology. DSC analysis was undertaken and is further discussed in section 6.3.9.

Figure 6.14 - A picture of the 5 myrcene containing pHIPEs ($St_{90}Myr_{10}1XL$, $St_{80}Myr_{20}1XL$, $St_{70}Myr_{30}1XL$, $St_{60}Myr_{40}1XL$, and $St_{50}Myr_{50}1XL$) immediately after being removed from the vacuum oven after drying at 45 °C.

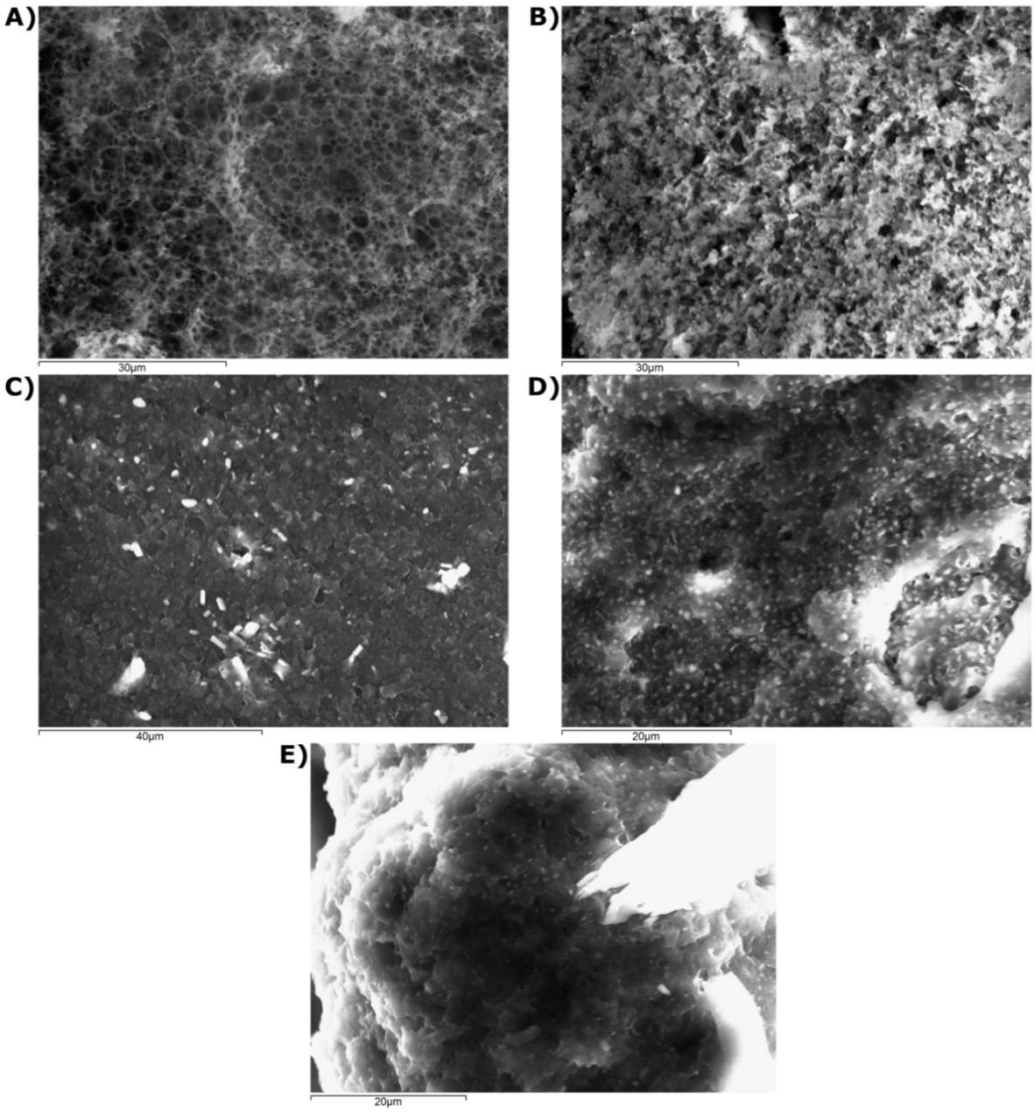

Figure 6.15 - Scanning electron micrographs of all the myrcene containing pHIPEs (A = $St_{90}Myr_{10}1XL$, B = $St_{80}Myr_{20}1XL$, C = $St_{70}Myr_{30}1XL$, D = $St_{60}Myr_{40}1XL$, and E = $St_{50}Myr_{50}1XL$) after drying in the vacuum oven at 45 °C.

6.3.8.3 Swelling of the collapsed pHIPEs

The SEM images suggested there was no interconnected porosity present in the collapsed samples (20 %, 30 %, 40 % and 50 % myrcene). To investigate whether the monoliths presented an increased swelling capacity as was expected from forming a pHIPE, swelling was carried out in methyl benzoate (Figure 6.16).

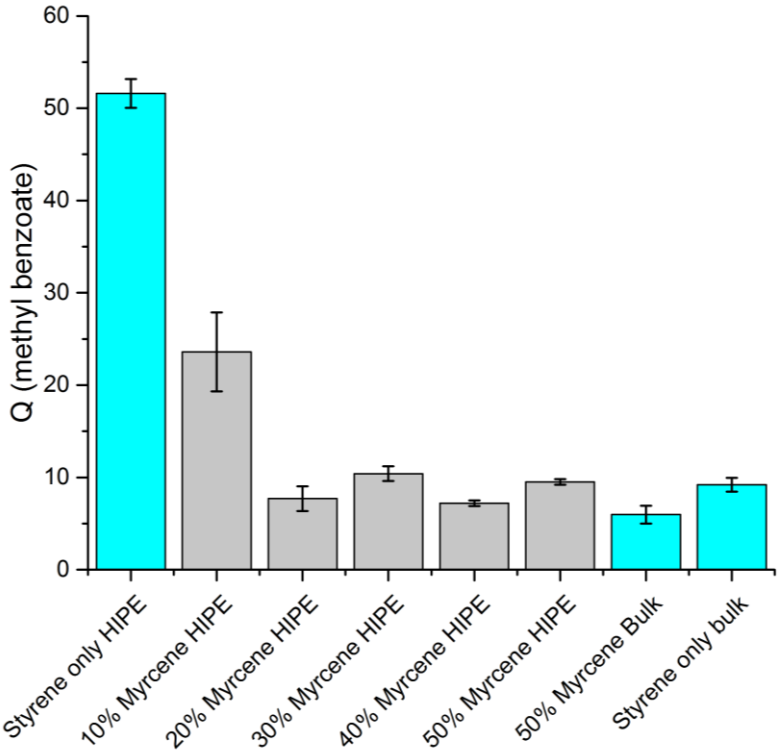

Figure 6.16 – The swelling performance of the myrcene containing pHIPEs with 1 % DDMA crosslinking (grey) against the swelling of three controls; styrene only pHIPE, styrene only polymer gel, and a 50 % myrcene polymer gel, each with 1 % DDMA crosslinking.

The results of the swelling suggested that the porous morphology had been lost completely. None of the samples swelled significantly higher than that of either of the bulk control samples, save for the styrene only, and 10 % myrcene content pHIPEs (Q = 51 and 23). The 10 % myrcene polymer was the only sample which retained some morphology by examination of the SEM. Despite the low swelling, the 10 % myrcene content did show that the HIPE was forming at some stage. The 0 % myrcene control showed that the crosslinker was not the cause of the problem, as this swelled to a level in line with the DVB samples of chapter 4.

6.3.8.4 Synthesis and drying of 5 % crosslinked myrcene containing pHIPEs

It was proposed that morphology losses could have been occurring due to the low levels of crosslinking present in these non-glassy systems (confirmed in 6.3.9); i.e. during the relatively harsh drying conditions, the crosslinks were not sufficient to retain the morphology of the polymer once the internal phase support was removed and the rubbery polymers would

collapse. A set of polymers were synthesised in an identical manner, except with a much higher level of crosslinking of 5 % (DDMA). This would demonstrate if higher crosslinking density could prevent the loss of porosity. The monoliths were slightly better in appearance than the 1 % crosslinked. The same loss of feature and morphology as before was however seen with 20 % myrcene onwards (Figure 6.17).

Figure 6.17 - Showing the 5 myrcene containing pHIPEs (left to right: $St_{90}Myr_{10}5XL$, $St_{80}Myr_{20}5XL$, $St_{70}Myr_{30}5XL$, $St_{60}Myr_{40}5XL$, and $St_{50}Myr_{50}5XL$) immediately after being removed from the vacuum oven after drying at 45 °C.

6.3.8.5 Resulting mass of the collapsed pHIPEs

When the yield of the polymers was calculated, they were seen to be dramatically low in all samples which contained myrcene (Figure 6.18). The only polymer with an acceptable yield was the styrene only sample (80 %). The polymers were seen to have a decreasing yield as the myrcene content increased with a large initial decrease seen at the first 10 % myrcene. Low yields were observed in the polymerisation trials with the 50 % myrcene so these results were not surprising. The 5 % crosslinked samples all showed a relatively higher yield. The 50 % myrcene samples in both only achieved 65 % and 36 % respectively.

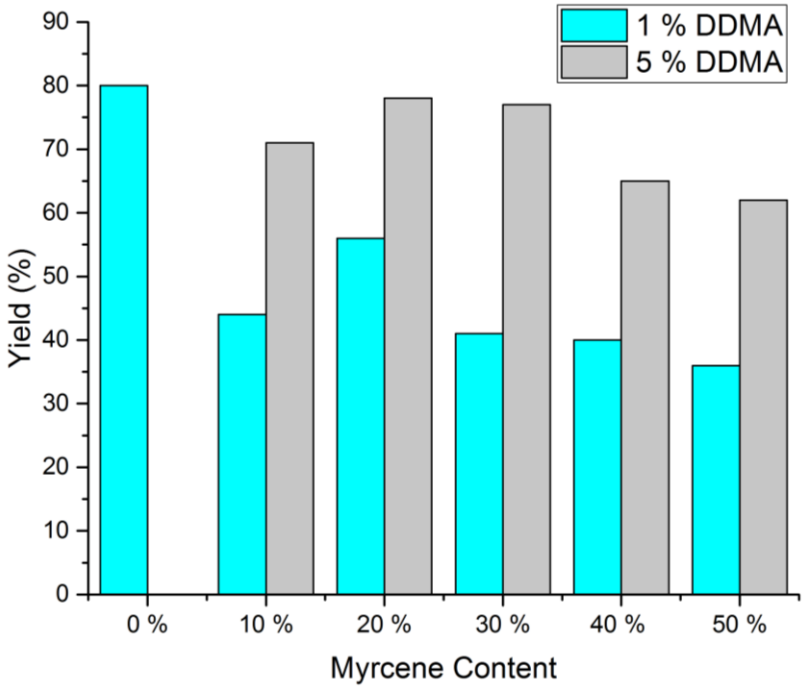

Figure 6.18 – The yields of each of the dry polymers both with 1 % and 5 % crosslinking.

The increased yield in the 5 % crosslinked could have explained why the polymers appeared visually to have a slightly better form. On the information presented it was likely the low polymer yields were a significant factor in the problems with the pHIPEs. Increasing the initiator 4 fold in the 50 % myrcene (1 % crosslinking) sample did not affect yield.

6.3.9 DSC analysis of the myrcene pHIPEs

As both a diagnostic technique for explaining the loss of morphology, but also as a general investigative technique for understanding the properties of this system, DSC was undertaken on the polymers synthesised with 1 % DDMA crosslinking. The T_g was determined for each by fitting a line between the plateaus of the onset and end of the endothermic curve, and finding the temperature value at half the distance between the points (Figure 6.19, Table 6.5).

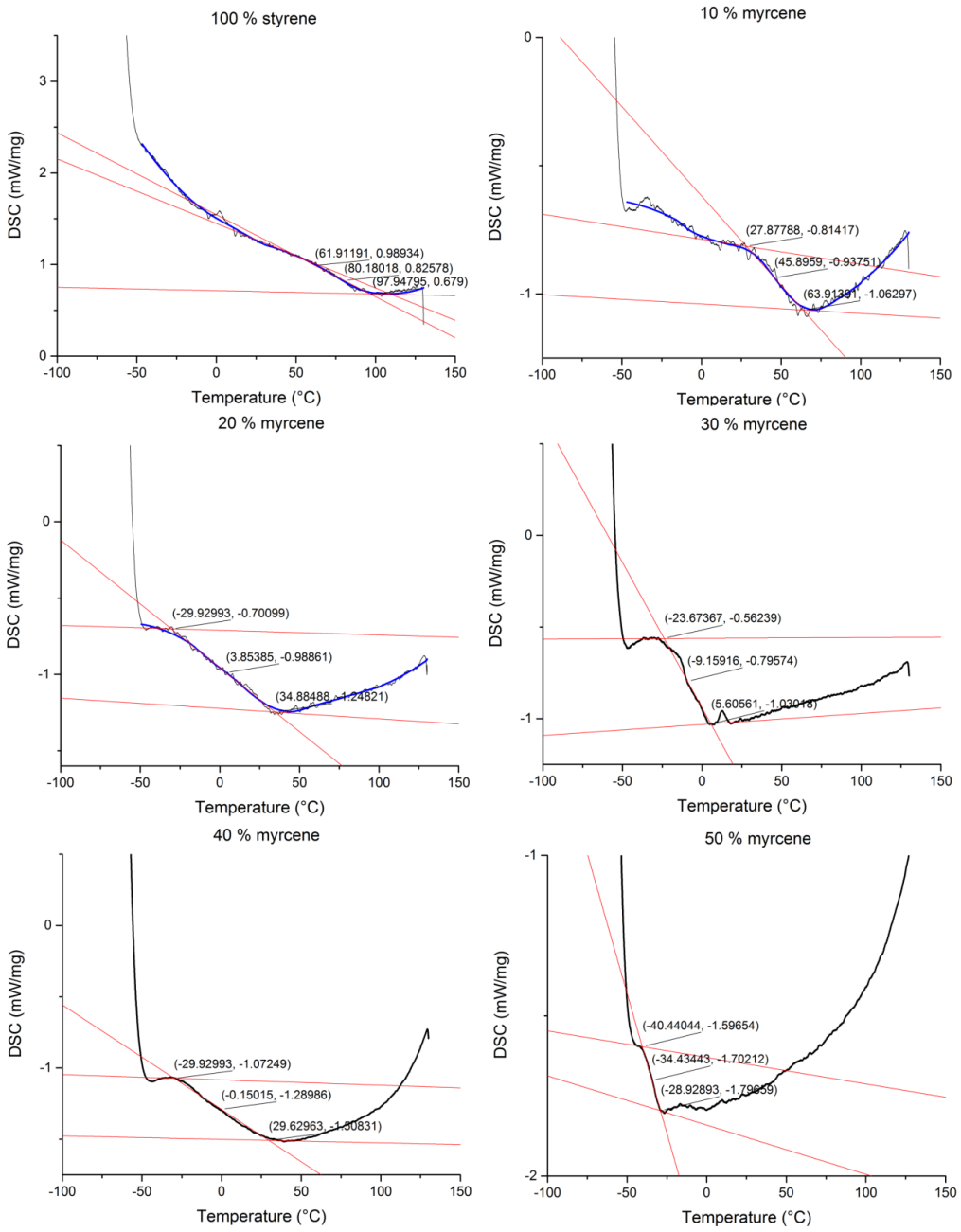

Figure 6.19 – The DSC heating curves (3rd cycle) for each of the 5 myrcene containing polymers and the control. The blue lines on the styrene only, 20 % and 30 % myrcene graphs is a 1000 point smoothed curve to help highlight the endothermic plateaus. The T_g was taken as the midpoint of the chord placed between the onset and offset plateaus.

There was a distinct lack of clear transition for all of the polymers, due to the crosslinking and surfactant present in the networks. The tentative assignments for the T_g showed that the 20 %, 30 %, 40 % and 50 % myrcene pHIPEs all showed sub-room temperature transitions.

Table 6.5 - The T_g from DSC of the 1 % DDMA crosslinked pHIPEs, along with literature values for poly(myrcene) and poly(styrene).

Polymer	T_g
poly(styrene)	c. 105 °C (no crosslinking) – 155 °C (30% DVB crosslinking)[27]
poly(myrcene)	c. -70 °C[28]
$St_{50}Myr_{50}$	-34 °C
$St_{60}Myr_{40}$	0 °C
$St_{70}Myr_{30}$	-9 ° C
$St_{80}Myr_{20}$	5 °C
$St_{90}Myr_{10}$	46 °C
St_{100}	80 °C

6.3.10 Solvent exchange drying of the myrcene pHIPEs

The literature was consulted and found that some research groups freeze dried their elastomeric / low T_g pHIPE systems to avoid the surface tension of the water damaging the pores on removal. These groups have also observed a skin forming on the surface during the drying process which was familiar to this system.[29,30,31]

Due to freeze drying being a very energy intensive process, an alternative approach was trialled first. The 50 % (1 % crosslinking) myrcene polymer was washed with ethanol overnight. This process causes ethanol to replace most of the water in the pores. This would likely also remove the surfactant, similarly to in chapter 4, which would reduce the interfacial tension of the liquid and the walls of the pores. This process was only trialled on the 50 % sample. During the washing the polymer became gradually more buoyant which suggested the exchange was occurring as the lower density ethanol replaced the water in the pores.

The dry polymer was examined with SEM (Figure 6.20) and the micrograph did not show an archetypal pHIPE porous, interconnected morphology as what would have been expected. Instead, they showed a very rough surface texture on the freshly cut surfaces. This suggested the swelling ability may have again become impaired during removal of the ethanol. The lack

of pores visible in SEM may have been due to shrinkage, analogous to the compressed polymer in chapter 4, therefore swelling was carried out.

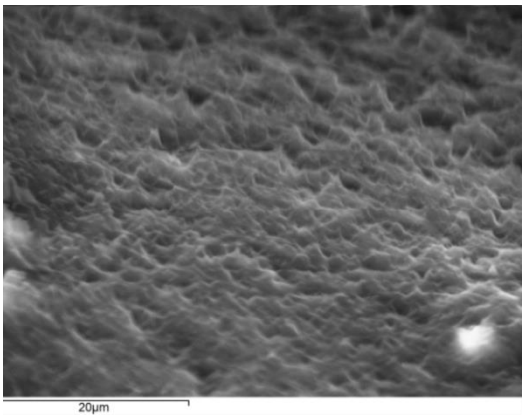

Figure 6.20 – A scanning electron micrograph of the $St_{50}Myr_{50}1XL$ polymer after having been dried following exchange of the internal phase water for ethanol.

6.3.10.1 Ethanol exchanged 50 % myrcene pHIPE swelling

The 50 % myrcene pHIPE sample was swollen in a small range of solvents to test whether exchanging the water for ethanol before drying had improved the properties of the polymer. The 6 solvents are shown in Figure 6.21.

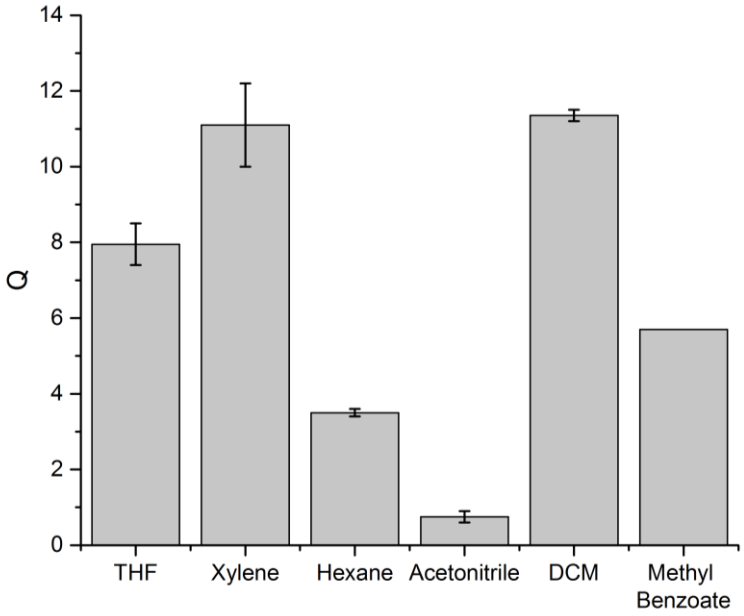

Figure 6.21 – The swelling of the 50 % myrcene pHIPE which was dried following exchange of the water for ethanol and removal of surfactant.

There was no noticeable difference in swelling of methyl benzoate in either the original vacuum dried sample, or the solvent exchanged / solvent removed sample. This suggested that there was no significant porosity being retained. The swelling of the xylene and hexane, although low, were actually improved slightly over the styrene only gels from chapter 2. The previous best swelling for xylene was Q = 8.8, and hexane Q = 0.

6.4 Conclusions and future work

6.4.1 General Conclusions

The new crosslinking agent worked effectively and did not disrupt the formation of the HIPE foams which was a concern for low chain length di-methacrylates. In the styrene only pHIPE with 1 mol% of this new crosslinker, the simulant swelling reaching over Q = 51. The previous equivalent polymers from chapter four which included VBC to increase the swelling reached only slightly higher swelling of Q = 55. It was also shown that the new crosslinker brought forward the apparent gel point by a significant margin over the DVB in a 50 % myrcene polymerisation. This was observed visually, and also inferred from the M_w parameter increases in GPC. It was clear that one of the main issues presented in this work was the low polymer conversions which were observed by NMR and yield, when any amount of myrcene was added into the polymerisation. Low yields of not over 60 % in the resulting pHIPEs, regardless of initiator quantity were observed. The pHIPEs were unable to maintain a porous monolithic form and on drying always collapsed. They appeared through SEM and swelling performance to have no distinct porosity and this was supported by the swelling results in the simulant. The swelling results of the dried 50 % myrcene polymer in xylene and hexane appeared to be promising as the swelling capacity exceeded that of a styrene only bulk system. If more time was allocated to this project and the archetypal pHIPE morphology could be obtained, an effective sorbent for low polarity solvents may be within reach. In chapter 4, the swelling increase from no morphology to a pHIPE was over 3.5 times which could result in hexane swelling easily over Q = 10 and xylene Q = 25 in this system.

6.4.2 Proposals for troubleshooting and future work

6.4.2.1 Yields

It was likely that the problems with losing the porosity began with the yield, or lack thereof. Two contrasting reports give largely different yields for myrcene styrene copolymerisation. The yield of an AIBN initiated myrcene polymerisation was reported to be low and in line with our non-crosslinked test of around 35 %.[32] The same article reported increasing the reaction temperature to 130 °C and utilizing living polymerisation methods such as RAFT allowed the conversions to exceed 65 %, but on equally long time scales. Emulsion polymerisation of myrcene and myrcene-styrene copolymers was seen to reach over 85 % in shorter reaction times of 16 - 28 hours.[33] The low yield could be affecting the resulting monoliths in various ways. Firstly, the polymer could simply not be forming a full network with sufficient modulus to maintain any morphology, and on drying the structure would collapse as the monomer and internal phase evaporated away under vacuum. This however does not explain why the collapsed pores would not refill with solvent during swelling. One proposal was that the polymer was undergoing adhesion between the walls of the pores on collapse, similarly to putty like material which would then prevent the pores re-expanding in solution. This would be intensified due to the low polymer conversion.

6.4.2.2 Window formation and porogen

Assuming the network had formed sufficiently, there was then no guarantee that the pores would form windows. As proposed in work by Cameron *et al*.,[34] and supported by authors such as Xu *et al*. [35], the windows only have a propensity to form when the polymer shrinks enough to 'rip' open the pores where the walls are thinnest. In our systems, the elastic nature of the polymers may have offset the ability of these holes to rip open which would leave a closed cell pHIPE. The bad yields could then aggravate this, where the left over monomers may swell the network as it forms, reducing both the pore volume and preventing window formation. This effect is similar to that of a porogen, which are known to reduce mechanical strength.[36] A pHIPE comprised of 40 % porogen (such as in these polymers with only 60 % yield) would

struggle to retain any morphology. This lack of open-cell nature may have explained why the polymers did not dry easily to the core.

6.4.2.3 Future work

It was clear that the yield was likely the leading cause for concern, as the resulting fraction of monomer could seriously affect the pHIPE through many mechanisms. Primarily, optimization and better understanding of the polymerisation of this co-polymer in the HIPE should be developed. Increased yields could solve all of the associated problems, however if they did not, then investigating the drying process more thoroughly with techniques such as cryo-SEM would likely give interesting data from the curing stage onward. Gaining access to freeze drying equipment where the drying could be carried out below T_g may result in the elastomer exhibiting the desired morphology and swelling performance, at least until it warmed.

6.5 References

1 A. F. Kingery and H. E. Allen, *Toxicol. Environ. Chem.*, 1995, **47**, 155–184.

2 G. E. Luckachan and C. K. S. Pillai, *J. Polym. Environ.*, 2011, **19**, 637–676.

3 D. H. (Midwest R. I. K. C. M. . American Chemical Society., T. M.J., S. J.S., M. R.R., B. R., C. J.R. and C. G., *Journal of agricultural and food chemistry.*, American Chemical Society, 1953.

4 J. C. Anastas, P. T.; Warner, *Green Chemistry: Theory and Practice*, Oxford University Press, New York, 1998.

5 V. Siracusa, P. Rocculi, S. Romani and M. D. Rosa, *Trends Food Sci. Technol.*, 2008, **19**, 634–643.

6 M. O. Carmody and W. H. Carmody, *J. Am. Chem. Soc.*, 1937, **59**, 1312–1312.

7 H.-H. Greve, in *Ullmann's Encyclopedia of Industrial Chemistry*, Wiley-VCH Verlag GmbH & Co. KGaA, Weinheim, Germany, 2000.

8 M. R. Thomsett, T. E. Storr, O. R. Monaghan, R. A. Stockman and S. M. Howdle, *Green Mater.*, 2016, **4**, 115–134.

9 M. F. Sainz, J. A. Souto, D. Regentova, M. K. G. Johansson, S. T. Timhagen, D. J. Irvine, P. Buijsen, C. E. Koning, R. A. Stockman and S. M. Howdle, *Polym. Chem.*, 2016, **7**, 2882–2887.

10 P. A. Wilbon, F. Chu and C. Tang, *Macromol. Rapid Commun.*, 2013, **34**, 8–37.

11 M. Firdaus, *Asian J. Org. Chem.*, 2017, **6**, 1702–1714.

12 M. Firdaus, L. Montero de Espinosa and M. A. R. Meier, *Macromolecules*, 2011, **44**, 7253–7262.

13 J. M. Bolton, M. A. Hillmyer and T. R. Hoye, *ACS Macro Lett.*, 2014, **3**, 717–720.

14 A. Behr and L. Johnen, *ChemSusChem*, 2009, **2**, 1072–1095.

15 D. L. Trumbo, *Polym. Bull.*, 1993, **31**, 629–636.

16 P. Sarkar and A. K. Bhowmick, *RSC Adv.*, 2014, **4**, 61343–61354.

17 A. J. Johanson, F. L. McKennon and L. A. Goldblatt, *Ind. Eng. Chem.*, 1948, **40**, 500–502.

18 K. Zimny, A. Merlin, A. Ba, C. Aristégui, T. Brunet and O. Mondain-Monval, *Langmuir*, 2015, **31**, 3215–3221.

19 N. R. Cameron and D. C. Sherrington, *J. Mater. Chem.*, 1997, **7**, 2209–2212.

20 J.-H. Chen, T. Le and K.-C. Hsu, *Membranes (Basel).*, 2018, **8**, 11.

21 Y. Tunc, N. Hasirci and K. Ulubayram, *Soft Mater.*, 2012, **10**, 449–461.

22 M. R. Moghbeli and M. Shahabi, *Morphology and Mechanical Properties of an Elastomeric Poly(HIPE) Nanocomposite Foam Prepared via an Emulsion Template*, 2011, vol. 20.

23 J. L. Mateo, M. Calvo and P. Bosch, *J. Polym. Sci. Part A Polym. Chem.*, 2001, **39**, 2049–2057.

24 S. Georges, M. Bria, P. Zinck and M. Visseaux, *Polymer (Guildf).*, 2014, **55**, 3869–3878.

25 E. Laur, A. Welle, A. Vantomme, J.-M. Brusson, J.-F. Carpentier, E. Kirillov, E. Laur, A. Welle, A. Vantomme, J.-M. Brusson, J.-F. Carpentier and E. Kirillov, *Catalysts*, 2017, **7**, 361.

26 S. Georges, M. Bria, P. Zinck and M. Visseaux, *Polymer (Guildf).*, 2014, **55**, 3869–3878.

27 M. Lu, J. Zhou, L. Wang, W. Zhao, Y. Lu, L. Zhang and Y. Liu, *J. Nanomater.*, 2010, **2010**, 1–8.

28 P. Sarkar and A. K. Bhowmick, *RSC Adv.*, 2014, **4**, 61343–61354.

29 X. Fan, S. Zhang, Y. Zhu and J. Chen, *RSC Adv.*, 2018,**8**, 10141-10147.

30 N. Annabi, J. W. Nichol, X. Zhong, C. Ji, S. Koshy, A. Khademhosseini and F. Dehghani, *Tissue Eng. Part B. Rev.*, 2010, **16**, 371–83.

31 M.-H. Ho, P.-Y. Kuo, H.-J. Hsieh, T.-Y. Hsien, L.-T. Hou, J.-Y. Lai and D.-M. Wang, *Biomaterials*, 2004, **25**, 129–38.

32 N. Bauer, J. Brunke and G. Kali, *ACS Sustain. Chem. Eng.*, 2017, **5**, 10084–10092.

33 A. J. Johanson, F. L. McKennon and L. A. Goldblatt, *Ind. Eng. Chem.*, 1948, **40**, 500–502.

34 N. R. Cameron, D. C. Sherrington, L. Albiston and D. P. Gregory, *Colloid Polym. Sci.*, 1996, **274**, 592–595.

35 H. Xu, X. Zheng, Y. Huang, H. Wang and Q. Du, *Langmuir*, 2016, **32**, 38–45.

36 N. R. Cameron and A. Barbetta, *J. Mater. Chem.*, 2000, **10**, 2466–2471.

37 G. Akay, Z. Bhumgara and R. J. Wakeman, *Chem. Eng. Res Des.*, 1995, **73**, 782.

Chapter 7 -

Final Conclusions

The overall purpose of this thesis was to develop a polymeric absorbent which could encapsulate to high swelling degrees, (Q > 25) and degrade, CWAs in a single SDM.

The beginning of the thesis looked at building on previously reported work with polyelectrolyte gels to learn how and why various solvents swelled in these systems. Chapter 2 saw that as the ionic content (THVBAC) of a styrene based, weakly crosslinked polyelectrolyte increased, its potential for high swelling also increased. Investigation found that for solvents which have both a good solubility parameter closeness to the polymer matrix and also a high level of dielectric, that extremely high swelling (Q > 150 in DMSO) could be achieved in the polyelectrolyte with increased ionic content. A mathematical model was developed which was able to predict the swelling of solvents using Ra and dielectric, and the correlation with the experimental results provided very goof fitment $R^2 = 0.979$. The model was not able to predict the correct swelling of VX, sarin and sulfur mustard. The experimental swelling results of these agents did help to identify methyl benzoate as a suitable physical simulant for VX and sulfur mustard, and showed that these two agents were incompatible with the ionic monomer moving forward.

Chapter 3 saw the modification of both the anion of the ionic monomer, and the non-ionic styrene in an attempt to increase the swelling of the agents. Alternative 'weakly-coordinating' anions were metathesized onto the THVBAC of chapter 2 and made into polymer gels. Correlations were made between the swelling of the polymers with alternative anions and the anion dissociation constants from literature. The variable dissociation constants led to varying amounts of osmotic pressure in the system which led to changes in swelling. The swelling of ethanol was seen to be related to the ability of the anion to accept hydrogen bonds. Alternative monomers to styrene were screened through exploration of HSPs and a range of other polymer gels were formed. None of the alternative systems swelled the CWAs significantly better than the non-ionic polymer of chapter 2.

The fourth part of the work introduced a morphological change to the polymer matrix. Styrene and divinylbenzene were polymerised using pHIPE templating techniques and were found to show significantly increased swelling (Q = 9.2 in St_{100} gel to Q = 55.6 in $St_{95}VBC_5IP_{95}$) of the methyl benzoate simulant over the non-HIPE gels due to the void expansion effect. The best performing polymer was able to swell to maximum capacity in less than 10 minutes, swell from a compressed state and be modified easily to be wholly hydrophobic or hydrophilic. Most importantly $St_{95}VBC_5IP_{95}$ showed record breaking absorption capacity for sulfur mustard (Q = 40) and all of the V-agents tested at no less than Q = 45 (Q_{VX} = 55). Sarin was also absorbed in line with the leading research of Q = 19. After proving the polymer was suitable for CWA encapsulation, the reaction was scaled up to produce batches totalling 9.5 kilograms of polymer, with no loss of swelling capacity over the process.

$St_{95}VBC_5IP_{95}$ was then brought into collaboration where active MOF-808 catalysts were incorporated into the pores of the matrix. This composite was able to hydrolyse VX with external buffering faster (k = 0.0267 min^{-1}) than the lone catalyst (k = 0.034 min^{-1}). Introducing 5 mol% of a piperidine based monomer required additional surfactant to stabilize the emulsion, but allowed the composite to possess some internal buffering potential. Slight loss of the swelling ability (Q = 32) was observed in the composite due to VBPP. The final composite MOF-HIPE-VBPP-S showed an increased rate (k = 0.0059 min^{-1}) of hydrolysis of VX compared to the control polymers (k = 0.0044 min^{-1}) in trials with no external buffer and excess water. In neat VX with no buffer or water, the VBPP containing polymer hydrolysed the VX slightly slower than the better swelling MOF-HIPE-S, yet the same conversion was reached after the full 14 days. Both MOF-HIPE-S and MOF-HIPE-VBPP-S proved to be effective SDMs for VX, with advantages over the closest alternative research, such as improved catalytic loading in addition to high swelling capacity.

The final chapter introduced some preliminary work on the potential for utilizing myrcene as an green alternative feed monomer to styrene in the pHIPE sorbents. The conversion to

polymer by NMR in trials with a 50:50 ratio of myrcene to styrene was low, and this was also seen by physical polymer yield. After also observing slow gelation of the polymerisation, an alternative crosslinker was synthesised (DDMA) which showed improved rates to gel. A range of pHIPEs were prepared with DDMA crosslinking and myrcene content from 10 % to 50 %. Visually the monoliths appeared to have formed in the archetypal manner for a pHIPE, but after removal of the internal phase, no porosity was observed by SEM in any of the polymers apart from the 0 % and 10 % myrcene systems. The swelling of the polymers also supported that the polymers were not porous after drying. Alternative approaches to processing the elastomers were carried out on the 50 % myrcene system but no porous morphology could be retained. Conclusions were discussed and the future work of this area of the project would revolve around a much more detailed understanding of the polymerisation of these two monomers and why the yields were so low before the synthesis of the pHIPEs was to be continued.

Overall, the aims of the thesis were met well in terms of the production of a versatile and effective sorbent for CWAs through the production of pHIPE $St_{95}VBC_5IP_{95.}$ The degradation of VX was effective in the SDM MOF-HIPE-VBPP-S and MOF-HIPE-S, although similar composites were not approached for either sarin, or sulfur mustard. A good understanding of why polyelectrolytes and non-electrolytes swell, as well as what compositions swell CWAs, was developed in the earlier work which allowed the pHIPE compositions to be established efficiently. Identification and successful trialling of a suitable swelling and physical simulant for VX and HD was also achieved.